Toward the Industrial Application of a Solid-Oxide Fuel Cell Power Plant with Compressed Air Energy Storage

Toward the Industrial Application of a Solid-Oxide Fuel Cell Power Plant with Compressed Air Energy Storage

Design, Simulation, Optimization, Techno-Economic Analyses and Life-Cycle Analyses

By JACOB NEASE, B.Eng.Mgmt.

A Thesis

Submitted to the School of Graduate Studies

in Partial Fulfillment of the Requirements for the Degree

Doctor of Philosophy

McMaster University

Ph.D. Candidate (2016) McMaster University
Chemical Engineering Hamilton, Ontario, Canada

TITLE: Toward the Industrial Application of a Solid-Oxide Fuel Cell Power Plant with Compressed Air Energy Storage

AUTHOR: Jacob Nease, B.Eng.Mgmt (Chemical Engineering)
McMaster University

SUPERVISOR: Dr. Thomas A. Adams II

NUMBER OF PAGES: **xiv, 136**

Abstract

The global electricity generation industry is very reliant on the use of fossil fuels, particularly natural gas and coal. However, it is quickly becoming a reality that the over-consumption of these resources will continue to lead to significant global damage via global warming, ecosystem destruction, and the depletion of these so-called non-renewable resources. To combat this issue, renewable sources such as wind, biofuels and solar are becoming much more prevalent in the power generation industry, but significant economic, reliability and availability barriers to entry will prevent these sources from being major contributors to the power industry for decades.

To this end, this thesis focuses on the design, operation, optimization and life cycle analysis of an integrated solid-oxide fuel (SOFC) cell power plant integrated with compressed air energy storage (CAES). This plant, fueled by either natural gas or coal, can make much more efficient use of their limited non-renewable fuel sources, and are capable of achieving nearly 100% carbon capture at the plant boundary. This plant is intended to serve as a more efficient and environmentally responsible alternative to current power generation methods while still exploiting remaining fossil fuels to their fullest extent.

This thesis details the design, sizing and simulation of integrated SOFC/CAES plants in Aspen Plus so that full feasibility and techno-economic analyses may be performed, the results of which are then compared to the current state-of-the-art (SOTA) options. In order to compare the plants on an environmental level, full cradle-to-grave life-cycle analyses using the *ReCiPe 2008* method are completed for each SOFC-based plant and all comparable SOTA options under a wide range of assumptions and plant configurations, such as the use of carbon capture strategies. Furthermore, detailed reduced-order dynamic models of the integrated SOFC/CAES plants are developed and simulated with a newly developed rolling-horizon optimization method to assess the load-following capabilities of the integrated plant. Real scaled demand data for the market of Ontario, Canada for the years 2013 and 2014 are used as the demand data for the simulations.

This thesis takes strides in proving the feasibility of an integrated SOFC/CAES power plant for providing clean, efficient, reliable and cost-effective power using fossil fuels. The next steps for this project involve the development of a lab-scale pilot plant, which would be used to validate simulation results and provide an opportunity for the real-time application and assessment of the potential of this plant design.

Research Contributions and Highlights

- This thesis contains the design and modeling of the first integrated solid-oxide fuel cell (SOFC) and compressed air energy storage (CAES) plants to provide peaking power from fossil fuels with zero gate-to-gate emissions.

- Up to 64% and 43% electrical efficiency (by higher heating value) can be achieved for natural gas- and coal-fueled plants with carbon capture and sequestration (CCS), which is at least 14 percentage points higher than any currently used state-of-the-art (SOTA) plant using CCS.

- SOFC-based plants are economically attractive under market conditions involving modest carbon emission taxes of $20 per tonne.

- Cradle-to-grave life cycle impacts for natural gas SOFC/CAES plants without CCS are equivalent to the natural gas combined cycle (NGCC) with CCS. The addition of CCS to SOFC plants decreases the total life-cycle impact by over 50%, and is nearly 80% lower than an NGCC plant without CCS.

- Cradle-to-grave life cycle impacts for coal SOFC/CAES plants without CCS are significantly lower than the currently used integrated gasification combined cycle (IGCC) and supercritical pulverized coal (SCPC) systems. The addition of CCS to SOFC plants decreases the total life-cycle impact by over 55%, and is at least 60% lower than any other SOTA option.

- The total life-cycle impact of any SOFC plant (coal or natural gas) with CCS is lower than any comparable SOTA plant, regardless of the type of fuel consumed.

- The use of rolling horizon optimization (RHO), formulated and simulated as a part of this work, can vastly improve the hour-by-hour load following capabilities of the SOFC/CAES plant when trying to match a typical demand profile for all fuel types. These effects are persistent even under the presence of significant forecasting uncertainty.

- Extension of the RHO scheme into two levels by making slow changes to the SOFC stack sizes allows for more effective seasonal load-following, resulting in an 86% improvement in annual load-following as measurement by the squared error between supply and demand.

Acknowledgments

When I approached the end of graduate school, I started to worry about what to write, how much to write, what to exclude, what to include and so on. However, there was one thing that stuck out in my mind from the outset: I will not skimp on the acknowledgments. If anything, it gives me a chance to be as verbose as I want without Dr. Adams cutting it down to a reasonable length! Kidding aside, I have a lot to be thankful for, and a lot of people that have made this project, this thesis, and my career a reality.

First and foremost, I want to thank my supervisor, Dr. Thomas Adams II. He has been my supportive mentor, my brilliant supervisor, my sounding board, my team mate, my tennis partner, and my friend. As a matter of fact, if it were not for Dr. Adams, I would never have pursued graduate studies. However, through my experiences with him as a TA in my fifth year of my undergraduate degree (which was by dumbfound luck, I will have you know), he convinced me that graduate school can be an exciting and fun time. He was right. Go figure. He's always right. Dr. Adams always told me to do what I love, and never to compromise for anything else. I hope we keep in touch no matter what happens, and that you keep going for that backhand passing shot.

To my committee members, Drs. Swartz and Petric, I owe a great deal of thanks as well. Dr. Petric taught me more about the actual workings of the technologies I simulate than I could have achieved on my own, and Dr. Swartz flat-out gave me the idea for an entire publication and gave me some invaluable funding proposal experience. You guys have been more than supportive, and this would not have happened without you.

Aside from my supervisor and committee, the entire Adams group has offered me a wealth of support over the last 5 years. A particularly special shout out to my bromantic buddy Jaffer "G-HOUSE" Ghouse for his intellectual and moral support throughout my time here. I would also like to thank Alicia and Handsome Yaser for their support during the formative years of the Adams group. Without you guys, I would never have had the motivation and the drive to come this far. I would like to extend this sentiment to all other members of the Adams group that have made my time here special: Kyle (in and beyond school), Dominik (aka "Brah"), Kush Ball, Vida, Chinedu, Giancarlo, James, Sarah, Leila, Hundey, and Nina (my fabulous summer student). You guys are awesome and I know you will all excel in grad school and beyond.

My final formal thanks goes to the department of Chemical Engineering here at McMaster, the faculty of which have made me feel at home for 10 years. A special thanks to Dr. Filipe, Dr. Zhu, and Kevin Dunn, who have nurtured my love of teaching and given me opportunities to develop a career that I could never have dreamed possible, especially as a student. I can only hope I continue with the stellar example you have set for me.

The whole "fun" promise about grad school would not have been possible without some pretty amazing friends that I have met along the way, and some that have been by my side for what seems my whole life. Scotty, Daryl, Trev, Corbett, Mudassir, Wallace, Cammers, Patty, Miles, BeWalt, Biebs, Neil, Stu, Graham, and Keith. Just a few names that come to mind when I think of softball, games nights, hockey, Frisbee, squash, the Phoenix, and

undying friendships forged through a life of good times and better company. Words cannot express my appreciation and love for all of you.

My family. Without my family I would be nothing like the person that I am today. Thank you to my parents, Brad and Val, for giving me everything and more. Constant love and support, a home, the freedom to follow my dreams, unforgettable memories and an unwavering interest in my life and academics are but some of the reasons that this degree has become a reality. To my brother Joe, you do not know what your presence and support has meant to me. I am honoured and graced to call you my brother and my friend. I am so proud of who you have become.

Last but not least, we come to Laura. The love of my life. My Rock. My best friend. It has been a long road, and you have made it that much better along the way. We have come a long way from me rambling about polymers at the Bean Bar. You have kept me level, made me happy, and been a tremendous supporter of everything I do in and beyond school. We finally made it, and I can't wait to start on a new path with you.

This work is dedicated in loving memory to my Gramps, Tom Nease, who always believed that my work could change the world. When I see you again, I will ensure that you were right. I promise.

Table of Contents

Nomenclature

Please note that the following list consists of abbreviations consistently used throughout all chapters of this thesis. Since chapters 2-6 (inclusive) are published reprints, they make use of mathematical symbols and variables native to their document, which may not be consistent across all chapters. For these symbols, please refer to the mathematical notation sections in each publication.

ALO	agricultural land occupation
ASU	air separation unit
ATR	auto-thermal reformer
CAES	compressed air energy storage
CC	climate change
CCS	carbon capture and sequestration
DCB	dichlorobenzene
ED	damage to ecosystem diversity
EOS	equation of state
FD	fossil depletion
FE	freshwater eutrophication
FET	freshwater ecotoxicity
HH	damage to human health
HHV	higher-heating value
HRSG	heat recovery and steam generation
HT	human toxicity
IESO	Independent Electricity Systems Operator
IGCC	integrated gasification combined cycle
IR	ionizing radiation
LCA	life cycle analysis
LCOE	levelized cost of electricity
MD	metal depletion
ME	marine eutrophication

MET	marine ecotoxicity
NGCC	natural gas combined cycle
NLT	natural land transformation
NMVOC	non-methane volatile organic compound
nWGS	no water-gas shift reactors
OD	ozone depletion
PEN	positive-electrolyte-negative
PM10	particulate matter with radius 10 mm
PMF	particulate matter formation
POF	photochemical oxidant formation
RD	damage to resource depletion
RHO	Rolling Horizon Optimization
SCPC	supercritical pulverized coal
SOFC	solid oxide fuel cell
SOTA	state-of-the-art
SSE	sum of squared error
TA	terrestrial acidification
TET	terrestrial ecotoxicity
TSD	train shutdown
ULO	urban land occupation
WD	water depletion
WGS	water-gas shift
WSSE	weighted sum of squared error

Chapter 1

Introduction

1.1 Preliminaries

Before describing the novelties and potential scientific and societal contributions of this thesis project, it is important to describe the technologies that will be (and have been) considered and analyzed. What follows in this section is a brief literature review and description of the current North American electricity industry and descriptions of the currently employed state-of-the-art (SOTA) in electricity generation in sections 1.2 and 1.3, respectively. Finally, descriptions of the two key technologies utilized in this project are given section 1.4.

1.2 Current State of the Electricity Generation Industry

On the global scale, the electricity generation industry is largely dependent on the use of fossil fuels such as natural gas and coal due to their high abundance and relative ease of access. Energy conversion with renewable fuel sources (wind, solar, bio-fuels etc.) is still decades away from being implemented on any significant scale. To illustrate, it is projected that the total electricity produced in the United States and Canada by renewable (non-hydro) sources in the year 2035 will be 16% and 10%, respectively [1],[2]. In fact, well over half of worldwide power production will still rely on fossil fuels into 2035 as illustrated in Figure 1 [3].

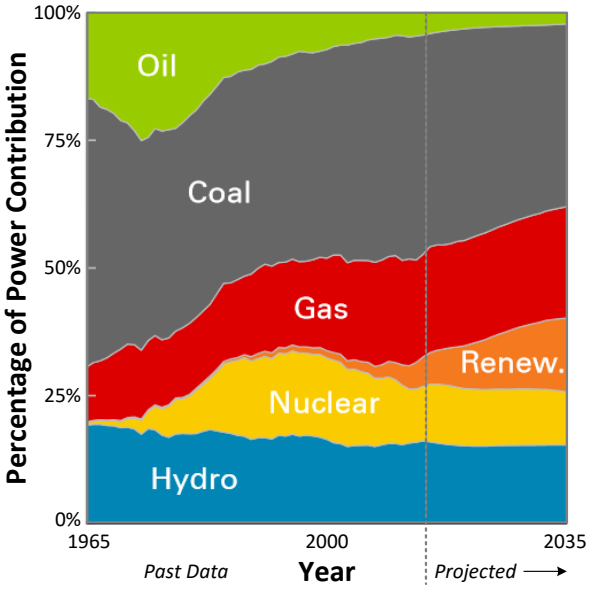

Figure 1: Projected worldwide electricity generation by fuel type. Adapted from [3]

For the near to medium term, it is desirable to maximize the efficiencies of current fossil-based power generation technologies while remaining cognizant that carbon capture and control requirements are likely going to be implemented in the near future, likely driven by a fixed carbon tax, emissions restriction or a cap-and-trade system. The electricity generation sector will likely be required to capture the CO_2 generated by their operations

and sequester it in underground spaces such as depleted oil fields, aquifers, and other geological storage sites [4]. As such, these industries will be faced with the decision to either invest in the required technology for CO_2 capture and sequestration, or bear the potential financial penalties associated with its emission. Either way, the impact to the end consumer will be increased electricity prices and therefore an increased cost of living.

With this outlook in mind, it is the objective of this thesis project to address the issue of medium- to long-term electricity generation utilizing fossil fuels. In order to make the most of our available resources, there is a need to improve efficiency, reliability and environmental impact while also addressing the economic and political concerns that are incumbent with the development of new technology and the consumption of limited resources. Not only does this thesis aim at developing technologies that can generate reliable base-load electricity, it is also targeted at developing processes that are capable of accurately following electricity demand patterns (known as "peaking power") with the same potential improvements regarding environmental impact and fuel efficiency. This project is motivated by these needs (economic feasibility, environmental impact and political acceptance) to satisfy what is known as the "triple-bottom-line" of sustainability. Over the past several years, this project has shown that significant impacts can be made on the electricity generation industry on the global scale, potentially changing not only how power is made and consumed, but also how different fuel sources and their potentially unflattering stigmas may be overcome.

1.3 Current State-of-the-Art Power Generation Techniques Using Fossil Fuels

Of course, in order to claim any benefits, the systems proposed in this project must be compared to the current SOTA in the electricity generation industry. What follows in the next subsections are brief descriptions of the status-quo for power generation technologies utilizing natural gas and coal.

1.3.1 The Natural Gas Combined Cycle (NGCC)

Natural gas-fed processes account for approximately 24% of all electricity generated in the United States and is anticipated to rise to 27% by 2035 [1]. In Canada, natural gas accounts for 9% of the electricity generated and is projected to increase to 15% by 2035 [2]. Natural-gas fired power plants produce inherently lower emissions per unit of electrical energy than coal (50.29 g/MJ and 90 g/MJ, respectively) [5], and therefore it is responsible for a proportionally smaller amount of the CO_2 emissions in the power sector. For example, in the United States, natural gas contributes to only 17.5% of the carbon emissions for the electricity sector [6],[1] while producing 24% of the power. However, the emissions from a standalone NGCC plant are still significant, and other approaches may be required to reduce the emissions of natural gas power plants to a sustainable level without the addition of expensive carbon capture strategies [7].

The NGCC process is briefly described as follows [7],[8]: First, the natural gas fed to the plant is cleaned and desulphurized if it was not done so prior to distribution. The gas is then combusted in air at a high temperature and pressure in a gas turbine unit, which produces electricity through a generator attached to the turbine. The waste heat from the exhaust stream may then be recovered through the generation of high pressure steam, which can be used to power steam turbines in a steam cycle for additional power generation (hence the name "combined cycle"). The exhaust, which now contains mostly CO_2, water and N_2 from the combustion step, may then be subjected to a solvent-based absorption process. This process would serve to separate the CO_2 from the flue gas with approximately 90% recovery should carbon capture and sequestration (CCS) be desired. Absorption can be performed with chemical solvents such as monoethanolamine (MEA) or methyldiethanol amine (MDEA), or physical solvent processes such as Rectisol^{TM} or Selexol^{TM} [9]. The CO_2 stream is then cooled and compressed to supercritical conditions suitable for transport in a CO_2 pipeline, and the decarbonized exhaust stream is vented to the atmosphere through a flue stack. However, a significant amount of energy is required for CO_2 capture in the NGCC process (up to 14% of the net power produced) which can cause up to a 40% increase in the levelized cost of electricity (LCOE) [8]. Other more recent approaches for CCS such as membrane-based processes, pressure swing adsorption and vacuum swing adsorption have also been investigated with promising results but have not yet been implemented at the industrial scale [10],[11].

1.3.2 Pulverized Coal and Gasification

Coal powers approximately 45% of the electricity generation in the United States and is expected to remain the dominant fuel choice through 2035 [1],[3]. On a global scale, coal accounts for approximately 33% of all electricity production and is expected to maintain a significant share over the next few decades [12]. Coal-fired power plants produce an inherently high amount of CO_2 per unit of electricity generated (approximately 90.29 g/MJ) and therefore account for a significant amount of the CO_2 emissions in the power generation sector [5]. For example, in 2010, coal-based processes contributed 80.9% of the total CO_2 emissions for the electricity generation sector in the United States, or 26.8% of all of the CO_2 emitted across all industries [6]. Reducing or eliminating the CO_2 emissions from coal-fed plants would contribute significantly towards the large-scale reduction of worldwide CO_2 emissions. In Eastern Canada, coal has been almost completely retired as a power generation option, which considerably narrows Canadian power generation options.

The supercritical pulverised coal (SCPC) process is chosen as the “status quo” coal-fed power generation process for the purposes of this investigation. The SCPC process is briefly described as follows [8]: coal is combusted with air in a boiler, generating heat to power steam turbines. Steam is generated above the critical point (hence “supercritical”) at 240 bar and 593°C to improve downstream power generation efficiency. The combustion products are mainly CO_2, H_2O, N_2, SO_2 and ash, as well as small amounts of other impurities (Hg, S, Cl). The ash and sulphur are removed through separate cleanup steps and the small amounts of impurities can be removed through various well-proven processes, yielding a final exhaust stream containing mainly H_2O, CO_2 and N_2. At this point, the exhaust

can be vented to the atmosphere (as is typically done), or post-combustion CO_2 absorption using the methods described in the previous section may be performed to remove CO_2 for capture and sequestration purposes. Approximately 90% of the CO_2 in the exhaust gas can be recovered at purities required for pipeline transport, with the rest being emitted to the atmosphere via the exhaust gas. Although they are effective, these absorption-based CCS strategies are energy-intensive and often lead to prohibitive decreases in overall system efficiency, leading to higher electricity costs [8]. In fact, the only example of an industrial-scale CCS system worldwide exists in Saskatchewan, Canada [13].

Gasified coal processes such as the integrated gasification combined cycle (IGCC) involve the gasification of coal into synthesis gas ("syngas," which is a combination of CO and H_2) as well as CO_2 and H_2O. The water-gas shift (WGS) reaction can then be performed downstream of the gasification step to increase the amount of H_2 in the syngas stream. After gas shifting, the same solvent-based absorption processes for CCS can be employed to remove CO_2 before the downstream use of the syngas. As in the post-combustion CCS case, approximately 90% of the CO_2 in the syngas stream can be recovered at pipeline purity [8].

1.4 Brief Description of Essential Technologies and Terminologies

1.4.1 Solid-Oxide Fuel Cells

A solid oxide fuel cell (SOFC) utilizes a fuel gas and an oxidant (typically air) to efficiently produce electrical power through electrochemical reactions on opposite sides of a solid oxide barrier, as depicted in Figure 2. The reactions that occur in the anode and cathode may include, but are not limited to:

$$H_2 + O^{=} \rightarrow H_2O + 2e^{-} \quad \text{(Anode)} \quad (1.1)$$

$$CO + O^{=} \rightarrow CO_2 + 2e^{-} \quad \text{(Anode)} \quad (1.2)$$

$$O_2 + 4e^{-} \rightarrow 2O^{=} \quad \text{(Cathode)} \quad (1.3)$$

Suitable fuel sources for the SOFC anode include hydrogen gas, carbon monoxide, natural gas [14], methanol, [15], and others. Moreover, fuels such as coal [16], diesel [15], ethane and even biomass [17] can be pre-processed into syngas and used as a fuel source. Provided that the fuel utilization is high and the SOFC is equipped with appropriate seals that maintain separation between the anode and cathode exhausts, the anode exhaust will consist mainly of H_2O and CO_2. The anode exhaust can hence be separated relatively easily, and the resulting captured CO_2 can be compressed for pipeline transport. The cathode exhaust is partially deoxygenized air at high temperatures (~900°C), which can be used for additional power generation through heat recovery and vented without posing an environmental risk. If the SOFC is operated at high pressures (10-20 bar), electricity can also be generated by feeding the hot, pressurized cathode exhaust to a gas turbine, thus forming a Brayton cycle. Prior studies have shown that pressurized SOFC systems of this type are capable of generating power at high efficiencies (up to 74% by higher heating value) with

essentially no CO_2 emissions [7]. Comparable studies by other groups have found similar results [18],[19]. Furthermore, the process of electrochemical energy conversion to electricity is more efficient than combustion and forgoes the typically required heat transfer to another medium, which allows the SOFC plant to achieve higher thermal efficiencies than systems that utilize the Carnot cycle.

However, one significant disadvantage of SOFC systems is that there are currently potentially cost-prohibitive operability challenges associated with their dynamic operation. For example, it is possible to change the power output of a SOFC relatively quickly (perhaps in response to load changes) [20], but this runs the risk of very high degradation rates or even destruction due to rapid thermal expansion or the backflow of gases [21]. To avoid these risks, it is probable that future large-scale SOFCs will operate at a fixed power output which will not be adjusted to follow the typical diurnal power demand profile of a power grid. Of course, a system with a fixed power output can be scaled large enough to always meet demand, but this approach would be wasteful since it would almost always produce more electricity than necessary. More details on the function and system design (both academic and industrial) of SOFCs may be found in a recent literature review [22].

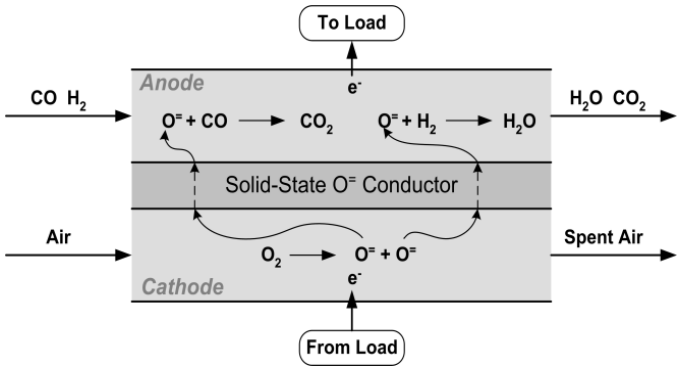

Figure 2: Simple schematic of a SOFC using syngas as a fuel source

1.4.2 Compressed Air Energy Storage

Compressed Air Energy Storage (CAES) plants operate as an intermittent source or sink for electrical power. The plant consumes power in order to compress air to high pressures and store it in an either man-made or naturally occurring void (which may be above- or below-ground) as elastic potential energy. During periods of high power demand or electricity prices, the stored compressed air is pre-heated (usually by combusting natural gas) and fed to gas turbines attached to an electric generator, thereby re-supplying the stored energy back to the power grid. A simplified schematic of a typical CAES system is shown in Figure 3.

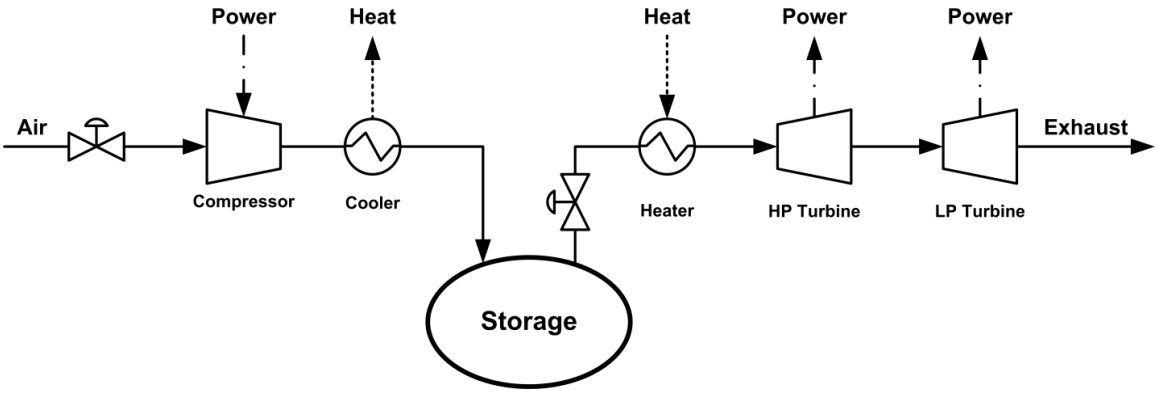

Figure 3: Simplified CAES system schematic. Reproduced from [22]

CAES technology has been utilized for over three decades. The Alabama Electric Corporation has been operating a 110 MW plant since 1991, and E.N. Kraftwerke has been running a 290 MW plant in Huntorf, Germany since 1978 [23]. There have been several other studies and plans to construct further CAES plants by Chamisa and Apex Energy, but at the time of writing this thesis no such projects have been completed [24].

CAES is advantageous for a variety of purposes; not only can it serve as a stand-alone plant capable of achieving profitability through compressing at times of low electricity prices and releasing at times of high prices, but it can also be combined with other processes to add flexibility or reliability. For example, there has been significant theoretical research in recent years examining the utilization of CAES as a method for levelling intermittent sources (such as wind power) to provide a consistent base load [23], [25]-[30]. However, there has not been much research concerning the integration of CAES with other power sources for the purposes of load following (or "peaking").

1.5 Opportunities and Potential Contributions

This thesis project investigates the integration of the two previously described technologies (SOFCs and CAES) at the systems level. The following sections are aimed at describing the novel and beneficial integration concept of these technologies, as well as the perspective in which this thesis will make comparisons of the integrated system to the current SOTA through the triple-bottom-line of sustainability.

1.5.1 Solid-Oxide Fuel Cell and Compressed Air Storage Integration Proposal

The main contributions of this research thesis involve the development, analysis, comparison and critical evaluation of an integrated SOFC/CAES system with optional CCS to provide peaking power with reduced or zero CO_2 emissions. In doing so, the integrated SOFC/CAES process makes use of the advantages of each individual technology (fuel flexibility, high efficiencies for the SOFC and rapid dynamics and controllability for the CAES)

and overcome their limitations when used exclusively (base-load only power for the SOFC, external power and heat source required for the CAES).

In order to provide reliable, peaking power with 100% CO_2 capture, this thesis proposes the integration of SOFCs (to provide base-load power), a CCS system (to achieve near-zero CO_2 emissions), and a CAES system (to follow peaking demand). The original SOFC and CCS models are based on those developed in literature, but have been updated using more recent works and modified to incorporate CAES [7],[31],[32] as necessary. During times of day in which demand is low, the CAES system can be used to charge the available storage space using a portion of the electrical power generated by the SOFC system to compress some or all of the cathode exhaust to the current pressure of the underground storage cavern. The portion of the cathode exhaust which is not sent to CAES is sent to a turbine attached to a generator to produce additional electricity, as shown in Figure 4(A). During times when the electricity demanded is high, all of the cathode exhaust is sent to the gas turbine, maximizing the electricity produced by the SOFC/GT system. In addition, air is released from the storage space and fed to a second gas turbine system, producing additional power, as expressed in Figure 4(B). With this approach, the proposed SOFC/CAES/CCS system is able to provide load-following power from fossil fuels while maintaining high efficiency and capturing nearly 100% of the CO_2.

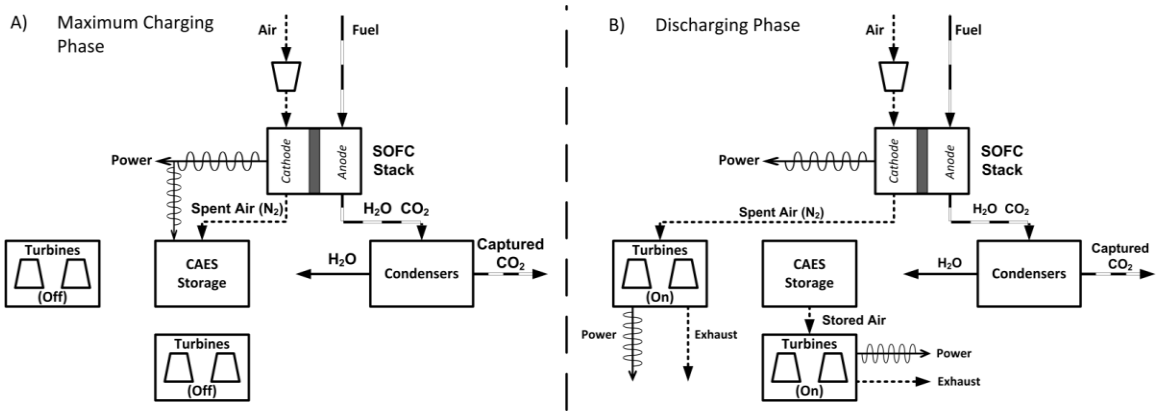

Figure 4: Simplified SOFC/CAES integration technique during (A) the maximum charging phase, and (B) the discharging phase.

1.5.2 Thesis Impact– The Triple-Bottom-Line of Sustainability

When comparing emerging and new technologies for power generation such as the integrated SOFC/CAES concept introduced above, it is not enough to only consider improvements or changes in performance (higher efficiencies, for example). Moreover, evaluating the economic advantages or disadvantages of such a process does not allow for a meaningful comparison between a SOFC-based power plant and one using a more traditional method (NGCC, for example). Instead, this thesis is targeted at critically analyzing these processes via their abilities to meet the *triple bottom line* of sustainability. This means that the processes must demonstrate:

(1) Improved or comparable **economic** performance versus the current state-of-the-art under a variety of scenarios and market conditions. Economic performance includes not only operating costs and revenues, but capital expenditures as well.

(2) A noticeably improved **environmental impact**, whether due to improved efficiency, carbon sequestration or a combination of the two. It should be noted that not only the operational environmental impact is to be considered, but the entire life-cycle impact of the proposed system will be assessed as well.

(3) Feasibility from a **political** point of view. The SOFC/CAES system must be shown to be safe, reliable and thus exhibit potential as a stand-alone peaking power plant. The application of optimization to the operation of the integrated plant will serve as proof that an SOFC/CAES plant has potential in a large scale peaking scenario.

By addressing each of the three issues of the triple-bottom-line via feasibility studies, techno-economic analyses and life cycle impact analyses, the SOFC/CAES system developed throughout this thesis project has the potential to change not only the infrastructure of the North American electricity generation industry, but the political viewpoint on fossil fuels and their role as a critical resource during the transition to an environmentally and economically sustainable economy.

1.6 Chapter and Publication Summaries

Chapter 2 consists of the first peer-reviewed publication resulting from this thesis project. It examines the design, simulation and techno-economic analysis of an SOFC/CAES plant for peaking power fueled by natural gas, largely with the objective of assessing its capability of meeting the economic requirements as outlined in the triple-bottom-line of sustainability. The paper goes into detail describing the design and operation of the system, units selected, and other methodologies. Rigorous steady-state plant simulations of the SOFC baseload portion and the CAES transient portion are performed in Aspen Plus, and dynamic simulations to assess the preliminary peaking capabilities of the plant are performed in MATLAB. In total, ten plants are modelled and compared from a techno-economic standpoint: The SOTA NGCC plants (with and without CCS), and eight permutations of the SOFC plant fueled by natural gas depending on the use of CAES, CCS, a heuristic partial plant shutdown schedule, or any combination of these. Sensitivity case studies are performed to assess the economic performance of each plant under a variety of assumptions such as fuel costs and potential CO_2 taxes, and the results are compared across all plants examined. The full paper citation is as follows:

> Nease J, Adams TA II. Systems for peaking power with 100% CO_2 capture by integration of solid oxide fuel cells with compressed air energy storage. *Journal of Power Sources*. 2013; 228(15): 281-293.

Chapter 3 consists of the second peer-reviewed publication resulting from this thesis. This publication builds on chapter 2 by designing an SOFC/CAES plant with CCS for

peaking power using gasified coal as a fuel source. The same design procedure is taken in which all permutations of the SOFC/CAES plant are designed and rigorously simulated in Aspen Plus before the peaking plants incorporating CAES are simulated dynamically in MATLAB. In this case, the use of WGS reactors ahead of the SOFC stacks to improve fuel cleanliness and cell efficiency is also assessed, resulting in 16 permutations of the SOFC plant including CAES, CCS, seasonal plant shutdowns and the use of WGS reactors. The results of these plant configurations are compared economically with the current SOTA coal power plant options: supercritical pulverized coal (SCPC) and integrated gasification combined cycle (IGCC) plants, both with and without CCS. Therefore, a total of 20 plants are simulated, costed, and compared in this work. The full paper citation is as follows:

> Nease J, Adams TA II. Coal-Fuelled Systems for Peaking Power with 100% CO_2 Capture Through Integration of Solid Oxide Fuel Cells with Compressed Air Energy Storage. *Journal of Power Sources*. 2014; 251: 92-107.

Chapter 4 is the fourth paper published in a peer-reviewed journal during this thesis and steps away from the design and economic evaluation portion of this thesis project in order to address the full environmental impact of the proposed SOFC/CAES plants fueled by natural gas. This objective is achieved by performing the first ever full cradle-to-grave life cycle analyses (LCAs) of SOFC power plants fueled by natural gas. For this, the *ReCiPe 2008* method is implemented through a combination of OpenLCA software and in-house calculation software based on the full life cycle inventory and impact data publicly available for *ReCiPe 2008*. The analyses are performed for the SOFC plant with and without CCS, and for the NGCC plant as a comparative case study. It should also be noted that this work features the first-ever *ReCiPe 2008* LCA for an NGCC plant, which was done for comparative purposes. Sensitivities to assumptions such as emissions and upstream plant impacts and the relative impact of each life cycle impact category are investigated as well. The full paper citation is as follows:

> Nease J, Adams TA II. Life Cycle Analyses of Bulk-Scale Solid Oxide Fuel Cell Power Plants and Comparisons to the Natural Gas Combined Cycle. *The Canadian Journal of Chemical Engineering*. 2015; 93: 1349-1363.

Chapter 5 is the fifth paper published in a peer-reviewed journal from this thesis project. It extends on the work in chapter 4 by performing the first-ever full LCAs of coal-fueled SOFC power plants with and without CCS using the *ReCiPe 2008* method. The same method is used for the first time for IGCC and SCPC plants with and without CCS for comparative purposes. These plants and their life cycle impact results are not only compared to each other, but since a consistent LCA method was used for these plants and the plants fueled by natural gas in the previous chapter, cross-fuel comparisons are possible. This paper thus offers insights into the actual environmental strengths and weaknesses of not only the SOFC plant versus a comparable SOTA option, but also natural gas versus coal as a fuel source. The full citation is as follows:

> Nease J, Adams TA II. Comparative life cycle analyses of bulk-scale coal-fueled solid oxide fuel cell power plants. *Applied Energy*. 2015; 150: 161-175.

Chapter 6 consists of the third paper published throughout this thesis project. In this work, the objective is to address the final component of the triple-bottom-line, namely the social and political feasibility of the proposed SOFC/CAES system. From this perspective, the purpose of this paper is to show that real-time demand forecasts, which are typically available in major North American markets such as Ontario [33], can be utilized in a rolling-horizon optimization scheme in which the peaking capabilities of the CAES system are optimally scheduled over the coming hours (the forecasting length is at the discretion of the user) based on operating and storage constraints. The main improvement brought on by this work is the avoidance of "large misses" which are very bad from an operability and reliability standpoint, especially if the integrated SOFC/CAES system is intended to provide power to a market exhibiting the typical diurnal demand fluctuations of a major power market. Instead, any potential shortcomings due to unavailability of stored energy in the CAES volume may be spread out over a longer period a series of predictable near-misses. This makes the acquisition of grid power or generation of additional power much easier to obtain, thus improving both the load-following performance of the plant and its ability to act as a reliable peaking power provider. Economically-oriented objectives and the impacts of demand and price forecasting uncertainties are also investigated and quantified in this work. Representative weeks of the Ontario market demand from 2013 are used as case studies. The full citation is as follows:

> Nease J, Adams TA II. Application of rolling horizon optimization to an integrated solid oxide fuel cell and compressed air energy storage plant for zero-emissions peaking power under uncertainty. *Computers & Chemical Engineering*. 2014; 68: 203-219.

Chapter 7 consists of the sixth and final paper submitted for publication as a part of this thesis project. This paper also addresses the reliability and peaking operation of the SOFC/CAES plant to target the socio-political component of the triple-bottom-line by significantly extending the work in chapter 6. In this work, slow movements to the upstream baseload plant in the form of incremental activations or deactivations of SOFC stacks are used as a part of a two-level rolling horizon optimization scheme to improve the ability of the SOFC/CAES plant to follow seasonal drifts in demand throughout the year as well as the hourly load-following made possible by the CAES system. Simulations are performed on a new reduced-order model of the SOFC/CAES plant fueled by gasified coal (different than the plant used in chapter 6) with a new set of decision variables. Furthermore, the integrated plant is subjected to the rolling horizon method for an entire year of scaled demand data from Ontario for the calendar year of 2014. The addition of small baseload changes and the second long-term level of the rolling horizon optimization approach is shown to substantially improve the annual load-following of the plant. Sensitivity analyses on storage volume size and comparisons to the previous single-level method are also investigated. The full paper citation is as follows:

> Nease J, Monteiro N, Adams TA II. Application of a two-level rolling horizon optimization scheme to a solid-oxide fuel cell and compressed air energy storage plant for the optimal supply of zero-emissions peaking power. *Computers & Chemical Engineering*. 2016 (Submitted).

1.7 Possible Overlap Between Papers

The reader should note that some parts of the following chapters, such as the introductory and technology description sections, will have some overlap. Although each paper has its own introduction and motivation to set up the work to follow, descriptions of the SOFC technology (a common request by reviewers), CAES systems, current SOTA power generation options, and the power generation outlook for North America and globally will be present in each work to some degree.

Other more focused areas of overlap may also be present based on the topic of the papers themselves. Specifically, chapters 4 and 5 both discuss life cycle analyses and the use of the *ReCiPe 2008* method since they are standalone publications in separate journals. Additionally, chapters 6 and 7 both make reference to the use of optimization software and problem formulations, certain components of which are shared. Note that although descriptions of technologies are repeated in some instances, no actual results are repeated in any papers.

1.8 Author's Contributions to Papers

As the author of this thesis, I can confirm that I was the primary investigator, developer of any and all methods, and first author of all published works featured in the proceeding chapters.

1.9 Chapter 1 References

[1] US Energy Information Administration, AEO2012 Early Release Outlook, US DOE/EIA- 0383ER (2012). January 2012.

[2] National Energy Board. Canada's Energy Future: Energy Supply and Demand Projections to 2035 - Electricity Outlook Highlights. [online] Accessed June, 2012. [online]. Available HTTP: http://www.neb-one.gc.ca/clfnsi/rnrgynfmtn/nrgyrprt/nrgyftr/2011/fctsht1134lctrct-eng.html.

[3] BP Energy. BP Energy Outlook 2035. *Corporate White Paper*. Updated February 2015. Available online: http://www.bp.com/content/dam/bp/pdf/energy-economics/energy-outlook-2015/bp-energy-outlook-2035-booklet.pdf.

[4] Herzog HJ, Golomb D. Carbon capture and storage from fossil fuel use, in: C.J. Cleveland (Ed.), Encyclopedia of Energy. New York: Elsevier Science, 2004, pp. 277–287.

[5] Energy Information Administration (EIA), Fuel emission factors, Appendix H of instructions to form EIA-1605, U.S. Department of Energy, Washington, D.C. [online]. Available HTTP: http://www.eia.gov/oiaf/1605/pdf/Form%20EIA-1605%20instructions.pdf.

[6] U.S. Environmental Protection Agency (EPA), Inventory of U.S. Greenhouse Gas Emissions and Sinks: 1990-2010. EPA 430-R-12-001, pg. 3-5. [online] Available HTTP: http://www.epa.gov/climatechange/ghgemissions/usinventoryreport.html.

[7] Adams TA II, Barton P, High-efficiency power production from natural gas with carbon capture. *J. Power Sources*. 195 (2010) 1971-1983.

[8] Haslbeck J, Keuhn N, Lewis E, Pinkerton L, Simpson J, Turner M, Varghese E, Woods M. Cost and Performance Baseline for Fossil Energy Plants. Volume 1: Bituminous Coal and Natural Gas to Electricity Final Report, DOE/NETL-2010/1397, Revision 2, November 2010.

[9] Adams TA II, Khojestah Salkuyeh Y, Nease J. *Processes and Simulations for Solvent-based CO_2 Capture and Syngas Cleanup*. Chapter in: Reactor and process design for in sustainable energy technology. *In Press*.

[10] Hasan M, Baliban R, Elia J, Floudas C. Modeling, Simulation, and Optimization of Postcombustion CO2 Capture for Variable Feed Concentration and Flow Rate. 2. Pressure Swing Adsorption and Vacuum Swing Adsorption Processes. *Ind. Eng. Chem. Res*. 51 (2012) 15665-15682.

[11] Hasan M, Baliban R, Elia J, Floudas C. Modeling, Simulation, and Optimization of Postcombustion CO_2 Capture for Variable Feed Concentration and Flow Rate. 1. Chemical Absorption and Membrane Processes. *Ind. Eng. Chem. Res.* 51 (2012) 15642-15664.

[12] Minchener AJ, McMullan JT. Strategy for sustainable power generation from fossil fuels. *J. Energy. Inst*. 81 (2008) 38-44.

[13] The Globe and Mail. "The world's first carbon capture plant opens in Saskachewan." Corporate white paper (2014). Available HTTP: http:// www.theglobe-andmail.com/report-on-business/rob-magazine/the-worlds-first-carbon-capture-plant-opens-in-saskachewan/article21877367/.

[14] Williams MC, Strakey JP, Surdoval WA. U.S. Department of Energy's solid oxide fuel cells: Technical advances. *Int. J. Appl. Cerma. Technol*. 2 (2005) 295.

[15] Trabold TA, Lylak JS, Walluk MR, Lin JF, Trojani DR. Measurement and analysis of carbon formation during diesel reforming for solid oxide fuel cells. *Int. J. Hydrogen Energy.* 37 (2012) 5190.

[16] Ming NQ. Coal based solid oxide fuel cell technology development. *ECS Trans*. 7 (2007) 45.

[17] Nagel FP, Schildhauer TJ, Biollaz SMA. Biomass-integrated gasification fuel cell systems – Part 1: definition of systems and technical analysis. *Int. J. Hydrogen Energy*. 34 (2009) 6809.

[18] Liso V, Oleson A, Nielson M, Kaer S. Performance comparison between partial oxidation and methane steam reforming processes for solid oxide fuel cell (SOFC) micro combined heat andpower (CHP) system. *Energy*. 35 (2011) 4216-4226.

[19] Kuramochi T, Turkenburg W, Faaij A. Competitiveness of CO_2 capture from an industrial solid oxide fuel cell combined heat and power system in the early stage of market introduction. *Fuel*. 90 (2011) 958-973.

[20] Achenbach E. Response of a Solid Oxide Fuel Cell to Load Change. *J. Power Sources.* 57 (1995) 105–109.

[21] Stiller C, Thorund B, Bolland O. Safe Dynamic Operation of a Simple SOFC/GT Hybrid System. *J. Eng. for Gas Turbines and Power*. 128 (2006) 551-559.

[22] Adams TA II, Nease J, Tucker D, Barton P. Energy conversion with solid oxide fuel cell systems: short and long term outlooks. *Ind. Eng. Chem. Res.* 52 (2013) 3089-3111.

[23] Raju M, Khaitan SK. Modeling and simulation of compressed air storage in caverns: A case study of the Huntorf plant. *Applied Energy*. 89 (2012) 474-481.

[24] Fertig E, Apt J. Economics of compressed air energy storage to integrate wind power: A case study in ERCOT. *Energy Policy*. 39 (2009) 2330-2342.

[25] Hoffeins H. Huntorf air storage gas turbine power plant. *Energy Supply,* Brown Boveri Publication (1994) DGK 90 202 E.

[26] Hounslow DR, Grindley W, Louglin RM. The development of a combustion system for a 110 MW CAES plant. *J. Eng. Gas Turbine Power*. 120 (1988) 875-883.

[27] Cavallo A. Controllable and affordable utility-scale electricity from intermittent wind resources and compressed air energy storage (CAES). *Energy*. 32 (2007) 120-127.

[28] Greenblatt JB, Succar S, Denkenberger DC, Williams RH, Socolow RH. Base load wind energy: modeling the competition between gas turbines and compressed air energy storage for supplemental generation. *Energy Policy*. 35 (2007) 1472-1492.

[29] Mason J, Fthenakis V, Zweibel K, Hansen T, Nikolakakis T. Coupling pv and case power plants to transform intermittent pv electricity into a dispatchable electricity source. *Prog Photovolt: Res Appl*. 16(8) (2008) 649-668.

[30] Succar S, Williams RH. Compressed air energy storage: theory, resources and applications for wind power. Princeton Environmental Institute: Princeton University, 2008.

[31] Adams TA II, Barton PI. Systems and methods for the separation of carbon dioxide from water. US Patent App. 12/434486 (2009).

[32] Adams TA II, Barton PI. High-efficiency power production from coal with carbon capture. *AIChE J*. 56 (2010) 3120.

[33] Independent Electricity System Operator. Ontario Demand and Market Prices. Accessed March 19, 2012. Available HTTP: http://www.ieso.ca/imoweb/siteShared/demand_price.asp?sid =ic.

Chapter 2

Systems for peaking power with 100% CO_2 capture by integration of solid oxide fuel cells with compressed air energy storage

The content of the following chapter is a **published reprint** of the following peer-reviewed publication:

Nease J, Adams TA II. Systems for peaking power with 100% CO_2 capture by integration of solid oxide fuel cells with compressed air energy storage. *Journal of Power Sources*. 2013; 228(15): 281-293.

Journal of Power Sources 228 (2013) 281–293

Contents lists available at SciVerse ScienceDirect

Journal of Power Sources

journal homepage: www.elsevier.com/locate/jpowsour

Systems for peaking power with 100% CO_2 capture by integration of solid oxide fuel cells with compressed air energy storage

Jake Nease, Thomas A. Adams II *

Department of Chemical Engineering, McMaster University, 1280 Main Street West, Hamilton, Ontario, Canada L8S 4L7

HIGHLIGHTS

- ► We model a novel CO_2 emission-free peaking power plant fueled by natural gas.
- ► Performance of different plant configurations are compared using defined metrics.
- ► Peaking power via CAES is possible with marginal impact on cost and efficiency.
- ► Partial shutdown for maintenance can be made while meeting demand and saving fuel.
- ► Proposed Plant becomes economically optimal at high fuel and carbon prices.

GRAPHICAL ABSTRACT

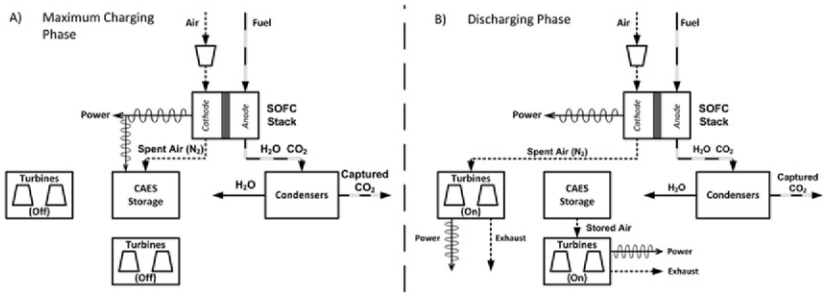

ARTICLE INFO

Article history:
Received 3 July 2012
Received in revised form
25 October 2012
Accepted 24 November 2012
Available online 1 December 2012

Keywords:
Solid oxide fuel cell
Compressed air storage
Carbon capture
Peaking power
Natural gas

ABSTRACT

In this study, the applicability and performance of an integrated solid oxide fuel cell (SOFC) and compressed air energy storage (CAES) plant with and without carbon capture and sequestration (CCS) in a load-following power production scenario is investigated. Ten different process configurations are simulated using a combination of Aspen Plus 2006.5 and MATLAB tools. It was found that the addition of CAES to an SOFC plant provided significant load-following capabilities with relatively small penalties to efficiencies (1.1%HHV) and levelized costs of electricity (LCOE) (0.08–0.3 ¢ kW^{-1} h^{-1}). The load-following capabilities of the CAES-enabled plants, as measured by proposed squared-error based metrics, were excellent and were not impacted by the addition of CCS. CCS-enabled configurations using SOFCs with and without CAES are able to reduce direct CO_2 emissions to essentially zero. The introduction of a seasonal, partial power train shutdown schedule, while useful for maintenance and cleaning purposes, also reduces fuel consumption by 9.5% with very small penalties to the overall load-following performance of the SOFC/CAES plant. Although SOFCs are perhaps decades away from being implemented on the scale discussed in this study, the forward-looking energy conversion strategy proposed in this work shows promise for providing future carbon-free peaking power.

1. Introduction

In most parts of the world, power production largely depends on the use of fossil fuels. Although efforts to utilize renewable energy sources such as solar, wind, and bio-fuels are ongoing, they currently only constitute a small portion of the energy portfolio due to cost and technical limitations. For the near term, it is desirable to maximize the efficiencies of current fossil-based power generation technologies, while remaining cognizant that carbon capture and control requirements may become a reality in the near future, likely driven by a carbon tax or emissions restriction. Consequently,

* Corresponding author. Tel.: +1 905 525 9140 x24782.
E-mail address: tadams@mcmaster.ca (T.A. Adams).

0378-7753/$ – see front matter © 2012 Elsevier B.V. All rights reserved.
http://dx.doi.org/10.1016/j.jpowsour.2012.11.087

industries that consume fossil fuels (such as electricity providers) may be required to capture the CO_2 generated by their operations and sequester it in underground spaces such as depleted oil fields, aquifers, and other geological storage sites [1]. As such, industries utilizing fossil fuels will be faced with the decision to either invest in the capture and sequestration of CO_2, or face the potential financial penalties associated with its emission.

With the above scenario in mind, this work investigates the combinatory effectiveness of an integrated solid oxide fuel cell (SOFC) and compressed air energy storage (CAES) plant for following demand-fluctuations (known as "peaking power") with and without CO_2 capture techniques enabled. Furthermore, the designs are also compared to a common natural gas-fed power process, the natural gas combined cycle (NGCC).

1.1. Natural gas combined-cycle plants

Natural gas-fed processes account for approximately 24% of all electricity generated in the United States and is anticipated to rise to 27% by 2035. [2]. In Canada, natural gas accounts for 9% of the electricity generated and is projected to increase to 15% by 2035 [3]. Natural-gas fired power plants produce inherently lower emissions per unit of electrical energy than coal (50.29 g MJ^{-1} versus 90.29 g MJ^{-1}) [4], and therefore are responsible for a proportionally smaller amount of the CO_2 emissions in the power sector. For example, in the United States, natural gas contributes to only 17.5% of the carbon emissions for the electricity sector [2,5] while producing 24% of the power. However, the emissions from a standalone NGCC plant are still significant, and other approaches may be required to reduce the emissions of natural gas power plants to a sustainable level [7].

The NGCC process is briefly described as follows [6,8]: First, the natural gas fed to the plant is cleaned and desulphurized if it was not done so prior to distribution. The gas is then combusted in air at a high temperature and pressure in a gas turbine unit, which produces electricity through a generator attached to the turbine. The waste heat from the exhaust stream may then be recovered through the generation of high pressure steam, which can be used to power turbines in a steam cycle for additional power generation (hence the name "combined cycle"). The exhaust, which now contains mostly CO_2, water and nitrogen from the combustion step, may then be subjected to a solvent-based absorption process which serves to separate the CO_2 from the flue gas with approximately 90% recovery should carbon capture be desired. The CO_2 stream is then cooled and compressed to supercritical conditions suitable for transport in a CO_2 pipeline, and the decarbonized exhaust stream is vented to the atmosphere through a flue stack. However, a significant amount of energy is required for CO_2 capture in the NGCC process (up to 14% of the net power produced) which can cause up to a 40% increase in the levelized cost of electricity (LCOE) [8].

1.2. Solid oxide fuel cells

A solid oxide fuel cell (SOFC) utilizes a fuel gas and an oxidant (typically air) to efficiently produce electrical power through electrochemical reactions on opposite sides of a solid oxide barrier, as depicted in Fig. 1. The reactions that occur in the anode and cathode include:

$$H_2 + O^{=} \rightarrow H_2O + 2e^{-} \quad \text{(Anode)} \tag{1}$$

$$CO + O^{=} \rightarrow CO_2 + 2e^{-} \quad \text{(Anode)} \tag{2}$$

$$O_2 + 4e^{-} \rightarrow 2O^{=} \quad \text{(Cathode)} \tag{3}$$

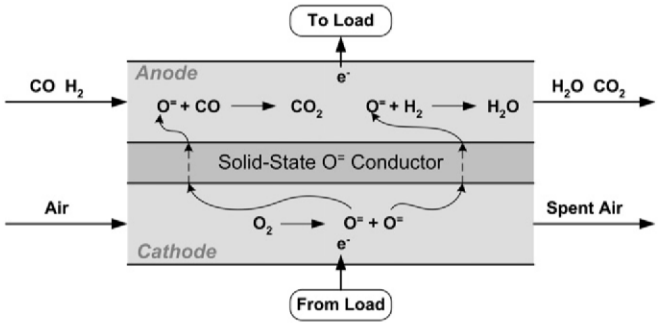

Fig. 1. Simple schematic of an SOFC using syngas as a fuel source as investigated in this study.

In addition to hydrogen gas and carbon monoxide (the two of which comprise synthesis gas or "syngas"), other suitable fuel sources for the SOFC anode include natural gas [9] and methanol [10] which can be used directly in the anode. Moreover, fuels such as coal [11], diesel [10], ethane and even biomass [12] can be pre-processed into syngas and used as a fuel source. Provided that the fuel utilization is high and the SOFC is equipped with appropriate seals that maintain separation between the anode and cathode exhausts, the anode exhaust will consist mainly of H_2O and CO_2. The anode exhaust can hence be separated relatively easily, and the resulting captured CO_2 can be compressed for pipeline transport. The cathode exhaust is partially deoxygenized air at high temperatures (~900 °C), which can be used for additional power generation through heat recovery and vented without posing an environmental risk. If the SOFC is operated at high pressures (10–20 bar), electricity can also be generated by feeding the hot, pressurized cathode exhaust to a gas turbine, thus forming a Brayton cycle. Our prior work has shown that pressurized SOFC systems of this type are capable of generating power at high efficiencies (up to 74% by higher heating value) with essentially no CO_2 emissions [6]. Comparable studies by other groups have found similar results [28,30]. Furthermore, the process of electrochemical energy conversion to electricity is more efficient than combustion, which allows the SOFC plant to achieve higher thermal efficiencies than systems that utilize the Carnot cycle.

However, one significant disadvantage of SOFC systems is that there are currently potentially cost-prohibitive operability challenges associated with their dynamic operation. For example, it is possible to change the power output of an SOFC relatively quickly (for example, in response to load changes) [13], but this runs the risk of very high degradation rates or even destruction due to rapid thermal expansion or the backflow of gases [14]. To avoid these risks, it is probable that future large-scale SOFCs will operate at a fixed power output which will not be adjusted to follow the typical diurnal power demand profile of a typical power grid. Of course, a system with a fixed power output can be scaled large enough to always meet demand, but this approach would be wasteful since it would almost always produce more electricity than necessary.

1.3. Compressed air energy storage

Compressed Air Energy Storage (CAES) plants operate as an intermittent source or sink for electrical power. The plant consumes power in order to compress air to high pressures and store it in an either man-made or naturally occurring void (which may be above- or below-ground) as elastic potential energy. During periods of high power demand or electricity prices, the stored compressed air

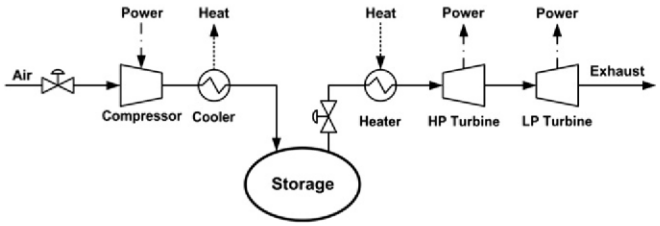

Fig. 2. Simplified CAES system schematic [23].

is pre-heated (usually by combusting natural gas) and fed to gas turbines attached to an electric generator, thereby re-supplying the stored energy back to the power grid. A simplified schematic of a typical CAES system is shown in Fig. 2.

CAES technology has been utilized for over three decades. The Alabama Electric Corporation has been operating a 110 MW plant since 1991, and E.N. Kraftwerke has been running a 290 MW plant in Huntorf, Germany since 1978 [15]. There have been several other studies and plans to construct further CAES plants in North America, but at the time of this publication no others have been constructed to the best of our knowledge [16].

CAES is advantageous for a variety of purposes; not only can it serve as a stand-alone plant capable of achieving profitability through compressing at times of low electricity prices and releasing at times of high prices, but it can also be combined with other processes to add flexibility or reliability. For example, there has been significant theoretical research in recent years examining the utilization of CAES as a method for leveling intermittent sources (such as wind power) to provide a consistent base load [15,17–22]. However, there has not been much research concerning the integration of CAES with other power sources for the purposes of load following (or "peaking").

1.4. SOFC/CAES integration concept

In order to provide reliable, peaking power with 100% CO_2 capture, we propose the integration of SOFCs (to provide base-load power), a CCS system (to achieve near-zero CO_2 emissions), and a CAES system (to following peaking demand). The SOFC and CCS systems used are modeled after the prior work of Adams and Barton (2010) [6] but modified to incorporate CAES. During the night or periods in which demand is low, the CAES system can be used to charge the available storage space in which a portion of the electrical power generated by the SOFC system is used to compress some or all of the cathode exhaust to the current pressure of the underground storage cavern. The portion of the cathode exhaust which is not sent to CAES is sent to a turbine attached to a generator to produce additional electricity, as shown in Fig. 3(A). During times when the electricity demanded is high, all of the cathode exhaust is sent to the gas turbine, maximizing the electricity produced by the SOFC/GT system. In addition, air is released from the storage space and fed to a second gas turbine system, producing additional power, as expressed in Fig. 3(B). A more detailed PFD of the proposed integrated process is provided in Fig. 4, and a detailed description of the process and its model is given in Section 2.

With this approach, the proposed SOFC/CAES/CCS system is able to provide load-following power from fossil fuels while maintaining high efficiency capturing nearly 100% of the CO_2. Because the system does not use SOFCs in load-following mode, there is a significantly lower risk of damage or shortened lifetime compared to using SOFCs in a load-following mode, as mentioned in Section 1.2. Furthermore, the system allows for the generation of large amounts of power during brief periods significantly above the normal power output of the SOFCs thanks to the use of CAES. This means that SOFCs need only be large enough for the "average" power produced, instead of the largest expected peak value which occurs for only a short time.

In this work, a techno-economic analysis of several configurations of the integrated SOFC/CAES process is presented. Simulations are used to compute mass and energy flows using Aspen Plus v7.3 for steady-state computations and in-house models implemented in MATLAB for dynamic simulations. For the economic analysis, the historical power demand profile for the province of Ontario, Canada in 2011 [25] was considered. Details are presented in the next section.

2. Simulation models

Many process systems have been proposed which use SOFCs or SOFCs with gas turbines using natural gas as a fuel source [24–30] (a comprehensive review can be found in Adams et al. (2012) [23]). The SOFC system selected for this work is based on the system presented in Adams and Barton (2010) [6] using the same modeling and design assumptions for consistency. This was integrated with CAES to form the proposed integrated SOFC/CAES process presented in Fig. 4. The SOFC system may be divided into the following sections, each discussed in turn: reforming, gas shifting, power generation, heat recovery and steam generation (HRSG), and CO_2 recovery. The CAES system may be divided into two sections, namely compression and storage, and expansion.

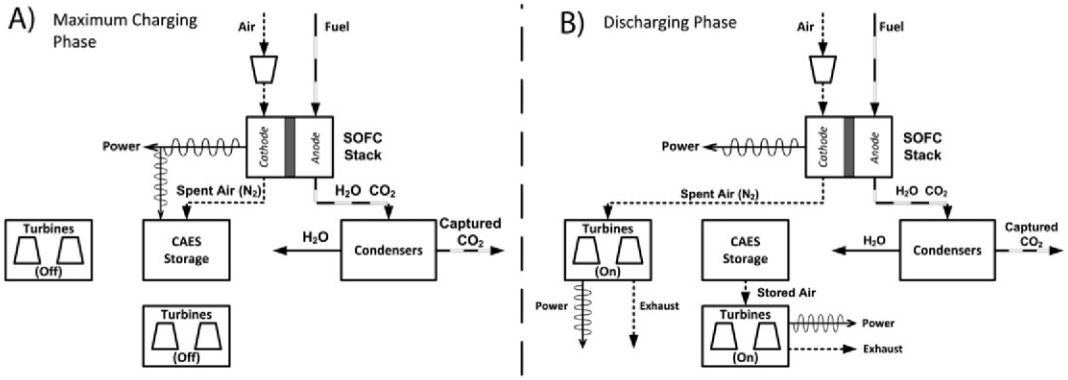

Fig. 3. Simplified SOFC/CAES integration technique during (A) the maximum charging phase, and (B) the discharging phase.

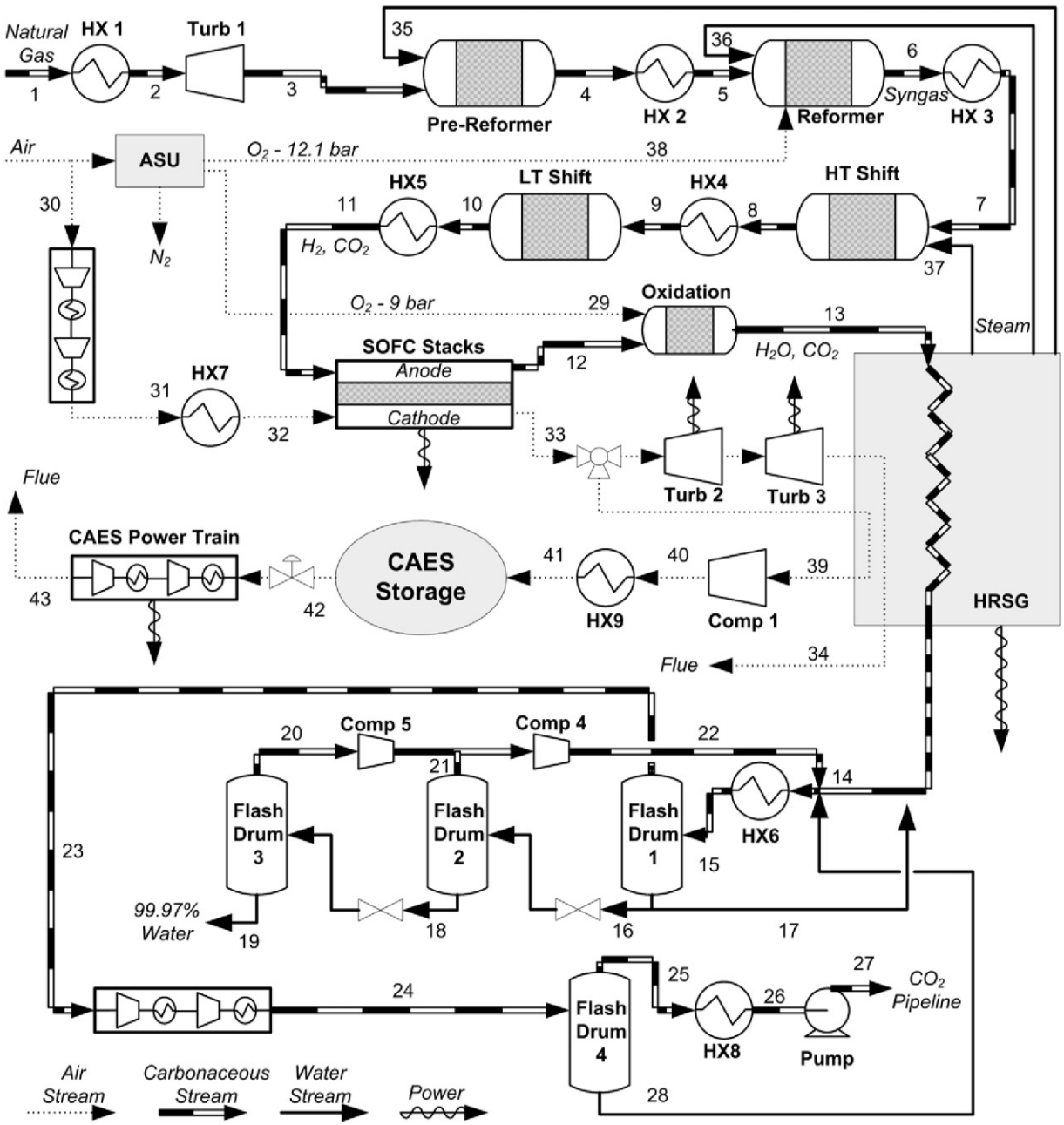

Fig. 4. PFD of proposed SOFC/CAES plant.

2.1. Basis of steady-state simulation and modeling approach

The SOFC plant examined in this study was modeled after that of the previous work, with a targeted base-load power output of 714.4 MW (including the net power produced by the SOFCs, the cathode Brayton cycle turbines 2 and 3, and the combined cycle in the HRSG). It should be noted that in the prior work, several process configurations were explored, and the configuration chosen for this paper is consistent with the configuration called the "autothermal reforming case" discussed therein [6]. The natural gas fed to the plant is assumed to be supplied at 30 bar and 38 °C and contains 93.9 mol% methane, 3.2% ethane, 0.7% propane, 0.4% *n*-butane, 1% CO_2 and the remainder N_2 [6]. Simulations of the SOFC/CAES plant were performed using Aspen Plus 2006.5 with the Peng–Robinson equation of state (EOS) including the Boston-Mathias modification throughout, except that the Redlich–Kwong–Soave EOS with predictive Holderbraum mixing rules was used for streams containing mostly CO_2 and H_2O below the critical point of CO_2, and the electrolyte-NRTL model with Henry coefficients and electrolyte specifications from the AP065 databank for H_2O/CO_2 streams near the critical pressure of CO_2. For sample stream conditions for a slightly different configuration of the SOFC plant, the reader is referred to the previous study [6].

2.2. Solid oxide fuel cell process and model

2.2.1. Natural gas reforming and syngas shifting

The reforming of natural gas involves its reaction with steam at temperatures above 700 °C to produce syngas through the following chemical reactions:

$$C_nH_m + nH_2O \leftrightarrow nCO + (0.5m + n)H_2 \quad (4)$$

In order to obtain high conversions (up to 99%) of this reaction at high pressures, very high temperatures are required (as high as 1000 °C at 15 bar pressure) [31]. The water-gas-shift (WGS) and CO_2 reforming reactions may also take place at these temperatures and pressures, leading to different overall yields of the desired H_2 and CO products [32]:

$$CO + H_2O \leftrightarrow CO_2 + H_2 \quad (5)$$

$$CH_4 + CO_2 \leftrightarrow 2CO + 2H_2 \quad (6)$$

It is possible to design the SOFC system such that natural gas reforming can take place inside the anode of the SOFC due to its high operating temperature and pressure (called "internal" natural gas reforming). Although this can be advantageous for reasons of thermal management (the endothermic reforming reaction can be used to regulate the exothermic electrochemical reaction in the fuel cell), there could be problems with carbon deposition and fouling inside the anode leading to serious challenges associated with the long-term operability of an internally-reforming fuel cell stack [33–35]. Although the most recently introduced commercial SOFCs use "internal" natural gas reforming (at the 1–200 kW stack scale) [23], it is unclear what configuration will be used at the megawatt scale since they are not yet commercially available. For example, "external" reforming may be preferred, in which natural gas is reformed (and possibly shifted) prior to entering the SOFC anode. In this work we consider the case where "external" reforming and gas-shifting are used (as shown in Fig. 4) in order to be consistent with the prior work. Although the external and internal reforming configurations will have some differences in cost and performance, the balance of the SOFC/CAES process is essentially the same regardless of the reforming and shifting strategy chosen.

In the process proposed in this work, natural gas is pre-heated to 615 °C and expanded to 12.5 bar through a turbine. The expanded gas is then sent to a pre-reformer, where the conversion of C_nH_m for $n > 1$ is assumed to be 99.9%. Reforming of C_nH_m where $n = 1$ as well as all side reactions are assumed to reach equilibrium. The pre-reformer effluent is then sent to an autothermal reformer (ATR) where restricted oxygen supplied from an air separation unit (ASU) at 92 mol% purity is used to oxidize a small portion of the remaining methane, generating the necessary heat to simultaneously reform the remaining methane with steam. The detailed design of the pre-reformer and ATR operating conditions are discussed in the previous work [6].

The syngas produced by the reforming section is reacted via the WGS reaction given in equation (5). The ATR effluent is sent to two plug-flow reactors in series. The first reactor operates at a high temperature (300–350 °C) and is assumed to achieve an 80% conversion of CO; the second reactor operates at a lower temperature (200–250 °C) and approaches equilibrium, therefore achieving an overall conversion of approximately 96% [8]. Details are available in the prior work [6].

2.2.2. Power generation and heat recovery

The SOFC generates electrical power through reactions (1) through (3). The SOFC stacks operate at a pressure of 10.1 bar and a temperature of approximately 950 °C. Although higher efficiencies are possible when higher temperatures are used, material limitations usually prevent the SOFC from surpassing 1000 °C [36]. The shifted syngas leaving the WGS unit is pre-heated to 910 °C, and fed to the anode of the fuel cell stack. Ambient air is compressed and heated to the same conditions and fed to the cathode. The anode and cathode exhaust streams are kept separate to prevent the mixing of N_2 and CO_2, allowing for cost-effective CO_2 capture and sequestration (see Section 2.2.3). The anode exhaust is fed to an oxidization unit where the unreacted H_2 and CO are completely oxidized with oxygen at 92 mol% purity (from the ASU) to H_2O and CO_2. The actual SOFC stacks were modeled using the same methods as in the prior work, where the achieved potential from a given cell is temperature and pressure dependant as described in Ref. [36].

The proposed design includes six parallel SOFC power generation trains of equal size, for several reasons. First, having multiple SOFC trains will allow for continued operation of the plant at 5/6 capacity should a malfunction in one train occur. Second, routine shutdowns of a particular stack may be scheduled for maintenance purposes (de-coking, re-sealing, replacement of electrical equipment, etc.). Finally, when incorporating the CAES design, it is possible to save fuel while still meeting demand by allowing for seasonal shutdowns of certain trains.

In the proposed SOFC/CAES system, the cathode exhaust may travel through one of two possible routes. During periods of low demand, all or a portion of the cathode exhaust stream is routed to a compressor that compresses it to the appropriate pressure in order to charge the CAES storage space. However, during periods of high demand the cathode exhaust is expanded to atmospheric pressure through a series of turbines to generate additional power. In both cases, the thermal energy contained after compression or expansion is recovered in the HRSG to improve thermal efficiency.

The design considerations of the HRSG and its associated heat exchanger network (HEN) are similar to the previous work [6] and are not discussed in this work. The two main assumptions made in modeling the HRSG are: (1) the HEN avoids temperature crossover but assumes an ideal ΔT_{min} of 0 °C for the sake of simplicity, and (2) all waste heat between 50 and 950 °C may be used as a heat source for the steam cycle, which contains 5 steam pressure levels.

2.2.3. CO_2 recovery

After heat recovery, the anode exhaust (containing mostly CO_2 and H_2O) is separated by a series of cascading flash drums as described by Adams and Barton (2010b) [37]. Some of the high purity water is fed to the HRSG to generate steam for other parts of the process, and the excess water from the final flash drum may be treated and used for other purposes. The CO_2 rich vapor is compressed to 74 bar (near the critical point) and flashed once more to remove most of the remaining water and achieve the CO_2 purity required for pipeline transit. The CO_2 stream is condensed to a liquid and pumped to 153 bar before it leaves the plant, destined for CO_2 sequestration.

2.3. Compressed air energy storage process and model

The CAES section was partially modeled in Aspen Plus. Design and operating parameters of the CAES process are given in Table 1. After leaving the SOFC, the cathode exhaust is split depending on the amount desired to be stored at that time (details on dynamic simulations will be provided in the following sections). The exhaust diverted to the CAES compression section is cooled to a temperature suitable for the compressor inlet (assumed to be 50 °C) via the HRSG. The stream is then compressed to a pressure between 42 and 72 bar (to reach a pressure 2 bar above the current air pressure within the cavern), and finally is cooled to 50 °C before being injected into the storage cavern. It is assumed that all of the heat recovered from cooling the compressed exhaust can be effectively recovered and used in the HRSG for the production of various grades of steam and heated water. The equipment selection for the CAES compression section was based on the heuristics provided by Luyben (2011) [38] as well as the Huntorf plant model developed by Raju and Khaitan (2012) [15]. It is also assumed that, once the storage air has entered underground storage cavern at

Table 1
Operating characteristics the CAES section of the proposed SOFC/CAES integrated system.

Operating condition	Value	Units
Air turbines (CAES power train in Fig. 4)		
Rated turbine power	200	MW
Maximum air flow rate	440	kg s^{-1}
Inlet pressure to HP turbine	40	bar
Inlet temperature to HP turbine	550	°C
Inlet pressure to LP turbine	6	bar
Inlet temperature to LP turbine	825	°C
Turbine efficiency	75	%
Compressor (Comp 1 in Fig. 4)		
Maximum air flow rate	210	kg s^{-1}
Rated compressor power	140	MW
Temperature at exit of after-cooler	50	°C
Pressure at exit of after-cooler	42–73	bar
Compressor isentropic efficiency	75	%
Cavern		
Volume of storage space	600,000	m^3
Cavern operating pressures	40–72	bar
Maximum cavern pressure	72	bar
Cavern wall temperature	50	°C

a temperature of 50 °C, there is negligible heat transfer between the stored air and the cavern walls [39] and the cavern is therefore considered to be isothermal. The CAES storage cavern is assumed to be a solution-mined salt dome with a volume of 600,000 m^3, which is comparable in size to the Huntorf plant [15]. The temperature changes due to friction by the transport to and from the storage cavern via the injection/withdrawal wells were calculated using the VALVE model in Aspen Plus and found to be on the order of 1 °C. Therefore, this temperature change was neglected for simplicity.

When the CAES cavern is to be discharged, all of the cathode exhaust is sent to turbine 2 and none is sent to the cavern (see Fig. 4). As such the power produced by turbines 2 and 3 are at their maximum level. The stored cathode exhaust in the CAES cavern is released at a rate depending on the desired total net power output of the integrated SOFC/CAES plant. The stored cathode exhaust is throttled to 40 bar with a valve, pre-heated to 550 °C and expanded through high- and low-pressure turbines, generating as much as 200 MW of power beyond the base-load of 714 MW (28%). It should be noted that the temperature losses across the valve were calculated using Aspen Plus and found to be at most 5 °C, which has very little impact on the overall performance of the CAES plant, and therefore was neglected for simplicity.

2.4. Dynamic simulation modeling approach

In order to simulate the SOFC/CAES plant dynamically while attempting to follow a transient load profile, the transient portions of the SOFC/CAES plant were modeled using a pseudo-steady-state approach. The transient portions included all units downstream of stream 33 (cathode exhaust Brayton cycle turbines, cathode exhaust compressors, the storage cavern, stored gas expansion, and related heat integration). In contrast, all units upstream of stream 33 (all natural gas processing, SOFCs, the CCS section, and related heat integration) are always steady-state and do not need to be considered in the pseuo-steady-state model.

Pseudo-steady-state Aspen Plus simulations of the transient portions of the plant were separated into two distinct modes of operation: charging and discharging of the CAES cavern. For each mode, a sensitivity analysis was run for a variety of cavern pressures and air flow rates to (in the charging mode) and from (in the discharging mode) the CAES cavern. These resulting data were regressed to multi-dimensional nonlinear equations in which the net power output of the plant (P_P, in MW) was the dependent variable. This yielded the following nonlinear pseudo-steady-state model to predict the power output of the combined SOFC/CAES plant:

$$P_P = I_M + a_{10}\frac{(F-\mu_F)}{\sigma_F} + a_{01}\frac{(P_C-\mu_{P_C})}{\sigma_{P_C}} + a_{20}\left(\frac{(F-\mu_F)}{\sigma_F}\right)^2 + a_{11}\frac{(F-\mu_F)}{\sigma_F}\frac{(P-\mu_{P_C})}{\sigma_{P_C}} + a_{02}\left(\frac{(P-\mu_{P_C})}{\sigma_{P_C}}\right)^2, \quad (7)$$

where I_M is the model intercept, F is the molar flow rate of air into the CAES storage cavern, P_C is the required pressure at the compressor outlet, a_{ij} is the model coefficient for the ith and jth power of F of P_C, respectively, and μ_k and σ_k are the arithmetic means and standard deviations where $k \in \{F, P_C\}$, respectively. Equation (8) may then be inverted in order to calculate the required flow rate to or from the cavern depending on the desired output of the plant at that time.

These resulting pseudo-steady-state models for the discharging and charging phases were programmed into MATLAB to allow for the dynamic calculation of the net output of the SOFC/CAES plant depending on the power demanded at any given time. Furthermore, the model anticipates the molar content and pressure of the CAES cavern at the end of each time step to ensure that they remain between the allowable operating ranges for the proposed system. The MATLAB calculation sequence is shown graphically in Fig. 5. For the purposes of the dynamic simulations in this study, 1-h control intervals were chosen for several reasons. Firstly, due to previous daily and seasonal power demand data, very accurate predictions of future power demand (up to 24 h in advance) are available [25]. Furthermore, the dynamics of CAES systems are limited only by the dynamics of the compressor and expansion turbines. A plant with one or more 135 MW generators can startup in 7–10 min, and ramp

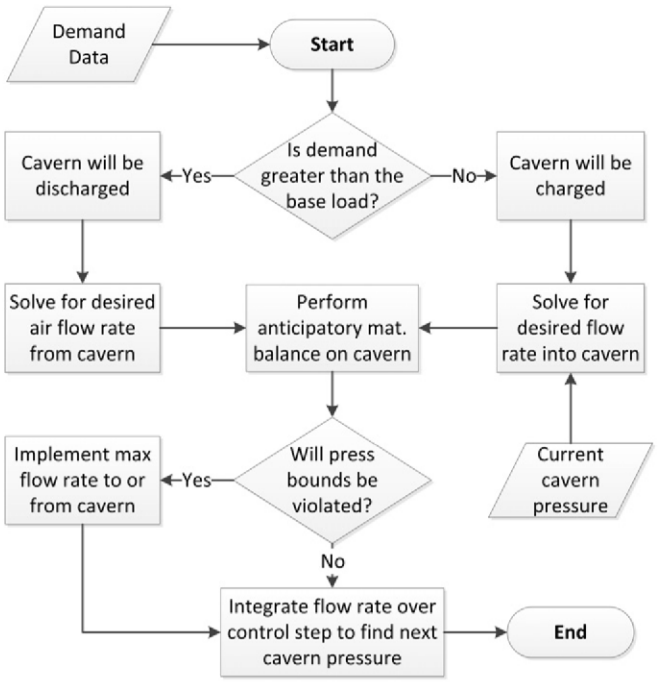

Fig. 5. MATLAB calculation sequence for a single simulation time step.

at approximately 4.5 MW per second (therefore requiring 30 s to obtain the maximum output) [40]. The CAES compressor starts in approximately 10–12 min and ramps at 20% per minute thereafter [16]. The dynamics of a CAES plant are therefore suitable for dynamic load-following, allowing for full operational changes in 15 min or less. With the above in mind, the dynamics associated with compressor and turbine adjustments as well as the actual control structure of the proposed plant is out of scope and was not considered in this study. Instead, it is assumed that the SOFC/CAES combined plant is capable of meeting the target power demand instantly at the beginning of each time step (1 h intervals), and therefore a pseudo-steady-state model is appropriate.

2.5. Combined plant scenario and operational objectives

The operational objective of the proposed SOFC/CAES plant in this study is to follow the power demanded as closely as possible over a year-long operational period. The effects of wear and tear during the lifetime of the plant are not considered. The scenario for this investigation is as follows: It is assumed that a plant must be constructed to meet the demand of a large (500–900 MW) community that exhibits a similar peaking profile (relative amplitude, frequency of peaks) to that of the actual grid demand for Ontario, Canada in 2011, scaled to an average of 714 MW [25]. Whenever the plant does not produce enough power to meet demand, it is assumed that the deficit is purchased from the grid at the current electricity price for that control interval (also from historical data for Ontario [25]). In addition to paying full price for the electricity purchased, it is assumed that the majority of the electricity obtained from the grid was produced by a natural gas-based peaking plant that emits 50.29 g of CO_2 equivalents per MJ of power produced [41]. Emissions from these grid-supplying plants are accounted for as indirect CO_2 emissions for each plant considered. It is further assumed that any excess power that is produced may be transmitted to the grid, but at no financial gain to the plant.

The metrics used to measure the performance of each plant configuration were the levelized cost of electricity (LCOE), the sum of squared-errors (SSE), and the weighted sum of squared-errors (WSSE) [43]:

$$\mathrm{LCOE} = \sum_{t=0}^{N}\left(\frac{\frac{I_t + M_t + \mathcal{F}_t}{(1+r)^t}}{\sum_{t=0}^{N}\frac{P_t}{(1+r)^t}}\right) \tag{8}$$

$$\mathrm{SSE} = \sum_{i=1}^{n}(P_{\mathrm{P},i} - D_i) \tag{9}$$

$$\mathrm{WSSE} = \sum_{i=1}^{n}\left[U_i^2 + \left(\frac{O_i}{2}\right)^2\right], \tag{10}$$

where in the LCOE calculation I_t, M_t, $\mathcal{F}_t$ and P_t are the capital expenditures, maintenance costs, fuel costs and total sellable power produced in year t, respectively. The plant lifetime is N years (20 years) and is discounted at a real interest rate of r (10%). The variable D_i represents the demand at interval i over n time steps (1 h per time step for one year). O_i is the amount of power over-produced by the plant and U_i is the amount under-produced by the plant at time step i.

The LCOE metric gives insight into the economic tractability, whereas the SSE and WSSE are meant to exhibit the load-tracking capabilities of each proposed plant configuration. The WSSE differs from the SSE in that WSSE does not fully penalize over-production; although this is wasteful from an operational standpoint, demand is fully met in this case and therefore is not penalized as much as underproduction.

2.6. Case studies

Ten different plant configurations have been simulated in order to compare their performance in the load-following scenario described in Section 2.5. Two cases are standard NGCC plants (with and without carbon capture and sequestration (CCS)), and eight cases are base-load SOFC power plants (also with and without CCS), both at fixed output of 714 MW. It is recognized that NGCC and other natural-gas fired power plants can sometimes have peaking capabilities, but according to the US Energy Information Administration: 'facilities that previously served peaking or more often intermediate load needs now contribute more significantly to base load electricity needs' [42]. The CCS method for the NGCC is solvent-based, and captures 90% of the CO_2 from the flue gas [6]. The remaining eight cases involve different configurations of the integrated SOFC/CAES plant with and without CCS and with and without the ability to shutdown one of the six SOFC trains on a seasonal basis. A summary of the features of each case is given in Table 2. The assumptions made with regards to the simulation and financial calculation parameters are provided in Table 3.

Train shutdown involves shutting down an SOFC train and reducing the process inlets proportionately to decrease the throughput of the plant for a period as long as several months. For this investigation, it is assumed that there are six SOFC process trains of equal size, and that the SOFC power generation section can operate at 5/6 capacity while one is shutdown. The assumptions about upstream operations reaching chemical equilibrium result in identical stream conditions (temperatures, pressures) upstream of the SOFC stacks. Thus no modeling changes to the units upstream of the SOFCs are required. A train shutdown not only allows for maintenance to be performed on the SOFC stacks, but also may be timed with seasonal decreases in demand to prevent unnecessary overproduction. Seasonal trends tend to show lower demand during the spring and fall and higher during the winter and summer [25]. The demand profile used in this study (shown as the average daily demand for improved readability) and the proposed train shutdown schedule are shown in Fig. 6. For this analysis, the proposed schedule was selected by manual inspection.

Capital cost estimates for the NGCC and SOFC plants were obtained using a combination of Aspen Icarus cost estimation software, published cost estimates, cost estimation methods provided by Seider et al. [44] and appropriate assumptions in order to be

Table 2
Description of simulated cases.

Case number	Tag	Base-load source	CCS enabled?	CAES enabled?	Train shutdown enabled?
1	NGCC	NGCC	No	N/A	N/A
2	NGCC–CCS	NGCC	Yes	N/A	N/A
3	SOFC	SOFC	No	No	No
4	SOFC–CCS	SOFC	Yes	No	No
5	SOFC–CAES	SOFC	No	Yes	No
6	SOFC–CAES–CCS	SOFC	Yes	Yes	No
7	SOFC–TSD	SOFC	No	No	Yes
8	SOFC–TSD–CCS	SOFC	Yes	No	Yes
9	SOFC–CAES–TSD	SOFC	No	Yes	Yes
10	SOFC–CAES–CCS–TSD	SOFC	Yes	Yes	Yes

Table 3
Assumed parameters for case studies.

Parameter	Value	Units[a]
Initial natural gas cost [47]	2.33	$ GJ^{-1}
HHV of natural gas [2]	52,970	kJ kg^{-1}
NG feed at full plant capacity (all 6 SOFC trains in service)	74,926	kg h^{-1}
NG feed at reduced plant capacity (only 5 SOFC trains in service)	62,436.4	kg h^{-1}
CO_2 tax[b]	50.00	$ tonne^{-1}
Plant lifetime	20	Years
Discount rate	10.0	%
Inflation rate	2.5	%

[a] Cost units are expressed in US$2007 using the Chemical Engineering Cost Index [49].
[b] This CO_2 tax is the "standard" for comparison, but is investigated in greater detail in Section 3.4.

consistent with the prior work [6]. The reader is referred to the prior work for details regarding the sizing, material selection and other assumptions with regards to the process costing step. The installed cost of an SOFC stack was assumed to follow a linear scaling profile of \$1000 kW^{-1}, and therefore the economy of scale penalties associated with using multiple, smaller power trains in parallel is already accounted for by this worst-case scaling assumption. The target for Fuel Cell Energy's SOFC stack costs in the year 2012 is \$496 kW^{-1} (US\$2007) and includes all of the appurtenances required for its operation [45], with other targets being even lower [46]. As such the estimate of \$1000 kW^{-1} is expected to be conservative for a mature plant [9]. CAES plant costs included the estimation of the injection/withdrawal wells, turbomachinery and storage cavern. The cost estimate for the storage cavern and its injection wells was obtained from Schainker (2009) [47] and assumes a linear cost \$1.5 MW^{-1} h^{-1} of storage. Turbomachinery costs were combined estimates of those from Mason (2012) [21], Seider [44], and Schainker (2009) [47]. Natural gas costs were assumed to begin at \$2.33 GJ^{-1} (\$2.46 MMBtu^{-1}) and then inflate at 2.5% per year over the lifetime of the plant [48].

3. Results and discussion

3.1. Overall system results and performance

A summary of the operational results for each case investigated is presented below in Table 4. The SOFC base-load plant has the highest efficiency of the configurations examined, and is consistent with the prior work [6]. Furthermore, the addition of the CAES component to the original base-load plant in both the CCS enabled and CCS disabled cases reduces the overall efficiency of each plant by approximately 0.6 percentage points due to losses from compression and throttling. The addition of CAES to any of the scenarios when train shutdown is enabled also decreases the overall efficiency of the plant by less than 1 percentage point in each case, although the addition of train shutdowns itself imposes a close to 1.1 percentage point decrease in efficiency largely due to lower attainable efficiencies in the HRSG. These results therefore indicate that, since the partially compressed cathode exhaust may be used as the energy storage medium, significant load-following capabilities may be introduced to an SOFC base-load plant in the form of CAES with a small reduction in plant efficiency.

The introduction of CCS has a large impact on the direct CO_2 emissions for each case, with complete capture for the SOFC base-load plant with CCS enabled. Furthermore, the introduction of train shutdowns decreases the direct natural gas consumed over the year and as such decreases the amount of direct CO_2 sequestered (in the CCS cases) or emitted (in the non-CCS cases). However, the introduction of train shutdowns also increases the amount of external grid power that must be purchased in order to meet demand, thereby increasing the indirect CO_2 emissions for the train shutdown cases. This leads to the interesting result that even though there is less direct fuel consumption by cases in which CAES and SOFC train shutdown are enabled, the indirect CO_2 emissions for these plants is higher than the SOFC cases where train shutdowns are not performed. For example, case 9, the integrated SOFC/CAES with train shutdowns (TSD) case, consumes approximately 9.5% less natural gas (directly) than the case in which a baseline SOFC plant is used without CAES or train shutdowns (case 3), but also produces 36% more indirect CO_2 emissions to meet the same peaking demand profile. However, the total CO_2 emissions (direct plus indirect) of case 9 are about 8.3% lower than case 3. This means that even though using CAES and train switching requires more external grid power, the total lifecycle CO_2 emissions are reduced by about 8.3%. In addition, case 9 has an advantage that by building periodic train shutdowns into the life of the plant, it is possible to schedule regular and necessary maintenance on an SOFC train every three years without disturbing production. This maintenance is essential to clean and replace degraded cells to maintain the performance of the overall plant without unwanted shutdowns.

Finally, the NGCC plant (cases 1 and 2) is inferior to that of the SOFC base-load plants with regards to both overall efficiency as

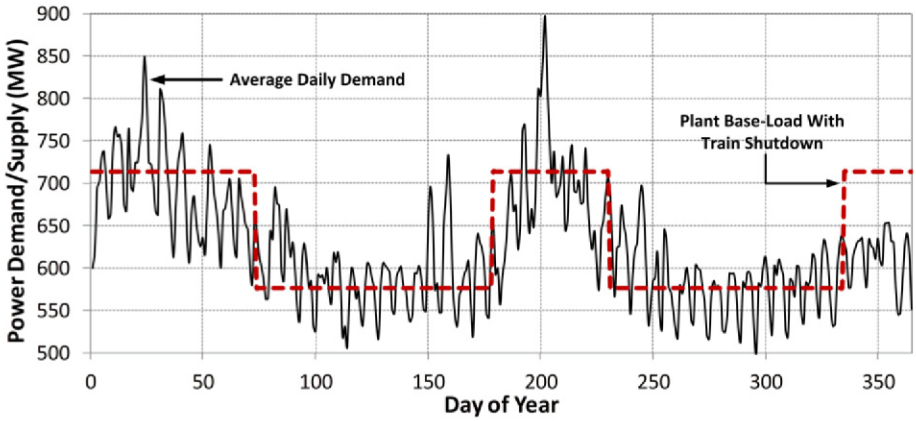

Fig. 6. Average daily demand and base-load plant train shutdown schedule for one simulated year of operation.

Table 4
Simulation and economic results for power generation case studies.

Case	1 NGCC	2 NGCC–CCS	3 SOFC	4 SOFC–CCS	5 SOFC–CAES
Direct fuel usage (tonne yr^{-1})	836,285	972,464	656,332	656,332	656,332
Direct CO_2 emitted (tonne yr^{-1})	2,194,420	219,440	1,722,220	0	1,722,220
Indirect CO_2 emitted (tonne yr^{-1})	47,059	47,059	47,059	47,059	18,991
Total CO_2 emitted (tonne yr^{-1})	2,241,480	266,501	1,769,280	47,059	1,741,210
CO_2 sequestered (tonne yr^{-1})	0	1,974,980	0	1,722,220	0
Electricity generated (MW-h yr^{-1})	6,254,640	6,254,640	6,338,740	6,254,640	6,278,900
Electricity sold (MW-h yr^{-1})	5,345,500	5,345,500	5,360,200	5,345,500	5,427,900
Electrical efficiency[a] (%HHV)	**50.8**	**43.7**	**65.6**	**64.8**	**65.0**

	6 SOFC–CAES–CCS	7 SOFC–TSD	8 SOFC–TSD–CCS	9 SOFC–CAES–TSD	10 SOFC–CAES–TSD–CCS
Direct fuel usage (tonne yr^{-1})	656,332	593,895	593,895	593,895	593,895
Direct CO_2 emitted (tonne yr^{-1})	0	1,558,390	0	1,558,390	0
Indirect CO_2 emitted (tonne yr^{-1})	18,991	117,812	117,812	63,845	63,845
Total CO_2 emitted (tonne yr^{-1})	18,991	1,676,200	117,812	1,622,230	63,845
CO_2 sequestered (tonne yr^{-1})	1,722,220	163,833	1,722,220	163,833	1,722,220
Electricity generated (MW-h yr^{-1})	6,193,000	5,640,700	5,564,640	5,525,100	5,456,200
Electricity sold (MW-h yr^{-1})	5,417,800	5,201,800	5,168,400	5,344,300	5,306,800
Electrical efficiency (%HHV)	**64.1**	**64.6**	**63.7**	**63.2**	**62.4**

[a] Electrical efficiency is calculated as the total power generated by the plant divided by the total HHV fuel input to the plant on a basis of 1 year, whether or not that electricity was actually "sold" to the grid for profit.

well as carbon capture capabilities. Although the NGCC plant has lower capital costs (as will be discussed in Section 3.4) its high fuel consumption, low efficiency and higher CO_2 emission rates are likely to make it less attractive should fuel prices increase and carbon restrictions of some fashion be implemented. For example, case 9 produces about 28% fewer total CO_2 emissions (direct and indirect) than case 1 (NGCC). When CCS is added, the SOFC/CAES plant with train shutdowns (case 10) produces 97% fewer total emissions than case 1 (NGCC), and 76% fewer emissions than case 2 (NGCC with CCS).

3.2. Economic results

The economic results of each of the ten cases examined are presented in Table 5. The LCOE for each case was calculated in the absence and presence of a carbon tax of \$50 $tonne^{-1}$. Due to its very low capital investment, the NGCC plant without CCS is unsurprisingly the most economically attractive configuration without a CO_2 tax and at the current market price of natural gas. However, due to its much lower efficiency and higher fuel utilization than the SOFC base-load plants, it becomes unattractive at a CO_2 tax of \$50 $tonne^{-1}$ or when fuel prices climb to the neighborhood of \$6.16 GJ^{-1} (\$6.50 $MMBtu^{-1}$) [6]. On that note, it is interesting to observe that when no CO_2 incentives are used the addition of CCS to any configuration based around the SOFC results in no more than a 0.08 ¢ kW^{-1} h^{-1} (1.6%) increase in LCOE. This is because a solvent-based CO_2 capture process is not required for the SOFC cases. CCS becomes economically attractive for all processes when a CO_2 tax of \$50 $tonne^{-1}$ is implemented, with the SOFC-based plants having the lowest LCOE.

The increase in capital costs associated with adding a CAES system to the SOFC base-load plant results in a slightly higher LCOE

Table 5
Economic results for each of the plant configurations simulated.

Case	1 NGCC	2 NGCC–CCS	3 SOFC	4 SOFC–CCS	5 SOFC–CAES
Capital cost (\$1,000s)	363,100	718,900	1,212,500	1,239,500	1,373,100
Grid power cost (\$1,000s yr^{-1})	5469	5469	5469	5469	2385
Fuel costs (\$1,000s yr^{-1})	101,800	118,400	79,900	79,900	79,900
CO_2 emission costs[c] (\$1,000s yr^{-1})	112,100	13,300	88,500	2353	87,100
Operating costs[a] (\$1,000s yr^{-1})	16,500	30,400	19,000	19,300	22,500
LCOE[b] (¢ kW^{-1} h^{-1})	**3.57**	**5.04**	**5.00**	**5.07**	**5.29**
LCOE[c] with CO_2 tax (¢ kW^{-1} h^{-1})	**6.084**	**5.335**	**6.967**	**5.123**	**7.206**

	6 SOFC–CAES–CCS	7 SOFC–TSD	8 SOFC–TSD–CCS	9 SOFC–CAES–TSD	10 SOFC–CAES–TSD–CCS
Capital cost (\$1,000s)	1,400,000	1,212,500	1,239,500	1,373,100	1,400,000
Grid power cost (\$1,000s yr^{-1})	2386	11,950	11,950	6880	6880
Fuel costs (\$1,000s yr^{-1})	79,900	72,300	72,300	72,300	72,300
CO_2 emission costs[c] (\$1,000s yr^{-1})	950	83,800	5890	81,100	3190
Operating costs[a] (\$1,000s yr^{-1})	22,500	19,300	19,300	22,500	22,500
LCOE[b] (¢ kW^{-1} h^{-1})	**5.35**	**5.12**	**5.22**	**5.30**	**5.40**
LCOE[c] with CO_2 tax (¢ kW^{-1} h^{-1})	**5.37**	**7.05**	**5.35**	**7.12**	**5.47**

[a] Operating costs include labor, maintenance, catalysts, water consumption, CO_2 transport costs, and materials.
[b] Does not include a CO_2 tax.
[c] Includes a CO_2 tax of \$50 $tonne^{-1}$.

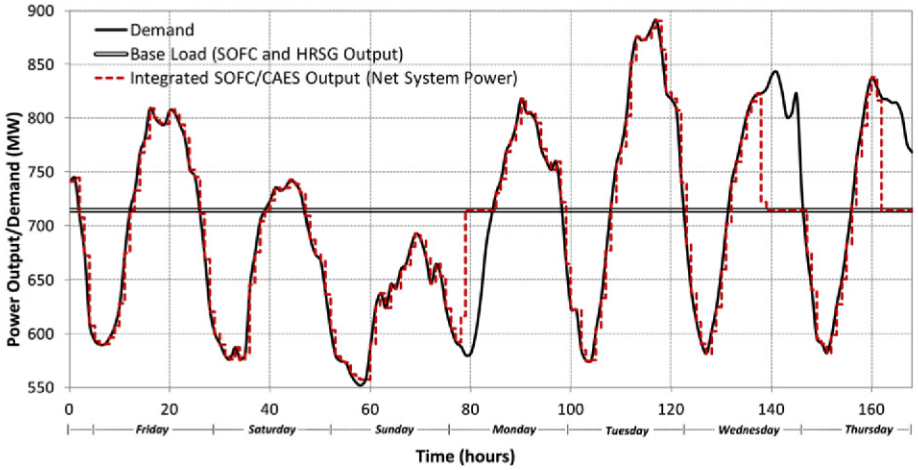

Fig. 7. Simulation results of the SOFC/CAES system for one selected week of operation (June 17–23, 2011). Times in which the output of the SOFC/CAES system matches the base load when demand is less than supply denote times when the cavern is full (at maximum allowable pressure). Times in which the SOFC/CAES system matches the base load when demand exceeds supply denote times when the storage cavern is empty (at minimum allowable pressure).

for the SOFC–CAES cases. However, this slight increase of approximately 0.1 ¢ kW^{-1} h^{-1} (2.0%) allows for much more accurate load-following when CAES is used than the base-load case, and significantly reduces the requirement for additional power being imported from the grid. The addition of train shutdowns, although not advantageous from a purely economic standpoint, reduces the direct fuel consumption cost of the proposed process by approximately 9.5%. Although this may not result in an immediate financial gain, the reduced fuel consumption will result in further fuel cost savings should the price of natural gas increase throughout the lifetime of the plant (see Section 3.4).

Since grid prices are always in flux, the CAES plant provides some protection from unexpected price increases. For example, instead of using the SOFC/CAES hybrid system to minimize load-following mismatch, as was the goal in the present work, one could use the CAES capabilities to maximize profit by storing energy during times of low prices and releasing at higher prices. Although this is left for future work, this property can have significant financial planning and forecasting benefits.

It is important to note that the economic results obtained in this study will be different at different scales, fuel prices, sale prices and other parameters used. For example, smaller system sizes would cause higher LCOEs of both the NGCC and SOFC-based plant designs since the proportion spent on capital increases due to economies-of-scale. For this investigation, our system scale was chosen such that the SOFC/CAES system design is comparable to that of the most reasonable alternative system for bulk power production, namely a modern NGCC plant operating at an output of approximately 700 MW. The effects of variations in many of the other economic parameters are explored in Section 3.4.

3.3. Load-following results and performance

A sample plot of demand and power provided by case 6 (SOFC–CAES–CCS) is given in Fig. 7, and the corresponding cavern pressure profile is displayed in Fig. 8. Table 6 summarizes the load-following metrics used in this investigation for each of the cases examined. It is clear that the CAES-enabled system is able to accurately follow demand above and below the level of the fixed SOFC and HRSG power output during most of the simulated control intervals.

The addition of the CAES component decreases the SSE and WSSE substantially when compared to the SOFC base-plant. From the standpoint of adding the CAES, this makes sense

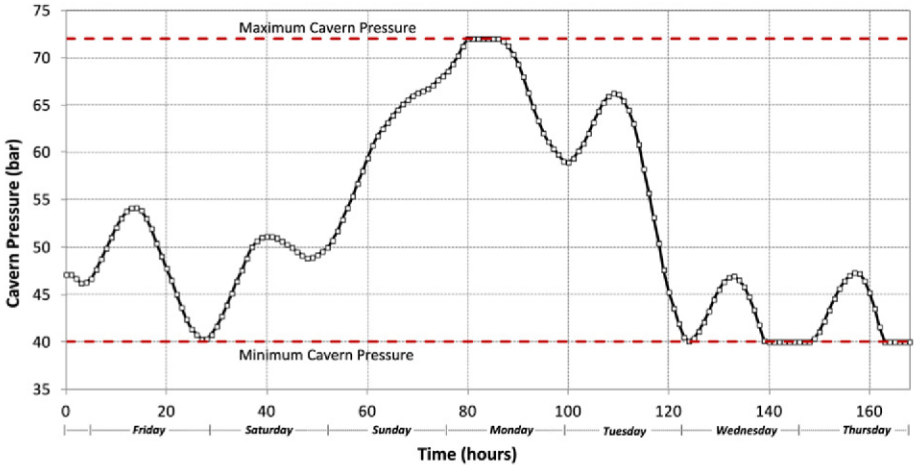

Fig. 8. Pressure profile for one week of simulated operation.

Table 6
Load-following metric results for cases investigated.

Case	Tag	SSE (10^6 [MW-h]^2)	WSSE (10^6 [MW-h]^2)	Relative SSE	Relative WSSE
1	NGCC	162.28	51.73	0.911	0.956
2	NGCC–CCS	162.28	51.73	0.911	0.956
3	SOFC	178.22	54.12	1.000	1.000
4	SOFC–CCS	162.28	51.73	0.911	0.956
5	SOFC–CAES	152.34	42.94	0.855	0.793
6	SOFC–CAES–CCS	135.98	40.13	0.763	0.742
7	SOFC–TSD	84.68	43.45	0.475	0.803
8	SOFC–TSD–CCS	81.95	46.34	0.460	0.856
9	SOFC–TSD–CAES	43.80	24.23	0.246	0.448
10	SOFC–TSD–CAES–CCS	43.70	26.24	0.245	0.485

because the amount over- and under-produced decreases substantially with the addition of load-following capabilities. Train shutdowns also decrease the SSE, and in the final case cause it to be as low as 24.5% of that of the base-load SOFC plant, indicating that the addition of CAES and train shutdowns result in about half as much demand/supply mismatch. For example, when comparing case 5 (SOFC–CAES) to case 9 (SOFC–CAES–TSD), the SSE for case 9 is 28.8% of that of case 5. Similarly to the SSE, the addition of train shutdowns decreases the WSSE, although not by as much. For example, when comparing cases 5 and 9 again, the WSSE for case 9 is 56.5% of that of case 5. This is largely due to the fact that the train shutdowns decrease the amount of overproduction while also slightly increasing the amount of underproduction, the latter of which is penalized more heavily in the WSSE metric. For this reason, the WSSE is likely a better performance metric than SSE; it is most important to meet demand as much as possible, even if over-production is highly wasteful. The only way to improve plant load-following performance with train shutdowns is through the introduction of the CAES plant, which brings the WSSE to 48.5% of the base-load plant when CCS is enabled.

The load-following performance of the CAES-enabled cases is highly dependent on the size of the storage cavern. A sensitivity analysis is shown in Fig. 9 that compares the WSSE of cases 4, 6, 8 and 10. It is clear that increasing the cavern size exhibits diminishing returns with regards to WSSE improvement, and very little improvement for either of cases 6 or 10 is made past 800,000 m^3. There is thus a trade-off to be investigated between increasing cavern sizes for the sake of improved load-following performance and the corresponding increase in capital investment, which is left to future work. The load-following performance of each system is also independent of the base-load system size. Since the demand profiles for the simulations were scaled to the size of the base-load plants investigated, the load-following results (SSE, WSSE, energy storage/withdrawal rates) are equivalent for any reasonable size.

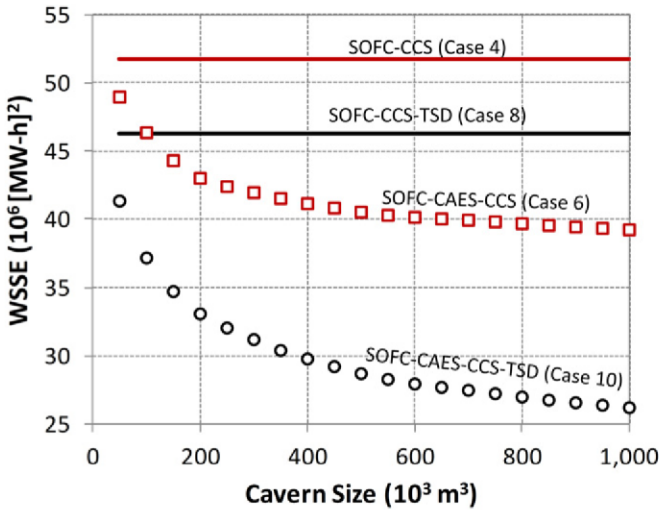

Fig. 9. Effect of cavern size on CCS-enabled system performance.

3.4. Sensitivity analyses

The LCOEs for the cases investigated have been computed as a function of the average lifetime carbon tax paid by the plant and are shown in Fig. 10. This analysis assumes a simple linear CO_2 tax on a per-tonne basis. With the price of natural gas at the current (June 2012) low price of \$2.33 GJ^{-1} (\$2.46 MMBtu^{-1}), it would require a CO_2 tax of \$30 tonne^{-1} to incentivize a system in which CCS is used; anything less would make CCS uneconomical compared to the non-CCS cases. Another interesting observation is that for the parameters investigated in this sensitivity analysis, the addition of CAES at no point becomes the most economical design. However, as mentioned previously, the addition of CAES improves the load-following capabilities of the SOFC base-load plant for a very modest increase in LCOE (only about 5% or 0.3 ¢ kW^{-1} h^{-1}), which is also evident in Fig. 10. SOFC based plants are not economically attractive unless CCS is enabled, where some are significantly less expensive than NGCC with CCS. This is an expected result, since the extremely cost-effective CO_2 capture of an SOFC plant is one of its major advantages in a future of sustainable energy.

Shown in Fig. 11 is a two-dimensional sensitivity map that shows which of the 10 cases has the lowest LCOE based changes in both fuel (natural gas) and CO_2 tax prices. One interesting observation from this plot is that the system of case 10 (SOFC–CAES–CCS–TSD) actually combines to offer the most cost-effective power generation at relatively high gas prices (~\$7.58 GJ^{-1} or \$8 MMBtu^{-1}) and CO_2 taxes (~\$60 tonne^{-1}). As a matter of fact, train shutdown configurations are almost exclusively used above a price of approximately \$7.58 GJ^{-1} (\$8 MMBtu^{-1}), which has occurred several times over the last few decades. Therefore, the CAES and SOFC train shutdown configurations not only protect a plant from sudden increases in fuel and external electricity costs, provide excellent load-following capabilities, reduce wasted energy and resources, and provide the capability to capture essentially 100% of direct CO_2 emissions at only a small cost premium, but it also becomes the outright most economically attractive option in a scenario with high emission taxes and fuel prices. The configuration which is generally the most economically optimal is case 4,

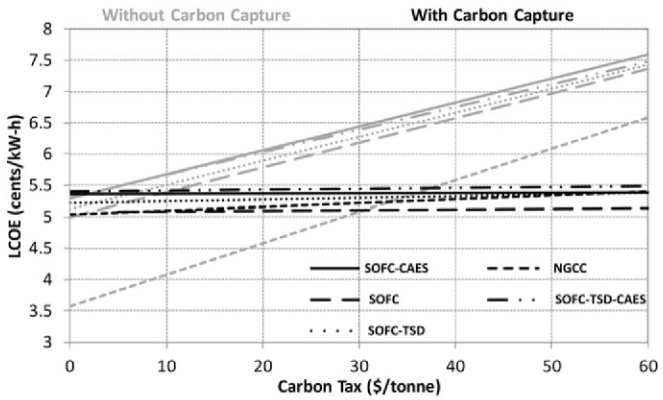

Fig. 10. Effect of CO_2 taxes on LCOE.

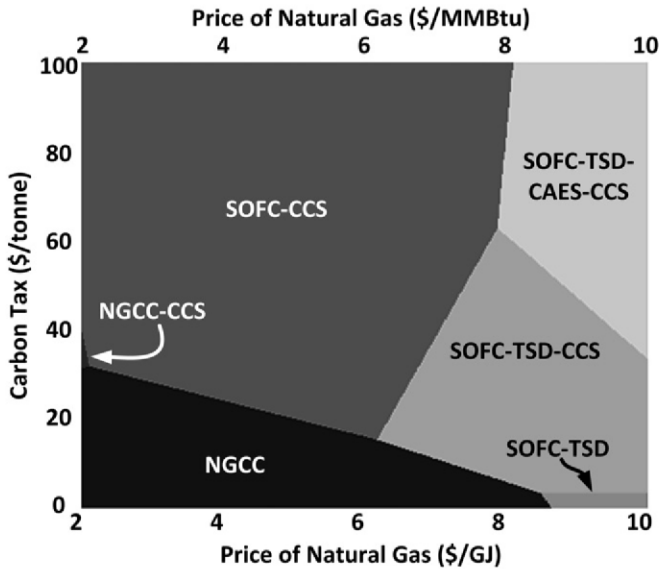

Fig. 11. Sensitivity map of processes exhibiting the lowest LCOE based on natural gas and CO_2 tax prices.

which becomes the most economically feasible with a CO_2 tax of approximately \$30 tonne^{-1} at the current price of natural gas.

4. Conclusions and future work

In this study, the applicability and performance of an integrated SOFC/CAES plant with and without CCS in a load-following power production scenario was investigated. Ten different process configurations were simulated using a combination of Aspen Plus and MATLAB tools. It was found that the addition of CAES to an SOFC plant provided significant load-following capabilities with relatively small penalties to efficiencies (1.1%HHV) and levelized electricity costs (0.08–0.3 ¢ kW^{-1} h^{-1}). The load-following capabilities of the CAES-enabled plants, as measured by the SSE and WSSE metrics, were significantly higher than the base-load cases and were not impacted by the addition of CCS. CCS-enabled configurations using SOFC/CAES strategies were able to reduce direct CO_2 emissions to essentially zero. The introduction of a train shutdown schedule, while useful for maintenance and cleaning purposes, was also found to help reduce fuel consumption with very small penalties to the overall load-following performance of the SOFC/CAES plant.

Overall, the SOFC/CAES process can provide very effective load-following power production with zero direct CO_2 emissions for only a marginal increase in LCOE. Furthermore, SOFC/CAES can be the most economical option should carbon taxes and natural gas prices rise above the range of \$40 tonne^{-1} and \$7.58 GJ^{-1} (\$8 MMBtu^{-1}), respectively. Although SOFCs are perhaps decades away from being implemented on the scale discussed in this study, the forward-looking energy conversion strategy proposed in this work shows great promise for providing future carbon-free peaking power.

Since this is the first known investigation of providing zero-emission peaking power using SOFCs to the best of our knowledge, several simplifying assumptions were made for the sake of this proof-of-concept study. Future work may include the consideration of CAES turbine dynamics, real-time optimization frameworks to maximize plant revenue or profitability (instead of minimizing underproduction and overproduction), market considerations when CO_2 has economic value (such as for enhanced oil recovery), control system considerations, stochastic fuel and material price planning, startup/shutdown penalties of the base load plant (specifically those involved with TSD), and the use of gasified coal, biomass, or other fuel sources instead of or in addition to natural gas. These considerations will likely affect the profitability (whether positively or negatively is unknown at this point) of integrated SOFC/CAES systems.

Nomenclature

Abbreviations

ASU	air separation unit
ATR	auto-thermal reformer
CAES	compressed air energy storage
CCS	carbon capture and sequestration
EOS	equation of state
HHV	higher-heating value
HRSG	heat recovery and steam generation
LCOE	levelized cost of electricity
SOFC	solid oxide fuel cell
SSE	sum of squared error
TSD	train shutdown
WGS	water-gas shift
WSSE	weighted sum of squared error

Mathematical symbols

a	model coefficient
D	demand
F	molar flow rate of air
$\mathcal{F}$	fuel costs
I_M	pseudo-steady-state model intercept
I	capital investment
M	maintenance costs
N	plant lifetime
O	plant over-production
P	pressure in cavern
$\mathcal{P}$	sellable power produced
P_C	compressor pressure at outlet
P_P	net power output of plant
r	discount rate
U	plant under-production
μ	mean
σ	standard deviation

References

[1] H.J. Herzog, D. Golomb, in: C.J. Cleveland (Ed.), Encyclopedia of Energy, Elsevier Science, New York, 2004, pp. 277–287.
[2] US Energy Information Administration, AEO2012 Early Release Outlook, US DOE/EIA- 0383ER (January 2012).
[3] National Energy Board, Canada's Energy Future: Energy Supply and Demand Projections to 2035-Electricity Outlook Highlights. (online). Available HTTP: http://www.neb-one.gc.ca/clf-nsi/rnrgynfmtn/nrgyrprt/nrgyftr/2011/fctsht1134lctrct-eng.html (accessed June 2012).
[4] Energy Information Administration (EIA), Fuel emission factors, Appendix H of instructions to form EIA-1605, U.S. Department of Energy, Washington, DC (online). Available HTTP: http://www.eia.gov/oiaf/1605/pdf/Form%20EIA-1605%20instructions.pdf.
[5] U.S. Environmental Protection Agency (EPA), Inventory of U.S. Greenhouse Gas Emissions and Sinks: 1990–2010. EPA 430-R-12–001, pp. 3–5 (online). Available HTTP: http://www.epa.gov/climatechange/ghgemissions/usinventoryreport.html.
[6] T.A. Adams II, P. Barton, J. Power Sources 195 (2010) 1971–1983.
[7] J. Conti, G.E. Sweetnam, et al., Emissions of Greenhouse Gases in the United States 2007. US DOE/EIA-0573(2007) (December 2008).
[8] M.C. Woods, P.J. Capicotto, J.L. Haslbeck, N.J. Kuehn, M. Matuszewski, L.L. Pinkerton, M.D. Rutkowski, R.L. Schoff, V. Vaysman, Cost and Performance Baseline for Fossil Energy Plants. Volume 1: Bituminous Coal and Natural Gas to Electricity Final Report, DOE/NETL-2007/1281, Revision 1, August 2007.
[9] M.C. Williams, J.P. Strakey, W.A. Surdoval, Int. J. Appl. Ceram. Technol. 2 (2005) 295.

[10] T.A. Trabold, J.S. Lylak, M.R. Walluk, J.F. Lin, D.R. Trojani, Int. J. Hydrogen Energy 37 (2012) 5190.
[11] N.Q. Ming, ECS Trans. 7 (2007) 45.
[12] F.P. Nagel, T.J. Schildhauer, S.M.A. Biollaz, Int. J. Hydrogen Energy 34 (2009) 6809.
[13] E. Achenbach, J. Power Sources 57 (1995) 105–109.
[14] C. Stiller, B. Thorund, O. Bolland, J. Eng. Gas Turbines Power 128 (2006) 551–559.
[15] M. Raju, S.K. Khaitan, Appl. Energy 89 (2012) 474–481.
[16] E. Fertig, J. Apt, Energy Policy 39 (2009) 2330–2342.
[17] H. Hoffeins, Huntorf Air Storage Gas Turbine Power Plant, Energy Supply, Brown Boveri Publication, 1994, DGK 90 202 E.
[18] D.R. Hounslow, W. Grindley, R.M. Louglin, J. Eng. Gas Turbine Power 120 (1988) 875–883.
[19] A. Cavallo, Energy 32 (2007) 120–127.
[20] J.B. Greenblatt, S. Succar, D.C. Denkenberger, R.H. Williams, R.H. Socolow, Energy Policy 35 (2007) 1472–1492.
[21] J. Mason, V. Fthenakis, K. Zweibel, T. Hansen, T. Nikolakakis, Prog. Photovolt. Res. Appl. 16 (8) (2008) 649–668.
[22] S. Succar, R.H. Williams, Compressed Air Energy Storage: Theory, Resources and Applications for Wind Power, Princeton Environmental Institute: Princeton University, 2008.
[23] T.A. Adams II, J. Nease, D. Tucker, P. Barton, Ind. Eng. Chem. Res., in press (2012), http://dx.doi.org/10.1021/ie300996r.
[24] T.S. Lee, J.N. Chung, Y. Chen, Energy Conv. Manage. 52 (2011) 3214–3226.
[25] Independent Electricity System Operator. Ontario Demand and Market Prices. Available HTTP: http://www.ieso.ca/imoweb/siteShared/demand_price.asp?sid=ic (accessed 19.03.12).
[26] F. Mueller, B. Tarroja, J. Maclay, F. Jabbari, J. Brouwer, S. Samuelson, J. Fuel Cell. Sci. Tech. 7 (2010). 031007-1-12.
[27] L. Yang, Y. Weng, J. Power Sources 196 (2011) 3824–3835.
[28] V. Liso, A. Oleson, M. Nielson, S. Kaer, Energy 35 (2011) 4216–4226.
[29] Y. Komatsu, S. Kimijima, J.S. Szmyd, Energy 35 (2010) 982–988.
[30] T. Kuramochi, W. Turkenburg, A. Faaij, Fuel 90 (2011) 958–973.
[31] N. Zhang, N. Lior, J. Eng. Gas Turbines Power 130 (2008) 051701-1–151701-11.
[32] K. Aasberg-Petersen, T.S. Christensen, I. Dybkjær, J. Sehested, M. Østberg, R.M. Coertzen, M.J. Keyser, A.P. Steynberg, in: A. Steynberg, M. Dry (Eds.), Fischer–Tropsch Technology, Elsevier, Amsterdam, 2004.
[33] R. Peters, E. Riensche, P. Cremer, J. Power Sources 86 (2000) 432–441.
[34] K.M. Walters, A.M. Dean, H. Zhu, R.J. Kee, J. Power Sources 123 (2003) 182–189.
[35] R.J. Kee, H. Zhu, A.M. Sukeshini, G.S. Jackson, Combust. Sci. Tech. 180 (2008) 1207–1244.
[36] EG&G Technical Services, DOE/NETL Fuel Cell Handbook, seventh ed., (November 2004).
[37] T.A. Adams II, P.I. Barton, AIChE J. 56 (2010) 3120–3136.
[38] W.L. Luyben, Ind. Eng. Chem. Res. 50 (2011) 13984–13989.
[39] R. Kushnir, Transport Porous Media 73 (2008) 1–20.
[40] Electric Power Research Institute, Wind Power Integration Technology Assessment and Case Studies. EPRI Report 1004806 (2004).
[41] US Energy Information Administration, Fuel Emission Factors (online), U.S. Department of Energy, 2010, Available HTTP: http://www.eia.gov/oiaf/1605/pdf/Form%20EIA-1605%20Instructions.pdf.
[42] US Energy Information Administration, Average utilization of the nation's natural gas combined-cycle power plant fleet is rising (online). Available HTTP: http://www.eia.gov/todayinenergy/detail.cfm?id=1730# (accessed 30.11.11).
[43] K. Branker, M.J.M. Pathak, J.M. Pearce, Renew. Sustain. Energy Rev. 12 (2011) 4470–4482.
[44] W.D. Seider, J.D. Seader, D.R. Lewin, S. Widago, Product and Process Design Principles, third ed., Wiley, Hoboken, NJ, 2009, pp. 534–597.
[45] G. Hossein, Progress in SECA-Based Program. Fuel Cell Energy, Inc. SECA Conference Proceeding, July 26, 2011.
[46] M.C. Williams, J.P. Strakey, W.A. Surdoval, U.S. DOE solid oxide fuel cells: technical advances, in: Proceedings of the 207th Meet. Electrochem. Soc., 2005, p. 1025.
[47] R. Schainker, Compressed Air Energy Storage Cost Analysis, The Electric Power Research Institute, 2009, Report 1016004.
[48] Bloomberg Commodity Prices: Energy. Henry Hub Spot Price of Natural Gas (online). Available HTTP: http://www.bloomberg.com/energy/ (accessed 08.05.12).
[49] D. Lozowski, Chem. Eng. 119 (6) (2012) 80.

Chapter 3

Coal-Fuelled Systems for Peaking Power with 100% CO_2 Capture through Integration of Solid Oxide Fuel Cells with Compressed Air Energy Storage

The content of the following chapter is a **published reprint** of the following peer-reviewed publication:

Nease J, Adams TA II. Coal-Fuelled Systems for Peaking Power with 100% CO_2 Capture Through Integration of Solid Oxide Fuel Cells with Compressed Air Energy Storage. *Journal of Power Sources*. 2014; 251: 92-107.

This paper makes reference to an online supplement submitted and reviewed with the full publication. The supplement is extensive and is not reproduced in this work, but has been made available electronically with the file name:

`Chapter_3_Supplement.xslx`

Journal of Power Sources 251 (2014) 92–107

Contents lists available at ScienceDirect

Journal of Power Sources

journal homepage: www.elsevier.com/locate/jpowsour

Coal-fuelled systems for peaking power with 100% CO_2 capture through integration of solid oxide fuel cells with compressed air energy storage

Jake Nease, Thomas A. Adams II *

Department of Chemical Engineering, McMaster University, 1280 Main Street West, Hamilton, Ontario, Canada L8S 4L7

HIGHLIGHTS

- A CO_2 emission-free peaking power plant fuelled by gasified coal is discussed.
- The performances of 16 different plant configurations are quantified.
- The direct impact of a water–gas shift process step is investigated and analyzed.
- Peaking power from coal is possible using CAES with little only minor impacts on electricity costs.
- SOFC/CAES plants can be economically advantageous at high fuel or carbon prices.

ARTICLE INFO

Article history:
Received 20 June 2013
Received in revised form
15 November 2013
Accepted 16 November 2013
Available online 28 November 2013

Keywords:
Solid oxide fuel cells
Compressed air energy storage
Carbon capture
Peaking power
Coal

ABSTRACT

In this study, a coal-fuelled integrated solid oxide fuel cell (SOFC) and compressed air energy storage (CAES) system in a load-following power production scenario is discussed. Sixteen SOFC-based plants with optional carbon capture and sequestration (CCS) and syngas shifting steps are simulated and compared to a state-of-the-art supercritical pulverised coal (SCPC) plant. Simulations are performed using a combination of MATLAB and Aspen Plus v7.3. It was found that adding CAES to a SOFC-based plant can provide load-following capabilities with relatively small effects on efficiencies (1–2% HHV depending on the system configuration) and levelized costs of electricity ($\sim$0.35 ¢ kW^{-1} h^{-1}). The load-following capabilities, as measured by least-squares metrics, show that this system may utilize coal and achieve excellent load-tracking that is not adversely affected by the inclusion of CCS. Adding CCS to the SOFC/CAES system reduces measurable direct CO_2 emission to zero. A seasonal partial plant shutdown schedule is found to reduce fuel consumption by 9.5% while allowing for cleaning and maintenance windows for the SOFC stacks without significantly affecting the performance of the system ($\sim$1% HHV reduction in efficiency). The SOFC-based systems with CCS are found to become economically attractive relative to SCPC above carbon taxes of \$22 ton^{-1}.

1. Introduction

On the global scale, the electricity generation industry is largely dependent on the use of fossil fuels such as natural gas and coal due to their high abundance and relative ease of access. Energy conversion with renewable fuel sources (wind, solar, bio-fuels etc.) is still decades away from being implemented on any significant scale. To illustrate, it is projected that the total electricity produced in the United States and Canada by renewable (non-hydro) sources in the year 2035 will be 16% and 10%, respectively [1,2]. Consequently, for the near term it is necessary to improve the performance of fossil-fuelled systems (both environmentally and economically) to drive society toward a sustainable future. Moreover, government incentives and emission restriction programs, such as cap-and-trade systems or taxes on equivalent CO_2 emissions may become a challenge for electricity providers in the coming years. To avoid these added costs, the electricity generation sector will be motivated to capture the CO_2 generated by their operations for underground sequestration (geological formation such as aquifers or depleted oil wells present viable options) or possibly resale as a value-added product for enhanced-oil recovery among other uses [3]. The coal-based power generation industry will thus be forced to develop and invest in CO_2 capture technology or pay the financial penalties that will accrue due to their emission to the atmosphere.

* Corresponding author. Tel.: +1 (905) 525 9140x24782.
E-mail address: tadams@mcmaster.ca (T.A. Adams).

0378-7753/$ – see front matter © 2013 Elsevier B.V. All rights reserved.
http://dx.doi.org/10.1016/j.jpowsour.2013.11.040

Either way, the impact to the end consumer will be increased electricity prices and therefore an increased cost of living.

In the interest of developing new methods to use coal for electricity generation, this work analyzes the performance of an integrated solid-oxide fuel cell (SOFC) and compressed air energy storage (CAES) plant, fuelled by gasified coal, that is capable of meeting demand variations (referred to hereafter as "peaking power"). The SOFC system uses gasified coal as the fuel source, and each of the designs are compared to a modern coal-based power process, the supercritical pulverized coal combustion process (SCPC). Sixteen system configurations with design decisions such as optional carbon capture and sequestration (CCS) and optional water–gas shift (WGS) reactors are considered.

1.1. Pulverized coal and gasification

Coal powers approximately 45% of the electricity generation in the United States and is expected to remain the dominant fuel choice through 2035 [1]. On a global scale, coal accounts for approximately 33% of all electricity production and is expected to maintain a significant share over the next few decades [4]. Coal-fired power plants produce an inherently high amount of CO_2 per unit of electricity generated (approximately 90.29 g MJ^{-1}) and therefore account for a significant amount of the CO_2 emissions in the power generation sector [5]. In 2010, coal-based processes contributed 80.9% of the total CO_2 emissions for the electricity generation sector in the United States, or 26.8% of all of the CO_2 emitted across all industries [6]. Reducing or eliminating the CO_2 emissions from coal-fed plants would contribute significantly towards the large-scale reduction of the United States' CO_2 emissions.

The SCPC process is chosen as the "status quo" coal-fed power generation process for the purposes of this investigation. The SCPC process is briefly described as follows [7]: coal is combusted with air in a boiler, generating heat to power steam turbines. Steam is generated above the critical point (hence "supercritical") at 240 bar and 593 °C to improve downstream power generation efficiency. The combustion products are mainly CO_2, H_2O, N_2, SO_2 and ash, as well as small amounts of other impurities (Hg, S, Cl). The ash and sulphur are removed through separate cleanup steps and the small amounts of impurities can be removed through various well-proven processes, yielding a final exhaust stream containing mainly H_2O, CO_2 and N_2. At this point, the exhaust can be vented to the atmosphere (as is typically done), or post-combustion CO_2 absorption may be performed to remove CO_2 for capture and sequestration purposes. Absorption can be performed with chemical solvents such as Monoethanolamine (MEA) or Methyldiethanol amine (MDEA), or physical solvent processes such as Rectisol™ or Selexol™. Approximately 90% of the CO_2 in the exhaust gas can be recovered at purities required for pipeline transport, with the rest being emitted to the atmosphere via the exhaust gas. Although they are effective, absorption-based CCS strategies are energy-intensive and often lead to prohibitive decreases in overall system efficiency, leading to higher electricity costs [7]. Other more recent approaches such as membrane-based processes, pressure swing adsorption and vacuum swing adsorption have also been investigated with promising results [8,9].

Gasified coal processes such as the integrated gasification combined cycle (IGCC) involve the gasification of coal into synthesis gas (syngas, CO and H_2) as well as CO_2 and H_2O. The water–gas shift (WGS) reaction can then be performed downstream of the gasification step to increase the amount of H_2 in the syngas stream. After gas shifting, the same solvent-based absorption processes for CCS can be employed to remove CO_2 before the downstream use of the syngas. As in the post-combustion CCS case, approximately 90% of the CO_2 in the syngas stream can be recovered at pipeline purity [7].

1.2. Solid oxide fuel cells

SOFCs make use of a hydrogen-based or carbonaceous fuel gas and an oxidant (air is typically used due to its availability and high oxygen content) to produce electricity through electrochemical reactions on either side of an impermeable partition, as depicted in Fig. 1. The reactions that occur in the anode and cathode are the oxidation of the fuel gas and the reduction of O_2, respectively. A sample of these reactions may include, but are not limited to, the following [10]:

$$H_2 + O^{=} \rightarrow H_2O + 2e^{-} \quad \text{(Anode)} \tag{1}$$

$$CO + O^{=} \rightarrow CO_2 + 2e^{-} \quad \text{(Anode)} \tag{2}$$

$$O_2 + 4e^{-} \rightarrow 2O^{=} \quad \text{(Cathode)} \tag{3}$$

SOFCs are fuel-flexible, and are able to utilize a variety of carbonaceous fuel sources. Examples of possible fuels include H_2 and CO (syngas), natural gas [11], methanol [12], jet fuel [12] and others [13]. Several other carbonaceous sources may be gasified, converted to syngas, and then used as a fuel source for the SOFC anode as well. Such options include coal [14], biomass [15,16], diesel [12] and others. See our prior work for a discussion of different fuel sources [13]. As shown in Fig. 1, the products on the anode side consist of H_2O, CO_2 and unspent fuel. If the anode and cathode outlet streams can be kept unmixed (which is possible), the anode products allow for simple and effective CCS to be employed. The unspent fuel in the anode exhaust may be combusted with stoichiometric amounts of O_2 (an excess of which may result in violating CO_2 pipeline restrictions) resulting in a mixture of nearly 100% CO_2 and H_2O. The CO_2 may then be captured at pipeline purities with minimal parasitic energy costs through a series of flash drums; see the patent by Adams and Barton (2009) for details [17]. The cathode exhaust contains mostly deoxygenized air at a high temperature (~900 °C) and pressure (10–20 bar), which facilitates several opportunities for additional power generation via a thermal (heat recovery steam generation (HRSG) cycle, for example) and/or pressure-driven (Brayton turbines, for example) bottoming cycle before being vented to atmosphere with essentially no environmental impact [10]. It has been shown in our prior work that gasified coal-fed SOFC processes can achieve electrical efficiencies of more than 45% by higher heating value (HHV) while completely capturing all CO_2 emissions [18,19]. Similar results have been obtained by other research groups (see Refs. [20–23] and Table 4 in Ref. [13], for example). The process of converting electrochemical potential to electricity is an inherently more efficient process than combustion, thus allowing for SOFC-based systems to make better

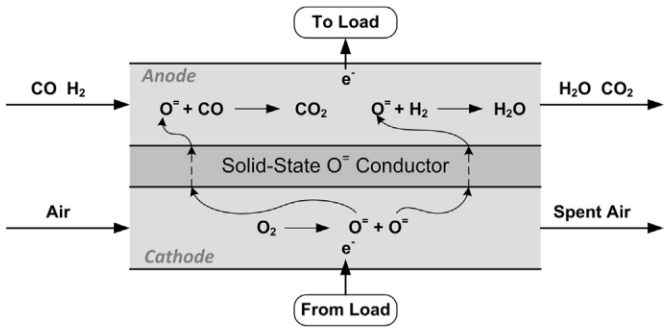

Fig. 1. Simple schematic of a SOFC using syngas as a fuel source with possible reactions shown. Reproduced from Ref. [10].

use of the energy contained within the resource than most modern commercially available technologies.

Although a very promising technology for bulk power generation, the SOFC is not without its disadvantages. A significant current limitation to SOFC technology is that there are cost-prohibitive challenges associated with operating the unit dynamically. For example, it is possible to attempt to provide peaking power by adjusting the power output from an SOFC stack in real time [24], but not without seriously risking cell degradation or destruction due to thermal expansion, gas backflow, and a variety of other problems [25]. Recent studies have shown that this remains an ongoing issue [26,27]. Therefore, we anticipate that future SOFC systems at the bulk scale will be used as fixed-output power suppliers that provide base-load power at high efficiency, with no capabilities of providing peaking power. It is possible to design an SOFC system to provide the maximum anticipated peak (and thereby always meet demand), but such a system would nearly always produce more electricity and consume more fuel than necessary.

1.3. Compressed air energy storage

CAES plants operate as intermittent sinks or sources of electrical power through the storage of mechanical energy in the form of compressed air. A CAES plant functions by consuming available electrical power to compress and store air as elastic potential energy in an above- or below-ground void. Typical storage voids may include depleted natural gas reserves, solution-mined salt domes and aquifers. The compressed air can then be pre-heated (typically by combusting it with natural gas) and released through expansion turbines attached to electrical generators in order to convert the stored elastic potential back into electrical power. CAES plants can be used as temporary storage options for large-scale processes that preclude the use of batteries or other distributed energy storage options, making it a prime candidate for bulk peaking power generation. A typical CAES system is shown diagrammatically in Fig. 2.

CAES is a mature technology that has successfully been utilized both in the United States and overseas for over 35 years. Examples of currently operating CAES plants include a 290 MW plant operated by E.N. Kraftwerke and a 110 MW plant operated by the Alabama Electric Company [28], alluding to the longevity and applicability of the technology. The two existing plants exploit the concept of peak electricity pricing; during periods of low electricity prices (night time), the CAES system consumes electricity, and re-feeds it to the electrical grid when the price of electricity is high (day time). The resulting arbitrage situation allows the CAES system to operate profitably. As of 2009, no other standalone CAES plants were planned on being constructed due to various issues [29]. However, in the summer of 2013 Apex announced an Award given to Dresser-Rand for a 317 MW system to be built in Texas valued at approximately $200 million, and another 270 MW facility from Chamisa Energy is scheduled to go online in 2014 [30,31].

Not only can a CAES system be used individually, but its rapid dynamics and controllability make it well-suited for combination with other process for added flexibility. One intriguing application of CAES is for the levelling of intermittent and somewhat unpredictable power generated by wind turbines in an attempt to provide reliable base-load power [28,32–37]. In much the same fashion, we feel that CAES can be used in an opposite role where it supplements an already reliable base load to provide controllable and reliable peaking power. There are two notable disadvantages to a CAES system: it requires an external electrical power source, and (in the absence of a significant heat sink), it requires the combustion of natural gas before (or in) the expansion turbines, resulting in CO_2 emissions.

1.4. Integration of SOFC and CAES systems

As an extension of our prior work, this study investigates the integration of gasified coal-fuelled SOFCs (to provide base-load power), a CCS system (to eliminate direct CO_2 emissions), and a CAES plant (to be used in an attempt to consume or supplement the base-load outlet, thereby resulting in peaking power), and is the first to do so to the best of our knowledge. As a further extension of our prior work, we quantify the impact of including the WGS step upstream of the SOFC stack on plant reliability and performance. The combined system exploits synergies that exist between each of the sections mentioned, effectively overcoming their individual disadvantages. The SOFC and CCS systems are modelled to be consistent with those of Adams and Barton (see Refs. [17–19,38]). The steady-state CAES model was kept the same as our prior work on natural gas systems with CAES for comparative purposes, but is applied with the process conditions of a SOFC plant fuelled by gasified coal. This SOFC/CAES/CCS system is capable of generating load-following power from gasified coal with essentially 100% carbon capture and high efficiencies relative to the current state-of-the-art. A simplified block diagram of the proposed integrated SOFC/CAES process is given in Fig. 3. A more detailed PFD of the proposed integrated process is provided in Fig. 4 and a more detailed model description is provided in Section 2.

In this work, we perform techno-economic, load following and overall system performance analyses of sixteen configurations of the integrated SOFC/CAES process described above. Aspen Plus v7.3 was used for the steady-state computations of mass and energy flows throughout the process, and in-house models implemented

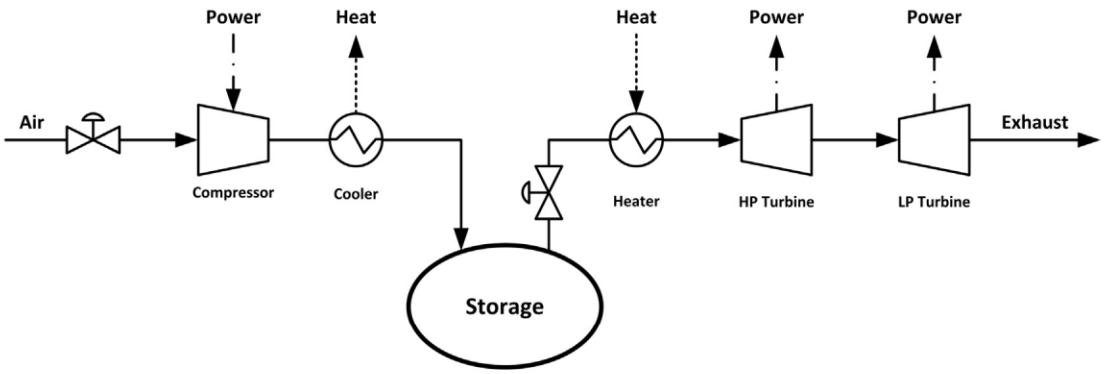

Fig. 2. Simplified CAES system schematic. Reproduced from Ref. [10].

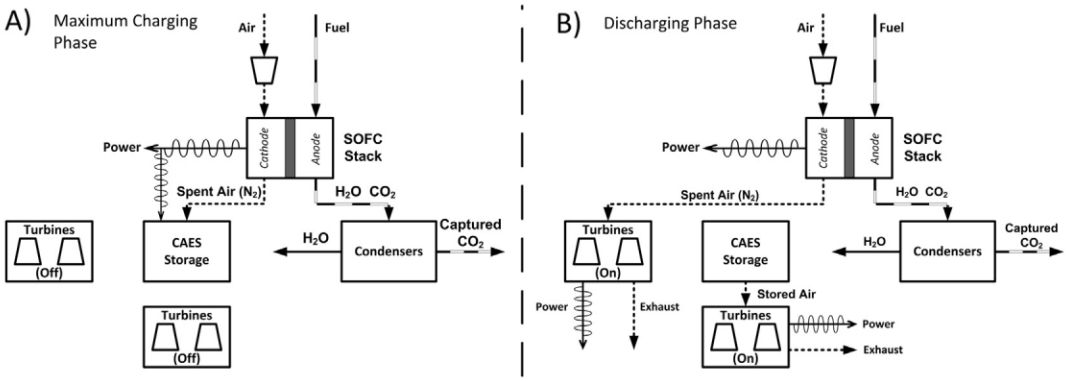

Fig. 3. Simplified SOFC/CAES integration technique during (A) the maximum charging phase, and (B) the discharging phase. Reproduced from Ref. [51].

in MATLAB were used for dynamic simulations performed using a pseudo steady-state approach. For load-following and economic performance evaluations, the historical power demand and price profiles for the province of Ontario, Canada in 2011 are used [39]. The boundaries for this analysis are the plant gates, and do not include transmission of electricity in or out of the plant, or the costs associated with the transport of fuels. These boundaries are chosen to be consistent with those of the NETL SCPC studies [7] to which the results are compared.

In this work, the SOFC/CAES system is shown to be a promising process which is able to produce load-following electric power from coal with very low direct and indirect CO_2 emissions. The CAES is shown to provide load-following abilities sufficient to the needs of actual grid behaviour at only a small price premium over baseline-only power generation using SOFCs. In addition, sensitivity analysis results show that the SOFC/CAES system can even be the best option from a pure economic point of view under certain realistic market conditions and carbon tax policies.

2. Simulation models

There have been several studies on the systems-level implementation of SOFCs and gas turbines for electricity generation using coal [20–23] or natural gas [40–45] as fuel sources (see Adams et al. (2012) for a review of these studies [13]). Detailed modelling decisions and assumptions for the SOFC model used in this work are available in Adams and Barton (2010); since this is an extension of our prior work, many of the same modelling parameters are used so that a meaningful comparison between the results may be drawn [18]. The SOFC model was integrated with a CAES process model to create the SOFC/CAES process presented in Fig. 4. Air separation, gasification and syngas cleaning, syngas shifting and impurity removal, power generation, heat recovery, and CO_2 recovery are the major components of the SOFC model. A brief description of each section is provided, but the reader is referred to our prior work for a more in-depth discussion [18]. The CAES system consists of compression, storage, and expansion models. The following sections give an overview of each of these process steps in turn.

2.1. Steady-state simulation and modelling approach

The SOFC was sized to target a base-load net power output of 719 MW when carbon capture is enabled (including the net power produced by the SOFCs, the bottoming expansion turbines utilizing stream 6.5 on the cathode side, and the HRSG). The US Department of Energy anticipates that MW-scale SOFC stacks will be available for demonstration by 2020, and therefore this scale of plant is considered to be reasonable for the forward-looking plant designs discussed in this work [46]. Multiple plant configurations are discussed in section 3. Each plant was scaled to achieve this same 719 MW output as the basis of comparison. The feedstock for this process was assumed to be Illinois #6 bituminous coal, which has a HHV of 27.267 MJ kg^{-1} [47]. By weight, the coal contains 63.75% C, 4.5% H, 1.25% N, 0.29% Cl, 2.51% S, 11.12% H_2O and the balance ash. Steady-state simulations of the SOFC/CAES system were performed in Aspen Plus v7.3 using the Peng–Robinson equation of state (EOS) with the Boston–Mathias modification with a few exceptions [48]: the NBC/NRC steam tables were used for pure water streams, the Electrolyte-NRTL method with Henry coefficients from the AP065 databank was used for streams consisting of mostly CO_2 and H_2O near the critical point of CO_2, and the Redlich–Kwong–Soave EOS with predictive Holderbraum mixing rules was used for streams containing mostly CO_2 and H_2O below the critical point of CO_2. A detailed discussion regarding the selection of each thermodynamic method and any other process assumptions (unless explicitly stated otherwise) for the portions of the process which do not involve CAES are available in our prior work [18].

2.2. Solid oxide fuel cell process model

2.2.1. Air separation

The air separation unit (ASU) serves to obtain high-purity oxygen from atmospheric air for use in various downstream process units. The majority of the separated O_2 is used in the gasifier, with small amounts also being used in the post-SOFC oxidation unit (stream 6.2 in Fig. 4) and the Claus unit for sulphur removal (stream 1.3 in Fig. 4). 94% of the oxygen in the feed air stream is recovered at 10 bar and 32.2 °C. The parasitic energy load of the ASU is accounted for by detracting from the steady-state base load of the plant. A more detailed description of this process and each unit is given in the prior work and is thus omitted here for the sake of brevity [18]. However, it is important to note that the ASU for this process was originally designed for an IGCC process in which the N_2 (which is a waste stream in this process) is used elsewhere in the process [7]. Consequently, it may be possible to improve the ASU process' efficiency by avoiding the production of high-pressure N_2, which is left as a future study in this work.

2.2.2. Gasification and syngas cleaning

The gasifier converts coal and water into syngas, which is modelled as a mixture of H_2, CO, H_2O, CO_2 and other gaseous impurities including N_2, Ar, HCl, COS, NH_3, Hg, CH_4 and H_2S. When possible, water is recycled to the gasifier from downstream processes, which contains small amounts of CO_2. The gasifier operates exothermically and the waste heat can be used for different

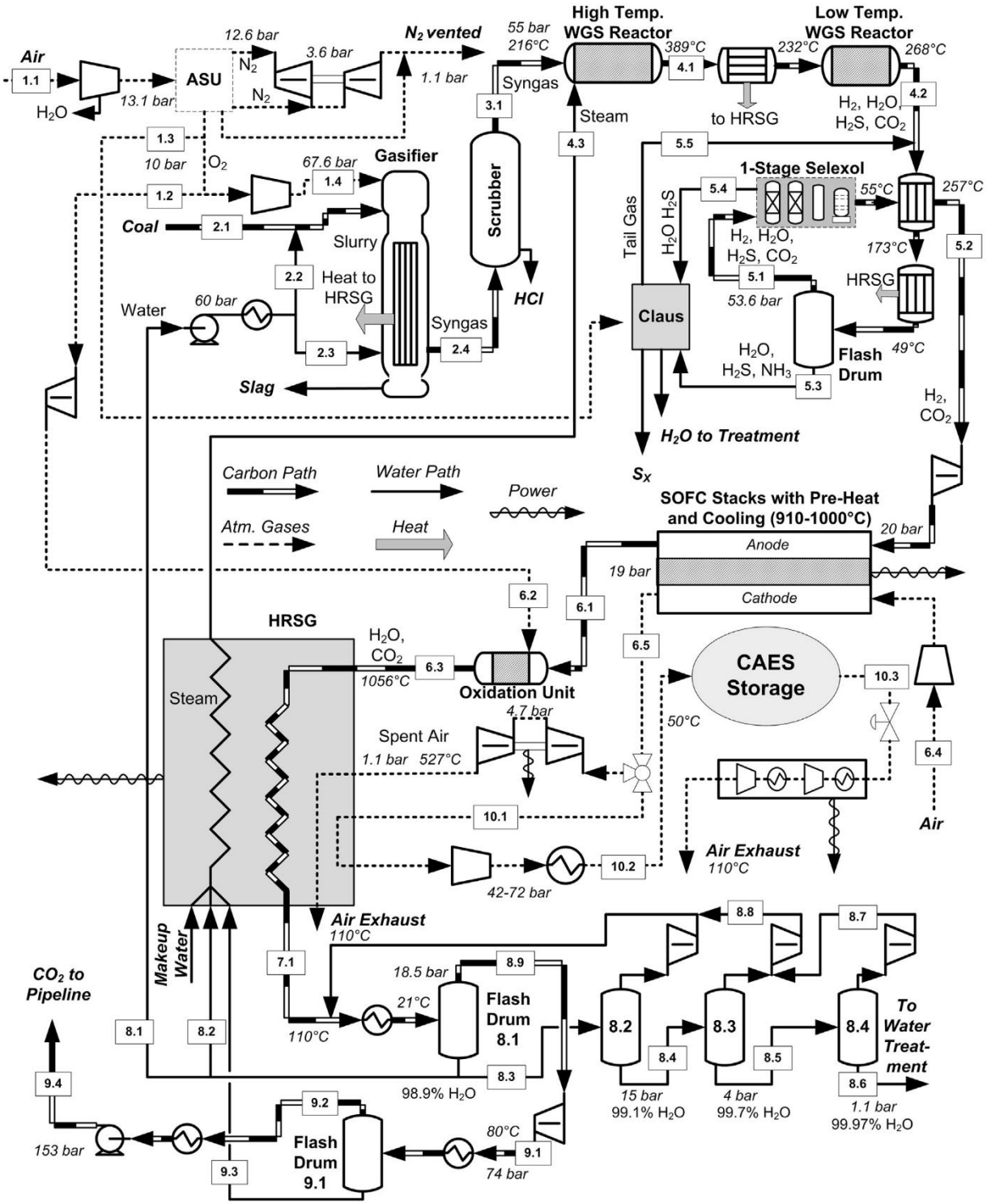

Fig. 4. PFD of proposed SOFC/CAES plant including optional WGS reactors, CAES storage/turbomachinery, and CCS.

purposes. For designs in which CAES is not used (i.e., the prior work [18]), the waste heat is used to generate steam for additional power generation in the HRSG. When CAES is enabled, some of the waste heat can instead be recovered for the pre-heating of the CAES discharge stream, which will be discussed in Section 2.3. Non-combustibles in the coal are recovered as a molten slag stream. To be consistent with our prior work and commonly used baseline studies [7], a GE Radiant-Only gasifier at 56 bar and 1300 °C was used. The syngas and slag product streams are assumed to be cooled to 210 °C before moving to any downstream processes. Further modelling details, including gasifier reactions, are given in our prior work [18].

SOFC stacks are very susceptible to impurities such as HCl and H_2S [49–51]. For simplicity, a detailed scrubbing step is omitted from this investigation, and 100% of the HCl produced in the gasifier is assumed to be removed. H_2S removal is described next.

2.2.3. Syngas shifting and impurity removal

After the syngas has been cleaned, it may optionally be sent to a water–gas shift (WGS) step in order to increase the H_2:CO ratio prior to entering the fuel cell. It is a subject of current debate as to whether or not the WGS step is required for SOFC systems, and it is not yet clear if future large-scale implementations of SOFCs will include this step during fuel preparation. Competing issues such as carbon deposition on the anode via the Boudouard equation, decreased theoretical cell voltage, sensitivity to sulfide poisoning depending on fuel gas CO content, exergetic losses, and increased capital costs must all be addressed before a consensus can be reached [52]. Therefore, in this study each system configuration was simulated both with and without the WGS step, which was not considered in our prior work.

When the WGS step is included most of the CO in the fuel stream is converted to CO_2 through two packed-bed reactors in series. First, a high-temperature (300–450 °C) reactor achieves about 80% conversion of the inlet CO, then a low-temperature (200–300 °C) reactor is assumed to reach chemical equilibrium, corresponding to an overall conversion of approximately 96%. One convenient side reaction that takes place in the WGS reactors is that of COS hydrolysis:

$$COS + H_2O \rightleftharpoons CO_2 + H_2S. \quad (4)$$

Due to the high H_2O:COS ratio in the WGS reactors, it is assumed that the COS hydrolysis reaction reaches 100% conversion. This is beneficial to the sulphur recovery step because H_2S is more easily recovered from the fuel stream than COS. Further design details (such as types of catalyst packing) and sample steady-state stream conditions are available in our prior work [18].

After the optional WGS step, impurities such as sulphur, ammonia and mercury must be removed prior to entering the SOFC anode. Mercury transport was not modelled in this investigation, and it is thus assumed that the trace amounts of mercury in the fuel stream are removed via a mercury removal process (not shown in Fig. 4). A one-stage Selexol process is used to remove H_2S (and any COS if a WGS step is not used) from the fuel stream because the SOFCs cannot tolerate sulphur concentrations higher than 100 ppm [53,54]. Since the fuel stream must be cooled to near-ambient conditions (49 °C) prior to entering the Selexol process, most of the NH_3 is condensed out with the entrained water vapour through a series of coolers and is sent to a Claus process for treatment. The Selexol process is designed to be able to remove 99.6% of the H_2S in the fuel stream [18]. The product sulphur stream is combusted with high-purity O_2 in a Claus furnace to form sulphur (S_x) compounds, with 4.2% of the H_2S present in the Claus process feed stream remaining unrecovered in the tail gas.

2.2.4. Power generation and heat recovery

The SOFC is the heart of this process and generates the bulk of the system's power through the electrochemical reactions (1), (2) and (3). It is assumed that the SOFC stacks operate at a 950 °C and 20 bar (primarily constrained by material limitations) [55]. The syngas leaving the impurity removal step (stream 5.2 in Fig. 4) is expanded to 20 bar, heated to 910 °C and fed to the anode of the fuel cell stack. Air obtained from the atmosphere is fed to the cathode at the same conditions after a compression and heating step. Separate anode and cathode exhausts prevent the mixing of N_2 and CO_2, promoting convenient CO_2 capture and sequestration (see Section 2.2.5) [10]. The anode exhaust is completely oxidized with high-purity O_2 provided by the ASU to mostly H_2O and CO_2 in a fuel completion step. The SOFC stack models were updated from Ref. [18] to account for the new design condition in two ways. First, the overall fuel utilization of the SOFC stacks was changed to 86% (from 99.5%). Second, the ideal cell voltage when the WGS step is omitted was lowered to 0.6 V to reflect the impact of H_2S (at approximately 20 ppm after the impurity removal step) on the anode in the presence of CO [51]. When running on near-pure H_2 (as is the case when the WGS step is included), the ideal cell voltage is maintained at 0.719 V [55]. It is assumed that 5% of the heat generated in the cell is lost to the surroundings, and that the DC/AC conversion is 96% efficient [53,55]. The proposed design uses six parallel SOFC trains such that each one can be turned off for a few months every three years for maintenance and seasonal power adjustments [10].

Table 1
Operating characteristics the CAES section of the proposed SOFC/CAES integrated system [53].

Operating condition	Value	Units
Air turbines (CAES power train in Fig. 4)		
Rated turbine power	200	MW
Maximum air flow rate	440	kg s^{-1}
Inlet pressure to HP turbine	40	bar
Inlet temperature to HP turbine	550	°C
Inlet pressure to LP turbine	6	bar
Inlet temperature to LP turbine	825	°C
Turbine efficiency	75	%
Compressor (compresses steam 10.1 in Fig. 4)		
Maximum air flow rate	210	kg·s^{-1}
Rated compressor power	140	MW
Temperature at exit of after-cooler	50	°C
Pressure at exit of after-cooler	42–73	bar
Compressor isentropic efficiency	75	%
Cavern		
Volume of storage space	600,000	m^3
Cavern operating pressures	40–72	bar
Maximum cavern pressure	72	bar
Cavern wall temperature	50	°C

After exiting the anode, the fuel exhaust stream (which still contains small amounts of CO and H_2) is sent to an adiabatic oxidation reactor where it is reacted with stoichiometric amounts of O_2, resulting in a stream consisting of almost entirely H_2O and CO_2. Before being sent to the CO_2 removal step, the heat contained in the anode exhaust is used to generate steam in the HRSG. The path of the cathode exhaust stream is dependent on the operational objective of the combined SOFC/CAES plant at any point in time. When the demand for electricity is below that of the plant's base load or its price is relatively low, the cathode exhaust is compressed beyond the 20 bar operating pressure of the SOFC to the necessary pressure for storage in the CAES cavern. When the price or demand for electricity is high, the cathode exhaust is sent to a steady-state bottoming cycle to recover as much energy as possible. In both cases, any excess thermal energy contained within the cathode stream is recovered via the HRSG.

The heat exchanger network (HEN) designs as well as the HRSG are modelled using a simple approach [18] and are not discussed here for the sake of brevity. However, the two main assumptions for this section are: (1) the HEN avoids temperature crossover but assumes an ideal minimum approach temperature of 0 °C, and (2) all waste heat between 110 and 950 °C is considered to be a useful heat source in the steam generation process. The techno-economic analysis presented in the results section includes all capital expenditures relating to the HRSG equipment.

2.2.5. CO_2 recovery and sequestration

Since the completed fuel stream is primarily CO_2 and H_2O, effective CO_2 separation can be obtained through a series of liquid/vapour flash unit operations after it is cooled in the HRSG [17].

Some of the high purity water that is recovered is used as make-up water for either process steam or power generation (via the HRSG). Surplus water is not considered in this analysis, but it may be treaded and used for other purposes if not released as a waste product. The CO_2 rich vapour is compressed to 74 bar and flashed once more to remove any remaining water, resulting in the CO_2 purity required for pipeline transit [56]. The CO_2 stream is compressed to a supercritical fluid and pumped to 153 bar before it leaves the plant for sequestration. Essentially 100% of the CO_2 in the incoming fuel stream is captured, and water is recovered at 99.97% purity.

2.3. Compressed air energy storage process and model

The CAES section was partially modelled in Aspen Plus in the same fashion as our prior work, with stream and unit connection adjustments made as necessary due to the differences between gasified coal- and natural gas-fed systems [10]. Moreover, the general design and operating parameters of the CAES process are typical of those used in other CAES literature, including those used in our prior investigation. These parameters are provided in Table 1, and further details describing the operation of the CAES system and its equipment selection can be found in our prior work but are omitted here for the sake of brevity [10,57,58].

2.4. Dynamic simulation modelling approach

The CAES dynamic modelling approach is modified from the approach developed in our prior work for natural gas fuelled SOFC/CAES systems [10] to adjust for the presence of coal fuels. A pseudo-steady-state model was used to account for the dynamics of the SOFC/CAES system. Streams and units that are considered transient involve those downstream of stream 6.5. In contrast, all units upstream of stream 6.5 and downstream of 6.1 (gasification and syngas shifting/cleanup, SOFC stacks, the CCS section, and related heat integration) are operated as a base-load plant and hence are not considered in the pseudo-steady-state model.

The goal of the pseudo-steady-state model is to compute the operating conditions of the SOFC/CAES at any given control interval. To do this, one-hour control intervals are used in which the system is assumed to achieve steady-state instantly and hold it for the hour. This is appropriate because accurate predictions of future power demand (up to 24 h in advance) are available at one hour increments [39] and because the compressor and turbine dynamics are very fast, requiring seconds to minutes to achieve major swings in power, [29,59].

At each control interval, the model must calculate the required flow rate of air to or from the cavern based on the power desired and the amount of air stored in the cavern. To do this with the rigorous Aspen Plus model requires an approximately 15 min of CPU time per control interval (Intel® Core-2 Quad @2.66 GHz and 7 GB RAM), or about 91 days per simulation. Instead, a reduced model was constructed by running the Aspen Plus model to generate a data table mapping the flow rate of air into the CAES cavern, the corresponding compressor pressure, and net operating power, and then fitting a nonlinear equation to that data. This brought the simulation time from 91 days to about 80 s. See the prior work for details such as the model structure and logical implementation [10].

2.5. Combined plant scenario and operational objectives

For the purposes of this study, it is assumed that the operational objective of the combined SOFC/CAES plant is to provide reliable peaking power for a large community (demand patterns ranging between 500 and 900 MW) that exhibits the same relative peaking load profile as the province of Ontario, Canada [39]. Consequently, historical market data for the province of Ontario for the calendar year of 2011 was scaled to a plant average of 719 MW and is used as the forecasted demand profile for dynamic simulations. Uncertainties and stochastic demand considerations are not considered; their impact on the optimal performance of the SOFC/CAES plant is left to future work. In the cases where the integrated SOFC/CAES system is incapable of providing the load demanded (whether due to operational constraints or the storage cavern being empty or unavailable), it is assumed that all supplementary power is purchased from the grid at the historical Ontario market price for that particular hour and day. Furthermore, it is assumed that a natural gas combined cycle (NGCC) peaking plant is used to generate any supplementary power and that it emits 50.29 g of CO_2-equivalents per MJ of electricity generated, which must be accounted for as an indirect emission of the proposed SOFC/CAES plant [61]. Finally, it is assumed that any power generated by the plant beyond the demanded load (for example, when the storage cavern is full and base-load operation is the only available mode of operation) is curtailed with no financial benefits (or penalties) to the plant.

This study associates the economic and load-following performance of the integrated SOFC/CAES plant using the following metrics [61]:

$$\mathrm{LCOE} = \sum_{t=0}^{N}\left(\frac{\frac{I_t+M_t+F_t}{(1+r)^t}}{\sum_{t=0}^{N}\frac{P_t}{(1+r)^t}}\right) \tag{5}$$

$$\mathrm{SSE} = \sum_{i=1}^{n}\left(P_{\mathrm{P},i} - D_i\right)^2 \tag{6}$$

$$\mathrm{WSSE} = \sum_{i=1}^{n} U_i^2 + \left(\frac{O_i}{2}\right)^2, \tag{7}$$

where LCOE, SSE and WSSE are the levelized cost of electricity, the sum of squared-errors, and the weighted sum of squared-errors between supply and demand. In the LCOE calculation I_t, M_t, F_t and P_t are the capital investment, maintenance costs, fuel costs and total sellable power produced in year t, respectively. The plant lifetime is N years (assumed to be 20 years) and is discounted at a real interest rate of r (10%). The variable D_i represents the demand at interval i over n time steps (1 h per time step for one year). O_i is the amount of power over-produced by the plant and U_i is the amount under-produced by the plant at time step i.

As is the case in industry, a balance is sought between economic, environmental and overall system performance. For these reasons, the LCOE is used to give insight into the economic performance of the proposed system configurations relative to each other and the current SCPC option. CO_2 emissions are accounted for using a carbon tax (which is the subject of a sensitivity analysis) and are reflected in the LCOE. The SSE and WSSE are used to compare the load-following capabilities of each system; the WSSE differs from the SSE in that it more heavily weights times when demand exceeds supply, and hence additional grid power must be purchased.

2.6. Case studies

Eighteen different plant configurations have been considered and their performances compared in each of the load-following scenario described in Section 2.5. The first two cases are standard SCPC plants scaled to a fixed output of 719 MW, one of which

includes CCS [7]. The SCPC plant using CCS is capable of 90% removal of CO_2 using a solvent-based technique [7]. The sixteen new cases that have been investigated involve every possible configuration of the SOFC/CAES plant incorporating any of the WGS step, CCS, and a train shut-down (TSD) schedule. A summary of the features of each case is given in Table 2. Simulation and financial calculation parameters are consistent with our prior work and are provided in Table 3 [10]. A base-case carbon tax of \$50/tonne of CO_2 emitted is considered, but is treated as a sensitivity variable in later analysis. Various carbon taxes of up to over \$100 tonnes^{-1} have been reported in other recent works [63,64]. Train shut-down involves the lowering of the plant's base-load output, and allows for consistent cleaning and maintenance of the SOFC stacks to be performed during periods of seasonally low demand while not affecting upstream units and saving fuel costs. The CAES system is able to, for the most part, meet the daily peaks during the seasons in which TSD is used, and any shortcomings are accounted for in the economic and performance analyses. See our prior work for more details [10].

Capital and operating cost results were obtained from making manual adjustments and using appropriate scaling factors in combination with Aspen Icarus cost estimation software, published cost estimates, and correlations provided by Seider et al. [65]. Unit sizing and justification can be found in our prior work and is not repeated here [18]. The most recent available target for FuelCell Energy's (a world leader in SOFC stack manufacturing) SOFC stack costs at maturity is \$317 kW^{-1} (US\$2007) and includes all accessories and balance-of-plant units for a 10 year stack lifetime [66]. Redox Power Systems, an emerging SOFC manufacturer, is targeting a release of their SOFC technology for purchase in 2014 at a cost of \$1000 kW^{-1} [67]. A price of \$500 kW^{-1} (requiring two stacks for a total of \$1000 kW^{-1} over the 20 year plant lifetime) is therefore assumed to be a conservative SOFC stack cost estimate for this future application. The CAES costs are those of the source wells, storage cavern construction, compressors, turbines and related heat equipment. The CAES plant is equal in size to our prior investigation, and hence the unit and process costs are the same as those used in our prior work and the references therein [10,65,68]. The price of Illinois Bituminous #6 coal is assumed to begin at \$45.0 tonnes^{-1} and be subjected to an inflation rate of 2.5% per year of operation. Overall, the base case cost estimates are meant to be as accurate as possible for the well-established technologies, but conservative for the up-and-coming technologies. A sample spreadsheet that itemizes the capital and operating costs for each of the plants examined is provided as Supplementary material.

Table 2
Description of simulated cases.

Case number	Tag	WGS enabled?	CAES enabled?	TSD enabled?	CCS enabled?
Pulverized Coal Systems					
1	SCPC	N/A	N/A	N/A	No
2	SCPC–CCS	N/A	N/A	N/A	Yes
SOFC Systems					
3	WGS	Yes	No	No	No
4	WGS–CCS	Yes	No	No	Yes
5	WGS–TSD	Yes	No	Yes	No
6	WGS–CCS–TSD	Yes	No	Yes	Yes
7	WGS–CAES	Yes	Yes	No	No
8	WGS–CCS–CAES	Yes	Yes	No	Yes
9	WGS-TSD-CAES	Yes	Yes	Yes	No
10	WGS–CCS–TSD–CAES	Yes	Yes	Yes	Yes
11	nWGS	No	No	No	No
12	nWGS–CCS	No	No	No	Yes
13	nWGS–TSD	No	No	Yes	No
14	nWGS–CCS–TSD	No	No	Yes	Yes
15	nWGS–CAES	No	Yes	No	No
16	nWGS–CCS–CAES	No	Yes	No	Yes
17	nWGS–TSD–CAES	No	Yes	Yes	No
18	nWGS–CCS–TSD–CAES	No	Yes	Yes	Yes

Table 3
Assumed parameters for case studies.

Parameter	Value	Units[a]
Initial price of coal	45.00	\$ tonnes^{-1}
HHV of coal	27,267	kJ kg^{-1}
CO_2 tax[b]	50.00	\$ tonnes^{-1}
Plant lifetime	20	Years
Discount rate	10.0	%
Inflation rate	2.5	%

[a] Cost units are expressed in US\$2007 using the Chemical Engineering Cost Index [62].
[b] This CO_2 tax is the "standard" for comparison, but is investigated in greater detail in Section 3.4.

3. Results and discussion

3.1. Overall system results and performance

3.1.1. Comparison of SCPC and SOFC processes

A summary of the operational results for each case investigated is presented below in Table 4. It is clear in this table that the SOFC systems, in general, behave differently than the traditional SCPC process. SOFC-based systems use less fuel that the SCPC plants, particularly in the cases where CCS is enabled. The base-load SOFC plant with WGS enabled, for example (case 3), uses 7% less coal (~150,000 tonnes per year) than the SCPC process. When CCS is enabled, the high parasitic energy costs associated with solvent-based CCS in the SCPC plant causes its fuel consumption to increase drastically in order to provide the same base load, whereas the SOFC–CCS (case 4) plant configuration is able to provide nearly the same amount of power without an increase in fuel consumption. When comparing cases 2 and 4, the fuel savings experienced by the SOFC base-load plant over its SCPC counterpart approaches 1,080,000 tonnes per year (35% savings). Furthermore, it can be seen that the direct CO_2 emissions from all of the SOFC plants with CCS are negligible, whereas they are still significant with the SCPC–CCS case due to the imperfect CO_2 recovery of the solvent-based CCS approach. It is also clear in Table 4 that all of the WGS-enabled SOFC processes (cases 3–10) have efficiencies 2.5–3.7 percentage points higher than the SCPC process, even with the inclusion of CAES and TSD (cases 7–10). When CCS is required, the SOFC-based systems are as much as 15 percentage points more efficient.

3.1.2. Effect of water–gas shift step

When comparing similar cases with and without the WGS step (cases 3–11, 4–12, etc.), it is clear that the overall efficiency of the plant decreases by approximately 3 percentage points. This lowered efficiency is mainly due to the decreased effectiveness of the SOFC stacks, caused by the presence of small amounts of H_2S in the cleaned fuel stream. The ideal potential of the SOFCs is more affected by H_2S in the presence of CO, leading to an overall lower efficiency of the SOFC stack, and therefore the entire plant. Furthermore, the CO oxidation reaction (Equation (2)) is more exothermic than the oxidation of H_2 (Equation (1)). Consequently, more energy from the fuel stream is lost to the surroundings through process inefficiencies as heat, and a greater degree of the chemical energy contained in the fuel stream is converted to thermal energy in the exhaust stream, instead of electricity. Although most of this additional heat is recovered in the HRSG, the lower overall efficiency of the HRSG compared to the SOFC stacks

Table 4
Overall and environmental system performance.

Case	1 SCPC	2 SCPC CCS	3 WGS	4 WGS CCS	5 WGS TSD	6 WGS CCS TSD	7 WGS CAES	8 WGS CCS CAES	9 WGS TSD CAES
Direct fuel usage (10^3 tonnes yr^{-1})	2137	3070	1988	1988	1799	1799	1988	1988	1799
Direct CO_2 emitted (10^3 tonnes yr^{-1})	5065	724.5	4463	0	4038	0	4463	0	4039
Indirect CO_2 emitted (10^3 tonnes yr^{-1})	48.99	48.99	40.48	48.99	85.02	102.4	14.51	20.56	54.25
Total CO_2 emitted (10^3 tonnes yr^{-1})	5114	773.5	4504	48.99	4124	102.4	4478	20.56	4093
CO_2 sequestered (10^3 tonnes yr^{-1})	0	7245	0	4463	0	4039	0	4463	0
Electricity generated (10^3 MW-h yr^{-1})	6300	6300	6422	6300	5809	5699	6345	6217	5640
Electricity sold (10^3 MW-h yr^{-1})	5390	5390	5411	5390	5301	5258	5474	5459	5377
Electrical efficiency[a] (%HHV)	39.1	28.4	42.9	42.0	42.8	42.0	42.3	41.5	41.6

Case	10 WGS–CCS TSD–CAES	11 nWGS	12 nWGS CCS	13 nWGS TSD	14 nWGS CCS TSD	15 nWGS CAES	16 nWGS CCS CAES	17 nWGS TSD CAES	18 nWGS–CCS TSD CAES
Direct fuel usage (10^3 tonnes yr^{-1})	1799	2175	2175	1969	1969	2175	2175	1969	1969
Direct CO_2 emitted (10^3 tonnes yr^{-1})	0	4939	0	4469	0	4939	0	4469	0
Indirect CO_2 emitted (10^3 tonnes yr^{-1})	76.05	39.60	48.99	83.21	102.4	13.35	19.75	30.35	45.69
Total CO_2 emitted (10^3 tonnes yr^{-1})	76.05	4979	48.99	4552	102.4	4952	19.75	4500	45.69
CO_2 sequestered (10^3 tonnes yr^{-1})	4039	0	4939	0	4469	0	4939	0	4469
Electricity generated (10^3 MW-h yr^{-1})	5509	6436	6300	5821	5699	6366	6226	5673	5551
Electricity Sold (10^3 MW-h yr^{-1})	5323	5413	5390	5305	5258	5477	5461	5435	5398
Electrical efficiency (%HHV)	40.6%	39.3%	38.4%	39.2%	38.41%	38.8%	38.0%	38.2%	37.4%

[a] Electrical efficiency is calculated as the total power generated by the plant divided by the total HHV fuel input to the plant on a basis of 1 year, whether or not that electricity was actually "sold" to the grid for profit.

lead to a decreased thermal efficiency of the plant overall. As such, in order to achieve comparable base-load plant outputs, the non-WGS cases require an overall higher fuel input to compensate for their lower efficiencies. Higher fuel consumption further causes as much as a 10% increase in the amount of carbon sequestered or emitted, causing increased operational costs. Whether or not the higher operating costs associated with omitting the WGS step outweigh the increased capital costs associated with its implementation in a purely economic sense is discussed in Section 3.2.

3.1.3. Effect of compressed air energy storage

As expected, the addition of CAES (cases 7–10 and 15–18) marginally decreases the overall thermal efficiency of the proposed system. This efficiency decrease is due to the higher losses associated with the CAES turbomachinery, as well as a less effective heat integration strategy due to an additional cooling/pre-heating step to/from 50 °C (recall it is assumed that the HRSG cannot recover energy in streams below 110 °C). However, these efficiency penalties are on the order of 1 percentage point, which is quite promising considering the significant practical value of peaking power which it enables. The improved peaking capabilities provided by the integrated CAES system significantly reduces the power that must be purchased from the grid over a one-year operating period. Consequently, the indirect CO_2 emissions for CAES-enabled plants are always lower than those of their non-CAES counterparts. This effect is even more prominent in the TSD cases, where the CAES system is utilized to a higher degree due to the seasonal shifts in base-load output. For example, when comparing cases 13 and 17 (See Table 4), case 13 requires approximately 177,000 MW-h less of purchased grid electricity, which corresponds to a decrease in CO_2 emissions of 53,000 tonnes (63.5%) over a one-year operating period. Finally, it should be noted that in scenarios when grid power is not available, the addition of CAES greatly improves reliability while also allowing for a much smaller base-load plant to be constructed.

3.1.4. Effect of train shutdown

As can be seen in Table 4, the addition of TSD to the SOFC-based systems has a negligible impact on the overall efficiency of the plant. However, adding TSD significantly reduces the amount of coal consumed due to its reduced operating level for several months of the year. For example, case 5 uses approximately 188,000 tonnes less of coal per year than case 3 (9.5%), which further leads to a proportional decrease in CO_2 emissions (when CCS is not implemented) or sequestration (when CCS is implemented). However, these decreases in fuel consumption and exiting CO_2 amounts come at the cost of meeting less consumer demand, leading to an increase in indirect CO_2 emissions stemming from grid electricity purchases. More detail regarding the effects of TSD on economics and load following are discussed in the proceeding sections.

3.2. Economic results

3.2.1. Comparison of SCPC and SOFC processes

Table 5 contains a summary of the economic data for each plant configuration examined in this work. Case 1 (SCPC) requires the

Table 5
Economic results for each of the plant configurations simulated.

Case	1 SCPC	2 SCPC CCS	3 WGS	4 WGS CCS	5 WGS TSD	6 WGS CCS TSD	7 WGS CAES	8 WGS CCS CAES	9 WGS TSD CAES
Capital cost ($1,000,000s)	1015	1849	1835	1873	1835	1873	2059	2097	2059
Grid power cost ($1000s yr^{-1})	5456	5456	4598	5456	8741	10,346	1762	2460	5159
Fuel costs ($1000s yr^{-1})	96,140	138,170	89,470	89,470	80,960	80,960	89,470	89,470	80,960
CO_2 Emission costs[c,d] ($1000s yr^{-1})	255,700	56,790	225,200	13,610	206,200	15,220	223,900	12,190	204,600
Operating costs[a] ($1000s yr^{-1})	39,700	85,270	60,960	72,110	60,680	70,780	60,960	73,870	62,430
LCOE[b] (¢ kW^{-1} h^{-1})	5.35	9.12	7.42	7.80	7.47	7.88	7.78	8.15	7.81
LCOE[c] with CO_2 tax (¢ kW^{-1} h^{-1})	11.04	9.98	12.40	7.85	12.13	7.99	12.69	8.17	12.36

Case	10 WGS–CCS TSD CAES	11 nWGS	12 nWGS CCS	13 nWGS TSD	14 nWGS CCS TSD	15 nWGS CAES	16 nWGS CCS CAES	17 nWGS TSD CAES	18 nWGS–CCS TSD CAES
Capital cost ($1,000,000s)	2097	1861	1901	1861	1901	2090	2130	2090	2130
Grid power cost ($1000s yr^{-1})	6877	4506	5456	8571	10,346	1635	2374	3537	5114
Fuel costs ($1000s yr^{-1})	80,960	97,900	97,900	88,580	88,580	97,900	97,900	88,580	88,580
CO_2 emission costs[c,d] ($1000s yr^{-1})	13,900	248,900	14,800	227,600	16,290	247,600	13,340	225,000	13,460
Operating costs[a] ($1000s yr^{-1})	72,530	61,220	73,570	60,930	72,100	62,970	75,320	62,680	73,850
LCOE[b] (¢ kW^{-1} h^{-1})	8.24	7.66	8.08	7.69	8.14	8.04	8.43	7.93	8.36
LCOE[c] with CO_2 tax (¢ kW^{-1} h^{-1})	8.32	13.17	8.13	12.83	8.26	13.45	8.46	12.89	8.41

[a] Operating costs include labour, maintenance, catalysts, water consumption, CO_2 transport costs, and materials.
[b] Does not include a CO_2 tax.
[c] Includes a CO_2 tax of $50 $tonnes^{-1}$.
[d] Includes sequestration costs of $2.5 $tonnes^{-1}$.

lowest total capital investment due to its high maturity and proven technology when compared to any of the SOFC-based cases. In fact, the SCPC plant costs at least $860 million less than any of the SOFC cases when CCS is not required. However, case 2 indicates that the addition of CCS to the SCPC plant would bring its capital costs up significantly, approaching the costs of an SOFC system while at the same time greatly increasing fuel requirements (due to the much lower efficiency resulting from CCS addition). Although the fuel costs for case 1 are higher than most of the SOFC cases (some non-WGS cases are less efficient overall than the SCPC plant), the increase in fuel costs is overshadowed by its lower capital and operating costs. The resulting LCOE for the SCPC case is 5.35 ¢ kW^{-1} h^{-1} and is the lowest among all cases when no CO_2 tax is implemented and CCS is not required. However, when a CO_2 tax of $50 $tonnes^{-1}$ is implemented it is clear that the high CO_2 emissions from the SCPC plant cause a significant increase in annual operating costs leading to an unattractive LCOE of 11.04 ¢ kW^{-1} h^{-1} (an increase of 106%). Even when CCS is added to the SCPC plant under a CO_2 taxed scenario, case 2 remains the most expensive option of any CCS-enabled processes investigated. In fact, case 2 has the highest LCOE among all cases examined when no CO_2 emission penalty is included.

3.2.2. Effect of water–gas shift step

When comparing any of the WGS-enabled processes to their non-WGS counterparts, it can be seen in Table 5 that the capital and operating costs for non-WGS cases are actually higher, leading to an increase in LCOE. The increased capital costs stem from the fact that since the non-WGS cases operate at a lower efficiency, the plant must be scaled up (using a higher fuel throughput as discussed in Section 3.1.2) to reach the required base-load output of 719 MW. Consequently, nearly all of the major process units must be scaled up to accommodate this throughput increase. The resulting added capital costs from scale-up slightly outweigh the cost of the WGS reactors themselves, leading to a modest (1–2%) increase in total capital investment. As a result, the higher capital and operating costs of the non-WGS cases lead to higher results for the LCOE metric, regardless of the design decisions. For example, when comparing cases 7 (WGS–CAES) and 15 (nWGS–CAES) in the absence of a CO_2 tax, case 15 has a $30 million higher capital cost and requires an additional $10.5 million per year in total operating and fuel costs, leading to a 3.2% higher LCOE (8.04 ¢ kW^{-1} h^{-1} versus 7.79 ¢ kW^{-1} h^{-1}). It can therefore be concluded from this investigation that the inclusion of a WGS step will decrease the total lifetime cost of the proposed SOFC/CAES plant, bearing in mind that these results are strongly dependant on the value of the ideal voltage when H_2S is in the presence of CO (see Section 2.2.4). It should further be mentioned that the assumed SOFC stack cost of $1000 kW^{-1} was maintained through each plant configuration. In the cases where WGS was not included, the SOFC electrical output decreased significantly, leading to a lower stack cost in the non-WGS cases. Should a constant physical stack size (and therefore cost) have been assumed, the capital cost for the non-WGS cases would have been even higher, further increasing their values for LCOE and motivating the inclusion of WGS.

3.2.3. Effect of compressed air energy storage

As expected, the addition of CAES to the SOFC base-load plant increases capital costs due to the additional turbomachinery and storage investments (see Table 5). However, the addition of CAES offers some decreases in the amount of supplementary grid power that must be purchased and costs associated with indirect CO_2 emissions. Comparing cases 4 and 8, it is clear that the addition of CAES results in a ~$225 million (12%) increase in capital costs. This increase is constant throughout all cases utilizing CAES since the turbomachinery and cavern sizes are all the same. However, the

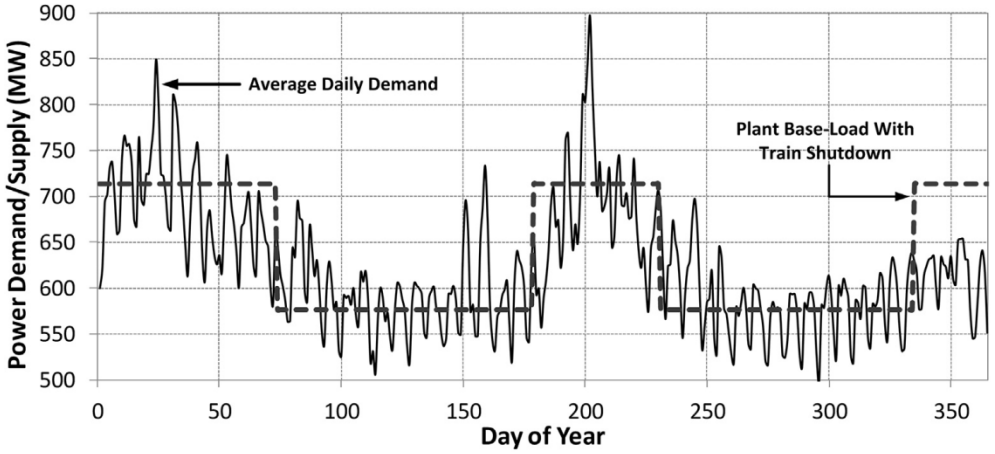

Fig. 5. Average daily demand and base-load plant train shutdown schedule for one simulated year of operation. Reproduced from Ref. [10].

annual amount of grid power that must be purchased decreases by ~$3 million per year (55%) when CAES is enabled. Furthermore, since the CAES-enabled plant in case 8 incurs 28,500 (58%) tonnes per year less indirect CO_2 emissions, it saves an additional $1.5 million per year in CO_2 taxes (assuming $50 tonnes^{-1}). When these effects are combined, the inclusion of CAES can be seen to cause a modest increase in a plant's LCOE of ~0.3 ¢ kW^{-1} h^{-1} or 0.35 ¢ kW^{-1} h^{-1} with or without a CO_2 tax of $50 tonnes^{-1}, respectively. Therefore, with a 3–4% increase in overall electricity costs, the addition of CAES can greatly improve reliability and grid independence. Finally, it is important to mention that if the assumed plant lifetime for this analysis were to increase, the decreased annual operating costs associated with adding CAES would further reduce its relative LCOE to a strictly base-load plant configuration.

3.2.4. Effect of train shutdown

It is clear in Table 5 that the inclusion of TSD has no effect on capital cost. Furthermore, cases with TSD have lower operating and significantly lower fuel costs than their constant base-load counterparts. For example, case 14 uses 9.5% less coal (equating to ~$9.3 million year^{-1}) than case 12. However, TSD significantly increases the amount of grid electricity that must be purchased and the indirect CO_2 emissions associated with it. Case 14 requires almost $5 million year^{-1} more in grid electricity purchases when compares to case 12, corresponding to a 90% increase. Furthermore, the TSD cases are able to sell less electricity by meeting less demand; even though the overall annual operating and fuel costs is lower for cases using TSD, the smaller amount of useable electricity produced results in a slightly higher LCOE. As expected, this gap increases when a CO_2 tax is implemented. Through the combination of TSD and CAES, both fuel savings and reduced dependence on grid electricity (and all associated indirect emissions) is possible but at higher capital cost, essentially providing a hybrid "best of both worlds" scenario.

3.3. Load-following results and performance

A sample plot of demand and power provided by case 8 (WGS–CCS–CAES) is given in Fig. 6, and the corresponding cavern pressure profile is displayed in Fig. 7. Table 6 summarizes the load-following results for each case. The CAES-enabled system is clearly able to follow demand fluctuations above and below the base-load output of the SOFC and HRSG together (the WGS–CCS case) with a high degree of reliability during most of the simulated control intervals.

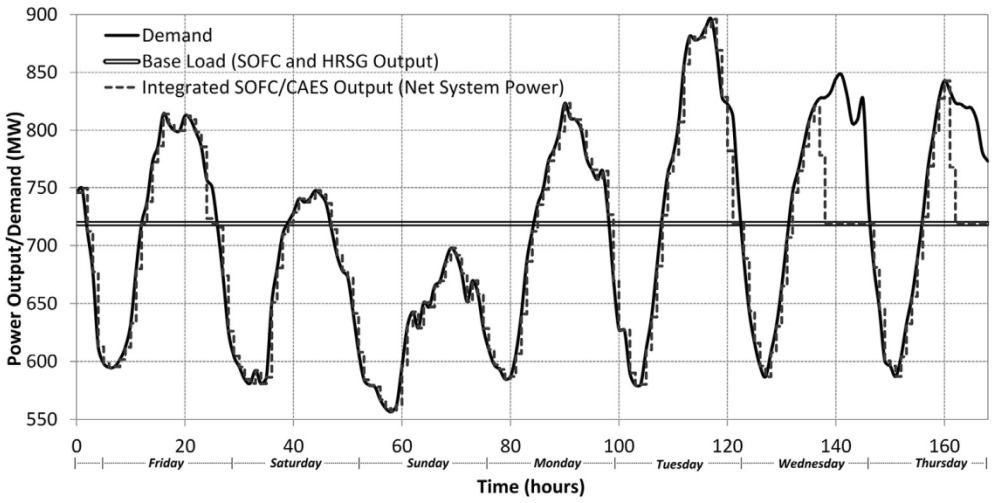

Fig. 6. Simulation results of the SOFC/CAES system for one selected week of operation (June 17–23, 2011). Times in which the output of the SOFC/CAES system matches the base load when demand is less than supply denote times when the cavern is full (at maximum allowable pressure). Times in which the SOFC/CAES system matches the base load when demand exceeds supply denote times when the storage cavern is empty (at minimum allowable pressure).

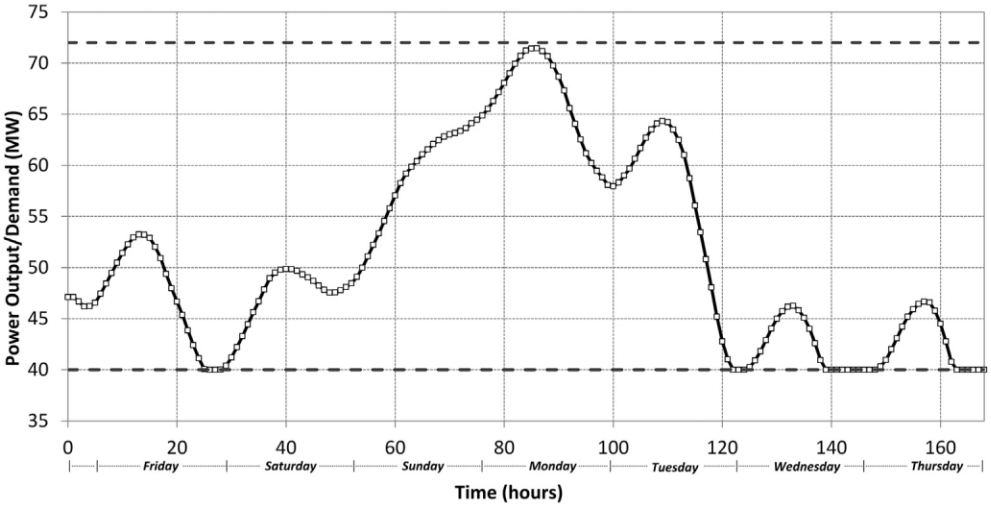

Fig. 7. Pressure profile for one week of simulated operation (June 17–23, 2011).

As reported in Table 6, the addition of CAES to any of the SOFC base-load configurations significantly improves the SSE and WSEE. For example, when comparing case 9 (WGS–CCS–CAES) to case 4 (WGS–CCS), the SSE and WSSE metrics decrease by 42.6% and 38.6%, respectively. Adding TSD also reduces the SSE and WSSE metrics when compared to a standard base-load SOFC plant due to a lower total demand/supply mismatch (this trend is evident in Fig. 5). However, the improvement in WSSE is less significant when TSD is added due to its higher weighting on the under-production of demand. For example, case 5 has a SSE less than 50% of that of case 3 due to the addition of TSD, but the WSSE is reduced by only 29%. Utilizing both CAES and TSD results in the best load following performance because the CAES system is able to minimize the amount of underproduction that arises due to the introduction of TSD. Interestingly, case 18 (nWGS–CCS–TSD–CAES) has the lowest overall SSE and WSSE. Since the SOFC stacks are inherently less efficient in the non-WGS cases, the reduction in base-load output is less significant when TSD is used. Consequently, the ability of the plant (while using TSD) to meet demand using the CAES system is improved, resulting in better load-following during those times.

Table 6
Load-following metric results for cases investigated.

Case	Tag	SSE (10^6 [MW-h]^2)	WSSE (10^6 [MW-h]^2)	Relative SSE	Relative WSSE
1	SCPC	162.6	51.8	0.86	0.93
2	SCPC–CCS	162.6	51.8	0.86	0.93
3	WGS	186.3	55.5	0.98	0.99
4	WGS–CCS	162.6	51.8	0.86	0.93
5	WGS–TSD	88.2	39.1	0.47	0.70
6	WGS–CCS–TSD	81.7	41.8	0.43	0.75
7	WGS–CAES	159.5	44.4	0.84	0.79
8	WGS–CCS–CAES	134.6	40.0	0.71	0.71
9	WGS–TSD–CAES	50.7	24.1	0.27	0.43
10	WGS–CCS–TSD–CAES	45.5	27.7	0.24	0.50
11	nWGS	189.1	55.9	1.00	1.00
12	nWGS–CCS	162.6	51.8	0.86	0.93
13	nWGS–TSD	89.0	38.9	0.47	0.70
14	nWGS–CCS–TSD	81.7	41.8	0.43	0.75
15	nWGS–CAES	163.2	45.0	0.86	0.80
16	nWGS–CCS–CAES	135.4	40.0	0.72	0.71
17	nWGS–TSD–CAES	45.68	20.06	0.24	0.36
18	nWGS–CCS–TSD–CAES	38.63	22.33	0.20	0.40

Given in Fig. 8 is a two-dimensional map that shows the relative positioning of each process investigated in terms of load-following and economic performance. System configurations toward the lower-left corner of Fig. 9 are those with the best LCOE and SSE results. It can be seen that cases using CCS, CAES and TSD offer the best load-following performance while also remaining economically superior or competitive with other configurations. In particular, case 10 offers the best LCOE/SSE trade-off while also being almost unaffected by the implementation of a \$50 tonnes^{-1} CO_2 tax.

3.4. Sensitivity of carbon tax on plant economics

The LCOEs for each of the cases examined computed as a function of the average lifetime carbon tax paid by the plant and are shown in Fig. 8. Note that the cases without a WGS step have essentially the same slopes as their WGS-enabled counterparts with only a small offset, and so for the sake of clarity are omitted from Fig. 8. This analysis assumes a simple linear CO_2 tax on a per-tonne basis. With the price of coal at \$45 tonnes^{-1}, it would require a CO_2 tax of \$22 tonnes^{-1} to incentivize a system in which CCS is used (noting that it is one of the SOFC designs); anything less would make CCS uneconomical compared to the non-CCS cases. Furthermore, it can be seen in Fig. 8 that once CCS is economically advantageous, only SOFC base-load plants with CCS are competitive. This analysis also confirms that the CAES system at no point becomes more economical than any of its non-CAES counterparts. This is not surprising, since added flexibility and reliability does not come without a cost, and no economic incentive for flexibility was included in this analysis. However, the added cost of a CAES system is small to the end consumer (0.35 ¢ kW^{-1} h^{-1}), and may become even more favourable if it is combined with current electricity price estimates and an economic optimization objective, which is left to future work. The closeness of the SOFC-based cases without a CO_2 tax owes to the very low cost of adding the CCS method described in Section 2.2.5. One of the strongest aspects of the SOFC/CAES system proposed in this work is that CCS may be retro-fitted to an already existing base-load plant with minimal process alterations, making it an excellent forward-looking insurance policy against future CO_2 emission regulations. Finally, this analysis indicates that SCPC with solvent-based CCS becomes economically advantageous compared to a SCPC process at a CO_2 tax of \$38 tonnes^{-1}, but is inferior to the SOFC-based systems at all CO_2 tax levels.

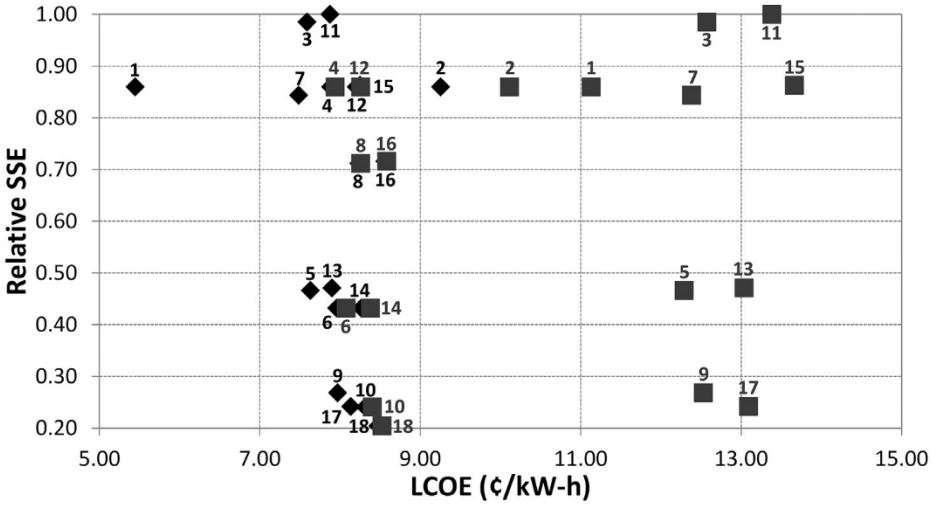

Fig. 8. Map of LCOE (economic indicator) versus SSE (load-following indicator) with (grey squares) and without (black diamonds) a \$50 tonnes^{-1} CO_2 tax. Each symbol is labelled with its corresponding case number as defined in Table 2.

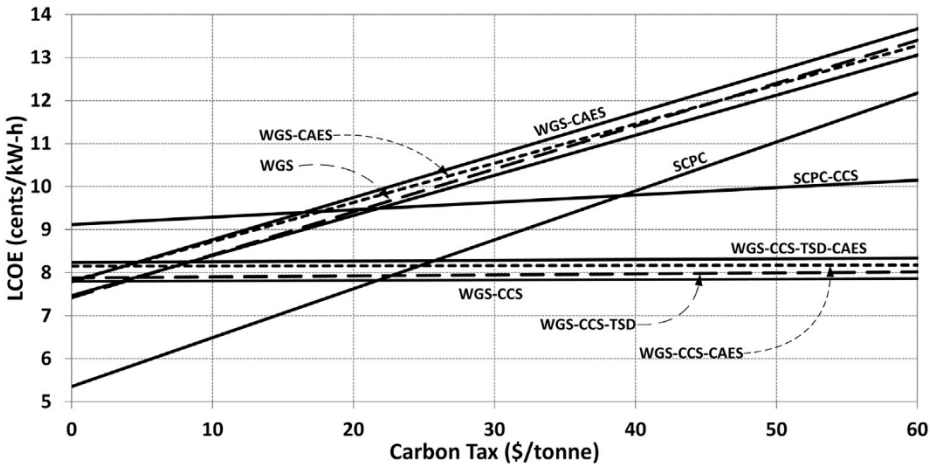

Fig. 9. Effect of CO_2 taxes on LCOE (WGS and SCPC cases).

3.5. Sensitivity analyses of assumed economic parameters

In order to assess the impacts of the assumptions made for this analysis, a comprehensive sensitivity analysis of the most uncertain variables was performed. Because of the high number of configurations investigated in this study, a candidate case was chosen to be the subject of the sensitivity analysis when analyzing the impact of the assumed parameters on LCOE (Section 3.5.1). To this end, case 10 (SOFC with WGS, CAES, CCS and TSD as described in Table 2) was chosen because it includes all of the possible design options and thus would be affected by all of the perturbed variables. A summary

Table 7
Variables and bounds for the sensitivity analysis.

Perturbed variable	Base case	Lowest value	Highest value	% Change (+/−)
CAES capital cost (\$ Thousands)	201,558	151,168	251,948	25
Discount rate (%)	10.0	7.5	12.5	25
SOFC stack cost (per kW)	500	300	700	40
Initial price of coal (\$ tonnes^{-1})	45	30	60	33
Plant lifetime[a] (years)	20	15	25	25
SOFC stack lifetime[a] (years)	10	8	12	20
Inflation rate (%)	2.5	1.5	3.5	40
CO_2 sequestration cost (\$ [tonne sequestered]$^{-1}$)	2.50	0	5.00	100

[a] Represents a variable where the higher value is a favourable case. All other variables are favourable when they are lowered.

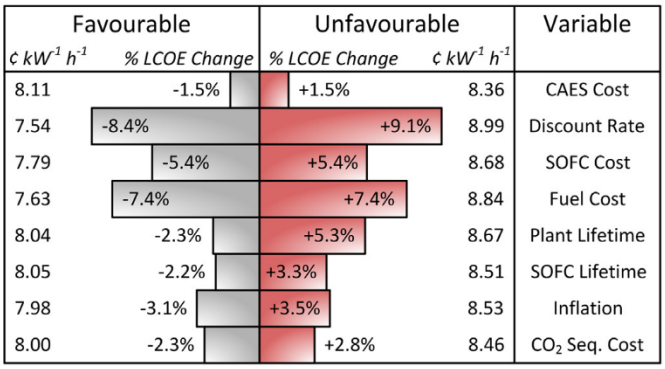

Fig. 10. Effect of sensitivity variables on the LCOE of the SOFC–WGS–CCS–CAES–TSD case.

of the variables that were altered for the sensitivity analysis is shown in Table 7, and a CO_2 tax of \$50 tonnes^{-1} was assumed for this sensitivity analysis.

A second sensitivity analysis was performed to specifically determine the effect on the breakeven CO_2 price (Section 3.5.2). In this analysis, the variables are altered in the same way (Table 7) as in the first sensitivity analysis, except that a constant CO_2 tax is no longer assumed. Instead, the CO_2 tax in which the SOFC-based plant becomes more economically favourable than the SCPC process is reported. A sensitivity analysis was not performed on the NETL pulverized coal plant cost estimates.

3.5.1. Effect of economic assumptions on LCOE of SOFC–CAES plant with CCS

The *Ceteris Paribus* ("all else being equal") sensitivity results that show the impact each of the main assumptions made in Table 7 have on the LCOE of the candidate plant are summarized in Fig. 10. It can be seen that the assumed discount rate (originally assumed to be 10%) has the largest effect on the LCOE of the candidate case. Increasing the discount rate by 2.5 percentage points (25%) increases the LCOE by 9.1% to almost 9 ¢ kW^{-1} h^{-1}. Moreover, the cost of coal has a large impact on the economics of the candidate case, changing the LCOE by ±7.4% (0.61 ¢ kW^{-1} h^{-1}) with a change of ±33% (\$15 tonnes^{-1}). Another interesting feature of Fig. 10 is that the capital cost of the CAES system does not have a large impact on plant economics. A 25% change in the cost of capital for the CAES system results in only a 1.5% change in LCOE. This means two things: a) the development of a SOFC/CAES plant is robust to uncertainties around the price of the CAES system, and b) a CAES can be retro-fitted on to an existing SOFC plant with a minimal impact on LCOE should peaking power be required. Finally, it is clear that LCOE is also strongly dependant on the SOFC stack cost (as it represents the largest capital expenditure), the lifetime of the plant, and the lifetime of the individual SOFC stacks (thereby requiring more frequent replacements). However, for all perturbations considered, the LCOE of the candidate case remains below that of SCPC (11 ¢ kW^{-1} h^{-1}) and SCPC–CCS (10 ¢ kW^{-1} h^{-1}) with a CO_2 tax of \$50 tonnes^{-1}.

3.5.2. Effect of economic assumptions on breakeven CO_2 tax

The sensitivity results that show the impact of the assumed economic parameters listed in Table 7 on the breakeven CO_2 tax (the point at which the SOFC plants become economically favourable over the current SCPC process) are shown in Fig. 11.

It can be seen that the SOFC stack cost and discount rate both have a large impact on the breakeven price of CO_2. Increasing the SOFC stack cost by \$300 kW^{-1} (30%) leads to an increase of \$3.6 tonnes^{-1} (16.4%) in the breakeven price of CO_2. This is not surprising, since the SOFC stack represents the majority of the plant cost and the main source of economic benefit for any of the SOFC-based plants compared to the SCPC plants is the avoidance of a potential CO_2 tax. Moreover, decreasing the SOFC stack cost by \$300 kW^{-1} (30%) leads to a \$4.4 (20%) tonnes^{-1} decrease in the breakeven price of CO_2. Perturbations of ±2.5 percentage points (25%) to the discount rate lead to changes in the breakeven CO_2 price of \$3.1 tonnes^{-1} (14%, unfavourable) and −\$2.75 tonnes^{-1} (12.5%, favourable), respectively. This is due to the large impact that the discount rate demanded by investors has on the capital investment, which is much higher for the SOFC cases than the SCPC cases. It is interesting to note that the CAES cost does not have an impact on the breakeven price of CO_2 in this scenario. This is because the plant configurations using CAES have a consistent (although small) price premium for the flexibility that the CAES system adds. Finally, it is interesting that the CO_2 sequestration cost has a much larger impact on the breakeven CO_2 price than the overall LCOE as discussed in section 3.5.1. An increase of \$2.5 tonnes^{-1} (100%) in the sequestration price increases the breakeven price of CO_2 by \$1.9 tonnes^{-1} (8.6%), whereas it only had a 2.8% impact on the LCOE. An increase in the sequestration cost of CO_2 has a direct impact on the potential net savings of CO_2 sequestration, which therefore leads to a significant impact on the required CO_2 tax to justify its use.

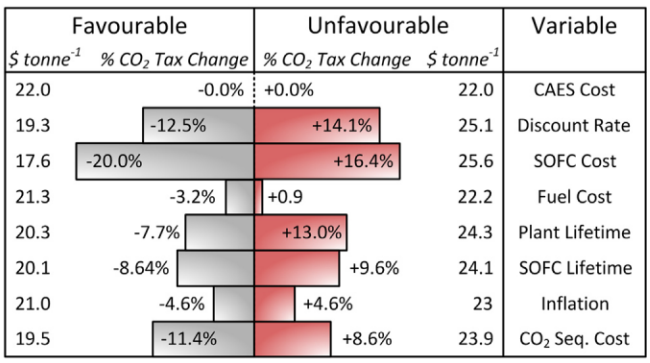

Fig. 11. Effect of sensitivity variables on the breakeven CO_2 tax.

4. Conclusions and future work

In this study, a novel integrated coal-fuelled SOFC/CAES system with and without optional WGS and CCS steps was investigated. Sixteen different SOFC plant configurations were simulated using a combination of Aspen Plus and MATLAB simulation tools (in-house models) and were compared to industrially standard SCPC processes. It was found that the addition of CAES to an SOFC-based system significantly improves load-following capabilities with minimal increases to LCOE (<0.3 ¢ kW^{-1} h^{-1}). Adding CAES significantly improved the load-following metrics (SSE and WSSE) of the proposed system, and was not negatively affected by the inclusion of CCS. Furthermore, the inclusion of CCS was able to reduce the total CO_2 emissions of the plant to nearly zero with a marginal increase in capital cost and no losses to overall plant operability. The inclusion of TSD was found to further improve the load-following capabilities of a CAES-enabled plant while also providing fuel savings and fuel cell maintenance windows. The addition of the WGS was found in this study to improve the overall economic performance of the plant due to the reduced electrical efficiency of the SOFC stacks when the fuel gas contains a combination of CO and H_2S. This resulted in higher capital costs, but reduced fuel and operating costs throughout the lifetime of the plant.

Overall, the SOFC/CAES process, when utilizing CCS and WGS, is capable of providing reliable load-following with zero direct (and nearly zero indirect) CO_2 emissions with only a marginal increase to LCOE. Furthermore, the SOFC-based systems with CCS become the most economically attractive option when CO_2 taxes of ~\$22 tonnes^{-1} or higher are considered. Sensitivity analyses show that the economic results for the SOFC-based plants depend on some key assumptions (listed in Table 7), but still consistently show improvement over the current state-of-the-art when CO_2 taxes are considered. Although SOFCs may be years away from being implemented at the bulk-generation scale, the forward-looking power production strategies proposed in this work show promise for providing clean and reliable peaking power in the future.

To the best of our knowledge, the investigation of peaking power generation from coal has not been explored yet. As a result, several simplifying assumptions were made in this study in order to provide a proof-of-concept framework. Future work may look at

dynamics associated with turbines, compressors and the HRSG and their effect on load-following capabilities. Furthermore, real-time optimization can be used with future predictions of demand to optimize the profitability or load-following capabilities of the SOFC/CAES system, potentially including stochastic fuel and electricity pricing, startup/shutdown penalties of using TSD, or considering CO_2 to have economic value. Different (potentially renewable) fuel sources may also be investigated, such as biomass and petroleum coke.

Nomenclature

Abbreviations

ASU	air separation unit
CAES	compressed air Energy storage
CCS	carbon capture and sequestration
EOS	equation of state
HHV	higher-heating value
HRSG	heat recovery and steam generation
LCOE	levelized cost of electricity
NGCC	natural gas combined cycle
SOFC	solid oxide fuel cell
SSE	sum of squared error
TSD	train shutdown
WGS	water–gas shift
WSSE	weighted sum of squared error
SCPC	supercritical pulverized coal
nWGS	no water–gas shift reactors

Mathematical symbols

D	demand
F	fuel costs
I	capital investment
M	maintenance costs
N	plant lifetime
O	plant over-production
P	sellable power produced
r	discount rate
U	plant under-production

Appendix A. Supplementary data

Supplementary data related to this article can be found at http://dx.doi.org/10.1016/j.jpowsour.2013.11.040.

References

[1] US Energy Information Administration, AEO2012 Early Release Outlook, US DOE/EIA-0383ER(2012), January 2012.
[2] National Energy Board. Canada's Energy Future: Energy Supply and Demand Projections to 2035 – Electricity Outlook Highlights, Available online: http://www.neb-one.gc.ca/clf-nsi/rnrgynfmtn/nrgyrprt/nrgyftr/2011/nrgsppldmndprjctn2035-eng.pdf (accessed June, 2012).
[3] H.J. Herzog, D. Golomb, in: C.J. Cleveland (Ed.), Encyclopedia of Energy, Elsevier Science, New York, 2004, pp. 277–287.
[4] A.J. Minchener, J.T. McMullan, J Energy Inst. 81 (2008) 38–44.
[5] Energy Information Administration (EIA), Fuel Emission Factors, Appendix H of Instructions to Form EIA-1605, U.S. Department of Energy, Washington, D.C., Available online: http://www.eia.gov/oiaf/1605/pdf/Form%20EIA-1605%20instructions.pdf.
[6] U.S. Environmental Protection Agency (EPA), Inventory of U.S. Greenhouse Gas Emissions and Sinks: 1990–2010, EPA 430-R-12–001, pp. 3–5, Available online:http://www.epa.gov/climatechange/ghgemissions/usinventoryreport.html.
[7] M.C. Woods, P.J. Capicotto, J.L. Haslbeck, N.J. Kuehn, M. Matuszewski, L.L. Pinkerton, M.D. Rutkowski, R.L. Schoff, V. Vaysman, Cost and Performance Baseline for Fossil Energy Plants. Volume 1: Bituminous Coal and Natural Gas to Electricity, August 2007. Final Report, DOE/NETL-2007/1281, Revision 1.
[8] M. Hasan, R. Baliban, J. Elia, C. Floudas, Ind. Eng. Chem. Res. 51 (2012) 15665–15682.
[9] M. Hasan, R. Baliban, J. Elia, C. Floudas, Ind. Eng. Chem. Res. 51 (2012) 15642–15664.
[10] J. Nease, T.A. Adams II, J. Power Sources 228 (2013) 281–293.
[11] M.C. Williams, J.P. Strakey, W.A. Surdoval, Int. J. Appl. Ceram. Technol. 2 (2005) 295.
[12] T.A. Trabold, J.S. Lylak, M.R. Walluk, J.F. Lin, D.R. Trojani, Int. J. Hydrogen Energy 37 (2012) 5190.
[13] T.A. Adams II, J. Nease, D. Tucker, P. Barton, Ind. Eng. Chem. Res. 52 (2013) 3089–3111.
[14] N.Q. Ming, ECS Trans. 7 (2007) 45.
[15] F.P. Nagel, T.J. Schildhauer, S.M.A. Biollaz, Int. J. Hydrogen Energy 34 (2009) 6809.
[16] H. Jin, E.D. Larson, F.E. Celik, Biofuels Bioprod. Bioref. 3 (2009) 142.
[17] T.A. Adams II, P.I. Barton, Systems and Methods for the Separation of Carbon Dioxide from Water, 2009, US Patent App. 12/434486.
[18] T.A. Adams II, P.I. Barton, AIChE J. 56 (2010) 3120–3136.
[19] T.A. Adams II, P.I. Barton, Fuel Proc. Technol. 92 (2011) 2105.
[20] P. Kuchonthara, S. Bhattacharya, A. Tsutsumi, Fuel 84 (2005) 1019–1021.
[21] A. Verma, A.D. Rao, G. Samuelsen, J. Power Sources 158 (2006) 417–427.
[22] M. Li, A. Rao, J. Brouwer, G. Samuelsen, J. Power Sources 195 (2010) 5707–5718.
[23] S. Park, J. Ahn, T. Kim, Appl. Energy 88 (2011) 2976–2987.
[24] E. Achenbach, J. Power Sources 57 (1995) 105–109.
[25] C. Stiller, B. Thorund, O. Bolland, J. Eng. Gas Turbines Power 128 (2006) 551–559.
[26] G. Almutairi, K. Kendall, W. Bujalski, Int. J Low-Carbon Technol. 7 (2012) 63–68.
[27] L. Barelli, G. Bidini, A. Ottoviano, Int J. Hydrogen Energy 37 (2012) 16140–16150.
[28] M. Raju, S.K. Khaitan, Appl. Energy 89 (2012) 474–481.
[29] E. Fertig, J. Apt, Energy Policy 39 (2009) 2330–2342.
[30] Dressler-Rand, Dresser-Rand Awarded Compressed Air Energy Storage (CAES) Project [press release], 2013. Available online: http://investor.dresser-rand.com/releasedetail.cfm?ReleaseID= 774720.
[31] L. Copelin, As Texas Worries about Power Generation, Is Answer Underground?, Statesman, April, 2013. Available online: http://www.statesman.com/news/business/as-texas-worries-about-power-generation-is-answe-1/nRmpY/.
[32] H. Hoffeins, Huntorf Air Storage Gas Turbine Power Plant, in: Energy Supply, Brown Boveri Publication, 1994. DGK 90 202 E.
[33] D.R. Hounslow, W. Grindley, R.M. Louglin, J. Eng. Gas Turbines Power 120 (1988) 875–883.
[34] A. Cavallo, Energy 32 (2007) 120–127.
[35] J.B. Greenblatt, S. Succar, D.C. Denkenberger, R.H. Williams, R.H. Socolow, Energy Policy 35 (2007) 1472–1492.
[36] J. Mason, V. Fthenakis, K. Zweibel, T. Hansen, T. Nikolakakis, Prog. Photovolt. Res. Appl. 16 (8) (2008) 649–668.
[37] S. Succar, R.H. Williams, Compressed Air Energy Storage: Theory, Resources and Applications for Wind Power, Princeton Environmental Institute: Princeton University, 2008.
[38] T.A. Adams II, P. Barton, J. Power Sources 195 (2010) 1971–1983.
[39] Independent Electricity System Operator, Ontario Demand and Market Prices, Available HTTP: http://www.ieso.ca/imoweb/siteShared/demand_price.asp?sid =ic (accessed 19.03.12).
[40] T.S. Lee, J.N. Chung, Y. Chen, Energy Convers. Manag. 52 (2011) 3214–3226.
[41] F. Mueller, B. Tarroja, J. Maclay, F. Jabbari, J. Brouwer, S. Samuelson, J. Fuel Cell Sci. Technol. 7 (2010) 031007-1–031007-12.
[42] L. Yang, Y. Weng, J. Power Sources 196 (2011) 3824–3835.
[43] V. Liso, A. Oleson, M. Nielson, S. Kaer, Energy 35 (2011) 4216–4226.
[44] Y. Komatsu, S. Kimijima, J.S. Szmyd, Energy 35 (2010) 982–988.
[45] T. Kuramochi, W. Turkenburg, A. Faaij, Fuel 90 (2011) 958–973.
[46] K. Krulla, in: SECA Conference Proceeding, United States Department of Energy – National Energy Technology Laboratory, Pittsburgh, PA, July 23–24, 2013.
[47] GREET, The Greenhouse Gases, Regulated Emissions, and Energy Use in Transportation Model, GREET 1.8d.1, Developed by Argonne National Laboratory, Argonne, IL, released, August 26, 2010. Available HTTP:, http://greet.es.anl.gov/.
[48] Aspen Technology, Inc., Aspen Plus User Guide, Version 2006.5, Software Documentation, Aspen Technology, Inc., Burlington, MA, 2006.
[49] J.P. Trembly, R.S. Gemmen, D.J. Bayless, J Power Sources 169 (2007) 347–354.
[50] K. Haga, S. Adachi, Y. Shiratori, K. Itoh, K. Sasaki, Solid State Ionics 179 (2008) 1427–1431.
[51] K. Sasaki, K. Susuki, A. Iyoshi, M. Uchimura, N. Imamura, H. Kusaba, Y. Teraoka, H. Fuchino, K. Tsujimoto, Y. Uchida, N. Jingo, J. Electrochem. Soc. 153 (2006) A2023–A2029.
[52] T.A. Adams II, P.I. Barton, J. Power Sources 195 (2010) 5152–5153.
[53] K. Lobachyov, J.H. Richter, J. Energy Resour. Technol. 118 (1996) 285–292.
[54] A.I. Marquez, T.R. Ohrn, J.P. Trembly, D.C. Ingram, D.J. Bayless, J Power Sources 164 (2007) 659–667.
[55] EG&G Technical Services, DOE/NETL Fuel Cell Handbook, seventh ed., November 2004.
[56] E. deVisser, C. Hendriks, M. Barrio, M.J. Mølnvik, G. de Koeijer, S. Liljemark, Y.L. Gallo, Int. J. Greenhouse Gas Control 2 (2008) 478–484.
[57] W.L. Luyben, Ind. Eng. Chem. Res. 50 (2011) 13984–13989.

[58] R. Kushnir, Transp. Porous Media 73 (2008) 1–20.
[59] Electric Power Research Institute, Wind Power Integration Technology Assessment and Case Studies, 2004. EPRI Report 1004806.
[61] K. Branker, M.J.M. Pathak, J.M. Pearce, Renew. Sustain. Energy Rev. 12 (2011) 4470–4482.
[62] D. Lozowski, Chem. Eng. 119 (2012) 80.
[63] H.C. Mantripragada, E.S. Rubin, Int. J. Greenhouse Gas Control 16 (2013) 50–60.
[64] R.D. Middleton, J.K. Eccles, Appl. Energy 108 (2013) 66–73.
[65] W.D. Seider, J.D. Seader, D.R. Lewin, S. Widago, Product and Process Design Principles, third ed., Wiley, Hoboken, NJ, 2009, pp. 534–597.
[66] G. Hossein, in: SECA Conference Proceeding, FuelCell Energy, Inc., Pittsburgh, PA, July 24–25, 2012.
[67] The Washington Post, At Redox Power Systems, the Future of Electricity Lies in Fuel Cells, 2013. Available online: http://articles.washingtonpost.com/2013-08-25/business/41446704_1_fuel-cells-warren-citrin-wind-power.
[68] R. Schainker, Compressed Air Energy Storage Cost Analysis, The Electric Power Research Institute, 2009. Report 1016004.

Chapter 4

Life Cycle Analyses of Bulk-Scale Solid Oxide Fuel Cell Power Plants and Comparisons to the Natural Gas Combined Cycle

The content of the following chapter is a **published reprint** of the following peer-reviewed publication:

Nease J, Adams TA II. Life Cycle Analyses of Bulk-Scale Solid Oxide Fuel Cell Power Plants and Comparisons to the Natural Gas Combined Cycle. *The Canadian Journal of Chemical Engineering*. 2015; 93: 1349-1363.

This paper makes reference to an online supplement submitted and reviewed with the full publication. The supplement is extensive and is not reproduced in this work, but has been made available electronically with the file name:

`Chapter_4_Supplement.xslx`

Life Cycle Analyses of Bulk-Scale Solid Oxide Fuel Cell Power Plants and Comparisons to the Natural Gas Combined Cycle

Jake Nease and Thomas A. Adams II*

Department of Chemical Engineering, McMaster University, 1280 Main Street West, Hamilton, ON, Canada

In this work, detailed cradle-to-grave life cycle analyses are performed for a current state-of-the art natural gas combined cycle and a bulk-scale solid fuel cell power plant fuelled by natural gas. Life cycle inventories are performed for multiple configurations of each plant, including designs with carbon capture capability. Consistent boundaries (including all supply chain and upstream processes) and unit bases for each process are defined for each process. The *ReCiPe 2008* life cycle assessment method is used to quantify the impacts of each plant at both mid- and end-point levels. Three impact assessment perspectives (individualist, hierarchist, and egalitarian) are considered. The results of these life cycle analyses are compared in order to determine the environmental trade-offs between potential power generation pathways. Results indicate that power generation using solid oxide fuel cells has a smaller life cycle impact than the natural gas combined cycle when the entire life cycle of each option is considered.

Keywords: energy, environment, fuel cells, process systems engineering, oil, gas and coal < energy

INTRODUCTION

In a time of dwindling natural resources, emphasis on sustainable alternatives, increasing human activity, and an increasing public awareness of global warming and environmental impact, the need for reliable and sustainable energy has become a matter of global importance.[1] With regard to power generation, there are several emerging methods that aim to convert sustainable sources such as biofuels, solar, and wind energy into usable and reliable electrical energy. However, although the growth rates of these industries are quite high, these methods are still decades away from being applied on a large scale even in the most developed and forward-looking economies. For example, renewable electricity is anticipated to contribute only 10 % and 16 % of the power produced in Canada and the United States by the year 2035, respectively.[2,3] Moreover, it is anticipated that the role of natural gas (NG) as a fuel source for electricity generation will only increase in the coming years, well exceeding that of all combined renewables. NG currently accounts for 9 % of the electricity generated in Canada and is anticipated to rise to 15 % by 2035.[2] In the United States, NG supplies the fuel requirements for 24 % of all electricity generated, and is anticipated to rise as high as 27 % by 2035.[3]

There is hence a strong motivation to improve the current methods that utilize NG as a fuel source for electricity production, both environmentally and economically. Moreover, there is a strong chance that policy-induced economic incentives (such as a cap and trade system, emission restriction, or carbon tax) will lead to the requirement for CO_2 capture and sequestration in various geological storage sites.[4] However, strictly quantifying direct emissions (mainly CO_2) may not be an appropriate method of assessing a plant's environmental impact. Instead, it is becoming more common to consider the entire life cycle emissions of a plant, including all upstream and downstream emissions associated with its operation. Moreover, additional considerations such as pollutants, ozone depleting species, and particulates have an effect on ecosystem and human health, and are hence being more closely considered.

To this end, this work performs a comprehensive life cycle analysis (LCA) using the *ReCiPe 2008* (using the version released in July 2013) method on a recently proposed power plant design utilizing solid-oxide fuel cells (SOFCs) for base-load power and compares the results with a state-of-the art natural gas combined cycle (NGCC) plant. This investigation is important because although the plant-gate emissions of bulk SOFC plants which use carbon capture and sequestration (CCS) have been shown to be nearly negligible, the complete cradle-to-grave life cycle impact of such a process might be much more significant due to upstream and downstream emissions, plant commissioning emissions, and the consumption of relatively rare resources required for the SOFC. The following sections briefly introduce the two power generation strategies to be compared and the LCA method used in this work.

Solid-Oxide Fuel Cells

A SOFC is a high-temperature device that electrochemically oxidizes a fuel gas by transporting oxygen ions through a solid-oxide barrier.[5] There are several advantages to this device that result in synergistic benefits to using SOFCs for power generation: they may run on a variety of gaseous fuels including methanol,[6] gasified coal,[7] natural gas,[8] biomass,[9] and others;[10,11] selective O_2 transport through the solid-state electrolyte acts as an effective O_2/N_2 separator from atmospheric air therefore allowing for low-cost and highly efficient carbon capture;[5] and its high operating temperatures and pressures lend itself to various system integration options, including bottoming cycles and energy storage techniques.[12–13] A simplified block diagram of a typical SOFC process with carbon capture is shown in Figure 1; detailed descriptions of the SOFC and its application to bulk power generation strategies are available in the literature.[11] Several

*Author to whom correspondence may be addressed.
E-mail address: tadams@mcmaster.ca
Can. J. Chem. Eng. 93:1349–1363, 2015

DOI 10.1002/cjce.22207
Published online 29 May 2015 in Wiley Online Library (wileyonlinelibrary.com).

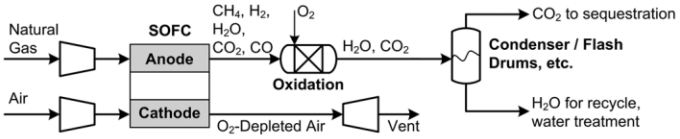

Figure 1. Simplified strategy for generating power from natural gas using SOFCs. Reproduced with permission from Adams et al.[11]

studies have shown that SOFC systems utilizing fossil fuels are capable of high electrical efficiencies (greater than 60 % in some cases) while potentially capturing and sequestering essentially 100 % of CO_2 emissions.[14–20] There have also been several studies that have investigated the full life cycle impact of constructing SOFC stacks and tubes and their associated appurtenances and balance-of-plant components, several of which are used as sources of information for this study.[21–22] There have been a number of life cycle impact studies on the operation of SOFCs. For example, SOFC-based auxiliary power units[23–24] and studies regarding the impact of using alternative fuels in SOFC stacks[27] have been a topic of recent study.

However, to the best of our knowledge, no studies have yet been performed to assess the entire cradle-to-grave life cycle impact of a bulk power generation system using NG as fuel and SOFCs as the main power source. Prior studies that claim SOFC-based systems can eliminate direct CO_2 emissions have not yet accounted for any emissions or environmental impacts of upstream NG processing, nor have they considered other factors that affect human health, ecosystem impact, or resource depletion.[25] Life-cycle cost analyses of household combined heat and power (CHP) SOFC units have been performed,[26] but they do not include the environmental or social impacts of bulk-scale SOFCs.

Natural Gas Combined Cycle Plants

NGCC plants are one of the most common strategies for power generation from NG in North America. NGCC plants burn NG with air in a combustion turbine at high temperatures and pressures, producing electricity through a generator. Waste heat from the system is typically used to generate high-pressure steam that can be used in a heat recovery steam generation (HRSG) system to produce additional power, or used for heating purposes as required elsewhere.[28] If desired, various CCS strategies may be employed to recover as much as 90 % of the CO_2 in the exhaust stream, including but not limited to solvent-based absorption, pressure-swing adsorption, or vacuum swing adsorption.[29,30] However, all of these CO_2 capture strategies have high parasitic energy costs, leading to reduced plant efficiencies, higher electricity costs, and greater resource consumption.

There are several LCA studies regarding the NGCC available in the literature, all of which were used as sources of information for this investigation. Several government-initiated studies have recently been performed in the United States that inventory the impact of NGCC plants and their associated upstream processes.[31,32] Other investigations have been performed as well using various impact analysis methods and levels of detail (see Table 1 in Singh et al.[33] and the references therein for a review of recent studies). However, at the time of this work, no studies have used the *ReCiPe 2008* method to assess the end-point impact of these analyses.

Description of Life Cycle Assessment Method: *ReCiPe 2008*

A LCA is a tool that is used to analyze the life cycle of a product or process in the context of its environmental impact and, to that end, its effect on the sustainability of our standard of living. Although

Table 1. *ReCiPe 2008* mid- and end-point factors and indication of their inclusion in this study[32]

Mid-Point Characterizations	Tag	Units	Considered
Agricultural Land Occupation	ALO	m^2	NO
Climate Change	CC	kg CO_2-Eq	YES
Fossil Depletion	FD	kg oil-Eq	YES
Freshwater Ecotoxicity	FET	kg (1,4)-DCB-Eq	YES
Freshwater Eutrophication	FE	kg P-Eq	NO
Human Toxicity	HT	kg (1,4)-DCB-Eq	YES
Ionizing Radiation	IR	kg U^{235}-Eq	NO
Marine Ecotoxicity	MET	kg (1,4)-DCB-Eq	YES
Marine Eutrophication	ME	kg N-Eq	YES
Metal Depletion	MD	kg Fe-Eq	YES$^{\alpha}$
Natural Land Transformation	NLT	m^2	NO
Ozone Depletion	OD	kg CFC-11-Eq	NO
Particulate Matter Formation	PMF	kg PM_{10}-Eq	YES
Photochemical Oxidant Formation	POF	kg NMVOC	YES
Terrestrial Acidification	TA	kg SO_2-Eq	YES
Terrestrial Ecotoxicity	TET	kg (1,4)-DCB-Eq	YES
Urban Land Occupation	ULO	m^2	NO
Water Depletion	WD	m^3	YES
End-Point Characterizations	**Tag**	**Units$^{\beta}$**	**Considered**
Damage to Human Health	HH	DALY$^{\delta}$	YES
Damage to Ecosystem Diversity	ED	Species-yrs	YES
Damage to Resource Depletion	RD	$	YES

α: Metal depletion is not included in the NGCC analyses used as sources for this study. As such metal depletion is included in the impact analysis for the SOFC systems for completeness, but is omitted from case comparisons.
β: End-point units are converted to "points" in this investigation. Please see the online supplement submitted with this article for conversion information.
δ: Daily Average Life Years.

there is no singular LCA method that has been identified to be all-encompassing, a common theme among most commonly accepted methodologies is to define a set of standardized metrics to categorize the impacts of products at the mid-point (such as climate change, ecotoxicity, or land occupation) and end-point (such as loss of human life and ecosystem degradation) levels. However, each model that attempts to characterize a product's life cycle impact contains underlying assumptions that lead to different results depending on the method used. For example, a recent study has shown that three relatively modern LCA methods can provide significantly different results in certain impact categories for some cases due to differing assumptions regarding the importance of certain elemental flows.[34] *ReCiPe 2008* offers a unified approach to quantify the impact of a product's life cycle at both the mid-point and end-point levels based on its inventory of flows to or from the environment (designated as elementary flows).[35] End-point results are normalized to a unified point system to obtain a description of the product's entire life cycle impact. The point system is scaled such that 1000 points is equivalent to the average human's impact over one year. Figure 2 shows a simplified depiction of the harmonized mid-point to end-point model adapted in *ReCiPe 2008*. It is also important to note that although there is no universally accepted life cycle assessment tool, a meaningful comparison between product life cycles can be obtained if a consistent model is employed.

The selection of what mid-point and end-point factors are to be considered in a LCA is at the discretion of the investigator. To this end, Table 1 lists the mid- and end-point impact categories for *ReCiPe 2008* and which of them are considered in this study. Mid-point impacts map material and energy flows to and from the environment into quantifiable metrics such as climate change potential (measured in kg of CO_2 equivalents) and fossil fuel depletion (measured in kg of oil equivalents). These mid-point metrics are objective, but have some degree of uncertainty. End-point methods map the mid-point metrics into smaller groups of impacts such as the damage to human health (measured in years of human life lost) or the damage caused to future generations by making it more expensive to recover non-renewable resources (measured in dollars). This too is objective, but with some additional uncertainty. These end-point metrics can then be mapped into one final metric called ecoPoints. A certain number of ecoPoints are assigned per year of life lost and a certain number of ecoPoints per dollar of damage inflicted to future generations, for example. This provides a single, useful metric from which one can compare all of the different categories of environmental impacts. However, this mapping into ecoPoints contains some degree of subjective judgement in determining the weighting factor between end-point categories. As such, *ReCiPe 2008* considers three different sets of weights, called "perspectives," based on various time horizons and cultural perspectives: Individualist (I), Hierarchist (H), and Egalitarian (E), each described as follows:[35]

- The individualist (I) perspective is based on humanity's short-term interests. It uses impact types that are not disputed (climate change and resource depletion, for example), and makes optimistic assumptions about the adaptability of humanity and technology to declining resource pools in the near future. This perspective puts a lower weighting on toxicity and acidification, but a higher weighting on short-term global warming potential.
- The hierarchist (H) perspective is based on common policy principles regarding time frames and other considerations. Generally speaking, it is the most evenly weighted of all perspectives.
- The egalitarian (E) perspective is the most pessimistic with regards to long-term global warming potential. It takes the longest time frames into account and considers some impact factors that are not yet fully established but are anticipated to have an impact (emphasizes long-term toxicity and acidification).

For details regarding the assumptions and implications of these perspectives, the reader is referred to the *ReCiPe 2008* documentation.[35] This study considers all three of these perspectives in order to form comprehensive conclusions.

For this work, agriculture is not a part of the supply chain, and so agricultural land occupation and freshwater eutrophication (commonly caused by fertilizer runoff) are not considered in the analysis. However, marine eutrophication was considered to account for effects such as oil leaks from the importation of LNG via ocean barge. Similarly, urban land occupation and natural

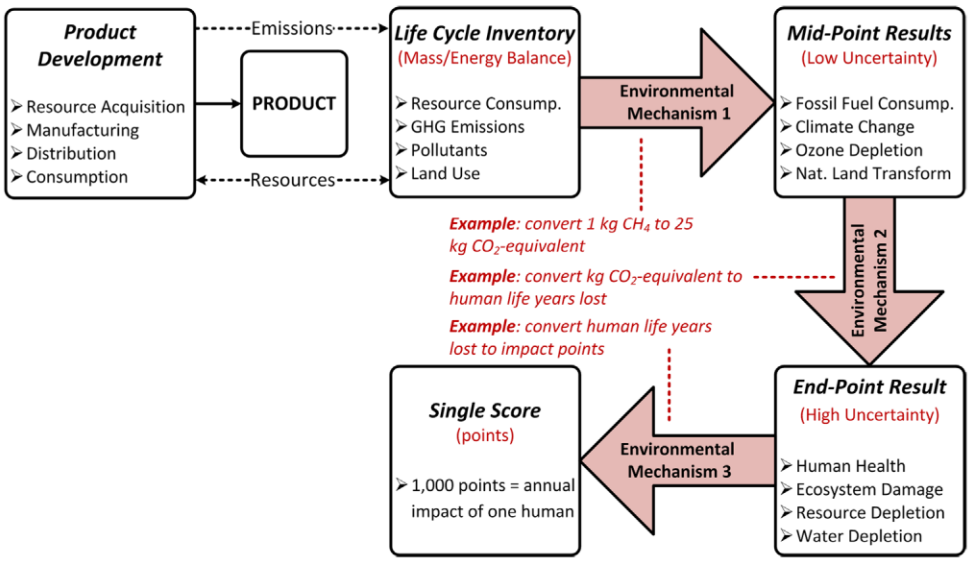

Figure 2. Example of a mid-point to end-point life cycle assessment strategy. Adapted from Skone et al.[32]

land transformation were also not considered because the environmental impact from occupying land required by the power plant is trivially small compared to the impacts of its heavy use throughout its lifetime. Ionizing radiation was not considered because nuclear energy plays only a tiny role in the supply chain in the form of the consumption of grid electricity during manufacturing processes and it was assumed that no radioactive components were emitted to the environment during this step. However, rare metal consumption (in the form of U^{235}) was accounted for resource depletion purposes. Ozone depletion was not considered because, based on the available data, no ozone-harming chemicals are released during the supply chain of either NGCC or SOFC in any significant quantity.

METHODOLOGY

Bases of Calculations

In order to compare the results of each process investigated in this study, a consistent unit basis for the product was defined. The final basis of comparison for each case was selected to be 1 MWh (3600 MJ) of useable electrical energy. 1 MWh of net electricity takes into account any process inefficiencies (and hence upstream implications), and distribution losses (considered in some specific cases). The "grave" of this electrical energy is assumed to be its final consumption, which is assumed to be 100 % efficient. It should be noted that when comparing different processes with the same end-product (in this case electrical energy being consumed), its final use bears no impact on the comparative life cycle impact of each process.

An exception to this basis is for the manufacturing of the SOFC stacks and their associated balance of plant (BoP). In this study, the entire life cycle impact, from construction to decommission, is desired for the SOFC process. However, current studies thus far have only considered the construction phase of the SOFC stacks. As such, the product basis for the SOFC manufacturing step is assumed to be 1 kW (net production) of finished SOFC stacks and their required BoP implementations. In order to apply these results to the entire lifetime LCA of an operating SOFC plant, a usable lifetime of 10 years when operating at full capacity (as previously reported in the literature) was assumed.[12,14] With this useful lifetime, the overall impact of constructing 1 kW of SOFC stacks may be normalized to a per-kWh basis, and therefore used in the overall LCA of the SOFC plant.

The basis unit of processed NG (used in each of the plants investigated) is taken to be 1 MJ by higher heating value (HHV). Assumptions regarding the energy density and sources of NG used for this study are discussed further in Natural Gas Supply Chain.

Natural Gas Supply Chain

In order to perform a full cradle-to-grave comparative study of NGCC and SOFC plants, the NG supply chain and its associated losses and inefficiencies had to be defined. The following subsections define the boundaries of the NG supply chain and any assumptions that were required for this investigation. Several sources were consulted to obtain this information.[32,36]

Boundary region definition

The boundary of the NG supply chain is shown below in Figure 3. The final product is defined to be 1 MJ of processed and delivered NG, which is derived from a combination of domestic and imported sources, each with different emissions resulting from their respective supply chains.

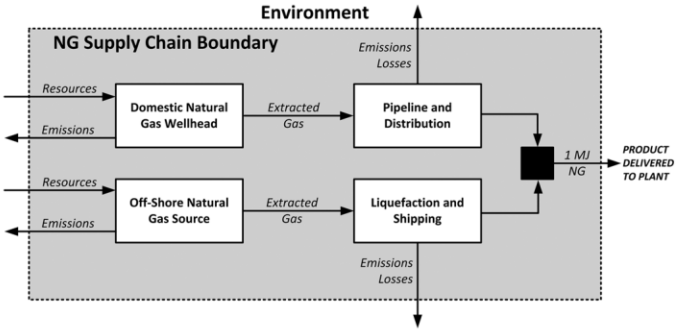

Figure 3. Cradle-to-gate life cycle boundary of the NG supply chain considered in this work.

Necessary assumptions

The NG used in the SOFC and NGCC plants is assumed to be the same composition in order to make fair comparisons. Literature sources defining the "average" NG used in the United States and the life cycle impacts of each source were considered for this study.[31,32,37] A summary of the contributions of each NG source is provided in Table 2. It is assumed that 98 % of the final NG is from domestic sources, and 2 % is liquefied NG (LNG) imported from Trinidad and Tobago. (Please see the supplement provided with this article for detailed emission breakdowns and calculations.) The further assumptions made in the definition of the upstream supply chain for NG are as follows:

- NG is assumed to have a HHV of 41.1 MJ/kg.[28]
- 13 % of the gas extracted from the wellhead is either flared or lost throughout the supply chain as fugitive emissions.[31,36]
- The only source of imported NG is assumed to be LNG that is liquefied off-shore, shipped via tanker, and re-vapourized domestically.[33]

SOFC Manufacturing Cradle-To-Gate Study

This section combines the results of previous SOFC manufacturing studies and adapts them to the unit basis of this investigation. Several sources were consulted and cross-referenced to obtain reliable life cycle inventories.[21,22,37] Shown in Figure 4 is a flowsheet describing the manufacturing process for the positive-electrolyte-negative (PEN) component of the SOFC, including resource inflows and potential emission sources. Figure 4 is a sub-network of the total cradle-to-grave boundary of the SOFC manufacturing process, which is described in the following section.

Table 2. Breakdown of NG sources in the United States

Domestic Gas[α]	Source	% of Domestic Gas
Conventional	Onshore	24.5
	Associated	12.5
	Offshore	7.0
Unconventional	Tight	31.0
	Shale	16.0
	CBM	9.0
Imported Source	**Source**	**% of Imported Gas**
Offshore	LNG	100.0

α: Domestic gas is assumed to account for 98 % of the NG consumed in the United States. 2 % is imported.

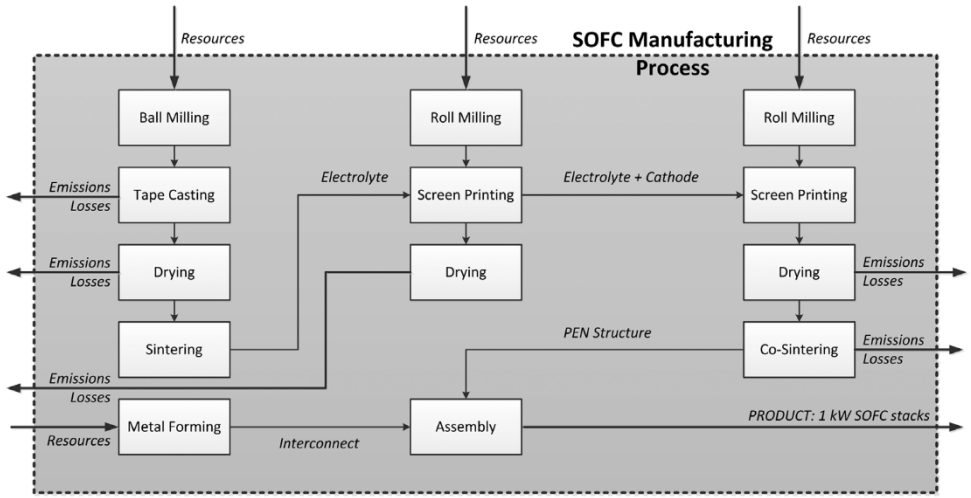

Figure 4. Example of a SOFC manufacturing process with resource entry points and potential emissions labelled. Adapted from Karakoussis et al.[22]

Boundary region definition

The boundaries of the SOFC and BoP manufacturing stage are depicted in the simplified block diagram of Figure 5. This sub-system contains all of the processes and contributions contributing to the cradle-to-gate life cycle impact of 1 kW of operating SOFC stacks, which are then normalized to the same basis units as the SOFC plant's operation (MWh) before being considered as an intermediate product in the full cradle-to-grave LCA. It should be noted that only metals that characterized by *ReCiPe 2008* were considered in this study. (Please see the online supplement for detailed emission rates for each sub-process.)

Necessary assumptions

Beyond the definition of the process boundaries, the following assumptions were also made with regards to the manufacturing of SOFC stacks:

- All energy consumed in the SOFC manufacturing process is assumed to be electricity. This is because the source data does not specify the type of energy consumed. However, most manufacturing processes of this type are typically electricity-driven.
- This electricity consumed in the SOFC manufacturing process and its associated emissions are assumed to comprise the average electricity mix in the United States. See Table 3 for a breakdown of each source. Typical system efficiencies are considered when tabulating resource depletion.[37–39]
- The GHG and pollutant emissions associated with electricity generation from renewable sources (i.e. wind, hydroelectric) are neglected since they generate no emissions during use and the emissions from their manufacture are small.
- The materials and energy required to develop the electricity generation infrastructure (plants, transmission systems, etc.) are assumed to already exist and therefore are not taken into account. Specifically, the effects of constructing the existing power grid are not within the boundaries of this study.
- All emissions are to the atmosphere since no liquid-phase emissions were reported in the source data (to-air).
- The BoP is assumed to account for the majority of unit operations extending beyond the SOFC stacks. The commissioning phase of the NGCC has been reported to be negligible when compared to the SOFC stacks, and therefore any units required beyond the SOFC/BoP structure are assumed to insignificantly contribute to the LCA impact of the SOFC commissioning phase.[14–28]
- Emissions caused upstream of the power grid from which the energy was consumed during SOFC manufacturing were omitted since they had a miniscule impact to the overall analysis.

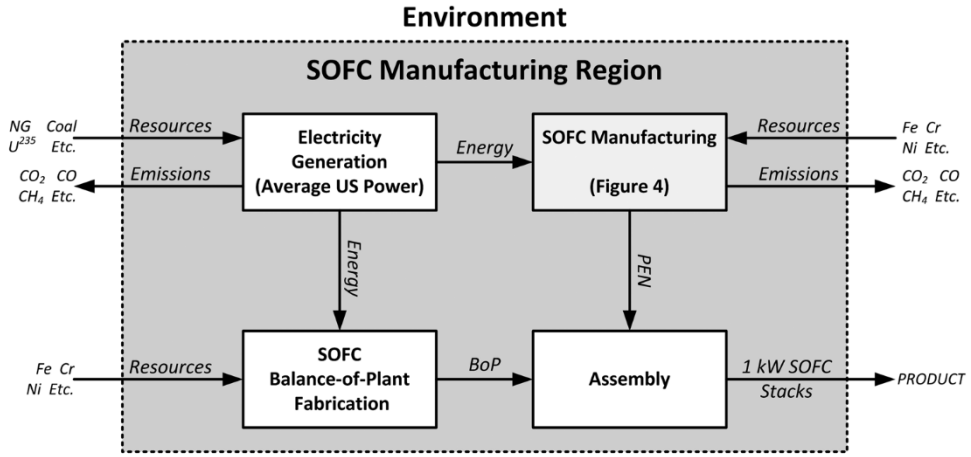

Figure 5. Life cycle boundary of the SOFC manufacturing step.

Table 3. Average United States electricity mix by source

Electricity Source	Percentage
Coal	44.50 %
Oil	1.12 %
Gas	23.30 %
Hydro	6.80 %
Nuclear	20.20 %
Other Renewables	4.08 %

NGCC Full Life Cycle Study

Boundary region definition

The boundary for a fully operating NGCC plant includes all species that are transferred to and from the natural environment in order to produce one unit of useable electrical power, including the commissioning and decommissioning of the plant itself. Furthermore, there are two decision points that are considered in this study: (1) whether or not CCS is utilized; and (2) whether or not the electricity distribution infrastructure (transmission lines) inefficiencies are considered. Utilizing CCS results in altered emissions to the environment at the cost of lower system efficiencies (and therefore greater upstream impacts) and accounting for the commissioning of a necessary CCS pipeline. Considering the transmission infrastructure further reduces the efficiency of the plant in question, leading to proportionally higher impacts for each sub-process within the LCA boundary. However, to consider the TML, assumptions must be made about the average energy losses between the power plant and the end user; we have assumed 7.0 %, which is a continental average and is used in a study by the NETL.[31] The results of this work are considered both with and without TML to make it easy for others to apply our results to different transmission infrastructures.

The full boundary region considered for the NGCC plant is depicted in Figure 6. Optional sub-processes and resulting emissions are denoted by dashed lines and borders. For this study, each of the combinations of optional cases accounting for CCS and transmission losses (TML) was considered. The definition of each case is given in Table 4. Plant efficiencies for the NGCC cases were obtained from the literature.[28] (Please see the online supplement for detailed emissions calculations for each sub-process.) It is assumed that the distribution network already exists in this study; hence the life cycle impacts of commissioning and decommissioning the network are assumed to be negligible.

Necessary assumptions

Beyond the definition of the process boundaries, the following assumptions were also made with regards to the NGCC cradle-to-grave impact:

- The transmission efficiency of the distribution infrastructure is assumed to be 93 %.[28]
- All emissions are to the atmosphere (to-air). No water emissions were indicated in the available data.
- 1 % of all sequestered CO_2 escapes from the CCS pipeline as a fugitive emission.[31]

SOFC Full Life Cycle Study

Boundary definition

The boundary region for the SOFC plant contains the same main sub-processes as the NGCC plant, namely plant commissioning, upstream NG acquisition and processing, the operating plant itself, and optional blocks for the transmission network and the CCS pipeline. Similarly to the NGCC study, four boundary regions are considered for the SOFC plant, each including a combination of CCS and TML, as summarized in Table 5. As mentioned previously, the product output of the SOFC manufacturing sub-process is normalized to units of energy in the same fashion as the NGCC plant.[28] The full LCA boundary region for the SOFC plant is shown in Figure 7, with the dashed blocks and lines representing optional sub-processes and consequent flows, respectively. It should be noted that the final unit of energy produced by the SOFC plant is the net result of the SOFC, HRSG, and other bottoming cycles less any parasitic energy loads. For detailed information about the operation of the SOFC plant the reader is referred to the literature.[12,14] Detailed emissions per basis unit of energy for each sub-process are provided in the online supplement, and are omitted for the sake of brevity.

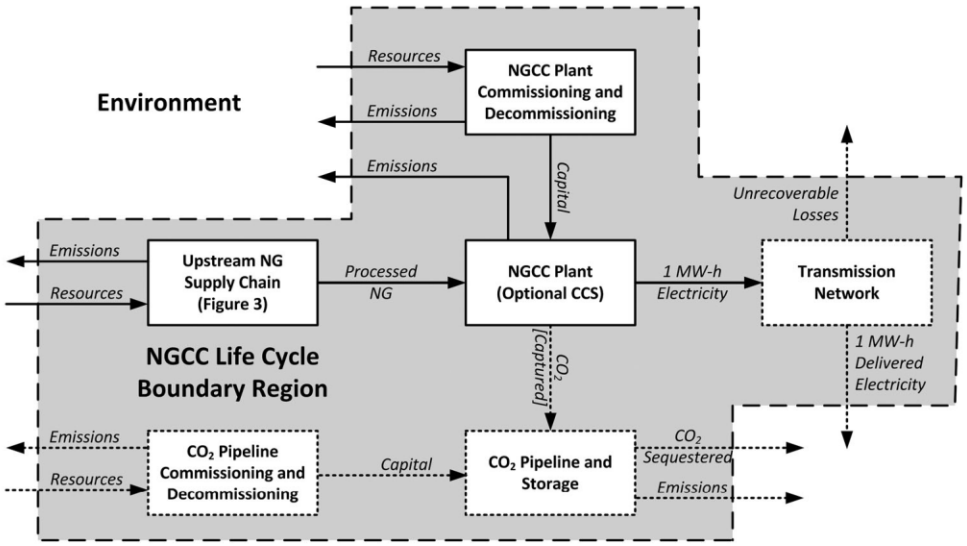

Figure 6. Cradle-to-grave boundary region block diagram for an NGCC plant including commissioning and decommissioning. Optional streams and sub-process are denoted by dashed lines.

Table 4. Description of each combination of optional sub-processes in the NGCC cradle-to-grave boundary region

Case Tag	TML Included?	CCS Included?	Net Efficiency (HHV)
NGCC-1	No	No	50.2 %
NGCC-2	Yes	No	46.7 %
NGCC-3	No	Yes	42.8 %
NGCC-4	Yes	Yes	39.8 %

Table 5. Description of each combination of optional sub-processes in the SOFC cradle-to-grave boundary region

Case Tag	TML Included?	CCS Included?	Net Efficiency (HHV)
SOFC-1	No	No	65.6 %
SOFC-2	Yes	No	61.0 %
SOFC-3	No	Yes	64.8 %
SOFC-4	Yes	Yes	60.3 %

Necessary assumptions

The assumptions for the SOFC boundary region include those listed in the assumption list for the NGCC plant. The following assumptions are unique to the SOFC plant:

- Since the fuel for the SOFC system is cleaned upstream of the power production step and is not combusted in air, the emissions of NO_x, SO_x, and N_2O were predicted to be negligible in prior studies and are therefore neglected for this analysis. However, the plant flue gas (with and without CCS) contains a non-trivial amount of H_2 that is accounted for (the studies consulted for the NGCC plant ignore this product).[12,14]

Calculation Strategy

Stream data for the SOFC plants were obtained from a combination of Aspen Plus v8.2 simulation files and previously documented results by the authors.[12,14] Mid-point characterization calculations were performed using OpenLCA v.1.3.0, an open-source life cycle inventory flowsheeting software.[40] However, due to the discovery of several bugs and inconsistent impact factor calculations in OpenLCA itself, all end-point characterization calculations were performed in-house using the *ReCiPe 2008* impact factor guidelines available in the literature.[41] Weighting factors for end-point impacts were selected as the average of those used in ReCiPe 2008 (40 % human health, 40 % ecosystem health, and 20 % resource depletion). (Please see the online supplement for more information.)

RESULTS AND DISCUSSION

For the sake of brevity, the results and discussion presented herein are those using the hierarchist (H) perspective for *ReCiPe 2008*. It should be noted that the perspective does impact the mid- and end-point results of each LCA, but the impact is consistent for each case investigated and therefore bears no impact on any comparative studies. The remaining perspectives (individualist and egalitarian) were calculated and are reported in the online supplement for the reader's interest.

SOFC Manufacturing Phase

Inventory and mid-point characterization results

Shown in Table 6 are the elemental flow inventory results for the construction of 1 kW of SOFC stacks and any required BoP materials. It can be seen that in order to manufacture a 1 kW stack of SOFCs, significant amounts of Ni, Cr, and Fe are required. Ni and Cr are particularly difficult to obtain and process, which has a large impact on resource depletion (as will be discussed later). Moreover, it can be seen that a high amount of coal (over 238 kg) must be consumed to partly fulfill the energy requirements of the manufacturing process. This is an expected result, since coal power is inefficient (with an optimistic process efficiency of 39 % by HHV), has a lower average energy density than other fossil fuels (24.8 MJ/kg versus the 44.1 MJ/kg in NG, for example) and accounts for the highest proportion of electrical energy consumed in the United States (see Table 3). This high consumption of coal in current pulverized coal (PC) power plants without CCS, combined with the consumption of other fossil fuels, leads to CO_2 emissions

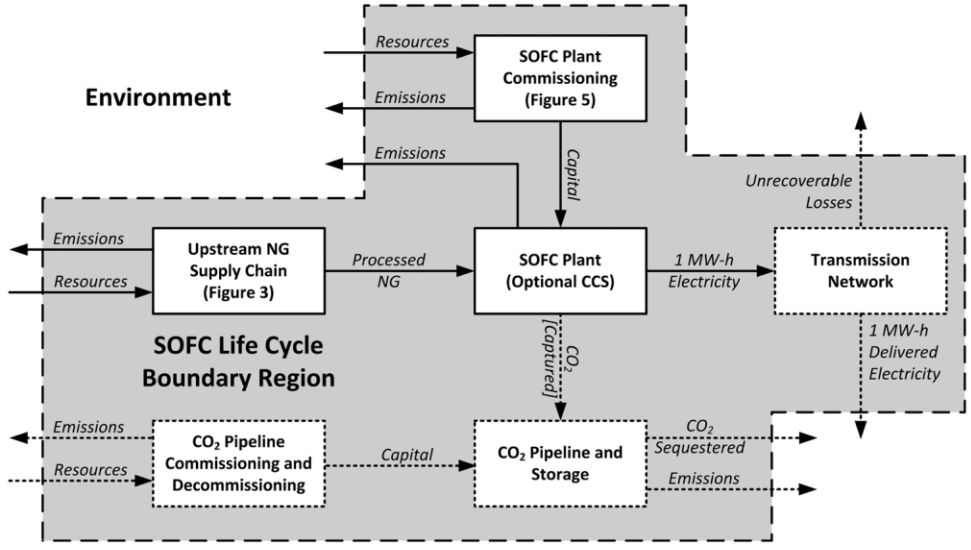

Figure 7. Cradle-to-grave boundary region block diagram for a SOFC plant including commissioning and decommissioning. Optional streams and sub-process are denoted by dashed lines.

Table 6. Cradle-to-gate life cycle resource flow inventory for the SOFC manufacturing stage

Inventory	Amount
Input Flows (kg)	
Chromium: 25.5 % (chromite); 11.6 % (crude ore)	26.79
Coal (hard)	283.29
Iron: 46 % (ore); 25 % (crude ore)	65.37
Natural Gas (44.1 MJ/kg)	64.88
Nickel: 1.13 % (sulfide); Ni 0.76% and Cu 0.76 % (crude ore)	8.75
Oil (crude)	4.30
Uranium (mined)	0.01
Output Flows (kg)	
Carbon Dioxide (CO_2)	944.19
Carbon Monoxide (CO)	0.29
Dinitrogen Monoxide (N_2O)	0.01
Methane (CH_4)	0.02
Nitrogen Oxides (NO_x)	0.87
Particulates $> 2.5\,\mu m$ and $< 10\,\mu m$	1.85
SOFC STACK (1 kW + BoP)	*1.00*
Sulfate	0.89
Sulfur dioxide (SO_2)	2.39

of over 944 kg per kW of SOFC stacks; the highest emission rate by a significant margin. Interestingly, the second- and third-highest emission rates are for SO_x (again from the high consumption of coal) and particulate matter.

Shown in Table 7 are the mid-point characterization results for the SOFC manufacturing process. Full detailed results are available in the online supplement. It can be seen that the high rate of CO_2 emission for this operation results in a high climate change (CC) potential of nearly one tonne of CO_2-equivalents (CO_2-Eq) per kW of SOFC stacks, or approximately the emissions of a typical passenger vehicle over a 2.5 month period.[42] Therefore, the CC potential of commissioning a 500 MW SOFC plant (ignoring operation) scales up to roughly 500 000 tonnes CO_2-Eq, or the equivalent impact of 100 000 vehicles operating for a calendar year. Due to the high consumptions of Ni, Cr, and Fe, the metal depletion impact for the construction of 1 kW of SOFC stacks is also significant at roughly 842 kg of Fe-equivalents (kg Fe-Eq), even though only 65 kg of Fe is actually consumed; this is due to the inaccessibility and much lower supplies of Ni and Cr occurring in the environment. Moreover, commissioning 1 kW of SOFC stacks consumes approximately 193 kg of oil-equivalents (oil-Eq), which is a significant amount of fossil fuels, especially when scaled to a bulk scale of 500 MW or larger. It should be noted that in the sources used to obtain the life cycle inventory information for this study, water consumption and toxic species were not documented.

Table 7. Mid-point characterization results (H perspective) for the SOFC manufacturing process per 1 kW SOFC stack constructed along with associated BoP

Mid-Point Inventory	Amount	Units
Climate Change	948.84	kg CO_2-Eq
Fossil Depletion	192.76	kg oil-Eq
Freshwater Ecotoxicity	0.00	kg 1,4-DCB-Eq
Human Toxicity	0.00	kg 1,4-DCB-Eq
Marine Ecotoxicity	0.00	kg 1,4-DCB-Eq
Marine Eutrophication	0.03	kg N-Eq
Metal Depletion	841.92	kg Fe-Eq
Particulate Matter Formation	2.52	kg PM_{10}-Eq
Photochemical Oxidant Formation	1.08	kg NMVOC
Terrestrial Acidification	2.88	kg SO_2-Eq
Terrestrial Ecotoxicity	0.00	kg 1,4-DCB-Eq
Water Depletion	0.00	m^3

End-point characterization results

Shown in Figure 8 are the cumulated end-point characterization results (in points, which are sometimes referred to as "EcoPoints") for the three main end-point impact categories. Breakdowns of the contributions of each mid-point characterization to specific end-points are omitted for the sake of brevity, but may be found in the online supplement.

The total impact for producing 1 kW of SOFC stacks is equal to 88.1 points, which is the equivalent to approximately 9 % of a human's impact on the environment over one year. Human health (HH) clearly experiences the largest impact (59 points), mainly due to the impacts of global warming chemicals and particulate emissions from the electricity supply chain. Resource depletion (RD, 26 points) is impacted by the high degrees of oil-Eq and Fe-Eq consumption. Interestingly, greenhouse gas species do not contribute significantly to ecosystem destruction (ED), resulting in a low contribution to the total (just over 3 points).

NGCC Plant Complete Life Cycle

Inventory and mid-point characterization results

Shown in Table 8 are the life cycle inventory results for each of the NGCC cases investigated in this study. Detailed results can be found in the online supplement. Note that metal and material consumptions were not available for this analysis and are therefore not present in the cradle-to-grave life cycle inventory for the NGCC process. As expected, the addition of CCS significantly decreases the global CO_2 emissions of the NGCC process (388 kg/MWh for case NGCC-1 versus 74.4 kg/MWh for case NGCC-3). However, the addition of CCS does not decrease global CO_2 emissions by 90 % (recall that this is the recovery of CO_2 for the NGCC) due to increased upstream emissions and pipeline losses; instead, only an 81 % reduction is achieved. Moreover, the addition of CCS requires 17.3 % more NG to achieve the same power output, which not only results in greater fossil fuel

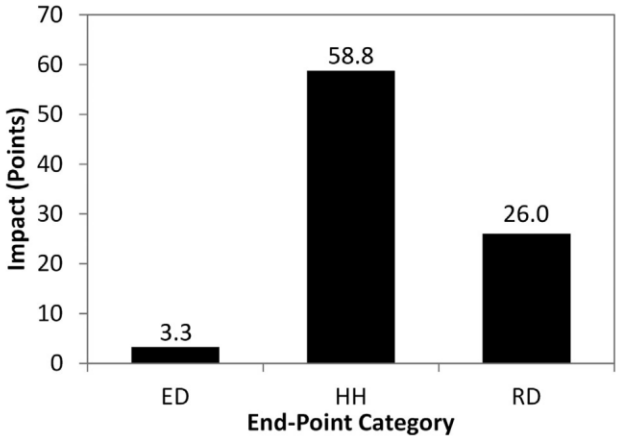

Figure 8. End-point impacts of the SOFC manufacturing process to produce 1 kW of SOFC stacks. Acronyms are defined in Table 1.

Table 8. Resource flow inventory for the NGCC cradle-to-grave life cycle

Inventory	NGCC-1	NGCC-2	NGCC-3	NGCC-4
Input Flows (kg)				
Natural Gas (44.1 MJ/kg)	186.91	200.99	219.23	235.73
Water (unspecified natural origin)	110.05	118.34	129.64	139.40
Output Flows (kg)				
Emissions to air (kg; unspecified population density and height)				
Ammonia (NH_3)	0.02	0.02	0.02	0.02
Carbon Dioxide (CO_2)	387.75	417.46	74.39	79.99
Carbon Monoxide (CO)	0.09	0.10	0.11	0.12
Dinitrogen Monoxide (N_2O)	6.35×10^{-4}	6.83×10^{-4}	7.50×10^{-4}	8.06×10^{-4}
Lead (Pb)	3.76×10^{-6}	4.04×10^{-6}	4.32×10^{-6}	4.64×10^{-6}
Mercury (Hg)	8.16×10^{-8}	8.77×10^{-8}	1.02×10^{-7}	1.09×10^{-7}
Methane (CH_4)	2.64	2.84	3.10	3.33
Nitrogen Oxides (NO_x)	0.37	0.40	0.43	0.47
NMVOC (non-methane volatile organics)	0.02	0.02	0.02	0.03
Particulates $> 2.5\,\mu m$ and $< 10\,\mu m$	0.01	0.01	0.01	0.01
Sulfur dioxide (SO_2)	0.02	0.02	0.02	0.02
Product Flows (MWh)				
Electricity Delivered, AC, Grid Quality	1.00	1.00	1.00	1.00

depletion, but also increases the amount of upstream fugitive CH_4 emissions by the same proportion. Depending on the LCA perspective used (all of which are reported in the online supplement), the impact of atmospheric CH_4 can vary significantly and thus such large increases in CH_4 emissions can have a large influence on a plant's global life cycle impact. The remaining inventories can be seen to increase in direct proportion to the NGCC plant's overall thermal efficiency.

Shown in Table 9 are the mid-point characterization results for the complete NGCC life cycle. Full detailed results are available in the online supplement. It can be seen that the addition of CCS to an NGCC plant reduces the CC impact by as much as 66.5 %. This is an important result, because it shows the importance of boundary definition and species tracking when performing a LCA. The addition of CCS is capable of reducing direct plant CO_2 emissions by 90 %, but extending the LCA boundary to include the full life cycle and additional species with global warming potential (GWP) reduces any apparent improvements in environmental impact by 23.5 percentage points. Moreover, it is important to note the trade-offs that exist between reducing life cycle CC potential and the impact that CCS has on other life cycle factors. It can be seen in Table 9 that although utilizing CCS yields a marked improvement to CC potential, every other mid-point impact category increases. Due to the decreased thermal efficiency of a NGCC plant using CCS, more NG and water is consumed, thereby eliciting higher fossil depletion and emissions from the upstream NG processing stage of the life cycle. Moreover, any species that are uncaptured at the gate of the NGCC plant (particulates, fugitive NO_x and SO_x) increase directly with fuel consumption (and inversely to thermal efficiency). An end-point analysis, discussed in the next section, is the best method with which to determine if this trade-off results in a lower total life cycle impact. As a final note, it is clear that accounting for transmission inefficiencies results in a proportional increase to all mid-point factors.

Table 9. Mid-point characterization results (H perspective) for the NGCC life cycle

Mid-Point Inventory	NGCC-1	NGCC-2	NGCC-3	NGCC-4	Units
Climate Change	454.04	488.72	152.12	163.58	kg CO_2-Eq
Fossil Depletion	170.46	183.30	199.94	214.99	kg oil-Eq
Freshwater Ecotoxicity	2.87×10^{-7}	3.08×10^{-7}	3.55×10^{-7}	3.82×10^{-7}	kg 1,4-DCB-Eq
Human Toxicity	0.10	0.11	0.12	0.13	kg 1,4-DCB-Eq
Marine Ecotoxicity	5.42×10^{-5}	5.83×10^{-5}	6.69×10^{-5}	7.19×10^{-5}	kg 1,4-DCB-Eq
Marine Eutrophication	0.02	0.02	0.02	0.02	kg N-Eq
Metal Depletion$^{\alpha}$	N/A	N/A	N/A	N/A	kg Fe-Eq
Particulate Matter Formation	0.10	0.11	0.11	0.12	kg PM_{10}-Eq
Photochemical Oxidant Formation	0.42	0.45	0.49	0.53	kg NMVOC
Terrestrial Acidification	0.27	0.29	0.27	0.34	kg SO_2-Eq
Terrestrial Ecotoxicity	8.61×10^{-6}	9.26×10^{-5}	1.07×10^{-5}	1.15×10^{-5}	kg 1,4-DCB-Eq
Water Depletion	110.05	118.34	129.64	139.40	m^3

α: The data required for computing metal depletion impacts were not available for the NGCC process.

End-point characterization results

Shown in Figure 9 are the cumulated NGCC end-point characterization results (in points) for the three main end-point impact categories. Breakdowns of the contributions of each mid-point characterization to specific end-points are omitted for the sake of brevity, but may be found in the online supplement. The total impact of producing 1 MWh of electricity from a NGCC without CCS is 44.2 points before TML and 47.5 points when considering TML. Interestingly, the global warming impact of an NGCC plant (reflected in the scores for ED and HH) is overshadowed by the resource depletion score. Consequently, according to *ReCiPe 2008* it is evident that, with regards to achieving a more sustainable life-cycle impact, the consumption of fossil fuels is just as important as (or even more important than) the emission of global warming species. This reinforces the notion that improved efficiencies will have a significant impact on the life cycle impact of generating electricity from fossil fuels; a lower fuel consumption for the same product not only decreases the largest life cycle impact contributor but also decreases all three of the main end-point impact categories simultaneously. However, it is clear that the addition of CCS reduces the ED and HH impacts of the NGCC by approximately 65 %, yielding a decrease of 9.5 life cycle impact points (21 %) overall in the case not considering TML. Two conclusions can be drawn from this result: (1) that capturing 90 % of the CO_2 generated in a NGCC plant only reduces its cradle-to-grave life cycle impact by 21 %; and (2) that the direct CO_2 emissions of a NGCC plant only account for approximately 23.3 % of its life cycle impact. The consideration of TML can be seen to increase all impact categories in direct proportion to the additional efficiency losses of the transmission infrastructure.

SOFC Plant Complete Life Cycle

Inventory and mid-point characterization results

Shown in Table 10 are the life cycle inventory results for each of the SOFC cases investigated in this study. Note that the results in Table 10 include the normalized SOFC manufacturing results discussed in the SOFC manufacturing life cycle study. Detailed results and breakdowns can be found in the online supplement. Unlike the NGCC plant, it can be seen that adding CCS to the SOFC plant greatly reduces its global CO_2 emissions with only very marginal increases in the other inventories (compare cases SOFC-1 and SOFC-3, for example). The small increases in other inventories are due to the marginal effect CCS has on the efficiency of the SOFC plant (approximately 1 percentage point). However, it should still be noted that although essentially 100 % of the direct CO_2 generated by the SOFC plant is captured at the plant gate, cradle-to-gate CO_2 emissions are only reduced by 93 % due to upstream emissions, the SOFC commissioning phase, and pipeline losses. Methane emissions are unable to be eliminated due to upstream NG losses that occur before the plant gate and increase with the addition of CCS and TML as the total system efficiency declines.

Shown in Table 11 are the mid-point characterization results for the complete SOFC life cycle (including the SOFC commissioning phase). Detailed results are available in the online supplement. As with the NGCC plant, CCS is able to eliminate the majority of the SOFC plant's CC potential, decreasing it by 77 % (274.3 points in the case of SOFC-1 versus SOFC-3). Although this decrease is significant, it exemplifies the role CH_4 leaks and the NG distribution network play in the cradle-to-grave life cycle impact of the SOFC process. However, unlike the NGCC process, the addition of CCS to the SOFC cases does not result in a marked increase in other mid-point characterizations; this is due in large part to the small parasitic energy load of CCS in a SOFC system. Overall, the SOFC process can be seen to compare favourably to the NGCC process in all mid-point categories and does not suffer from increased characterizations peripheral to CC potential with the introduction of CCS.

End-point characterization results

Shown in Figure 10 are the cumulated SOFC end-point characterization results (in points) for the three main end-point impact categories. Breakdowns of the contributions of each mid-point characterization to specific end-points are omitted for the sake of brevity, but may be found in the online supplement.

Due to higher system efficiencies and low parasitic energy costs for CCS, each SOFC case can be seen to have a lower overall life cycle impact compared to the equivalent NGCC case. As expected, the addition of CCS to the SOFC system reduces ED and HH each by over 70 %. However, as the mid-point characterization results may suggest, the increase in RD due to CCS addition is slight (less than 1 point). The overall improvement to end-point impact is approximately 35 %. Even for the more efficient SOFC process, RD clearly has the highest end-point impact (18–19 points) and accounts for more than 50 % of the total plant life cycle impact even when CCS is not utilized. This further reinforces that improved utilizations of fossil fuels are an important route through which the life cycle impact of electricity generation may be reduced regardless of the energy conversion strategy. As a final

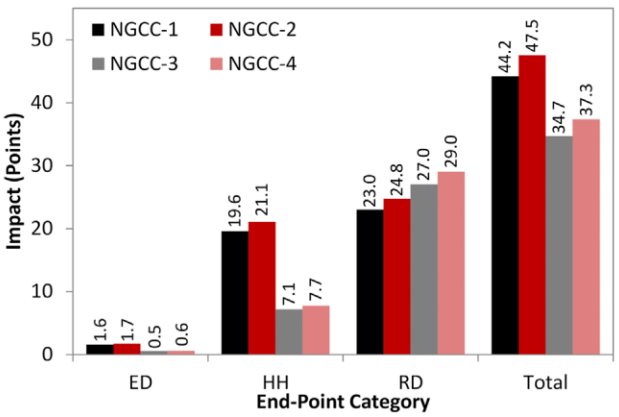

Figure 9. End-point impacts of the NGCC process to produce 1 MWh of delivered electricity. Acronyms are defined in Table 1.

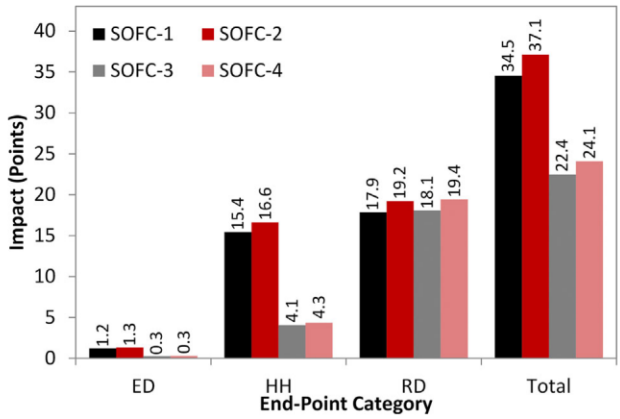

Figure 10. End-point impacts of the SOFC process to produce 1 MWh of delivered electricity. Acronyms are defined in Table 1.

Table 10. Resource flow inventory for the SOFC cradle-to-grave life cycle

Inventory	SOFC-1	SOFC-2	SOFC-3	SOFC-4
	Input Flows (kg)			
Chromium: 25.5 % (chromite); 11.6 % (crude ore)	0.31	0.31	0.31	0.31
Coal (hard)	3.23	3.23	3.23	3.23
Iron: 46 % (ore); 25 % (crude ore)	0.75	0.75	0.75	0.75
Natural Gas (44.1 MJ/kg)	143.78	154.56	145.54	156.35
Nickel: 1.13 % (sulfide) (crude ore)	0.10	0.10	0.10	0.10
Oil (crude)	4.91×10^{-2}	4.91×10^{-2}	4.91×10^{-2}	4.91×10^{-2}
Uranium (mined)	1.24×10^{-5}	1.24×10^{-5}	1.24×10^{-5}	1.24×10^{-5}
Water (unspecified natural origin)	83.65	89.96	84.68	91.00
	Emissions to air (kg; unspecified population density and height)			
Ammonia (NH_3)	1.41×10^{-3}	1.51×10^{-3}	1.42×10^{-3}	1.53×10^{-3}
Carbon Dioxide (CO_2)	306.51	328.81	31.81	33.36
Carbon Monoxide (CO)	7.73×10^{-2}	8.29×10^{-2}	7.19×10^{-2}	7.70×10^{-2}
Dinitrogen Monoxide (N_2O)	4.75×10^{-4}	5.11×10^{-4}	4.81×10^{-4}	5.17×10^{-4}
Hydrogen (H_2)	2.95×10^{-2}	3.17×10^{-2}	2.95×10^{-4}	3.15×10^{-4}
Lead (Pb)	9.41×10^{-7}	1.01×10^{-6}	9.53×10^{-7}	1.02×10^{-6}
Mercury (Hg)	4.52×10^{-8}	4.86×10^{-8}	4.58×10^{-8}	4.92×10^{-8}
Methane (CH_4)	2.03	2.19	2.05	2.20
Nitrogen Oxides (NO_x)	0.26	0.28	0.27	0.28
NMVOC (non-methane volatile organics)	1.72×10^{-2}	1.85×10^{-2}	1.74×10^{-2}	1.86×10^{-2}
Particulates $> 2.5\,\mu m$ and $< 10\,\mu m$	3.30×10^{-3}	3.55×10^{-3}	3.39×10^{-3}	3.64×10^{-3}
Sulfur dioxide (SO_2)	4.08×10^{-2}	4.18×10^{-2}	4.10×10^{-2}	4.20×10^{-2}
	Product Flows (MWh)			
Electricity Delivered, AC, Grid Quality	1.00	1.00	1.00	1.00

note, it should be mentioned that even though the commissioning and manufacture phase of the SOFC accounts for a significant amount of CO_2 emissions (which can add up to the equivalent of about 100 000 cars driving for one year for a 500 MW power plant), it still pales in comparison to the environmental impact of the regular use of the system; only approximately 1 % of the total life cycle impact of 1 MWh of electricity from the SOFC plant arises from commissioning and manufacture. This is typical of bulk-scale power plants.

Selected Case Comparisons

Next, some interesting comparisons between the NGCC and SOFC systems are discussed. For the sake of brevity, only the results for cases without TML are discussed in this section (NGCC-1, NGCC-3, SOFC-1 and SOFC-3) because the equivalent cases with TML (NGCC-2, NGCC-4, SOFC-2, SOFC-4) only differ from their non-TML equivalents by small amounts and in the same proportions. Moreover, only the hierarchist perspective is discussed in this section for the same reason: the individualist and egalitarian results show essentially the same trends and lead to the same conclusions. However, all of the results for those cases not discussed in this section are contained in the online supplement.

Shown in Figures 11 and 12 are selected mid-point and end-point characterization comparisons between each of the NGCC and SOFC cases investigated, respectively. It can be seen in Figure 11 that even when CCS is not used the SOFC plant is capable of producing electricity with lower values of all mid-point characterizations than NGCC without CCS. When CCS is

Table 11. Mid-point characterization results (H perspective) for the SOFC cradle-to-grave life cycle

Mid-Point Inventory	SOFC-1	SOFC-2	SOFC-3	SOFC-4	Units
Climate Change	355.85	382.64	81.55	86.93	kg CO_2-Eq
Fossil Depletion	132.31	142.28	133.92	143.78	kg oil-Eq
Freshwater Ecotoxicity	1.53×10^{-7}	1.65×10^{-7}	1.55×10^{-7}	1.67×10^{-7}	kg 1,4-DCB-Eq
Human Toxicity	0.04	0.04	0.04	0.04	kg 1,4-DCB-Eq
Marine Ecotoxicity	2.83×10^{-5}	3.04×10^{-5}	2.86×10^{-5}	3.07×10^{-5}	kg 1,4-DCB-Eq
Marine Eutrophication	0.01	0.01	0.01	0.01	kg N-Eq
Metal Depletion$^{\alpha}$	N/A	N/A	N/A	N/A	kg Fe-Eq
Particulate Matter Formation	0.09	0.09	0.09	0.09	kg PM_{10}-Eq
Photochemical Oxidant Formation	0.31	0.34	0.32	0.34	kg NMVOC
Terrestrial Acidification	0.19	0.21	0.19	0.21	kg SO_2-Eq
Terrestrial Ecotoxicity	4.69×10^{-6}	5.04×10^{-6}	4.75×10^{-6}	5.10×10^{-6}	kg 1,4-DCB-Eq
Water Depletion	83.65	89.96	84.68	91.00	m^3

α: Metal depletion statistics were not available for the NGCC process and are therefore considered only for the SOFC manufacturing stage for reference

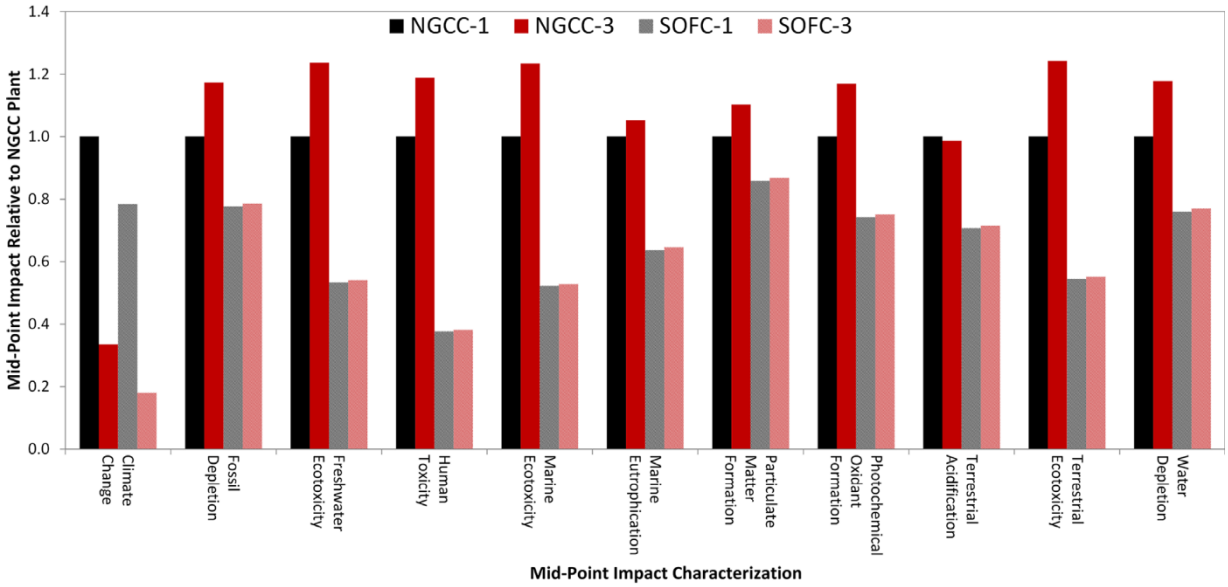

Figure 11. Selected normalized mid-point characterization comparisons of the NGCC and SOFC systems.

introduced to the SOFC system as in Figure 11, CC potential drops significantly to only 18 % of that of the NGCC plant without CCS. Moreover, the other mid-point characterizations do not increase substantially for the SOFC process due to the low parasitic energy cost (and therefore upstream impact) of adding CCS to the SOFC plant. This result can be extended to the end-point characterization results as shown in Figure 12, where it can be seen that case SOFC-3 scores approximately 80 % lower than NGCC-1 for ED and HH, and 21 % lower for RD.

Another interesting comparison is shown in Figure 11, wherein the NGCC plant with CCS (case NGCC-3) is compared to a SOFC plant without CCS (case SOFC-1). Although using CCS with a NGCC plant results in a marked reduction in CC potential (42.7 % of that of the SOFC plant without CCS), each of the other mid-point characterizations are still inferior to the SOFC plant. This is in large part due to the increased consumption of NG by case NGCC-3, which results in higher upstream impacts and greater emissions of uncaptured species at the plant gate.

The end-point characterization results for this comparison are particularly interesting. As shown in Figure 12, the ED and HH impacts of case NGCC-3 are less than 50 % of those of SOFC-1. However, due to the much lower efficiency of NGCC-3 versus

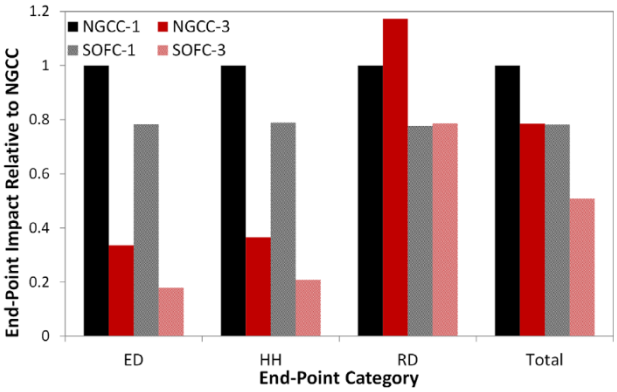

Figure 12. Selected normalized end-point characterization comparisons of the NGCC and SOFC systems.

SOFC-1, the RD metric for NGCC-3 is more than 50 % higher than for SOFC-1. Consequently, since RD has been shown to be the most significant contributor to each life cycle impact, the improvements to ED and HH for case NGCC-3 relative to SOFC-1 are outweighed by its higher RD score. This leads to the very interesting result that a NGCC plant operating with CCS actually has a slightly higher life cycle impact than a SOFC process without CCS (although for all practical purposes they are statistically indistinguishable due to the uncertainty inherent in the *ReCiPe* method). This result is significant in that it motivates the pursuit of developing electricity generation strategies utilizing SOFCs. Not only were SOFC systems shown to be economically favourable for many potential future market conditions in prior studies,[12–16] but their total life-cycle impact (including all upstream impacts and material requirements) are lower than the current state-of-the-art strategies for generating electricity from NG.

It is possible to combine the results of this study with that of previous techno-economic analyses to determine the added cost of CO_2 reductions and eco-point reductions for the SOFC and NGCC cases. Based on the results of our prior work,[12] the costs of adding CO_2 capture to bulk scale NGCC and SOFC plants (assuming a NG price of $2.33 per GJ) are $52.92 per MWh and $2.52 per MWh, respectively. Therefore, the cost of reducing global CO_2-Eq emissions can be calculated to be $175.28 and $9.19 per tonne of CO_2-Eq avoided for the NGCC and SOFC plants, respectively. Similarly, the cost per ecoPoint avoided can be computed to be $5.56 and $0.21 per point avoided, respectively. It is therefore evident that the addition of CCS to a SOFC plant is both economically and environmentally preferable. Moreover, adding CCS to the SOFC plant effectively provides an impact reduction of 1000 points (one human over a calendar year) at the cost of $210, which is an extremely effective trade-off between cost and environmental sustainability.

Sensitivity Analyses

As mentioned in the LCA Methodology section, the assumptions regarding mid- and end-point weighting and conversion factors can significantly impact the results of any given LCA. To this end, the following subsections describe the results of sensitivity

analyses of some of the most important assumptions made during this analysis. Again, only four selected cases are shown for brevity.

Ceteris paribus effects of end-point conversion factors

The largest degree of uncertainty in a typical LCA stems from the conversion of mid-point inventories to end-point impacts; the value of such things as human lives or species extinction is sometimes very different to compare. Therefore, each mid-to-end factor was adjusted exclusively to the others (*ceteris paribus*) by +/− 20 % of its original value, and the total end-point impact of each plant was recorded. Shown in Figure 13 is a tornado plot of the four most significant factors and their effects on each of the plant configurations considered. All other mid-to-end point conversion factors had a smaller effect on the end-point LC impact of the plants and are omitted here for brevity, but the results can be found in the online supplement.

It can be seen in Figure 13 that, unsurprisingly, the climate change impact conversion has a large impact on the total points for any process without CCS. However, it is interesting to note that a change to the fossil depletion end-point conversion factor has the largest impact on the end-point impact for any given plant (NGCC or SOFC), yielding at least a +/− 10 % change in end-point impact for a +/− 20 % change in the assumed factor. These results reinforce the conclusion that resource depletion is the largest contributing factor to the end-point impact of the systems considered in this study. Moreover, it is clear in Figure 13 that the relative impact of changing each factor is similar for the non-CCS cases (NGCC-1 and SOFC-1) as well as the with-CCS cases (NGCC-3 and SOFC-3). For example, both NGCC-3 and SOFC-3 suffer from larger relative deviations from their base-case value for a change in the fossil depletion factor because, due to the reduction in climate change impact brought about by CCS, the effect of resource depletion is emphasized for both cases.

Factor Decrease		Factor Increase		Plant
Points	*% Change in Points*	*% Change in Points*	*Points*	
+/- 20% Change in Fossil Depletion				
39.6	-10.4%	+10.4%	48.8	NGCC-1
29.3	-15.6%	+15.6%	40.1	NGCC-3
31.0	-10.3%	+10.3%	38.1	SOFC-1
18.8	-16.1%	+16.1%	26.0	SOFC-3
+/- 20% Change in Climate Change				
40.1	-9.2%	+9.3%	48.3	NGCC-1
33.3	-3.9%	+3.9%	36.0	NGCC-3
31.3	-9.3%	+9.3%	37.7	SOFC-1
23.2	-3.3%	+3.3%	21.7	SOFC-3
+/- 20% Change in Particulate Matter Formation				
44.0	-0.3%	+0.3	44.4	NGCC-1
34.5	-0.5%	+0.5	34.8	NGCC-3
34.4	-0.4%	+0.4	34.7	SOFC-1
22.3	-0.6%	+0.6%	22.6	SOFC-3
+/- 20% Change in Terrestrial Acidification				
44.1	-<0.1%	+<0.1%	44.3	NGCC-1
34.7	-<0.1%	+<0.1%	34.7	NGCC-3
34.5	-0.0%	+0.0%	34.5	SOFC-1
22.4	-0.0%	+0.0%	22.4	SOFC-3

Figure 13. Ceteris paribus sensitivity results for the four most significant mid-to-end point conversion factors.

Furthermore, the lower efficiencies of the plants using CCS result in higher natural gas consumption, which further drives up the impact of fossil depletion. In a similar vein as (but to a lesser extent than) fossil depletion, the impact of changing particulate matter formation increases with the addition of CCS for both systems due to the higher consumption of natural gas. The climate change conversion factor also has a large impact on the end-point results of each plant configuration, although its alteration has a noticeably smaller effect on the systems utilizing CCS. Moreover, it is important to note that a change in the climate change factor has a smaller impact on case SOFC-3 than NGCC-3 due to the higher rate of carbon capture (and lower upstream emissions) of the SOFC plant. A final observation that can be made in Figure 13 is that changing certain parameters significantly affects which system of NGCC-3 and SOFC-1 has a lower life cycle impact overall. This further reinforces that the two plants are nearly equivalent when it comes to their cradle-to-grave life cycle impacts.

Monte Carlo analysis

For this analysis, all assumed characterization factors were perturbed using a normally distributed pseudo-random mutation with a mean (μ) equal to the base-case value of the parameter and a standard deviation (σ) of 20 %. This procedure was repeated 10 000 times, with the end-point impact being recorded for each instance. The resulting end-point probability density distributions for each of the four case studies investigated are shown in Figure 14. Detailed data corresponding to this figure for each case study are reported in the online supplement.

It can be seen that, even in the presence of significant (and often compounding) uncertainties, case SOFC-3 has a significantly lower end-point impact than NGCC-1. Furthermore, the standard deviations of the SOFC systems (9.3 and 7.4 points per MWh for SOFC-1 and SOFC-3, respectively) are significantly lower than the standard deviations of the NGCC systems (11.9 and 11.2 points per MW-h for NGCC-1 and NGCC-3, respectively). Since the NGCC plants consume more natural gas (thereby requiring additional upstream processing) and produce more emissions (CO_2 and others), they have a higher dependence on the assumed factors for this study. Furthermore, it can be seen that the addition of CCS to the SOFC system significantly tightens the distribution of expected end-point impacts (σ is reduced from 9.3 to 7.4 points per MWh). Due to the significant parasitic energy cost and therefore increased resource consumption of adding CCS to the NGCC plant, the reduction of uncertainty from adding CCS is not nearly as significant. Finally, Figure 14 shows

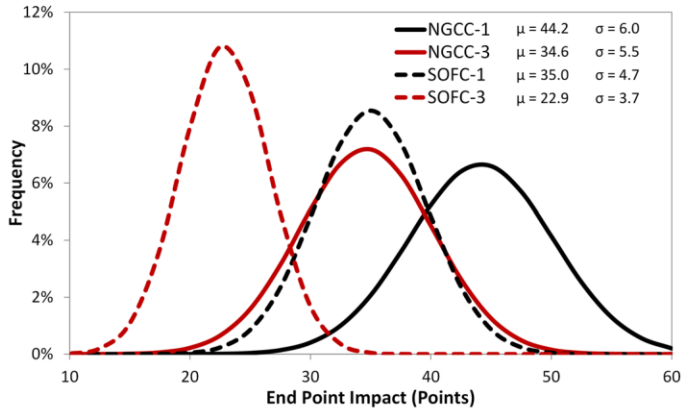

Figure 14. End-point probability distributions of each case study investigated.

how cases NGCC-3 and SOFC-1 give very similar results even under high degrees of uncertainty; a recurring theme throughout this study.

CONCLUSIONS AND FUTURE WORK

A complete life cycle analysis was performed for a system that generates electricity using natural gas-fueled solid oxide fuel cells (SOFCs) and compared it to the state-of-the-art natural gas combined cycle. Both LCAs accounted for all upstream material and fuel acquisition and processing in order to form a complete cradle-to-grave perspective. The LCA method *ReCiPe 2008* was used to perform both mid- and end-point characterization calculations for three socioeconomical perspectives, all of which are documented in the online supplement. The boundary regions for each process and any necessary sub-process were defined and any required assumptions were made to develop a consistent basis of comparison between the processes. Carbon capture and sequestration and transmission network losses and their impacts on the life cycles of each process were also considered.

It was found that the manufacturing stage of 1 kW of SOFC cells and their associated balance of plant contributes a noticeable portion to the entire life cycle impact of the SOFC process. The manufacturing of 1 kW of SOFC cells was found to release approximately 950 kg CO_2-equivalents, consume 193 kg of oil-equivalents, and require approximately 840 kg of iron-equivalents. Most emissions from SOFC manufacturing are the result of consuming electricity during the manufacturing process, which was assumed to be supplied by the average electricity mix in the United States. With regard to end-point impacts, the manufacturing of 1 kW of SOFCs has the impact of 88.1 points, which is approximately 9 % of the impact of a human being over one year.

The addition of CCS to the NGCC process reduced direct CO_2 emissions by 90 %, but reduced global CO_2 emissions by only 81 %. Moreover, the decreased efficiency of the NGCC plant with CCS resulted in increases of NG and water consumptions of 17 % in order to produce the same amount of electricity. Uncaptured direct emissions were found to increase with added fuel consumption as well. The NGCC process without CCS was found to have an end-point impact of 44 points per MWh of electricity generated, which is approximately 4.4 % of a human's impact over one year. The end-point reduction of adding CCS to the NGCC plant was found to be partially offset by increased resource consumption, but yielded an overall decrease of approximately 21 % to 35 points. Considering TML was found to increase all life-cycle impact categories proportionally to its added inefficiency, details of which can be found in the online supplement.

The addition of CCS to the SOFC process reduced direct CO_2 emissions by 100 % and decreased global CO_2 emissions by approximately 93 %. However, adding CCS to a SOFC process has a very low parasitic energy penalty and hence does not facilitate the need for significantly more NG. As such, the impacts of upstream NG acquisition and processing were small. The SOFC process without CCS was found to have an end-point impact of 35 points per MWh of electricity generated, which is approximately 3.5 % of a human's impact over one year and 9 points (20 %) lower than the NGCC plant without CCS. The end-point reduction of adding CCS to the SOFC plant was significant, yielding an overall decrease of approximately 35 % to 22 points. Considering TML was found to increase all life-cycle impact categories proportionally to its added inefficiency, details of which can be found in the online supplement.

A comparison of cases showed that the SOFC plant without CCS is capable of producing 1 MWh of electricity with a lower life-cycle impact than the NGCC process in all scenarios, even when CCS is used with the NGCC exclusively. As a final note, if a current NGCC plant running without CCS were to be replaced with an equivalent SOFC system utilizing CCS, the complete life cycle impact of generating electricity of such a scenario would be reduced by 50 % for the same amount of power produced.

This work has reinforced the applicability and potential of utilizing NG in SOFC systems to produce clean, reliable electricity when compared to the current state-of-the-art systems. Not only can direct system CO_2 emissions be essentially eliminated, but the entire life cycle impact of the electricity generation infrastructure using NG can be reduced by as much as 50 % without requiring any changes to the upstream NG supply chain.

NOMENCLATURE

ALO	agricultural land occupation
ASU	air separation unit
CAES	compressed air energy storage
CC	climate change
CCS	carbon capture and sequestration
DCB	dichlorobenzene
ED	damage to ecosystem diversity
FD	fossil depletion
FE	freshwater eutrophication
FET	freshwater ecotoxicity
HH	damage to human health
HHV	higher-heating value
HRSG	heat recovery and steam generation
HT	human toxicity
IR	ionizing radiation
LCA	life cycle analysis
MD	metal depletion
ME	marine eutrophication
MET	marine ecotoxicity
NGCC	natural gas combined cycle
NLT	natural land transformation
NMVOC	non-methane volatile organic compound
OD	ozone depletion
PEN	positive-electrolyte-negative
PM_{10}	particulate matter with radius 10 μm
PMF	particulate matter formation
POF	photochemical oxidant formation
RD	damage to resource depletion
SOFC	solid oxide fuel cell
TA	terrestrial acidification
TET	terrestrial ecotoxicity
ULO	urban land occupation
WD	water depletion

REFERENCES

[1] Intergovernmental Panel on Climate Change, "Climate Change 2013: The Physical Science Basis," *Fifth Assesment Report of the Intergovernmental Panel on Climate Change*, Camberidge University Press, Cambridge **2013**.

[2] National Energy Board, "Canada's Energy Future: Energy Supply and Demand Projections to 2035 - Electricity Outlook Highlights," accessed June, 2012, http://www.neb-one.gc.ca/clfnsi/rnrgynfmtn/nrgyrprt/nrgyftr/2011/fctsht1134lctrct-eng.html

[3] US Energy Information Administration, *AEO2012 Early Release Outlook*, US DOE/EIA-0383ER **2012**.

[4] H. J. Herzog, D. Golomb, "Carbon capture and storage from fossil fuel use," *Encyclopedia of Energy*, C. J. Cleveland Ed., Elsevier Science, New York **2004**, p. 277.

[5] EG&G Technical Services, *DOE/NETL Fuel Cell Handbook*, 7th edition, November 2004.

[6] T. A. Trabold, J. S. Lylak, M. R. Walluk, J. F. Lin, D. R. Trojani, *Int. J. Hydrogen Energy* **2012**, *37*, 5190.

[7] N. Q. Ming, *ECS Trans.* **2007**, *7*, 45.

[8] M. C. Williams, J. P. Strakey, W. A. Surdoval, *Int. J. Appl. Cerma. Technol.* **2005**, *2*, 295.

[9] F. P. Nagel, T. J. Schildhauer, S. M. A. Biollaz, *Int. J. Hydrogen Energy* **2009**, *34*, 6809.

[10] H. Jin, E. D. Larson, F. E. Celik, *Biofuels Bioprod. Bioref.* **2009**, *3*, 142.

[11] T. A. Adams II, J. Nease, D. Tucker, P. Barton, *Ind. Eng. Chem. Res.* **2013**, *52*, 3089.

[12] J. Nease, T. A. Adams II, *J. Power Sources* **2013**, *228*, 281.

[13] J. Nease, T. A. Adams II, *J. Power Sources* **2014**, *251*, 92.

[14] T. A. Adams II, P. Barton, *J. Power Sources* **2010**, *195*, 1971.

[15] T. A. Adams II, P. I. Barton, *AIChE J.* **2010**, *56*, 3120.

[16] T. A. Adams II, P. I. Barton, *Fuel Proc. Tech.* **2011**, *92*, 2105.

[17] P. Kuchonthara, S. Bhattacharya, A. Tsutsumi, *Fuel* **2005**, *84*, 1019.

[18] A. Verma, A. D. Rao, G. Samuelsen, *J. Power Sources* **2006**, *158*, 417.

[19] M. Li, A. Rao, J. Brouwer, G. Samuelsen, *J. Power Sources* **2010**, *195*, 5707.

[20] S. Park, J. Ahn, T. Kim, *Appl. Energy* **2011**, *88*, 2976.

[21] L. Zhao, J. Brouwer, *ECS Transactions* **2012**, *42*, 247.

[22] V. Karakoussis, N. P. Brandon, M. Leach, R. van der Worst, *J. Power Sources* **2001**, *101*, 10.

[23] F. Baratto, U. M. Diwekar, *J. Power Sources* **2005**, *139*, 188.

[24] C. Strazza, A. Del Borghi, P. Costamagna, A. Traverso, M. Santin, *Appl. Energy* **2010**, *87*, 1670.

[25] K. Tanaka, C. Wen, K. Yamada, *Fuel* **2000**, *79*, 1493.

[26] R. J. Braun, *J. Fuel Cell Sci. Tech.* **2010**, *7*, 031018–1.

[27] J. Lin, C. W. Babbit, T. A. Trabold, *Bioresource Technol.* **2013**, *128*, 495.

[28] L. Haslbeck, N. J. Kuehn, E. G. Lewis, L. L. Pinkerton, J. Simpson, M. J. Turner, E. Varghese, M. C. Woods, *Cost and Performance Baseline for Fossil Energy Plants. Volume 1: Bituminous Coal and Natural Gas to Electricity Final Report*, DOE/NETL-2010/1397 Revision 2 **2010**.

[29] M. Hasan, R. Baliban, J. Elia, C. Floudas, *Ind. Eng. Chem. Res.* **2012**, *51*, 15665.

[30] M. Hasan, R. Baliban, J. Elia, C. Floudas, *Ind. Eng. Chem. Res.* **2012**, *51*, 15642.

[31] L. Drauker, R. Bhander, B. Bennett, T. Davis, R. Eckard, W. Ellis, J. Kauffman, J. Littlefield, A. Malone, R. Munson, M. Nippert, M. Ramezan, R. Bromiley, *Life Cycle Analysis: Natural Gas Combined Cycle (NGCC) Power Plant*, DOE/NETL-403-110509 **2010**.

[32] T. J. Skone, J. Littlefield, J. Marriott, *Life Cycle Greenhouse Gas Inventory of Natural Gas Extraction, Delivery and Electricity Production*, DOE/NETL-2011/1522 **2011**.

[33] B. Singh, A. H. Strømman, E. Hertwich, *Int. J. Greenhouse Gas Control* **2011**, *5*, 457.

[34] M. Owsianiak, A. Laurent, A. Bjørn, M. Z. Hauschild, *Int. J. Life Cycle Assessment* **2014**, *19*, 1007.

[35] M. Goedkoop, R. Heijungs, M. Huijbregts, A. De Schryver, J. Struijs, R. van Zelm, *Recipe 2008 First Edition* (revised, version 1.08), Ministerie van Volkshuivesting, Ruimtelijke Ordening en Milieubeheer **2013**.

[36] T. J. Skone, "Life Cycle Greenhouse Gas Analysis of Natural Gas Extraction and Delivery in the United States," *U. S. Department of Energy Lecture*, Cornell University, 12 May **2011**.

[37] United States Environmental Protection Agency, "2009 Boiler, Generator, Plant, State, PCA, eGRID Subregion, NERC Region, US, and Grid Loss (%) Data," **2009**, accessed November 2013, http://www.epa.gov/cleanenergy/energy-resources/egrid/

[38] R. D. Dumas, *Energy Usage and Assumptions Associated with Electrical Energy Consumption as a Part of a Solid Waste Management Life Cycle Inventory Model*, Department of Civil Engineering, North Carolina State University **1997**.

[39] C. Jiminez-Gonzalez, D. J. Constable, *Green Chemistry and Engineering: A Practical Design Approach*, John Wiley & Sons, Hoboken, NJ, USA **2011**.

[40] A. P. Acero, C. Rodriguez, A. Ciroth, "LCIA methods: Impact assessment methods in Life Cycle Assessment and their impact categories," *GreenDelta GMBH* **2014**, http://www.openlca.org/documents/14826/3bbaecf3-5efa-4a00-a965-4dc91c25b531

[41] M. Goedkoop, R. Heijungs, M. Huijbregts, A. De Schryver, J. Struijs, R. van Zelm, *Recipe 2008 First Edition* (version 1.08), Characterization Factor Spreadsheet, Pré Consultants **2013**.

[42] United States Environmental Protection Agency, "Greenhouse Gas Emissions from a Typical Passenger Vehicle," *EPA Office of Transportation and Air Quality* **2011**, http://www.epa.gov/otaq/climate/documents/420f11041.pdf

---

Manuscript received June 4, 2014; revised manuscript received August 14, 2014; accepted for publication September 16, 2014.

Chapter 5

Comparative Life Cycle Analyses of Bulk-Scale Solid Oxide Fuel Cell Power Plants

The content of the following chapter is a **published reprint** of the following peer-reviewed publication:

Nease J, Adams TA II. Comparative life cycle analyses of bulk-scale coal-fueled solid oxide fuel cell power plants. *Applied Energy*. 2015; 150: 161-175.

This paper makes reference to an online supplement submitted and reviewed with the full publication. The supplement is extensive and is not reproduced in this work, but has been made available electronically with the file name:

`Chapter_5_Supplement.xslx`

Applied Energy 150 (2015) 161–175

Contents lists available at ScienceDirect

Applied Energy

journal homepage: www.elsevier.com/locate/apenergy

Comparative life cycle analyses of bulk-scale coal-fueled solid oxide fuel cell power plants

Jake Nease, Thomas A. Adams II *

Department of Chemical Engineering, McMaster University, 1280 Main Street West, Hamilton, Ontario, Canada

HIGHLIGHTS

- A full LCA of a solid oxide fuel cell power plant fuelled by coal is performed using *ReCiPe 2008*.
- LCAs are performed for modern state of the art (IGG, SCPC) coal plants for comparative purposes.
- Mid- and end-point impacts are tabulated for each plant with and without the use of carbon capture.
- SOFC plants with carbon capture have much lower life cycle impacts than state of the art plants.
- Results are compared with natural gas plants using *ReCiPe* to assess the impact of different fuels.

ARTICLE INFO

Article history:
Received 27 January 2015
Received in revised form 18 March 2015
Accepted 21 March 2015

Keywords:
Life cycle analysis
Solid oxide fuel cells
Coal
Natural gas
Gasification

ABSTRACT

Detailed cradle-to-grave life cycle analyses are performed for bulk-scale solid oxide fuel cell power plants fueled by gasified coal. These results are compared to cradle-to-grave life cycle analyses of the supercritical pulverized coal and integrated gasification combined cycle power generation plants, which are also performed as a part of this study. Life cycle inventories for each plant including the inputs (resources and fuels) and outputs (emissions and waste) of the gate-to-gate plants and their associated up- and down-stream sub-processes are computed. The impact of carbon capture and sequestration on each plant is quantified and assessed using the *ReCiPe 2008* life cycle inventory method for three socioeconomic perspectives. The results of each coal plant are compared to one another and to plants generating power from natural gas at the end-point level. Results indicate that not only do coal-fed SOFCs generate power with a significantly lower life cycle impact than the current state-of-the-art coal plants, but when carbon capture is enabled they can do so with a lower impact than the most modern plants utilizing natural gas, as well.

1. Introduction and motivation

The growth of industrialization, worldwide population and overall quality of life in most regions of the world has led to increasing demands for the production of reliable electricity. Moreover, increasing concern regarding greenhouse gas emissions and the environmental impact of fossil fuel consumption has resulted in the need for efficient, reliable and environmentally responsible energy production strategies [1]. Research dedicated to the development of wind, solar and biofuel energy sources has been significant, but these technologies are not yet ready to completely replace more traditional methods utilizing fossil fuels [2]. Over the next 20 years, it is anticipated that wind, solar, and biomass use will comprise approximately 10% and 16% of the electricity markets in Canada [3] and the United States [4], respectively. Contrarily, electricity derived from natural gas (NG) is anticipated to account for 15% and 34% of all power produced by 2035 for Canada [3] and the United States [4], respectively. Furthermore, even with the expected growth of renewable technologies, coal is still anticipated to be a dominant contributor to the United States' power mix in 2035, supplying approximately 34% of demand [4]. Not only is coal anticipated to remain a large contributor, but over 250 years of coal capacity (at the current usage rate) is available in North America. The abundance of coal coupled with its forecasted importance in the North American energy mix motivates the development of processes that can use it in an environmentally and socially sustainable manner [5].

Solid oxide fuel cell (SOFC) power plants with integrated carbon capture and sequestration technology (CCS) have been proposed as

* Corresponding author at: 1280 Main Street West, Hamilton L8S 4L7, Ontario, Canada. Tel.: +1 (905) 525 9140x24782.
E-mail address: tadams@mcmaster.ca (T.A. Adams II).

http://dx.doi.org/10.1016/j.apenergy.2015.03.105
0306-2619/

Nomenclature

ALO	agricultural land occupation
ASU	air separation unit
CAES	compressed air energy storage
CC	climate change
CCS	carbon capture and sequestration
DCB	Dichlorobenzene
ED	damage to ecosystem diversity
FD	fossil depletion
FE	freshwater eutrophication
FET	freshwater ecotoxicity
HH	damage to human health
HHV	higher-heating value
HRSG	heat recovery and steam generation
HT	human toxicity
IR	ionizing radiation
LCA	life cycle analysis
MD	metal depletion
ME	marine eutrophication
MET	marine ecotoxicity
NGCC	natural gas combined cycle
NLT	natural land transformation
NMVOC	non-methane volatile organic compound
OD	ozone depletion
PEN	positive-electrolyte-negative
PM_{10}	particulate matter with radius 10 μm
PMF	particulate matter formation
POF	photochemical oxidant formation
RD	damage to resource depletion
SOFC	solid oxide fuel cell
TA	terrestrial acidification
TET	terrestrial ecotoxicity
ULO	urban land occupation
WD	water depletion
WGS	water gas shift

a way of producing electricity from coal with almost no CO_2 emitted directly from the power plant itself, while also significantly reducing water consumption [6]. This process and its many variants have been studied by many different groups (see [6] for an extensive review) and has repeatedly been shown to be a very promising way of using coal with potentially higher efficiencies and reduced direct CO_2 emissions than the current state-of-the-art supercritical pulverized coal (SCPC) process or even the integrated gasification combined cycle (IGCC) process with carbon capture.

However, to the best of our knowledge, a cradle-to-grave life cycle analysis (LCA) of large-scale coal-based SOFC power plants has not been presented in the open literature. This is important because, although the downstream CO_2 emissions of this process are lower than state-of-the-art coal-based processes, the effects of upstream portions of the supply chain have not previously been considered. Similarly, other environmental factors such as resource depletion, human health impacts, and acid rain formation should also be considered in order to understand if global warming potential might be reduced at the expense of other forms of environmental damage. There have been prior investigations for plants at smaller scales such as auxiliary power units without CCS [7,8], studies focused on the impact of using alternative fuels in SOFC stacks [9], or studies which only considered the life-time cost impact of using SOFCs [10]. However, none of these investigations have used a method to incorporate a broad range of environmental factors such as human health, ecosystem destruction and resource consumption, and none have considered gasified coal as a feedstock [11].

To this end, this work presents a comprehensive cradle-to-grave life cycle analysis (LCA) of a large-scale power plant utilizing solid oxide fuel cells (SOFCs). The SOFC plant is fueled by the gasification of coal. The LCA is determined using the *ReCiPe 2008* (revised 2013) method, which is also applied to the state-of-the-art supercritical pulverized coal (SCPC) process and a more futuristic integrated gasification combined cycle (IGCC) for the first time. This work is a significant extension of our prior work in which a similar analysis was applied to NG-based power plants [12]. The supply chains for coal and NG-based processes are very different, and thus required separate consideration. However, since the methodology, standards, and assumptions are consistent, useful comparisons between the coal and NG-based processes can be made, which are also presented in this work.

1.1. Solid-oxide fuel cells

The SOFC is an emerging device in which a fuel gas is electrochemically oxidized by the transport of oxygen ions through an impermeable solid oxide barrier which can be formed from a variety of zirconia and perovskite materials [14–19]. SOFCs are an exciting frontier for power generation because they possess some very strong synergistic advantages. First, the anode of the SOFC can accept a variety of carbonaceous or hydrogen-based fuels such as gasified coal [20], methanol [21], natural gas [22], gasified biomass [23] and more [6,24–27]. Furthermore, the cell drives exothermic electrochemical reactions and typically operates at high temperatures (up to 1000 °C depending on material limitations), and is thus well-suited to downstream heat, power and even energy storage integration to improve its efficiency and utility at the systems level [25,26]. Moreover, the impermeable electrolytic barrier separating the anode and cathode of the SOFC prevent the mixing of fuel with air, therefore resulting in an exhaust stream of H_2O, CO_2 and unspent fuel. This allows for efficient and reliable carbon capture without the use of solvents or other methods of absorption that encumber typical CCS strategies [14]. A more detailed SOFC description is omitted from this work for the sake of brevity, but a simplified diagram depicting a typical planar SOFC is provided for reference in Fig. 1. There have been multiple studies in literature that have shown the effectiveness of SOFCs at the systems level for providing highly efficient power (beyond 60% electrical efficiency) [26–33]. A comprehensive review of the industrial and academic status of SOFC research is given by Adams et al. [6].

1.2. Producing power from coal: the current state-of-the-art

1.2.1. Supercritical pulverized coal process description

For this study, the SCPC process is assumed to be the plant of choice were a new greenfield plant to be constructed. What follows is a brief description of the SCPC process for the reader's reference; however, a full detailed process description and plant diagram are omitted for the sake of brevity, and can be found in the NETL bituminous baseline report [34].

Coal is combusted with air in a high-efficiency boiler, the energy from which is used to generate supercritical steam at approximately 240 bar and 593 °C. The steam is expanded in a series of turbines to generate power. The combustion products are

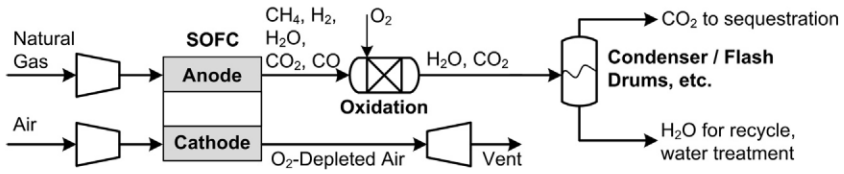

Fig. 1. Simplified schematic of producing power from NG using SOFCs. Reproduced with permission from [6].

primarily CO_2, H_2O, SO_2, ashes and any inerts that were in the air (N_2, Ar). Small amounts of impurities such as Hg, Cl, NO_x and dust are also produced. Various well-proven processes are used to remove ash, Cl, Hg, SO_2 and NO_x, although these processes are typically not able to completely remove these components. The final clean exhaust stream, containing mainly H_2O, CO_2, N_2 and trace Ar can then be vented to the atmosphere (as is typically done), or post-combustion CO_2 removal can be used to extract and sequester CO_2 if desired. A typical post-combustion CCS process uses solvent-based absorption employing a variety of chemical (such as MEA) or physical (such as Rectisol™) solvents, the optimal selection of which strongly depends on the composition and physical conditions of the flue gas [35]. Approximately 90% of the CO_2 in the flue gas is captured at pipeline purities, with the remainder being too costly to recover and thus is vented via the exhaust stream [34]. The most significant drawback of solvent-based absorption CCS methods is that they are highly energy intensive, leading to high parasitic energy loads on the plant and therefore significant penalties to overall electrical and thermal efficiencies. These decreased efficiencies result in higher fuel and overhead costs, when combined with the additional capital investment of installing the CCS system leads to increased break-even life cycle electricity prices of as much as 73% [36]. Other CCS approaches such as pressure swing adsorption, vacuum swing adsorption and membrane separations are possible [37,38], although they are not considered in this work. A life cycle inventory (LCI) of the gate-to-gate SCPC process has been performed by the NETL, but it does not include environmental life cycle impact assessments (LCIA) or the application of *ReCiPe 2008* [36]. Therefore, the LCIA is presented in this work. LCIAs using other methodologies have been performed on other electricity generation processes using coal and other fuel sources (see [39] for example), but no investigation, to the best of the authors' knowledge, has included all of the life cycle impact factors accounted for in *ReCiPe 2008*. Therefore, this work presents LCIAs using *ReCiPe 2008* which were computed using the published inventory data, to provide a consistent basis for comparison.

1.2.2. Integrated gasification combined cycle process description

IGCC plants operate in a similar fashion to SCPC plants, with a few modifications. What follows is a brief description of an IGCC process, with greater details contained in the literature [34]. A coal slurry is fed with O_2 from an air separation unit (ASU) to an oxygen-blown gasifier, producing synthesis gas ("syngas", a mixture of H_2 and CO) as well as a solid slag and many of the same impurities (e.g.: Hg, Cl, and NO_x.) as the SCPC plant. After cleaning and dehydration, the syngas stream may be upgraded via the water-gas shift (WGS) reaction mechanism, but this is not typically done in IGCC plants not attempting CCS. The syngas is then mixed with N_2 as a diluent (the other product from the ASU) and is burnt in a combustion turbine, producing power. The exhaust stream is then sent to a heat recovery steam generation (HRSG) cycle to generate additional power before being vented to the atmosphere.

Carbon capture can be performed using many of the same methods as the SCPC plant, however the location of CCS is different. Although post-combustion CCS is a possibility, it is usually better to use the WGS reaction after the gasifier to convert the syngas stream into mainly H_2, CO_2 and impurities, and then separate the H_2 and CO_2 prior to combustion using a two-stage Selexol™ or other solvent-based absorption method. The products from the combustion turbine in this case are mainly H_2O and N_2 combined with any of the CO_2 that slipped through the upstream CCS stage. As with the SCPC plant, approximately 90% of the CO_2 generated in the process is recovered with significant parasitic energy losses [34].

Although there have been several studies presenting a LCA of IGCC plants, the examples currently in the literature typically only account for GHG emissions and, in rare cases, material consumption during plant commissioning [40–42]. Prior to this work, no studies to the best of our knowledge have presented a LCA using *ReCiPe 2008* or have included any of the many end-point impact factors therein.

1.3. Producing power from natural gas: the natural gas combined cycle

In this work, the natural gas combined cycle (NGCC) is considered for comparative purposes. The NGCC process consists of an integrated compressor–combustor–turbine–generator system, where waste heat from the hot combustion exhaust is recovered and used to make steam to power steam turbines for additional power. If desired, carbon capture is employed using a solvent-based post-combustion method. All LCA results were taken directly from our prior work, to which the reader is referred for a more detailed description of this process and its life cycle [12].

1.4. Description of life cycle assessment method: ReCiPe 2008

ReCiPe 2008 offers a unified life cycle analysis method which attempts to quantify the impact of a product's life cycle at both the mid-point (kg CO_2 equivalents, kg of oil equivalents consumed, etc.) and end-point (human life years lost, environmental species destroyed, etc.) levels based on an inventory of flows to or from the environment (designated as elementary flows) [43]. End-point results are normalized to a unified point system to obtain a quantified scale of the product's entire life cycle impact. By using a unified point-based system, it is possible to not only compare the life cycles of similar products, but those in entirely separate industries as well. The calculations in *ReCiPe 2008*, as with any life cycle analysis tool, consist of a series of unit conversions (such as kg of CH_4 emissions to kg of equivalent CO_2 emissions) based on characterization factors with varying degrees of uncertainty [43]. Since these characterizations are somewhat subjective, *ReCiPe 2008* considers three so-called life cycle perspectives, all of which are considered in this work and can be found in the online supplement:

- The individualist (I) perspective is based on humanity's short-term interests. It uses impact types that are not disputed (climate change and resource depletion, for example), and makes optimistic assumptions about the adaptability of humanity

and technology to utilize declining resource pools in the near future. This perspective puts a lower weighting on toxicity and acidification, but a higher weighting on short-term global warming potential (20 year outlook).

- The heirarchist (H) perspective is based on common policy principles regarding time frames and environmental stability. Generally speaking, it is the most evenly weighted of all perspectives and is often used as a default perspective (100 year outlook).
- The egalitarian (E) perspective is the most pessimistic with regards to long-term global warming potential. It takes the longest time frames into account for factors such as atmospheric CO_2 retention and considers some impact factors that are not yet fully established but are anticipated to have an impact (500 year outlook).

A more detailed description of *ReCiPe 2008* is outside the scope of this work (see the *ReCiPe* manual for an in-depth discussion [43]), but a general description of *ReCiPe* as it applies to this work can be found in our prior publication [12].

The environmental considerations used in this work are consistent with our prior work, and so agricultural land occupation, freshwater eutrophication (commonly caused by fertilizer runoff), urban land occupation, natural land transformation, ionizing radiation and ozone depletion were not considered [12]. A summary of the mid-point factors for *ReCiPe 2008* that were and were not considered in this work are provided in Table 1. *ReCiPe 2008* is used for all processes in this work so that the results may be compared on a consistent basis, but it is important to note that results can vary depending on the LCA method chosen [44].

Table 1
ReCiPe 2008 mid- and end-point factors and indication of their inclusion in this study [43].

Category	Tag	Units	Considered
Mid-point characterizations			
Agricultural land occupation	ALO	m^2	NO
Climate change	CC	kg CO_2-eq	YES
Fossil depletion	FD	kg oil-eq	YES
Freshwater ecotoxicity	FET	kg (1,4)-DCB-eq	YES
Freshwater eutrophication	FE	kg P-eq	NO
Human toxicity	HT	kg (1,4)-DCB-eq	YES
Ionizing radiation	IR	kg U^{235}-eq	NO
Marine ecotoxicity	MET	kg (1,4)-DCB-eq	YES
Marine eutrophication	ME	kg N-eq	YES
Metal depletion	MD	kg Fe-eq	YES[a]
Natural land transformation	NLT	m^2	NO
Ozone depletion	OD	kg CFC-11-eq	NO
Particulate matter formation	PMF	kg PM_{10}-eq	YES
Photochemical oxidant formation	POF	kg NMVOC	YES
Terrestrial acidification	TA	kg SO_2-eq	YES
Terrestrial ecotoxicity	TET	kg (1,4)-DCB-eq	YES
Urban land occupation	ULO	m^2	NO
Water depletion	WD	m^3	YES
Category	Tag	Units[b]	Considered
End-point characterizations			
Damage to human health	HH	DALY[c]	YES
Damage to ecosystem diversity	ED	Species-yrs	YES
Damage to resource depletion	RA	$	YES

[a] Data for metal depletion is not available for the SOTA systems used in this study, but it is available for the SOFC plants and several of their associated subsystems. As such metal depletion is included in the impact analysis for the SOFC systems for completeness, but is omitted from case comparisons.

[b] End-point units are converted to "EcoPoints" (measured in "points") in this investigation using the standard *ReCiPe 2008* method. Please see the online supplement submitted with this article for conversion information.

[c] Daily average life years.

2. Methodology

2.1. Bases of calculations

The basis unit chosen for each plant is 1 MW h of delivered electricity to the consumer (equivalent to 3600 MJ). This includes any system losses, waste, and transmission losses that occur at all points in the supply chain network upstream and downstream of the plant in question. The "grave" of each unit of electricity is the consumption of the electric power in whatever device in which it is used. Since it is impossible to predict what that device may be, the device itself is not in the life cycle.

The SOFC manufacturing stage uses a basis unit of 1 kW of net useable SOFC capacity, including any balance-of-plant (BoP) materials and resources required for their operation. In order to convert this to a basis of MW h of power, the lifetime of the SOFCs was assumed to be 10 years when operating at full capacity. This is a realistic forward-looking lifetime for SOFC stacks and has been used in multiple prior studies investigating the economics of SOFC systems [25,26]. With a lifetime assumed, it is possible to convert the impact of 1 kW of SOFC stacks to a per-MW h basis, which was consistent with our prior work.

The fuel (NG and coal) is reported on a per-unit of energy basis by higher heating value (HHV). This was possible by assuming constant energy densities of NG and coal on a per-mass basis, the details of which are discussed in the assumptions in Sections 2.2 and 2.3.

2.2. Natural gas supply chain

The state-of-the-art coal plants considered in this work use a measurable amount of NG during start-up and shut-down procedures. The boundary region definition and breakdown of what NG sources contribute to the average supply are shown in Fig. 2 and Table 2, respectively [12]. Several sources were used to obtain this information [46,47,49]. It is assumed that 98% of the final NG is from domestic sources, and 2% is liquefied NG (LNG) imported from Trinidad and Tobago.

2.3. Coal supply chain

For a complete LCA of all coal-fired plants investigated in this study, the upstream coal supply chain was modeled as a sub-process. The following subsections define the boundary regions of this sub process and any assumptions that were made throughout the modeling process. Multiple sources were considered and cross-referenced to obtain this information [36,42].

2.3.1. Boundary region definition

The boundary of the coal supply chain is shown in Fig. 3. The final product is defined on a basis of 1 MJ of processed and delivered coal to the gate of the power plant, including the locating, mining, cleaning and transportation requirements of the coal.

2.3.2. Necessary assumptions

All coal in this study was assumed to be Illinois Bituminous coal #6, mined and upgraded in the continental United States. All transportation is performed via a General Electric 4400 hp (3281 kW) diesel locomotive towing 100 rail cars each with a loaded capacity of 91 tonnes. A list of further assumptions is as follows:

- The HHV of the coal arriving at the plant gate is 27,135 kJ/kg [34].
- 45% of the coal extracted from the mine is assumed to be unusable. For the purposes of this study, this means that the resources required to obtain and process 1 kg of raw coal out of the ground only results in 0.55 kg of coal delivered to the plant gate [36,42].

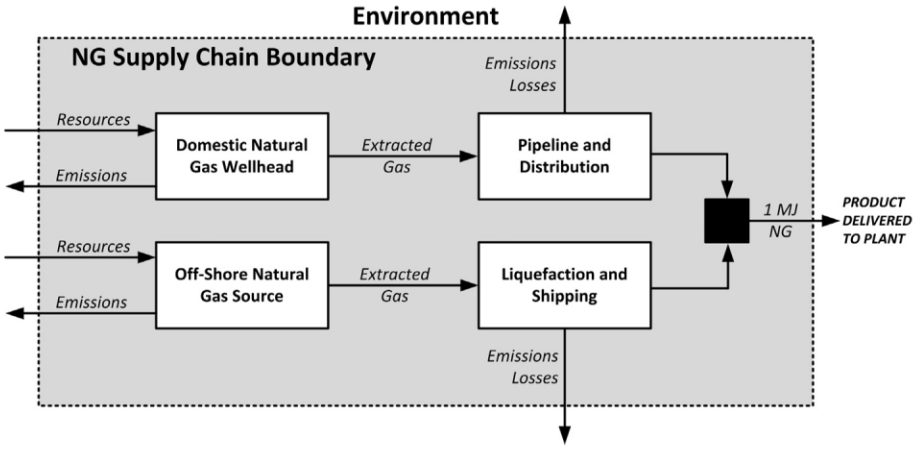

Fig. 2. NG supply chain showing different sources. Reproduced with permission from [12].

Table 2
Breakdown of NG sources in the United States.

Domestic gas[a]	Source	% of Domestic gas
Conventional	Onshore	24.5
	Associated	12.5
	Offshore	7.0
Unconventional	Tight	31.0
	Shale	16.0
	CBM	9.0
Imported source	Source	% of Imported Gas
Offshore	LNG	100.0

[a] Domestic gas is assumed to account for 98% of the NG consumed in the United States. 2% is imported.

- Any unsuitable raw coal that is rejected during the mining and refining process is assumed to be returned to the environment in its original form and is thus not counted as a resource consumed or displaced during the mining process. The proper treatment of coal returned during the mining process is a topic of some debate, but not classifying returned coal as a consumed resource is the most common practice. This assumption, as discussed later, is very important when quantifying the resource depletion of coal-fueled plants, and is relaxed in the sensitivity analysis section.
- The rail distance from the mine to any average plant in the continental United States is 1872 km [36].
- It is assumed that approximately 40 km of new rail spurs are required to connect the existing rail network (assumed to already exist) to the mine and plant gates [42].
- Fugitive dust emissions from the open coal rail cars are considered, but any significant losses of coal during the transportation stage are assumed to be included in the coal rejection rate of 45%.
- Water is not consumed in an appreciable amount during the mining and transportation stage [36].
- All mining is performed via underground long-wall mining [36].

2.4. SOFC manufacturing cradle-to-gate study

As in our prior work, the manufacturing stage of the SOFC plant life cycle is an important consideration. The reader is referred to our prior work for a detailed description of the SOFC manufacturing boundaries and their associated assumptions; the figures are reproduced in the appendix for convenience. As mentioned in Section 2.1, the per-kw of stacks output from the SOFC manufacturing process is normalized to a per-MW h delivered electricity basis by assuming a useable SOFC stack lifetime of 10 years.

2.5. NGCC full life cycle study

The NGCC life cycle is consistent with our prior investigation, with the inclusion of emissions and efficiency losses from the transmission network [12]. The boundary definition is shown in Fig. 4. All assumptions used are consistent with that of the prior work.

2.6. SCPC and IGCC life cycle studies

Since the SCPC and IGCC plants considered in this work have similar structures to their life cycle boundaries and possess largely the same set of assumptions, they are presented together in this section.

2.6.1. Boundary definition

Fig. 5 depicts the life cycle boundary definition for the SCPC and IGCC plants considered in this work. The upstream NG supply chain is included in this boundary region because modern coal plants also consume a modest amount of NG to maintain high

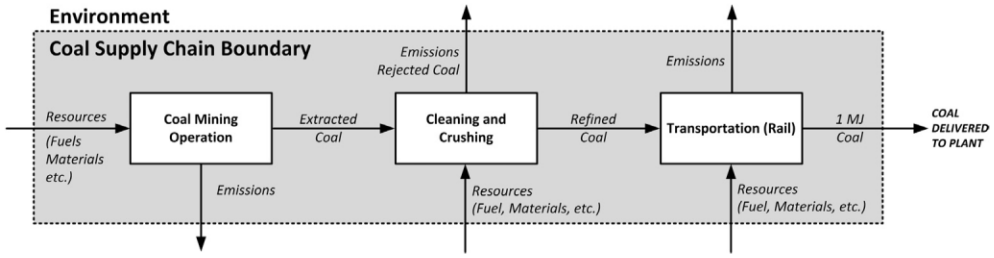

Fig. 3. Coal supply chain sub process.

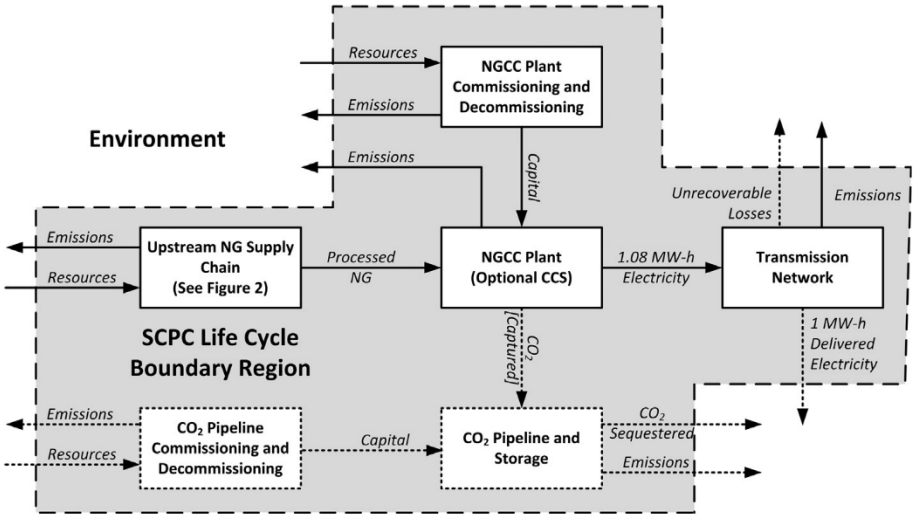

Fig. 4. NGCC cradle-to-grave life cycle boundary with compulsory transmission network emissions and losses.

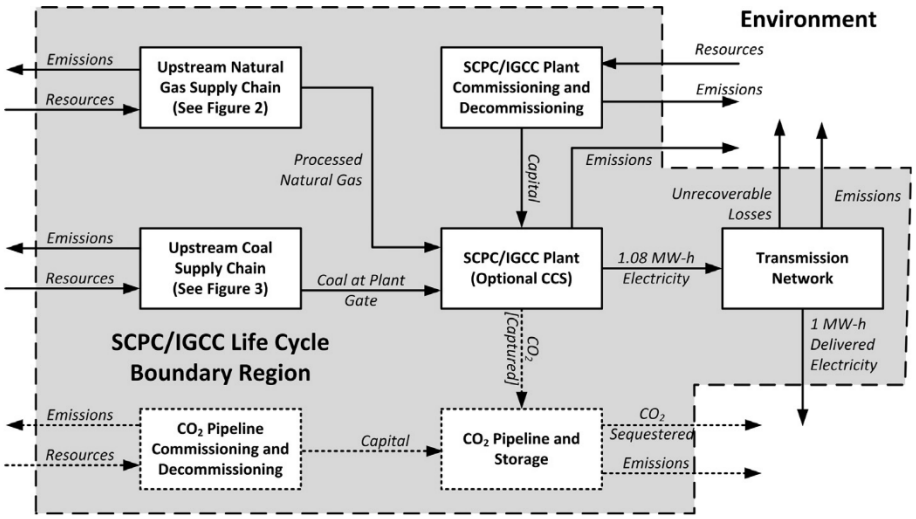

Fig. 5. Current SOTA coal plant (SCPC and IGCC) boundary region definitions. Dashed lines and boxes (all CCS-related sub processes and products) represent optional additions that are considered in this work.

temperatures in certain process units during temporary shutdowns which can occur at various points during the life of the plant [36,42]. The transmission network includes the material usage and emissions associated with maintaining the transmission network over an allocated duration of 20 years (annualized to a per-MW h of electricity delivered basis). The final basis unit of electrical energy is the net output of either the boiler steam cycle (in the case of the SCPC) or combustion turbine with bottoming cycle (for the IGCC) after all parasitic loads have been considered, including compression, the ASU sub-process, and any energy loads associated with CCS.

2.6.2. Necessary assumptions

Beyond the definition of the life cycle boundary for these coal plants, the following assumptions were also made:

- The electrical efficiencies of the SCPC and IGCC plants are assumed to be 39.3% and 39.0% by HHV, respectively [34,36,42].
- The electrical efficiencies of the SCPC and IGCC plants with chemical absorption-based Selexol™ CCS processes are assumed to be 28.4% and 32.6% by HHV, respectively [34,36,42].
- The WGS reactions upstream of the combustion turbines in the IGCC plant are assumed to reach approximately 98% conversion [34].
- 90% of the CO_2 in the flue/syngas stream is recovered and delivered to the CO_2 pipeline.
- 1% of the CO_2 that is pipelined is lost to the atmosphere as fugitive emissions.
- Any NG consumed for both coal plants is assumed to be of the same origin and quality as that which is consumed by the NGCC and NG-fed SOFC plants.
- The transmission efficiency of the power grid over the average transmission distance is assumed to be 93% [36].
- All emissions are to the atmosphere via stack gases and fugitive emissions.

2.7. Coal-fueled SOFC life cycle study

2.7.1. Boundary definition

The coal-fueled SOFC boundary region is similar to that of the state-of-the-art coal plants. The SOFC boundary region includes the sub-processes for coal mining and transport, SOFC plant

commissioning and decommissioning, and downstream transmission networks. However, unlike the state-of-the-art coal plants, NG is not included as a flow into the SOFC coal plant process block because no NG is required for the day-to-day operation of the SOFC coal plant, and there is no known requirement to use NG in any appreciable amount during startup or maintenance phases. Although startup and maintenance issues for coal-fueled SOFC bulk systems are not well-studied, we do not expect that any NG use that may be required during these times would contribute significantly to the total life cycle impact.

Optional sub-processes for CCS are included as dashed blocks. The output of the SOFC commissioning stage is normalized to a basis unit of 1 MW h as mentioned previously by assuming a useful life 10 years for the SOFC stacks. The final electrical energy output from the plant gate is the power produced by the SOFC stacks and HRSG bottoming cycle minus all parasitic loads, many of which are similar to the state-of-the-art coal plants. Details regarding the operation and specific stream conditions within the SOFC plant can be found in the literature [25,6,28]. Furthermore, there have been several studies that have investigated the life-cycle impact of the fabrication of SOFC stacks and their associated balance-of-plant, several of which were used in our prior work and are thus continued to be used in this work [12,45,50]. With these points in mind, the complete cradle-to-grave life cycle boundary of the coal-fueled SOFC plant considered in this study is shown in Fig. 6.

2.7.2. Necessary assumptions

The assumptions for the SOFC boundary region include all of those listed in Section 2.6.2. The following assumptions are unique to the SOFC plant:

- The emissions of N_2O, NO_x, Cl, Hg and SO_x are not assumed to be negligible for this process. However, since there is no stream data in the literature regarding coal-fueled SOFC plant design regarding pollutant emissions, it is assumed that the SOFC plant emits these pollutants at the same rate as the IGCC plant referred to in literature on a per-kg of coal consumed basis [42]. The IGCC plant is chosen because it also uses gasification as a method of processing coal.
- The SOFC plant emits a non-negligible amount of unreacted H_2 in the stack exhaust. It is therefore assumed that this H_2 enters the atmosphere alongside the other pollutants.

Table 3
Summary of all cases investigated and compared in this study.

Case tag	Fuel source	CCS included?	Net efficiency before transmission (HHV) (%)
SCPC	Coal	No	39.3
SCPC-CCS	Coal	Yes	39.0
IGCC	Coal	No	28.4
IGCC-CCS	Coal	Yes	32.6
SOFC-C	Coal	No	42.9
SOFC-C-CCS	Coal	Yes	42.0
NGCC[a]	NG	No	50.2
NGCC-CCS[a]	NG	Yes	42.8
SOFC-NG[a]	NG	No	65.6
SOFC-NG-CCS[a]	NG	Yes	64.8

[a] NGCC, NGCC-CCS, SOFC-NG and SOFC-NG-CCS are cases NGCC-1, NGCC-3, SOFC-1 and SOFC-3 from [12], respectively.

2.8. Summary of cases investigated

Table 3 shows a summary of all cases subjected to a full LCA in this study and the cases used from the prior study for comparative purposes. The net electrical efficiencies before transmission losses of each plant are also shown. In total there are 6 plants operated using coal and 4 plants operated using NG.

2.9. Calculation strategy

Stream data for the SOFC plants were taken from simulation files developed and published by the authors in *Aspen Plus v8.2* [26,28]. All mid-point characterizations were obtained through the life cycle inventory flowsheeting software *OpenLCA v1.3.4* [51]. Since there were several bugs in the *OpenLCA* software that were found during cross-validation of end-point calculations, all end points were ultimately determined using in-house calculations by referencing the *ReCiPe 2008* calculation guidelines and impact factors freely available in the literature [52]. *Ceteris Paribus* sensitivity analyses were performed by perturbing flows and mid-point conversions in *OpenLCA* and *Excel*, while Monte Carlo simulations of end-point conversion factors were performed in *MATLAB*. As a final note, when determining end-point impacts the average weightings of those used in *ReCiPe 2008* were adopted (40% human health, 40% ecosystem health and 20% resource depletion) [52].

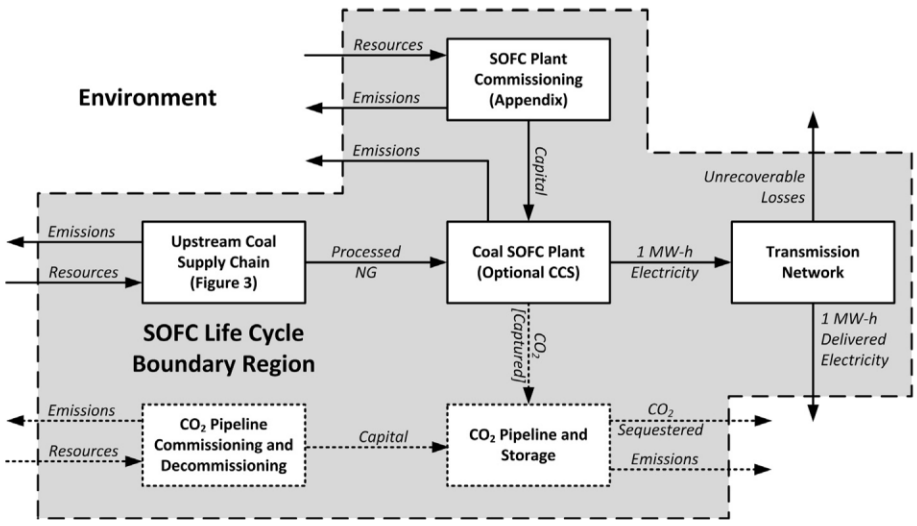

Fig. 6. Coal-fueled SOFC plant life cycle boundary. Dashed boxes and lines represent optional sub processes and flows for CCS.

3. Results and discussion

For the sake of brevity, all results and discussion discussed herein considers the LCA results using the "heirarchist" (H) perspective in *ReCiPe 2008*. This was chosen as a representative perspective because it assumes a medium-length outlook and impact length for all factors considered. It should be noted that although different perspectives result in slightly different results in an absolute sense, the comparative results of each plant investigated and general conclusions do not change as long as the same perspective is used for each. The other perspectives (egalitarian and individualist) were also calculated and are available in the online supplement for the reader's interest.

3.1. Supercritical pulverized coal life cycle analysis

3.1.1. Inventories and mid-point characterization results

Table 4 shows the life cycle inventory results for the cradle-to-grave LCA of the SCPC processes with and without the addition of CCS. Full results and details for all perspectives can be found in the online supplement. It can be seen that, as expected, the largest required input to the process for both case studies is coal. However, the 363 kg of coal consumed in the production of 1 MW h of power using the SCPC plant is approximately 7.5% higher than the required plant-gate coal to generate 1 MW h of power at an electrical efficiency of 39%. Approximately 7% of this extra coal must be consumed in order to overcome the electrical losses that occur throughout the transmission network, and approximately 0.5% of this coal is used during the commissioning and decommissioning stage of the SCPC plant. The most significant emissions for the SCPC (regardless of CCS) is, unsurprisingly, CO_2. The life-cycle emission of CO_2 for the SCPC plant is 1020.5 kg/MW h, which is 26% higher than the plant gate emissions of 811 kg/MW h reported in the literature [26], which clearly reinforces the need for complete cradle-to-grave perspectives when determining the CO_2 footprint of power generation. Adding CCS to the SCPC plant increases coal consumption by 38%, which is mainly due to the parasitic energy costs associated with the chemical absorption CCS method used to capture CO_2 in SCPC plants. Furthermore, even though 90% of CO_2 is assumed to be captured at the plant gate, the addition of CCS to a SCPC plant decreases its cradle-to-grave CO_2 emissions by 82.1%, down to 182.6 kg/MW h. Upstream emissions during the mining and transportation of coal as well as leakages from the CO_2 pipeline and geological storage site for CO_2 thus have a significant impact on the effectiveness of CCS.

The other most prominent emissions from the SCPC plant include methane (from coal mine gases and the upstream processing of NG to be used in the SCPC plant), SO_2, NO_x and particulates. Although there are cleaning and capture stages designed to trap SO_2, NO_x and particulates within the gates of the SCPC process, they are not 100% effective. One point of interest is that the SCPC plant releases more particulates than the IGCC or SOFC plants (discussed later) because it is the only process that combusts pulverized coal, allowing for far more particulates to escape through the flue gases. Adding CCS to the SCPC plant has the expected effect of increasing all uncontrolled emissions due to a lower electrical efficiency. However, it is interesting to note that SO_2 emissions actually decrease with the addition of CCS, which is due to slippage of SO_2 and NO_x into the Selexol™ solvent, therefore ending up in the CCS pipeline stream instead of the atmosphere.

Table 5 shows the mid-point characterization results for the SCPC process. Full details for all perspectives are available in the online supplement. It can be seen that the high rate of CO_2 emissions for the SCPC plant result in a very high climate change (CC) potential of 1094 kg CO_2-eq/MW h of electricity delivered. To put this in perspective, a 500 MW (net) SCPC plant, when considering the entire cradle-to-grave lifecycle, has the GHG impact equivalent to 958,344 passenger vehicles in the United States [53]. Adding CCS to the SCPC plant reduces its CC potential by 74.1% to 283.2 kg CO_2-eq/MW h, but this is still a significant amount of CC potential. Note also that the reduction of cradle-to-grave kg of CO_2-eq by adding CCS to the SCPC plant (74.1%) is significantly lower than the reduction of cradle-to-grave CO_2 emissions 82.1%). This result emphasizes the importance of accounting for all emissions, not just CO_2, that potentially contribute to CC. In this case, the increased methane, SF_6 and N_2O emissions of the SCPC plant with CCS detract from the overall efficacy of the CCS system. Another significant mid-point impact factor for the SCPC plant is fossil depletion (FD), which is 165.4 and 228.8 kg oil-eq/MW h for the SCPC and SCPC-CCS plants, respectively. Since large amounts of coal are consumed in this process at a relatively low efficiency, the FD metric becomes quite significant. This result is consistent with what was found in our prior work investigating plants using NG as a fuel source [12]. CCS addition increases FD of the SCPC plant by 38.4%, which is a significant offset to the reduction in CC when considering end-point impacts (discussed in the next section). Human toxicity (HT) is another category that is significant for the SCPC plant, mainly due to the high Hg and Pb content in coal and thus some eventual escape to the atmosphere.

Table 4
Life cycle inventory results for the cradle to grave life cycles of SCPC plants.

Inventory	SCPC	SCPC-CCS
Input flows (kg)		
Coal (hard, in ground, 27.135 MJ/kg)	362.99	502.30
Natural gas (in ground, 44.1 MJ/kg)	0.22	0.26
Oil (crude, in ground)	6.70	9.27
Water (unspecified natural origin)	2315.41	3866.60
Emissions to air (kg; unspecified population density and height)		
Ammonia (NH_3)	4.93×10^{-4}	6.82×10^{-4}
Carbon dioxide (CO_2)	1020.51	182.62
Carbon monoxide (CO)	4.86×10^{-2}	6.11×10^{-2}
Dinitrogen monoxide (N_2O)	4.95×10^{-4}	6.90×10^{-4}
Lead (Pb)	5.29×10^{-5}	5.40×10^{-5}
Mercury (Hg)	5.36×10^{-6}	8.54×10^{-6}
Methane (CH_4)	2.81	3.88
Nitrogen oxides (NO_x)	0.37	0.28
NMVOC (non-methane volatile organics)	4.02×10^{-3}	5.34×10^{-3}
Particulates > 2.5 μm and < 10 μm	0.11	0.10
Sulfur dioxide (SO_2)	0.46	0.11
Sulfur hexaflouride (SF_6)	1.42×10^{-4}	1.43×10^{-4}
Product flows (MW h)		
Electricity delivered, AC, grid quality	1.00	1.00

Table 5
Mid-point characterization results (H perspective) for the SCPC life cycle.

Mid-point inventory	SCPC	SCPC-CCS	Units
Climate change	1094.06	283.16	kg CO_2-eq
Fossil depletion	165.36	228.79	kg oil-eq
Freshwater ecotoxicity	1.79×10^{-5}	2.83×10^{-5}	kg 1,4-DCB-eq
Human toxicity	3.61	5.28	kg 1,4-DCB-eq
Marine ecotoxicity	3.26×10^{-3}	5.14×10^{-3}	kg 1,4-DCB-eq
Marine eutrophication	0.01	0.01	kg N-eq
Metal depletion[a]	N/A	N/A	kg Fe-eq
Particulate matter formation	0.28	0.18	kg PM_{10}-eq
Photochemical oxidant formation	0.44	0.34	kg NMVOC
Terrestrial acidification	0.67	0.2657	kg SO_2-eq
Terrestrial ecotoxicity	5.52×10^{-4}	8.77×10^{-4}	kg 1,4-DCB-eq
Water depletion	2.32	3.87	m^3

[a] The data required for computing metal depletion impacts were not available for the SCPC process.

3.1.2. End-point characterization results

Shown in Fig. 7 are the cumulated SCPC end point results, broken into the three main categories of ecosystem destruction (ED), human health (HH) and resource depletion (RD). The breakdowns and calculations of how each mid-point result contributes to an end-point category are omitted for the sake of brevity, but may be found in the online supplement. It can be seen that the total end-point impact of delivering 1 MW h of electricity using a SCPC plant is 73.8 points (in the *ReCiPe 2008* method, a point is defined such that 1000 points is the average human's impact in a one year period). The most significant contributor to the overall life cycle impact of the SCPC plant is HH, contributing approximately 64.5% of the total life cycle impact. The HH totals are affected by the high levels of GHG emissions (CO_2-eq in the mid-point categories) and toxic species (kg DCB_4-eq in the mid-point categories). However, RD is also a very important factor, contributing approximately 30.2% of the total points for the SCPC process. This means that, according to *ReCiPe 2008*, the inclusion of resource depletion in the discussion of life cycle impact is very significant, although this is a facet that is all too commonly disregarded in LCAs. Moreover, the overall weighting of RD with regards to the total life cycle impact of a process was assumed to be 20% in this study; although it was weighted lowest, it still contributes the second highest number of points to the total life cycle impact of the SCPC plant. Overall, ED contributes only a small portion (3.8 points or 5.1%) of the SCPC's end-point impact.

The addition of CCS to the SCPC plant has a very interesting result in that it actually reverses the importance of FD and HH. Since such a high amount of CO_2 is removed via CCS, the HH impact reduces to 13.2 points (29.3% of the total impact for the SCPC-CCS plant). However, the high parasitic energy costs of solvent-based absorption and thus additional fuel consumption result in the points contributed by FD increasing to 30.9 points, or 68.5% of the impact of the SCPC-CCS plant. This further reinforces the imperativeness of including RD in LCAs since more than half of the total life cycle impact of the SCPC plant with CCS comes from the depletion of fossil fuels and other resources. Overall, the total end-point impact of the SCPC plant is reduced by 28.7 points (38.9%) through the addition of CCS, which is a much more sobering result than a gate-to-gate GHG reduction of 90% assumed by many studies.

3.2. Integrated gasification combined cycle life cycle analysis

3.2.1. Inventories and mid-point characterization results

Table 6 shows the cradle-to-grave life cycle inventory results for the IGCC plant. Please note that the full results for all perspectives are available in the online supplement. It can be seen that, due to the slightly lower overall efficiency of the IGCC plant (39.0% compared to 39.3% for the SCPC case), it consumes a slightly higher amount of coal than the current state-of-the-art. However, due to the use of gasification instead of combustion, the total CO_2 emissions from the IGCC plant are significantly lower at 863.7 kg/MW h. Furthermore, the emission of particulates, SO_2 and NO_x are lower for the IGCC plant when compared to the SCPC case. The addition of CCS to the IGCC plant has roughly the same benefit for CO_2 emissions as the SCPC plant (an 84.1% reduction), but with a much smaller penalty in the amount of coal consumed to do so. Similarly, the lower parasitic energy cost of CCS upstream of the combustion stage used in the IGCC plant provides a significantly higher electrical efficiency compared to the SCPC plant, leading to less fuel and water consumption overall. In addition, unlike the SCPC plant, the addition of CCS does not have a significant impact on other uncontrolled emissions when added to the IGCC plant. Only marginal increases in toxic species such as Hg and Pb are observed, and those were lower than the SCPC plant to begin with since many of the toxic or otherwise harmful emissions from the SCPC plant leave the IGCC plant via the solid ash or slag waste stream from the gasifier, preventing their release into the atmosphere.

Table 7 shows the mid-point characterization results for the complete IGCC life cycle using the H perspective. Full details and additional perspectives can be found in the online supplement. It can be seen that the addition of CCS reduces the CC potential of the IGCC plant by approximately 75.9%, which is a slightly greater relative reduction than the SCPC plant due to the lower efficiency penalty of CCS and thus less additional upstream emissions when CCS is enabled. It is still clear that CC is very significant for the IGCC plant, contributing almost 938 kg CO_2-eq per MW h delivered; a 500 MW IGCC plant therefore emits the equivalent of almost 821,700 passenger vehicles on an annual basis, which is reduced to just under 198,000 vehicles when CCS is added. Moreover, the IGCC plant contributes less than half of the human toxicity (1.65 versus 3.61 kg 1,4-DCB eq.) compared to the SCPC plant. Since the parasitic energy cost of CCS is lower for the IGCC, this gap widens even further once CCS is enabled. Table 7 also indicates that the rate of particulate matter formation (PMF) is significantly lower for the IGCC plant, which is further reinforced by the end-point results discussed next. Overall, these results demonstrate that the IGCC plant is a more environmentally-friendly

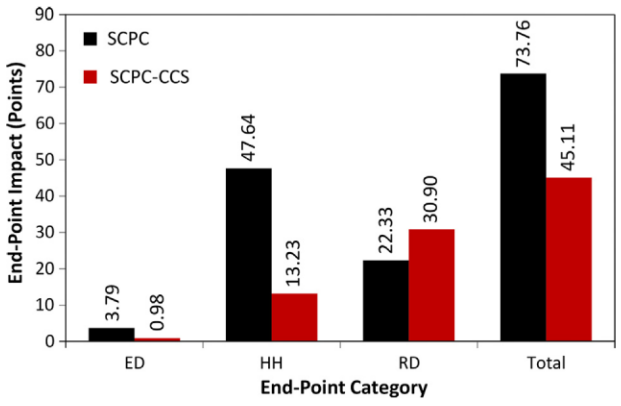

Fig. 7. End-point characterization results (H perspective) for the SCPC plant.

Table 6
Life cycle inventory results for the cradle to grave life cycles of IGCC plants.

Inventory	IGCC	IGCC-CCS
Input flows (kg)		
Coal (hard, in ground, 27.135 MJ/kg)	365.78	437.59
Natural gas (in ground, 44.1 MJ/kg)	0.26	0.26
Oil (crude, in ground)	6.75	8.07
Water (unspecified natural origin) [m^3]	1456.88	2432.95
Emissions to air (kg; unspecified population density and height)		
Ammonia (NH_3)	4.97×10^{-4}	5.98×10^{-4}
Carbon dioxide (CO_2)	863.67	137.50
Carbon monoxide (CO)	4.34×10^{-2}	5.71×10^{-2}
Dinitrogen monoxide (N_2O)	4.79×10^{-4}	4.94×10^{-4}
Lead (Pb)	1.36×10^{-5}	1.66×10^{-5}
Mercury (Hg)	2.78×10^{-6}	3.24×10^{-6}
Methane (CH_4)	2.83	3.39
Nitrogen oxides (NO_x)	0.27	0.28
NMVOC (non-methane volatile organics)	3.78×10^{-3}	4.80×10^{-3}
Particulates > 2.5 μm and < 10 μm	7.76×10^{-2}	9.16×10^{-2}
Sulfur dioxide (SO_2)	9.24×10^{-2}	9.39×10^{-2}
Sulfur hexaflouride (SF_6)	1.42×10^{-4}	1.42×10^{-4}
Product flows (MW h)		
Electricity delivered, AC, grid quality	1.00	1.00

Table 7
Mid-point characterization results (H perspective) for the IGCC life cycle.

Mid-point inventory	IGCC	IGCC-CCS	Units
Climate change	937.83	226.00	kg CO_2-eq
Fossil depletion	166.67	199.34	kg oil-eq
Freshwater ecotoxicity	9.21×10^{-6}	1.07×10^{-5}	kg 1,4-DCB-eq
Human toxicity	1.65	1.94	kg 1,4-DCB-eq
Marine ecotoxicity	1.67×10^{-3}	1.94×10^{-3}	kg 1,4-DCB-eq
Marine eutrophication	1.07×10^{-2}	1.10×10^{-2}	kg N-eq
Metal depletion[a]	N/A	N/A	kg Fe-eq
Particulate matter formation	0.16	0.17	kg PM_{10}-eq
Photochemical oxidant formation	0.32	0.33	kg NMVOC
Terrestrial acidification	0.25	0.25	kg SO_2-eq
Terrestrial ecotoxicity	2.85×10^{-4}	3.32×10^{-4}	kg 1,4-DCB-eq
Water depletion	1.46	2.43	m^3

[a] The data required for computing metal depletion impacts were not available for the SCPC process.

strategy than SCPC when CCS is desired, even when considering the entire life cycle and many different environmental factors.

3.2.2. End-point characterization results

Fig. 8 shows the end-point life cycle impacts of the IGCC plant with and without CCS. The HH impact is the highest contributor to the life cycle impact of the IGCC plant when CCS is not enabled, accounting for 60.9% (40.1 points) of the total impact. This is because the CC potential for the IGCC plant, while lower than that of the SCPC case, is still overwhelmingly high compared to any other potential impact factors. Unsurprisingly, the high amount of fuel consumed by the IGCC results in RD being the second highest contributor at 22.5 points (34.1%). Overall, the IGCC plant has a slightly lower total impact than the SCPC case of 65.9 points per MW h delivered. The addition of CCS lowers both ED and HH by approximately 75%, which results in a significant reduction of 29.4 points in the HH category. However, as was the case with the SCPC plant, the RD contribution increases, although by only 4.4 points (19.5%). After CCS is added, RD is the most significant impact category, contributing more than 70% of the total end-point impact of the IGCC-CCS plant. However, the large relative reductions of ED and HH result in the total impact of the IGCC plant to be reduced by 41.7%, which is a greater reduction than was possible with the SCPC case. These results indicate that, although it has a lower thermal efficiency, the IGCC plant has a lower total life-cycle impact than the SCPC plant when the full cradle-to-grave perspective and all relevant facets of *ReCiPe 2008* are considered. Furthermore, the performance gap between IGCC and SCPC widens when CCS is enabled, indicating that the IGCC is the most promising state-of-the-art technology currently available for the generation of power from coal from a life-cycle impact perspective.

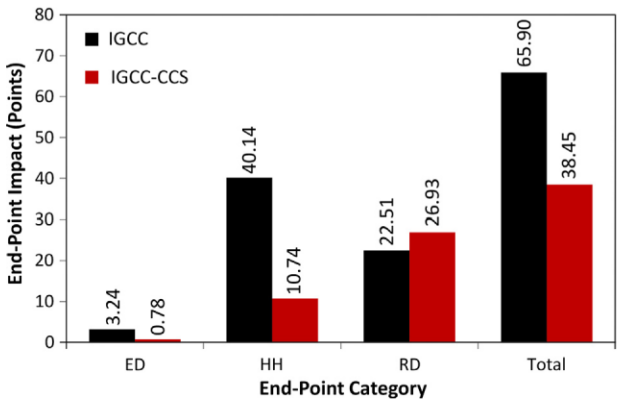

Fig. 8. End-point characterization results (H perspective) for the IGCC plant.

3.3. Coal-fueled SOFC life cycle analysis

3.3.1. Inventories and mid-point characterization results

Table 8 displays the SOFC-C life cycle inventories with and without CCS as investigated in this study. Please note that the results in Table 8 include the SOFC manufacturing results presented in our prior work and reported in the online supplement for the reader's convenience. One point of interest for the SOFC plant results is that rare earth metals and other manufacturing resources are included in Table 8. This is because this information was available for the SOFC manufacturing stage and its therefore included for the sake of completeness. However, the use of metals is not included in the comparative mid- or end-point calculations shown in Section 3.4 and 3.5 so that the SOFC plants may be fairly compared to the SCPC and IGCC case studies.

The SOFC plant without CCS is actually not much more efficient than a typical IGCC plant, and thus the CO_2 emissions from the SOFC plant are still quite high (784 kg CO_2/MW h), especially when compared with the SOFC plant fueled by NG without CCS from our prior work (488.7 kg/MW h) [12]. This is because the ASU used in the SOFC plant causes significant parasitic losses. However, the addition of CCS to the SOFC plant has a very low parasitic energy cost, and thus allow for a significant reduction in CO_2 emissions (over a 95% reduction) with marginal increases to fossil fuel consumption and uncontrolled emissions. A low parasitic energy cost for CCS causes the cascade of added resources and upstream life cycle impact to be significantly smaller for the SOFC plant than either of the other state-of-the-art options, leading to the best ratio of climate change reduction per trade-off impact of any of the plants investigated in this study. For the purposes of this study and since no other data were available, it was assumed that the toxic species emitted from the SOFC plant (using gasification as the main coal conversion process) was the same as the IGCC plant

Table 8
Life cycle inventory results for the cradle to grave life cycles of SOFC-C plants.

Inventory	SOFC-C	SOFC-C-CCS
Input flows (kg)		
Chromium: 25.5% (chromite); 11.6% (crude ore)	0.22	0.22
Coal (hard, 27.135 MJ/kg)	334.89	340.74
Iron: 46% (ore); 25% (crude ore)	0.55	0.55
Natural gas (44.1 MJ/kg)	0.23	0.24
Nickel: 1.13% sulfide (crude ore)	0.07	0.07
Oil (crude, in ground)	6.45	6.59
Uranium (mined)	1.61×10^{-5}	1.64×10^{-5}
Emissions to air (kg; unspecified population density and height)		
Ammonia (NH_3)	4.50×10^{-4}	4.6×10^{-4}
Argon (Ar)	35.52	22.59
Carbon dioxide (CO_2)	784.02	35.93
Carbon monoxide (CO)	5.83×10^{-2}	3.96×10^{-2}
Dinitrogen monoxide (N_2O)	4.19×10^{-4}	4.29×10^{-4}
Hydrogen (H_2)	6.57×10^{-2}	6.69×10^{-4}
Hydrogen sulfide (H_2S)	3.49×10^{-2}	3.48×10^{-4}
Lead (Pb)	1.25×10^{-5}	1.27×10^{-5}
Mercury (Hg)	2.52×10^{-6}	2.58×10^{-6}
Methane (CH_4)	2.59	2.64
Nitrogen oxides (NO_x)	3.81×10^{-2}	3.95×10^{-2}
NMVOC (non-methane volatile organics)	6.59×10^{-3}	6.75×10^{-3}
Particulates > 2.5 μm and < 10 μm	5.16×10^{-2}	5.28×10^{-2}
Phosphates (PO_4)	1.16×10^{-5}	1.18×10^{-5}
Sulfates (SO_4)	3.09×10^{-2}	3.15×10^{-2}
Sulfur dioxide (SO_2)	6.50×10^{-2}	6.64×10^{-2}
Sulfur hexaflouride (SF_6)	1.41×10^{-4}	1.42×10^{-4}
Product flows (MW h)		
Electricity delivered, AC, grid quality	1.00	1.00

on a per-kg of coal consumed basis. Using this technique, realistic estimates of Hg and Pb emissions were obtained and are shown in Table 8.

The mid-point characterization results for the coal-fueled SOFC plants are shown for the H perspective in Table 9. Other perspectives and calculations can be found in the online supplement. It is clear in Table 9 that although the SOFC-CCS plant has a cradle-to-grave CO_2 emission rate of 35.9 kg CO_2/MW h, the total CC potential of the SOFC-CCS plant is still a significant 105.3 kg CO_2-eq/MW h. The addition of CCS to the SOFC plant therefore reduces its total CC potential by 87.6% from the original total of 852.1 kg CO_2-eq/MW h. As expected based on the methods in which toxic species were calculated, the SOFC plant has a slightly lower total HT than the IGCC plants. [26]. Finally, note that the metal depletion is significant for SOFC plants; this is due to the high uses of chromium, nickel and other metals that are consumed during the SOFC manufacturing process.

3.3.2. End-point characterization results

In a similar fashion to the state-of-the-art case studies, Fig. 9 shows that the SOFC plant without CCS has a very high HH end-point impact (35.9 points or 60% of the total impact) due to its high emission rate of CO_2 and toxic species. Unsurprisingly, RD contributes the other majority (35%) of the end-point impact for the SOFC plant. However, the total end-point impact of the SOFC plant is only 59.9 points, which is 6 points (9.1%) and 13.9 points (18.8%) lower than the IGCC and SCPC plants, respectively. By adding CCS, the total impact of the SOFC plant is reduced by 55.3% to 26.8 total points. As expected, the addition of CCS increases RD, but due to the very low energy costs of achieving CCS with the SOFC plant this increase is marginal (less than 0.5 points). Conversely, there is a marked reduction in HT due to the very high reduction in CC potential, lowering it by 86% to approximately 5 points. Furthermore, the high CC reduction without a notable increase in uncontrolled emissions lowers the end-point impact of ED to effectively zero.

Once CCS is added to the SOFC plant, the gap between it and the state-of-the-art plants widens to 11.6 points (30%) and 18.3 points (41%) for the IGCC and SCPC plants, respectively. These results show great potential for coal-fueled SOFC plants to use an otherwise tabooed resource such as coal in an environmentally and socially responsible way.

3.4. Sensitivity analyses

The two highest degrees of uncertainty in this investigation are the assumed mid-to-end point conversion factors and the assumption that replaced and rejected coal at coal mine gate is not considered as a depleted resource. In order to address these assumptions, sensitivity analyses were performed and are discussed in the following sections.

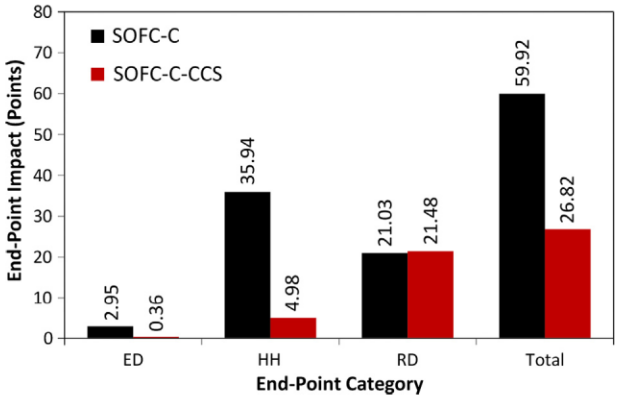

Fig. 9. End-point characterization results (H perspective) for the SOFC-C plant.

3.4.1. Effect of end-point conversion factors

In order to quantify the dependence of each process' end-point results on the high-uncertainty mid-to-end point conversion factors in *ReCiPe 2008*, 10,000 case studies were performed using a Monte Carlo approach in which each mid-to-end point conversion factor was randomly perturbed by ±20% using a uniform distribution. The resulting (normal) distributions and the statistical parameters for each of the six case studies in this work (using the H perspective) are presented in Fig. 10. Please note that the curves shown are descriptive trends; the actual histograms and data are available in the online supplement.

It is clear from Fig. 10 that the end-point results for all case studies are somewhat subjective to the end-point conversion factors, although there are still some significant disparities between certain cases. For example, the SOFC-C plant is significantly different within two standard deviations from any of the non-CCS plants (including the SOFC system). This yields and important result in that it can be concluded with confidence that a SOFC plant with CCS provides a significant cradle-to-grave life cycle improvement over any plant not using CCS. In a slightly more surprising result, the IGCC-CCS case is almost significantly different from its non-CCS counterpart, and is significantly different from the SCPC case. Consequently, it is evident that coal-to-electricity conversion methods are possible that have significantly lower environmental and social impact than the current state-of-the-art, which could

Table 9
Mid-point characterization results (H perspective) for the SOFC-C life cycle.

Mid-point inventory	SOFC-C	SOFC-C-CCS	Units
Climate change	852.07	105.25	kg CO_2-eq
Fossil depletion	152.65	155.92	kg oil-eq
Freshwater ecotoxicity	8.37×10^{-6}	8.55×10^{-6}	kg 1,4-DCB-eq
Human toxicity	1.50	1.54	kg 1,4-DCB-eq
Marine ecotoxicity	1.52×10^{-3}	1.55×10^{-3}	kg 1,4-DCB-eq
Marine eutrophication	1.52×10^{-3}	1.56×10^{-3}	kg N-eq
Metal depletion[a]	7.07	7.21	kg Fe-eq
Particulate matter formation	0.07	0.07	kg PM_{10}-eq
Photochemical oxidant formation	0.08	0.08	kg NMVOC
Terrestrial acidification	0.09	0.09	kg SO_2-eq
Terrestrial ecotoxicity	2.59×10^{-4}	2.65×10^{-4}	kg 1,4-DCB-eq
Water depletion	0.01	0.01	m^3

[a] Metal depletion statistics were not available for the NGCC process and are therefore considered only for the SOFC manufacturing stage for reference.

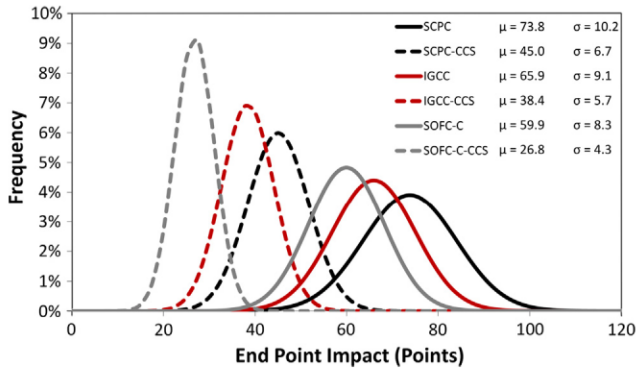

Fig. 10. Monte Carlo sensitivity results for the cases investigated in this study by perturbing all end-point conversions by ±20%. Full histogram statistics are available in the online supplement.

Table 10
Effect of considering 45% rejected coal at mine gate in resource depletion score.

Case	Fossil depletion score (kg Oil-eq)			End point score (points)		
	Does not count rejected coal as fossil depletion	Counts rejected coal as fossil depletion	% Change	Does not count rejected coal as fossil depletion	Counts rejected coal as fossil depletion	% Change
SCPC	165.36	300.79	81.90	79.33	92.05	16.03
SCPC-CCS	228.79	416.20	81.92	52.83	70.43	33.31
IGCC	166.67	303.14	81.88	71.52	84.33	17.92
IGCC-CCS	199.34	362.61	81.90	45.17	60.50	33.93
SOFC-C	152.65	276.72	81.28	65.03	76.68	17.91
SOFC-C-CCS	155.92	284.52	82.48	32.04	44.79	39.81

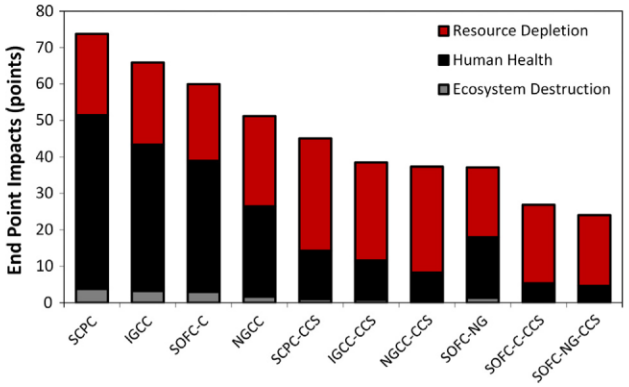

Fig. 11. Total end-point impact for all coal-fueled cases investigated in this study and NG cases investigated in out prior work in order of decreasing end-point impact.

allow for coal to become "unlocked" as a resource that can be used in a sustainable and reliable energy future.

Furthermore, it can be seen that adding CCS decreases the standard deviation for any of the three plant configurations investigated. This is an expected result, since the lower overall mid-point inventories for each plant with CCS deceased their dependence on the mid-to-end point conversions for their end-point results. Due to its low variance, there is a very strong chance (within 99% confidence according to these results) that the SOFC-CCS plant will have an end-point impact of less than 40 points per MW h of delivered electricity. Thus, even in a worst-case scenario, it is expected that generating power with a SOFC-CCS plant will have a 45.8% lower life-cycle impact than a state-of-the-art SCPC process.

3.4.2. Effect of rejected coal handling

The impacts of altering the assumption that the 45% of coal rejected at the mine gate is returned to the mine and thus not included in the consideration of resource depletion are shown in Table 10. It is clear that the FD score for all cases in this work are strongly dependent on this assumption as they all increase by more than 81%. This is because coal is by far the highest consumed fossil resource in these cases, and therefore considering nearly twice as much coal as "displaced" that is actually used in any of the plants has a significant impact. This change is also reflected in the end-point scores for each plant. However, it can be seen that the cases with CCS show larger end-point score changes (33–39% increase) when compared to their non-CCS counterparts (16–18% increase). This makes sense, as FD is a larger contributor to the end-point impact for plants with CCS enabled, as discussed in Sections 3.1–3.3. Furthermore, the relative impact of this assumption is higher for the SOFC-C-CCS case than the other systems using CCS. This is due to the higher efficacy of CCS for the SOFC system (and therefore larger relative decreases in HH and ED with the addition of CCS) which thus further increases the importance of this assumption on the performance of the SOFC system. Regardless, it is clear that the decision as to whether or not unusable coal should be categorized as fossil depletion or not is a very important aspect of the life cycle impact of coal-fueled power plants, motivating the need for further investigation into this area in future research.

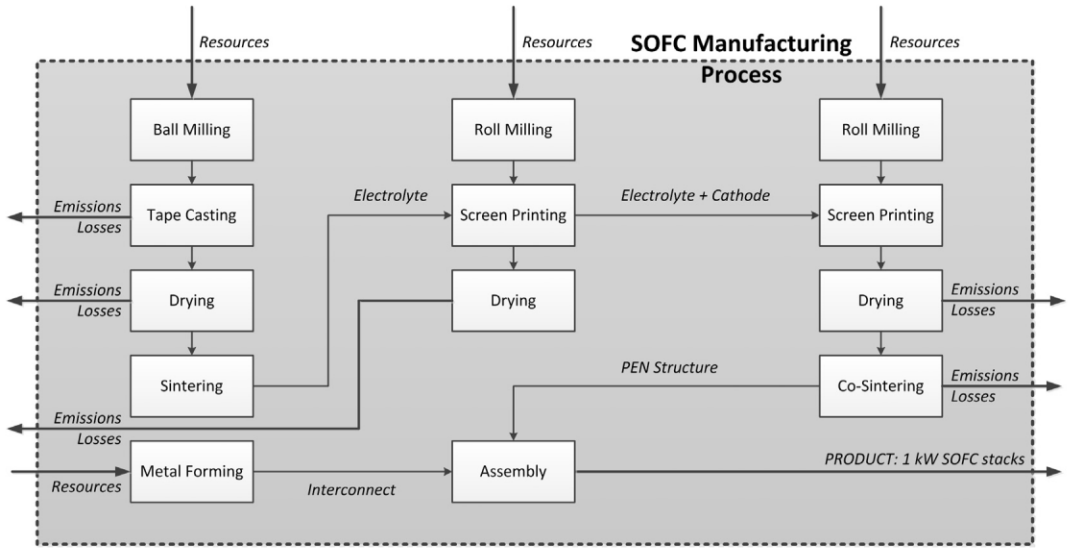

Fig. 12. Example manufacturing process for a SOFC stack. Reproduced with permission from [12].

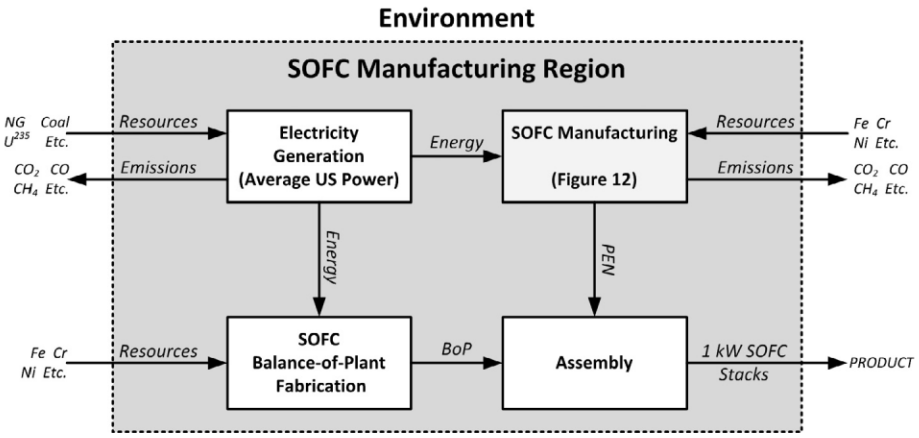

Fig. 13. Life cycle boundary of the SOFC manufacturing step. Reproduced with permission from [12].

3.5. Cross-fuel comparisons using LCA: natural gas and coal

Shown in Fig. 11 are the end-point impacts of all cases studies in this work and four cases using NG from our prior work for comparative purposes. Because of the unified end-point approach taken by *ReCiPe 2008*, the coal and NG power generation strategies can be compared in a fair and consistent manner. It is clear from Fig. 11 that the coal-based state-of-the-art system have the highest end-point impacts before the addition of CCS. When compared with a state-of-the-art NGCC plant, the most telling disadvantage of the coal plants are their much higher HH impacts (shown as the black bars) due to the much higher CC potential and toxic species emissions resulting from the consumption of coal. However, since HH is most affected by the addition of CCS, the gap between the state-of-the-art coal plants and the NGCC narrows with the addition of CCS since a similar relative reduction (90% at plant gate) of CO_2 emissions causes a larger deduction in HH impact for coal plants than the NG case. For example, the gap between NGCC and SCPC (22.6 points/MW h) narrows considerably (7.8 points/MW h) when comparing their CCS-enabled counterparts. Furthermore, the significant decrease in HH impact for the IGCC-CCS case with a low increase in FD (due to the relatively low parasitic energy penalty of pre-combustion CCS in an IGCC plant) results in the IGCC-CCS and NGCC-CCS cases having very similar environmental impact, with less than 1 point/MW h of separation. This leads to a very interesting conclusion that IGCC and NGCC plants have (within the uncertainty of this study) the same end-point environmental impact when CCS is used.

When considering the SOFC plants, the SOFC-NG case has approximately the same end point impact as the NGCC-CCS and IGCC-CCS cases. In other words, running a SOFC system on natural gas and venting the CO_2 to the atmosphere has ultimately the same net environmental impact as carbon capture from coal or natural gas state-of-the-art power plants. However, when CCS is added to the SOFC-C plant, its environmental impact according to this end-point analysis becomes significantly less than the NGCC-CCS case, and is comparable to that of the SOFC-NG-CCS scenario, with less than 3 points separating the two results. This leads to the interesting conclusion that, using the inherent advantages of SOFC systems, it is possible to produce reliable power using coal with a lower environmental impact than the current state-of-the-art plants using NG, which is currently regarded as the cleaner of the two fuel sources. This means that SOFCs could be the key to harnessing the ample supplies of coal in North America for future power generation without the taboo of it being "dirty."

4. Conclusions

In this study, a complete cradle-to-grave life cycle analysis was performed for a system generating electricity using solid oxide fuel cell (SOFC) stacks fueled by gasified coal. These analyses were also performed for two state-of-the-art alternatives to the SOFC, namely the supercritical pulverized coal (SCPC) and integrated gasification combined cycle (IGCC) plants. All upstream and downstream processes were accounted for and quantified using *ReCiPe 2008* using three socioeconomical perspectives. All sub-processes and their respective inputs, outputs and assumptions were defined in order to allow for a meaningful comparison between processes. Carbon capture and sequestration (CCS) was added to each process to assess its impact on the life cycle of each plant.

It was found that the addition of post-combustion CCS (Selexol™ with 90% recovery) to a SCPC plant reduced its global climate change potential from approximately 1094 to 283 kg CO_2-eq/MW h (74.1%). However, the parasitic energy cost of CCS was found to increase the amount of coal consumed by the SCPC plant from 165 to 229 kg oil-eq (38%). Uncaptured emissions and fugitive emissions of species such as Pb, Hg and NH_3 also increased significantly with the addition of CCS. Overall, it was found that resource depletion is a major contributor to the end-point life cycle impact of the SCPC plant, contributing 22.3 of its 73.8 total life cycle impact points. The higher resource consumption of the SCPC plant with CCS somewhat offsets its reduction in human health impact, but still has a net 39% lower (45.1 points) cradle-to-grave end-point impact than its non-CCS counterpart.

When pre-combustion CCS (also with 90% recovery) was added to the IGCC plant, it was found that its cradle-to-grave climate change potential dropped from 938 to 226 kg CO_2-eq/MW h (a 76% reduction). The parasitic energy costs for CCS in the IGCC plant are relatively lower than those of the SCPC system, yet adding CCS still caused a significant increase in the amount of fossil fuel consumed by the IGCC plant from 167 to 199 kg oil-eq/MW h (13% increase). Furthermore, as with the SCPC plant, uncaptured or fugitive emissions of toxic species increased nearly proportionally to the increase in coal consumption. The major end-point contributors of the IGCC plant were found to be its impacts on human health and fossil depletion, contributing 40 and 22.5 points/MW h (95% combined) to the total life-cycle impact of 65.9 points/MW h, respectively. Adding CCS to the IGCC system reduced its total end-point impact to 38.5 points/MW h, which is a slightly higher drop (41.6%) relative to the SCPC process, largely due to the lower fossil depletion of an IGCC plant using CCS.

Adding CCS to the SOFC plant had the most marked impact on climate change potential of all plants investigated, dropping it from 852 to 105 kg CO_2-eq/MW h (87.6%). Furthermore, the relatively low energy costs of CCS in the SOFC plant caused it to have a very modest increase in the amount of coal required at the plant gate, causing a small increase from 152.7 to 155.9 kg oil-eq/MW h (2%) in fossil fuel consumption. The resulting end-point reduction for the SOFC with CCS therefore widened the gap between it and the two aforementioned competitor processes, causing it to drop from 59.9 to 26.8 points/MW h (a 55% reduction). Even in the presence of significant uncertainties in the mid-to-end point conversion factors of *ReCiPe 2008*, the SOFC system with CCS stands alone as the system with the lowest cradle-to-grave impact of those investigated.

A significant conclusion that can be drawn from this work is that the proper use of coal allows for reliable and environmentally responsible electricity, even when compared to plants using NG. In fact, it was found that the coal SOFC system with CCS outperforms a NGCC plant with CCS by a significant margin from a life-cycle perspective, and an IGCC plant with CCS does not perform significantly worse than the NGCC. Furthermore, it was found that SOFC plants with CCS, which have the lowest life-cycle impact, have very similar results regardless of the chosen fuel source. With the negative annotation associated with coal combustion and mining, it is a very positive result that using SOFCs can unlock coal as a potential resource for future sustainable electricity generation. Furthermore, the fuel flexibility of SOFCs allow for flexible plants that can generate power in the most economically attractive fashion based on market conditions (driven by fuel prices, for example) without the risk of one mode of operation being environmentally favourable over another. This work thus not only reinforces the applicability of SOFCs in a sustainable future, but provides some positive outlooks on the use of coal in a responsible and socially acceptable manner.

Acknowledgements

The authors would like to acknowledge funding from the National Science and Engineering Research Council Vanier Scholar program, and the Ontario Research Fund for support on this project.

Appendix A. SOFC manufacturing boundary regions

The SOFC manufacturing boundary region combines the results of previous SOFC manufacturing studies and adapts them to the unit basis of this investigation. Several sources were consulted and cross-referenced to obtain reliable life cycle inventories [45,50,48]. Shown in Fig. 12 is a flowsheet describing the manufacturing process for the positive-electrolyte-negative (PEN) component of the SOFC, which is a sub-network of the total cradle-to-gate boundary of the SOFC manufacturing process. The boundaries of the SOFC and balance of plant manufacturing stage are depicted in the simplified block diagram of Fig. 13.

Appendix B. Supplementary data

Supplementary data associated with this article can be found, in the online version, at http://dx.doi.org/10.1016/j.apenergy.2015.03.105.

References

[1] Intergovernmental Panel on Climate Change. Climate change 2013: the physical science basis. Fifth assessment report of the intergovernmental panel on climate change. Cambridge University Press; 2013.
[2] Murphy, Hall. Ann NY Acad Sci 2010;1185:102–18.
[3] National Energy Board. Canada's energy future: energy supply and demand projections to 2035 – electricity outlook highlights. <http://www.neb-one.gc.ca/clfnsi/rnrgynfmtn/nrgyrprt/nrgyftr/2011/fctsht1134lctrct-eng.html> [Accessed June, 2012].
[4] US Energy Information Administration. Annual energy outlook 2014. US DOE/EIA- 0383(2014). April 2014.
[5] BP Energy. BP statistical review of world energy June 2014 (2014). <http://www.bp.com/content/dam/bp/pdf/Energy-economics/statistical-review-2014/BP-statistical-review-of-world-energy-2014-full report.pdf>.
[6] Adams II TA, Nease J, Tucker D, Barton P. Energy conversion with solid oxide fuel cell systems: short and long term outlooks. Ind Eng Chem Res 2013;52:3089.
[7] Baratto F, Diwekar UM. Life cycle assessment of fuel-cell based APUs. J Power Sources 2005;139:188.
[8] Strazza C, Del Borghi A, Costamagna P, Traverso A, Santin M. Comparative LCA of methanol-fuelled SOFCs as auxiliary power systems on-board ships. Appl Energy 2010;87:1670.
[9] Lin J, Babbit CW, Trabold TA. Life cycle assessment integrated with thermodynamic analysis of bio-fuel options for solid oxide fuel cells. Bioresour Technol 2013;128:495.
[10] Braun RJ. Techno-economic optimal design of solid oxide fuel cell systems for micro-combined heat and power applications in the U.S. J Fuel Cell Sci Technol 2010;7. 031018-1.
[11] Tanaka K, Wen C, Yamada K. Design and evaluation of combined cycle system with solid oxide fuel cell and gas turbine. Fuel 2000;79:1493.
[12] Nease J, Adams II TA. Life cycle analyses of bulk-scale solid oxide fuel cell power plants and comparisons to the natural gas combined cycle. Can J Chem Eng. http://dx.doi.org/10.1002/cjce.22207.
[13] EG&G Technical Services. DOE/NETL fuel cell handbook, 7th ed. November 2004.
[14] Tao S, Irvine JTS, Kilner JA. An efficient solid oxide fuel cell based upon single-phase perovskites. Adv Mater 2005;17:1734–7.
[15] Sora IN, Pelosato R, Simone A, Montanaro L, Maglia F, Chiodelli G. Characterization of LSGM films obtained by electrophoretic deposition (EPD). Solid State Ionics 2006;177:1985–9.
[16] Chiodelli G, Malavasi L. Electrochemical open circuit voltage (OCV) characterization of SOFC materials. Ionics 2013;19:1135–44.
[17] Tealdi C, Chiodelli G, Flor G, Leonardi S. Electrode stability and electrochemical performance of Lamox electrolytes under fuel cell conditions. Solid State Ionics 2010;181:1456–61.
[18] Ishihara T, Honda M, Shibayama T, Minami H, Nishiguchi H, Takita Y. Imtermediate temperature solid oxide fuel cells using a new $LaGaO_3$ based oxide ion conductor. J Electrochem Soc 1998;145:3177–83.
[19] Trabold TA, Lylak JS, Walluk MR, Lin JF, Trojani DR. Measurement and analysis of carbon formation during diesel reforming for solid oxide fuel cells. Int J Hydrogen Energy 2012;37:5190.
[20] Ming NQ. Coal based solid oxide fuel cell technology development. ECS Trans 2007;7:45.
[21] Williams MC, Strakey JP, Surdoval WA. U.S. Department of Energy's solid oxide fuel cells: technical advances. Int J Appl Cerma Technol 2005;2:295.
[22] Nagel FP, Schildhauer TJ, Biollaz SMA. Biomass-integrated gasification fuel cell systems – Part 1: definition of systems and technical analysis. Int J Hydrogen Energy 2009;34:6809.
[23] Jin H, Larson ED, Celik FE. Performance and cost analysis of future, commercially mature gasification-based electric power generation from switchgrass. Biofuels Bioprod Bioref 2009;3:142.
[24] Nease J, Adams II TA. Systems for peaking power with 100% CO_2 capture by integration of solid oxide fuel cells with compressed air energy storage. J Power Sources 2013;228:281.
[25] Nease J, Adams II TA. Coal-fuelled systems for peaking power with 100% CO_2 capture through integration of solid oxide fuel cells with compressed air energy storage. J Power Sources 2014;251:92.
[26] Adams II TA, Barton P. High-efficiency power production from natural gas with carbon capture. J Power Sources 1971;2010:195.
[27] Adams II TA, Barton PI. High efficiency power production from coal with carbon capture. AIChE J 2010;56:3120.
[28] Adams II TA, Barton PI. Combining coal gasification, natural gas reforming, and solid oxide fuel cells for efficient polygeneration with CO_2 capture and sequestration. Fuel Proc Technol 2011;92:2105.
[29] Kuchonthara P, Bhattacharya S, Tsutsumi A. Combination of thermochemical recuperative coal gasification cycle and fuel cell for power generation. Fuel 2005;1019:84.
[30] Verma A, Rao AD, Samuelsen G. Sensitivity analysis of a Vision 21 coal based zero emission power plant. J Power Sources 2006;158:417.
[31] Li M, Rao A, Brouwer J, Samuelsen G. Design of highly efficient coal-based integrated gasification fuel cell power plants. J Power Sources 2010;195:5707.
[32] Park S, Ahn J, Kim T. Performance evaluation of integrated gasification solid oxide fuel cell/gas turbine systems including carbon dioxide capture. Appl Energy 2011;88:2976.
[33] Haslbeck L, Kuehn NJ, Lewis EG, Pinkerton LL, Simpson J, Turner MJ, et al. Cost and performance baseline for fossil energy plants. Volume 1: Bituminous coal and natural gas to electricity final report. DOE/NETL-2010/1397. Revision 2; 2010.
[34] Adams II TA, Khojestah Salkuyeh Y, Nease J. Processes and simulations for solvent-based CO_2 capture and syngas cleanup. In: Reactors and process

design in sustainable energy technology. Amsterdam, Netherlands: Elsevier [chapter 1].
[35] Skone T, James R. Life cycle analysis: supercritical pulverized coal (SCPC) power plant. DOE/NETL-403-110609; 2010.
[36] Hasan M, Baliban R, Elia J, Floudas C. Modeling, simulation, and optimization of postcombustion CO_2 capture for variable feed concentration and flow rate. 2. Pressure swing adsorption and vacuum swing adsorption processes. Ind Eng Chem Res 2012;51:15665.
[37] Hasan M, Baliban R, Elia J, Floudas C. Modeling, simulation, and optimization of postcombustion CO_2 capture for variable feed concentration and flow rate. 1. Chemical absorption and membrane processes. Ind Eng Chem Res 2012;51:15642.
[38] Zhang Y, McKechnie J, Cormier D, Lyng R, Mabee W, Ogino A, et al. Life cycle emissions of producing electricity from coal, natural gas and wood pellets in Ontario, Canada. Environ. Sci. Technol. 2010;44:538–44.
[39] Fiaschi D, Lombardi L. Integrated gasifier combined cycle plant with integrated CO_2–H_2S removal: performance analysis, life cycle assessment and exergetic life cycle assessment. Int J Appl Thermodyn 2002;5(1):13–24.
[40] Odeh N, Cockerill TT. Life cycle GHG assessment of fossil fuel power plants with carbon capture and storage. Energy Policy 2008;36:367–80.
[41] Skone T, James R. Life cycle analysis: integrated gasification combined cycle (IGCC) power plant. DOE/NETL-403/110209; 2013.
[42] Goedkoop M, Heijungs R, Huijbregts M, De Schryver A, Struijs J, van Zelm R. Recipe 2008 first edition (revised, version 1.08). Ministerie van Volkshuivesting, Ruimtelijke Ordening en Milieubeheer; 2013.
[43] Owsianiak M, Laurent A, Bjørn A, Hauschild MZ. Impact 2002+, ReCiPe 2008 and ILCD's recommended practice for characterization modelling in life cycle impact assessment: a case study-based comparison. Int J Life Cycle Assess 2014;1007:19.
[44] Zhao L, Brouwer J. Life cycle analysis of ceramic anode-supported SOFC system manufacturing processes. ECS Trans 2012;42:247.
[45] Drauker L, Bhander R, Bennett B, Davis T, Eckard R, Ellis W, et al. Life cycle analysis: natural gas combined cycle (NGCC) power plant. DOE/NETL-403-110509; 2010.
[46] Skone TJ, Littlefield J, Marriott J. Life cycle greenhouse gas inventory of natural gas extraction, delivery and electricity production. DOE/NETL-2011/1522; 2011.
[47] United States Environmental Protecion Agency. 2009 boiler, generator, plant, state, PCA, eGRID subregion, NERC region, US, and grid loss (%) data. 2009. <http://www.epa.gov/cleanenergy/energy-resources/egrid/> [Accessed November 2013].
[48] Skone TJ. Life cycle greenhouse gas analysis of natural gas extraction and delivery in the United States. U.S. Department of Energy Lecture Cornell University; May 12, 2011.
[49] Karakoussis V, Brandon NP, Leach M, vand der Worst R. The environmental impact of manufacturing planar and tubular solid oxide fuel cells. J Power Sources 2001;101:10.
[50] Acero AP, Rodriguez C, Ciroth A. LCIA methods: impact assessment methods in Life Cycle Assessment and their impact categories. *GreenDelta GMBH*. April, 2014. <http://www.openlca.org/documents/14826/3bbaecf3-5efa-4a00-a965-4dc91c25b531>.
[51] Goedkoop M, Heijungs R, Huijbregts M, De Schryver A, Struijs J, van Zelm R. Recipe 2008 first edition (version 1.08): characterization factor spreadsheet. Pré Consultants; 2013.
[52] United States Environmental Protection Agency. Greenhouse gas emissions from a typical passenger vehicle. EPA Office of Transportation and Air Quality. 2011. <http://www.epa.gov/otaq/climate/documents/420f11041.pdf>.

Chapter 6

Application of Rolling Horizon Optimization to an Integrated Solid Oxide Fuel Cell and Compressed Air Energy Storage Plant for Zero-Emissions Peaking Power Under Uncertainty

The content of the following chapter is a **published reprint** of the following peer-reviewed publication:

Nease J, Adams TA II. Application of rolling horizon optimization to an integrated solid oxide fuel cell and compressed air energy storage plant for zero-emissions peaking power under uncertainty. *Computers & Chemical Engineering*. 2014; 68: 203-219.

Computers and Chemical Engineering 68 (2014) 203–219

Contents lists available at ScienceDirect

Computers and Chemical Engineering

journal homepage: www.elsevier.com/locate/compchemeng

Application of rolling horizon optimization to an integrated solid-oxide fuel cell and compressed air energy storage plant for zero-emissions peaking power under uncertainty

Jake Nease, Thomas A. Adams II*

Department of Chemical Engineering, McMaster University, 1280 Main Street West, Hamilton, Ontario, Canada

ARTICLE INFO

Article history:
Received 9 March 2014
Received in revised form 29 May 2014
Accepted 1 June 2014
Available online 7 June 2014

Keywords:
Solid oxide fuel cell
Compressed air energy storage
System design
Peaking power
Optimization
Natural gas

ABSTRACT

In this study, the application of a rolling horizon optimization strategy to an integrated solid-oxide fuel cell/compressed air energy storage plant for load-following is investigated. A reduced-order model of the integrated plant is used to simulate and optimize each optimization interval as a mixed integer nonlinear program. Forecasting uncertainties are considered through the addition of measurement noise and use of stochastic Monte Carlo simulations. The addition of rolling horizon optimization gives significant reductions to the sum-of-squared-errors between the demand and supply profiles. A sensitivity analysis is used to show that increasing the forecasting and optimization horizon improves load tracking with diminishing returns. Incorporating white Gaussian noise to demand forecasts has a marginal impact on error, even when a relatively high noise power of is used. Consistently over- or under-predicting demand has a greater impact on the plant's load-tracking error. However, even under worst-case forecasting scenarios, using a rolling horizon optimization scheme provides a more than 50% reduction in error when compared to the original system. An economic objective function is formulated to improve gross revenue using electricity spot-prices, but results in a trade-off with load-following performance. The results indicate that the rolling horizon optimization approach could potentially be applied to future municipal-scale fuel cell/compressed air storage systems to achieve power levels which closely follow real grid power cycles using existing prediction models.

1. Introduction

The electricity generation industry in North America is strongly dependent on the consumption of fossil fuels such as coal and natural gas due to their abundance and the availability of mature industrial technologies which use them. In an effort to move away from these "non-renewable" fuel sources, significant research has been invested into the conversion of energy from renewable sources (wind, solar, biofuels, etc.) in an effort to drive a more sustainable electricity generation industry. It is projected that the portion of electricity generated in the United States and Canada from renewable (non-hydroelectric) resources will be 16% and 10% by the year 2035, respectively (NEB, 2011; US Energy, 2012). A limitation to these technologies, however, is that they are still decades away from being implemented on the scale required to completely replace power production from non-renewable sources. Consequently, it is desirable to maximize the efficiencies and minimize the environmental impacts of fossil fuel-based electricity generation technologies for the near- to medium-term. Furthermore, economic incentives such as carbon taxes or cap-and-trade systems are likely to promote the development and implementation of CO_2 capture and sequestration (CCS) technologies in order to control the CO_2 emissions generated by the power generation industry. These CCS systems will likely involve the capture and compression of CO_2 followed by sequestering it in underground storage spaces such as aquifers, depleted oil fields and other geological storages sites (Herzog & Golomb, 2004).

To this end, this work investigates the application of rolling horizon optimization (RHO) of the solid-oxide fuel cell (SOFC) and compressed air energy storage (CAES) electricity generation plant

Abbreviations: CAES, compressed air energy storage; CCS, carbon capture and sequestration; EOS, equation of state; GT, gas turbine; HHV, higher-heating value; HRSG, heat recovery and steam generation; IESO, independent electricity systems operator; LCOE, levelized cost of electricity; RHO, rolling horizon optimization; SOFC, solid oxide fuel cell; SSE, sum of squared error.

* Corresponding author at: 1280 Main Street West, Hamilton, Ontario, Canada L8S 4L7. Tel.: +1 905 525 9140x24782.
E-mail address: tadams@mcmaster.ca (T.A. Adams II).

http://dx.doi.org/10.1016/j.compchemeng.2014.06.001
0098-1354/

Nomenclature

Mathematical symbols

$\bar{E}$	actual power produced at each time step
I_m	psuedo-steady-state model intercept
$\bar{P}$	actual pressure recorded in cavern at each time step
$\bar{n}$	actual number of moles in cavern at each time step
$\Re$	total revenue
D	demand
E	net power output of plant (calculated)
F	molar flow rate of air
N	RHO forecasting maximum time horizon
P	pressure in cavern (calculated)
R	universal gas constant
V	volume
a	model coefficient
f	SOFC/CAES reduced model
n	number of moles in cavern (calculated)
w	Gaussian noise weighting factor
$\mathcal{N}$	normal Gaussian distribution
δ	binary charge/discharge decision variable
μ	mean
σ	standard deviation
ω	price of electricity
ψ	user-defined economic/load-following weight factor
Φ	economic/load-following objective function

Subscripts

i	simulation/control time step
t	RHO calculation time horizon step
m	reduced model identifier
k	reduced model variable identifier
α,β	reduced model power identifier

fueled by natural gas proposed in our prior work (Nease & Adams, 2013). The proposed plant utilizes SOFC stacks to provide base-load power, and CAES to follow demand fluctuations above or below the plant's base load capacity (known as peaking power), while also capturing essentially 100% of all CO_2 emissions. The performance of the RHO scheme is established in both load-following (demand/supply mismatch minimization) and revenue maximization scenarios. Case studies examining the effects of design and uncertainty conditions are also investigated.

1.1. Solid oxide fuel cells

A SOFC uses a fuel gas and an oxidant (which is typically atmospheric air) to efficiently produce electrical power through several electrochemical reactions occurring on opposite sides of an impermeable oxide barrier. These reactions may include, but are not limited to (EGG, 2004):

$$H_2 + O^{=} \rightarrow H_2O + 2e^{-} \quad \text{(Anode)} \tag{1}$$

$$CO + O^{=} \rightarrow CO_2 + 2e^{-} \quad \text{(Anode)} \tag{2}$$

$$O_2 + 4e^{-} \rightarrow 2O^{=} \quad \text{(Cathode)} \tag{3}$$

One of the greatest advantages of SOFCs is their fuel flexibility. SOFCs are capable of converting a wide variety of carbonaceous gasses such as H_2, synthesis gas (a mixture of H_2 and CO, or 'syngas') (EGG, 2004), natural gas (Williams, Strakey, & Surdoval, 2005), jet fuel (Trabold, Lylak, Walluk, Lin, & Trojani, 2012), methanol (Trabold et al., 2012), and others (Adams, Nease, Tucker, & Barton, 2013). In addition, solid carbonaceous fuels such as coal (Ming, 2007; Adams & Barton, 2010a) and biomass (Jin, Larson, & Celik, 2009; Nagel, Schildhauer, & Biollaz, 2009) can be gasified into syngas and run in the SOFC as well. The products of the anode side consist of mostly H_2O, CO_2 and unspent fuel. From a CCS perspective, maintaining separate anode and cathode exhausts is therefore very advantageous as it precludes the requirement of separating CO_2 from the N_2 on the cathode side. As such, after a fuel completion step (typically done by oxidizing the unspent fuel with stoichiometric amounts of O_2) the CO_2 can be separated from the H_2O with minimal parasitic energy costs by condensing the H_2O in a series of pressurized flash drums (Adams & Barton, 2009). The exhaust streams are at high temperatures (~900 °C) and pressures (10–20 bar in a pressurized SOFC) which allow for additional bulk power generation using thermal and/or pressure-driven bottoming cycles. For example, the cathode exhaust may be expanded through a series of gas turbines (GTs), forming a Brayton cycle. The high-quality heat in the turbine exhaust may then also be recovered by generating high-pressure steam in a heat recovery steam generation cycle (HRSG). The exhaust (mostly N_2) may then be vented to the atmosphere with negligible environmental impact. Our prior work has shown that natural-gas fed SOFC systems are capable of achieving overall thermal efficiencies of 74% (on a higher heating value (HHV) basis) for natural gas with essentially zero CO_2 emissions (Adams & Barton, 2010b). Similar results have been reported in recent literature by other groups (see (Becker, Braun, Penev, & Melaina, 2012; Campanari, 2002; Komatsu, Kimijima, & Szmyd, 2012; Kuramochi, Turkenburg, & Faaij, 2011; Liso, Oleson, Nielson, & Kaer, 2011; Mueller et al., 2010; Yang & Weng, 2010), and table in Adams et al. (2013) and the references therein). Converting chemical potential directly to electrochemical potential is an inherently more efficient process than combustion and expansion through a turbine, which allows for SOFC systems to achieve higher net thermal efficiencies than systems utilizing Rankine or Carnot engines.

Although a very promising bulk power generation technology, SOFCs also have several disadvantages. One major disadvantage is that there are currently significant cost and operational challenges associated with running SOFCs dynamically. Although it is possible to change the power output from a SOFC dynamically (Achenbach, 1995), doing so runs the risk of cell degradation due to thermal expansion, backflow of gasses, and a variety of other operational concerns (Almutairi, Kendall, & Bujalski, 2012; Barelli, Bidini, & Ottoviano, 2012; Stiller, Thorund, & Bolland, 2006). This is an area of active research, but our approach is to avoid any potential shortfalls of operating an SOFC system dynamically by operating it as a base-load power provider, with CAES instead used to provide the peaking capabilities (Nease & Adams, 2013).

1.2. Compressed air energy storage

CAES plants operate as intermittent sinks or sources of mechanical energy. The plant functions by consuming excess or available electrical power to compress air and store it in a large above- or below-ground void such as a depleted natural gas reserve, aquifer or solution-mined salt dome. The stored air may then be re-heated (which usually requires the consumption of fossil fuels such as natural gas) and expanded through turbines attached to electrical generators to convert the stored elastic potential energy in the storage cavern to useful electricity. CAES can therefore be used as a round-trip electricity storage option for large-scale (hundreds of MW-h of energy stored) bulk and distributed power generation strategies, making it an excellent candidate for peaking power generation.

CAES technology is mature and has been implemented in the power generation industry for over three decades. The Alabama Electric Company and E. N. Kraftwerke have been operating stand-alone CAES plants since 1991 and 1978, respectively (Raju &

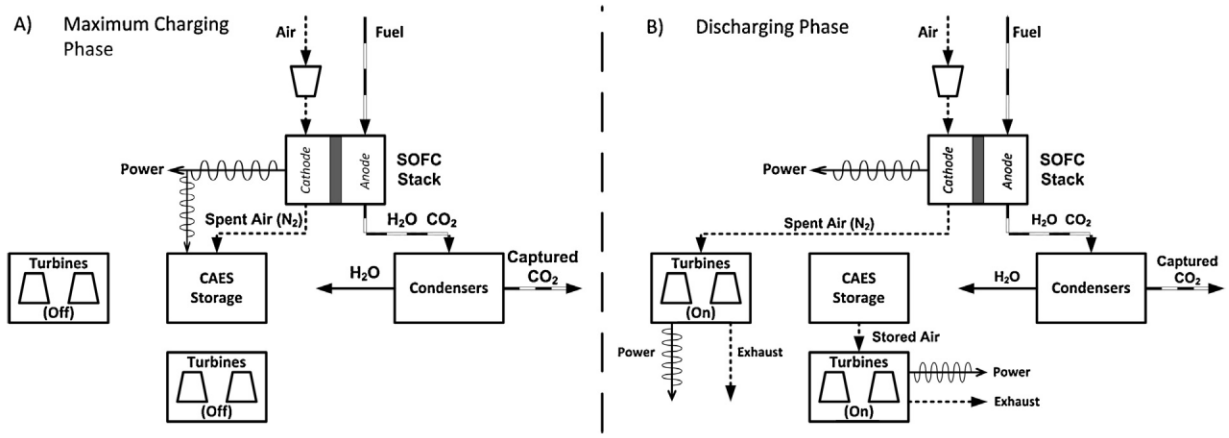

Fig. 1. Simplified SOFC/CAES integration technique during (A) the maximum charging phase and (B) the discharging phase. Reproduced from Nease and Adams (2013).

Khaitan, 2012). These plants operate profitably by purchasing electricity from the grid when the price is low (typically night time), temporarily store it underground as compressed air, and re-supply it back to the grid when the price of electricity is high (typically the day time). Several new CAES plants have been planned or investigated in North America, with two plants scheduled to go online in 2014: Dresser-Rand was awarded a 317 MW project by Apex Energy (valued at $200 million) to be constructed in Texas, and Chamisa Energy is planning a 270 MW system (Copelin, 2013; Dressler, 2013).

Although the Alabama and Kraftwerke plants exemplify the ability of the CAES system to act as a stand-alone plant, its rapid dynamics and controllability allow it to be combined with other systems to increase their flexibility or reliability. For example, there have been several studies recently that investigate using CAES to level intermittent power sources (such as wind turbines) to provide a consistent base-load from an otherwise unreliable power source (Cavallo, 2007; Fertig & Apt, 2009; Greenblatt, Succar, Denkenberger, Williams, & Socolow, 2007; Hoffeins, 1994; Hounslow, Grindley, & Louglin, 1988; Mason, Fthenakis, Zweibel, Hansen, & Nikolakakis, 2008; Raju & Khaitan, 2012; Succar & Williams, 2008). Our prior work investigated the applicability of integrating SOFCs and CAES in order to provide reliable peaking power with essentially zero CO_2 emissions (Nease & Adams, 2013).

1.3. Integrated SOFC/CAES plant

Our prior work discussed the integration of a SOFC plant (to provide base-load power) with a CAES system (to provide peaking power) and a CCS system to provide cost-effective and highly efficient peaking power with 100% carbon capture (Nease & Adams, 2013). During periods of operation when demand is lower than the base-load supply, cathode exhaust is diverted from the fuel cell to the CAES compressors, which consume excess electricity generated by the SOFC to compress and store the (inert) exhaust underground as shown in Fig. 1(A). During periods when the demand for electricity is high, the cathode exhaust is diverted to the already existent expansion turbine, thus reverting back to the base-load power output of the plant. In addition, compressed air is released from storage as required to supplement the base-load plant output in order to meet demand as demonstrated in Fig. 1(B). The fast CAES dynamics discussed in Section 1.2 allow for accurate load-following using one-hour optimization intervals.

There are several inherent synergies to linking a SOFC and CAES system that allow for the utilization of their unique strengths while overcoming their individual weaknesses. Specifically, the integrated system takes advantage of the high efficiency, fuel flexibility, and low-cost CO_2 capture properties of the SOFC system. At the same time, the CAES system provides load-following capability without the need for an external heat source since waste heat from the fuel cell stack can be used instead. Moreover, since the partially compressed cathode exhaust from the SOFC is used as the storage medium instead of air, significantly less energy is required to compress the cathode exhaust to the CAES storage pressure (10 bar to 40–70 bar, or a compression ratio of ~4–7) when compared to using air from the atmosphere (1 bar to 40–70 bar, or a compression ratio of 40–70). This yields a higher-round trip efficiency of the CAES system. Further details on the potential synergies and advantages of an integrated SOFC/CAES system and the overall analysis of the SOFC/CAES system are available in our prior work (Nease & Adams, 2013).

The integrated SOFC/CAES system could be located anywhere with sufficient underground storage availability and a natural gas pipeline connection. This study assumes that the SOFC/CAES plant is placed in Ontario, Canada, where there are already 73 active salt storage domes with a total volume of 3.5 million cubic meters and 35 depleted natural gas wells with a total volume of 7.3 billion cubic meters currently used for the temporary storage of natural gas (Ontario, 2013). Such a plant could also be located in the United States, where there are many depleted gas wells and salt caverns that are used for intermittent natural gas storage. For example, Michigan, Ohio and Pennsylvania possess a large portion of over 18 billion cubic meters of available storage space in the United States (USEIA, 2013).

2. Simulation models

2.1. SOFC model development

The basis for the SOFC system model is equivalent to the system discussed in our prior work (Adams & Barton, 2010b; Nease & Adams, 2013). The system was designed and simulated using Aspen Plus v7.3 with the Peng–Robinson equation of state (EOS) using the Boston–Mathias modification throughout, with the exceptions of using the Redlich–Kwong–Soave EOS with predictive Holderbraum mixing rules for streams consisting of mainly CO_2 and H_2O below the critical point of CO_2, and the Electrolyte-NRTL model with Henry coefficients and electrolyte specifications from the AP065 data bank for streams consisting of H_2O and CO_2 near or above the critical pressure of CO_2. The simulation considers a total of 15 components, 131 unit operations and three combined design specifications and calculator blocks. The system is assumed to be

Table 1
Characteristics the CAES section of the proposed SOFC/CAES integrated system. Reproduced from Nease and Adams (2013).

Operating condition	Value	Units
Air turbines (CAES power train in Fig. 2)		
Rated turbine power	200	MW
Maximum air flow rate	440	$kg\,s^{-1}$
Inlet pressure to HP turbine	40	bar
Inlet temperature to HP turbine	550	°C
Inlet pressure to LP turbine	6	bar
Inlet temperature to LP turbine	825	°C
Turbine efficiency	75	%
Compressor (compresses steam 39 in Fig. 2)		
Maximum air flow rate	210	$kg\,s^{-1}$
Rated compressor power	140	MW
Temperature at exit of after-cooler	50	°C
Pressure at exit of after-cooler	42–73	bar
Compressor isentropic efficiency	75	%
Cavern		
Volume of storage space	600,000	m^3
Cavern operating pressures	40–72	bar
Maximum cavern pressure	72	bar
Cavern wall temperature (constant (Krulla, 2013))	50	°C

fueled by natural gas at 30 bar and 38 °C and contains 93.9 mol% CH_2, 3.2% ethane (C_2H_6), 0.7% propane (C_3H_8), 0.4% *n*-butane (*n*-C_4H_{10}), 1% CO_2 and the remainder N_2. The SOFC process has a net output of 714 MW, which is the base-load capacity of the integrated SOFC/CAES plant. The size of the base-load was selected to be the same as our prior work and as a typical NGCC plant as defined by Woods et al. (2007) for comparative purposes. Although this is a large plant size relative to what is currently commercially available (Bloom Energy currently provides SOFC modules of up to 210 kW), the US Department of Energy is expecting to have MW-scale SOFCs available for demonstration by 2020 and commercially available by 2030. (FCT, 2011; Krulla, 2013; Vora, 2013). Therefore, it is reasonable for the forward-looking plant discussed in this work to be constructed by 2030. A detailed description of each process step and unit design considerations are provided in detail in our prior works (Adams & Barton, 2010b; Nease & Adams, 2013), but are omitted here for the sake of brevity.

2.2. CAES model development

The CAES turbomachinery section was partially modeled in Aspen Plus v7.3. The design and operating parameters of the CAES system were chosen based on the design recommendations provided by Luyben (2011) and to be comparable with the E.N. Kraftwerke plant simulated by Raju and Khaitan (2012). The design assumptions made for the CAES plant are summarized in our prior work, and can be found in Table 1. The CAES cavern size was selected to be a Pareto-optimal trade-off between load following performance and capital costs. This is described in our prior work, along with further details and assumptions on the integration of the CAES system with the base-load SOFC plant (Nease & Adams, 2013).

2.3. SOFC/CAES integration and reduced model

The integrated SOFC/CAES plant used for this study can be seen in Fig. 2. The CAES dynamic modeling approach is the same that was developed in our prior work (Nease & Adams, 2013). The transient portions of the SOFC/CAES plant were modeled using a pseudo-steady-state approach, where all mass and other related balances are calculated in MATLAB. The transient portions included all units downstream of streams 33 and 39–43 (cathode exhaust Brayton cycle turbines, cathode exhaust compressors, the storage cavern, stored gas expansion, and related heat integration). In contrast, all other units and streams with the exception of the HRSG (steam reforming, gas shifting, air separation and CCS) are a part of the base-load plant and hence are always steady-state and do not need to be considered in the pseudo-steady-state model. Details regarding stream and unit conditions of the upstream plant can be found in our prior works (Adams & Barton, 2010b; Nease & Adams, 2013).

The goal of the dynamic model is to compute the operating conditions of the SOFC/CAES at any given time. To do this, one-hour optimization intervals are used in which the system is assumed to achieve steady-state instantly and hold it for the hour. This is appropriate because accurate predictions of future power demand (up to 24 h in advance) are available at one hour increments from the Independent Electricity System Operator of Ontario (IESO) (IESO, 2012) and because the compressor and turbine dynamics are very fast, requiring seconds to minutes to achieve major changes in power consumption or generation, respectively (EPRI, 2004; Fertig & Apt, 2009).

At each optimization interval, the model must calculate the required flow rate of air to or from the cavern based on the power desired and the amount of air stored in the cavern. To do this with the rigorous Aspen Plus model requires an approximately 15 min of CPU time per optimization interval to converge (Intel® Core-2 Quad @2.66 GHz and 7 GB RAM), or about 1.75 CPU days per week-long (or 91 CPU days per year-long) simulation. Instead, a reduced model was constructed by running the Aspen Plus model to generate a table mapping the flow rate of air into the CAES cavern, the corresponding compressor pressure, and net operating power, and then fitting the parameters of a nonlinear model to that data. This brought the simulation time from 91 days to about 80 s. See our prior works for details (Nease & Adams, 2013, 2014). The reduced model used in this work, for the valid operating ranges of the SOFC/CAES plant, has a R^2 value of less than 0.99 and a mean-squared error of 1.16 MW (<0.2% of the nominal load) compared to the rigorous plant model. The reduced model considered in this work is thus considered to be an accurate representation of the rigorous plant model.

Furthermore, for the purposes of this investigation we wish to optimize the performance of the SOFC/CAES plant throughout week and year-long operating periods. The reduced model described in our prior work and in Section 3.1 was therefore used in order to expedite calculations. Since the optimization routine is run at every simulation time step to determine the optimal output over the future optimization horizon (see Section 3.2 for details) and may require (depending on the solver) 50 or more iterations, using the rigorous Aspen Plus model as the model being optimized would result in impractically long computation times. With this information in mind, the optimal operation of the SOFC/CAES plant can be established. The following section describes the rolling horizon optimization framework and problem formulation.

3. Rolling horizon optimization framework

Due to CAES cavern storage pressure and maximum flow rate limitations, it is often not possible to exactly meet the market load requirements at all times, even with an infinitely large cavern. The purpose of using a rolling horizon optimizer to schedule the output of the SOFC/CAES plant at each optimization interval is to improve either its overall load-following or its economic performance. Many other studies in the field of chemical engineering have been performed that utilize some form of time-varying optimization to improve plant reliability, economics and other factors (Chachuat, Srinivasan, & Bonvin, 2009; De Souza, Odloak, & Zanin, 2010; Khajuria & Pistikopoulos, 2012; Young, 2006; Zanin, Tvrska de Gouvea, & Odloak, 2010; Zhao, Fu, & Xu, 2013). The following

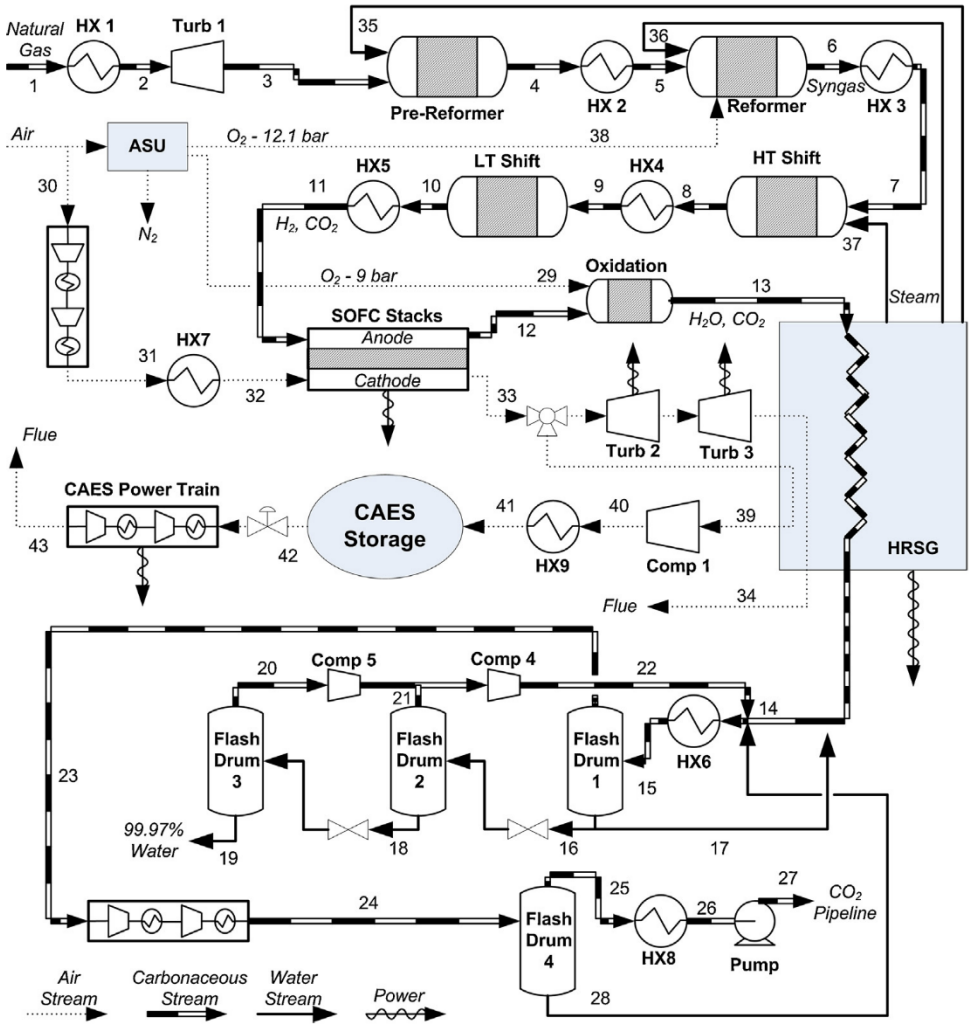

Fig. 2. Integrated SOFC/CAES process flow diagram. Reproduced from Nease and Adams (2013).

sections describe the implementation of the RHO routine in the SOFC/CAES dynamic simulations and the problem formulations.

3.1. Problem formulation

In the load-following optimization case, it is the objective of the RHO to determine the plant output over the control horizon that will either minimize the sum-of-squared errors (SSE), maximize the total revenue, or some weighted combination of both over the optimization's horizon ($\Re$). The primary decision variable of interest determined by the RHO program is the flow rate to or from the CAES cavern, which is then used to calculate the power output of the combined SOFC/CAES plant at each time step.

3.1.1. Objective function formulation

In the load-following scenario, the RHO maximizes a weighted objective function (Φ) that balances a trade-off between the plant's total revenue ($\Re$) and load-following performance (measured by the negative of SSE):

$$\max_{\delta_{i,t}F_{it,t}} \Phi_i = \{\psi R_i - (1-\psi)\mathrm{SSE}_i\} \tag{4}$$

$$\mathrm{SSE}_i = \sum_{t=1}^{N} (E_{i,t} - D_{i,t})^2 \tag{5}$$

$$\Re_i = \sum_{t=1}^{N} (E_{i,t}\omega_{i,t}), \tag{6}$$

where SSE_i is the sum of squared error difference at each simulation time step i between the power produced E and forecasted demand D (both in MW) at each control move t across the forecast time horizon N, $\omega_{i,t}$ is the forecasted market spot-price of electricity (POE) for each one-hour optimization interval over the optimization horizon, and $\psi \in [0,1]$ is a pre-defined weighting factor. The optimization is repeated each timestep. It can be seen that in the case of $\psi = 1$ the load-following term will be ignored and the problem reduces to a revenue maximization problem without any penalties due to sporadic or aggressive production patterns. Selecting $\psi = 0$ results in a minimization of SSE problem (called the load-following problem), which will attempt to produce electricity as close to the demand curve as possible without any concern for economic performance. Problems with ψ in between 0 and 1 result in scenarios where both economic and load-following performance are considered with different weights.

It is assumed that the SOFC/CAES plant is a price-taker in the market, and therefore has no control over the POE at any given time. Price and demand data are obtained from the IESO (IESO, 2012), except that since demand data are given for the entire province of Ontario, demand data for one calendar year are scaled to an average of 714 MW (approximately the size of one major power plant).

3.1.2. Model equations

For the purposes of this investigation, the optimization interval was assumed to be one hour to correspond with our prior work. $E_{i,1}$ is therefore the power actually produced in timestep i, and $E_{i,t}$ is the power the optimizer plans on producing $t-1$ timesteps in the future for $t=(2\ldots N)$, which may or may not be implemented in future time steps. Similarly, $D_{i,1}$ is the actual, known demand at timestep i, and $D_{i,1}$ is the predicted demand given to the optimizer at timestep i for $t-1$ timesteps in the future. The power production $E_{i,t}$ is a combination of the reduced models corresponding to our prior work, namely:

$$E_{i,t} = \delta_{i,t} f_{c,i,t}(P_{i,t}, F_{i,t}) + (1-\delta_{i,t}) f_{d,i,t}(P_{i,t}, F_{i,t}), \quad [\forall t = (1\ldots N)] \tag{7}$$

where $\delta_{i,t}$ is a binary decision variable corresponding to the decision to charge ($\delta=1$, reduce the net plant output) or discharge ($\delta=0$, increase the net plant output) at each future timestep $t-1$ steps ahead of given optimization interval i. Similarly, $F_{i,t}$ and $P_{i,t}$ are the molar flow rate to/from the storage cavern (in kmol/h) and the pressure (in bar) in the cavern at each time step, respectively. $f_{m,i,t}$ are the reduced models for the charging and discharging of the CAES cavern where $m \in \{c, d\}$, respectively:

$$\begin{aligned} f_{m,i,t}(P_{i,t}, F_{i,t}) = I_m &+ a_{10,m}\frac{(F_{i,t}-\mu_{F,m})}{\sigma_{F,m}} + a_{01,m}\frac{(P_{i,t}-\mu_{P,m})}{\sigma_{P,m}} \\ &+ a_{20,m}\left(\frac{(F_{i,t}-\mu_{F,m})}{\sigma_{F,m}}\right)^2 \\ &+ a_{11,m}\frac{(F_{i,t}-\mu_{F,m})}{\sigma_{F,m}}\frac{(P_{i,t}-\mu_{P.m})}{\sigma_{P,m}} \\ &+ a_{02,m}\left(\frac{(P_{i,t}-\mu_{P,m})}{\sigma_{P,m}}\right)^2 \end{aligned} \tag{8}$$

where I_m is the model intercept, $a_{\alpha,\beta,m}$ is the model coefficient for the αth and βth power of F of P in model m, respectively, and $\mu_{k,m}$ and $\sigma_{k,m}$ are the arithmetic means and standard deviations in model m where $k\varepsilon\{F, P\}$, respectively. The mass balance on the cavern is described as:

$$\begin{aligned} n_{i,1} &= n_{i-1,1} + F_{i,1}\delta_{i,1} - F_{i,1}(1-\delta_{i,1}), \\ n_{i,t} &= n_{i,t-1} + F_{i,t}\delta_{i,t} - F_{i,t}(1-\delta_{i,t}), \quad [\forall t = (2\ldots N)] \end{aligned} \tag{9}$$

where $n_{i,t}$ is the number of moles of cathode exhaust (mostly consisting of N_2) contained in the CAES cavern at any given time step i. Note again that $n_{i,1}$ is the actual molar holdup of the cavern as a result of executing the decision variables $F_{i,1}$ and $\delta_{i,1}$, and $n_{i,t}$ for $t=(2\ldots N)$ is the predicted molar holdup $t-1$ timesteps in the future based on the current optimization results, and may or may not change in the future.

The pressure of the CAES cavern is calculated using the SRK equation of state:

$$P_{i,t} = \frac{RT_{i,t}}{V_{M,t} - b_{\mathrm{SRK}}} - \frac{a_{\mathrm{SRK}}}{T_{i,t}^{0.5} V_{M,i,t}\left(V_{i,t} + b_{\mathrm{SRK}}\right)}, \quad [\forall t = (1\ldots N)] \tag{10}$$

where a_{SRK} and b_{SRK} are the SRK model coefficients for the cathode exhaust with units of m^6bar/mol^2 and m^3/mol, respectively, that may readily be obtained from literature (Smith, Van Ness, & Abbot, 2005). R is the universal gas constant and $T_{i,t}$ is the temperature. $V_{M,i,t}$ is the molar volume of the CAES cavern contents at each control step, and is determined as:

$$V_{M,i,t} n_{i,t} = V_{i,t}. \tag{11}$$

Pressure is calculated at each time step to ensure that it never exceeds the operating limits of the CAES system, namely:

$$40 \le P_{i,t} \le 72. \quad [\forall t = (1\ldots N)] \tag{12}$$

Finally, the flow rate into the CAES cavern must not exceed the maximum cathode exhaust molar flow rate $F_{\max}$:

$$\delta_{i,t} F_{i,t} \le F_{\max}. \quad [\forall t = (1\ldots N)] \tag{13}$$

The resulting compiled problem (4) is a mixed-integer nonlinear program (MINLP), the size of which increases linearly with the optimization horizon N. For a prediction horizon of $N=24$ h, the optimization formulation at each time step i contains 217 variables (143 of which participate in nonlinear terms and 24 of which are discrete) and 169 constraints. A one-year simulation of the SOFC/CAES plant using 1-h optimization intervals and 24 h prediction horizons would therefore require that problem (4) is solved 8760 times in sequence (for $i=1$–8760), for a total 1.9 million mixed-integer and continuous variables solved (though not simultaneously).

3.2. Optimization scheme and method

The rolling horizon optimizer is implemented at each time step of the SOFC/CAES simulation. The overall algorithm for any given simulation is summarized in Fig. 3. At each optimization interval, forecasted demand for the same number of future time steps as the optimization horizon (which is a user-defined parameter) is given to the RHO with the current power output of the plant, current pressure of the CAES cavern and molar content of the CAES cavern. The RHO returns the optimal SOFC/CAES plant output ($E_{i,t}$), cavern pressure ($P_{i,t}$) and cavern molar content ($n_{i,t}$) trajectories over the optimization horizon. The first of the power output trajectories is recorded as the "current" optimal output for the ith simulation and control move (i.e., $\bar{E}_i = E_{i,1}$, where $\bar{E}_i$ is the actual power achieved at timestep i). The first of the pressure and molar content trajectories are also recorded, and assigned as the initial values for the next round of optimization (as in: $\bar{P}_i = P_{i,1}$ and $\bar{n}_i = n_{i,1}$). If the simulation has not reached the final time ($i < N_{\max}$), the time step is updated and the new initial conditions and updated demand data are provided to the rolling horizon optimizer. Fig. 4 shows an example of executing three time steps of the rolling horizon optimizer, including the determination of the optimal output trajectory from the RHO and the implementation of the first RHO control move to the actual plant.

3.3. Initial guesses and solver selection

The generation of initial guesses for the variables was automated by assigning the solution to the previous time step as the initial guesses for the variables in the next step. This is important because if one chooses all zero flows as an initial guess (which is the default setting), this is almost always a feasible solution which, according to the solver reports, is also a local minimum.

A hierarchical selection of three commercial packages were used in GAMS to solve the optimization at each simulation time step: DICOPT, BONMIN and KNITRO (Rosenthal, 2012). If one of the solvers did not report a global optimal solution, the next solver down in the hierarchy was used. The first solver used at each simulation time step was DICOPT due to its high speed relative to the other options, followed by BONMIN and finally KNITRO if necessary. It was found that although DICOPT usually reported a global optimal solution, in about 2% of cases it did not. In only very few cases (about 0.3%) did none of the three solvers find a global optimal solution. When this occurred, if a feasible, local minimum was found, then that solution was used. Otherwise, if no feasible solution was found, the solution for this time step as suggested from

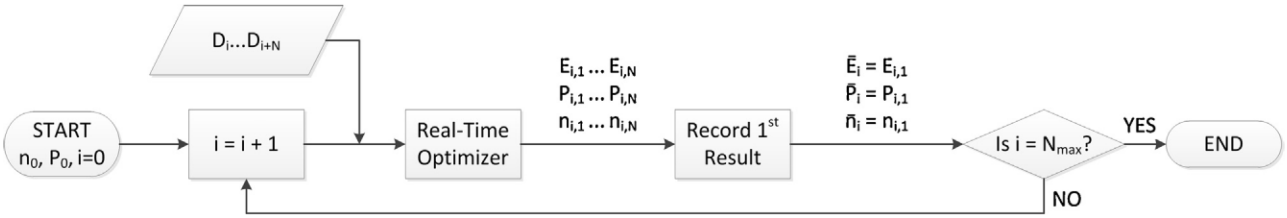

Fig. 3. Flow chart describing the implementation of RHO to determine the optimal power output at each simulation time step.

the results of the optimization for the previous timestep were used instead. This occurred very rarely and had a negligible impact on the results.

4. Effect of rolling horizon optimization on plant performance

One of the primary purposes of using the RHO scheme discussed in the previous sections is to improve the load-following performance as measured by the SSE of the integrated SOFC/CAES system. To this end, consider Fig. 5, which shows the output of the SOFC/CAES plant compared to the scaled demand over a week of operation in July of 2011 with a RHO horizon of $N = 1$ and weighting factor $\psi = 0$ are used, meaning that SSE is minimized and revenue maximization is not considered in the objective. This is equivalent to the "greedy" algorithm previously used in our prior work, where only the demand for the next optimization interval is known, and hence the integrated SOFC/CAES system attempts to identically match demand without considering future requirements. It can be seen that although the load-following capabilities of the integrated plant are significant, there are times ($t \approx 75$, $t \approx 140$ and $t \approx 162$) where the CAES storage cavern becomes either filled or emptied, resulting in the SOFC/CAES plant reverting back to its original base-load production level of 714 MW. Fig. 6 shows the CAES cavern pressure profile for this time period, which confirms that its maximum and minimum operating pressures are indeed hit at the same time periods, resulting in the incapability of the CAES system to supplement the base-load as required. Although it is attractive that demand can be met almost perfectly most of the time, sudden drop-offs in the SOFC/CAES plant's output cause large gaps between supply and demand. From an operational standpoint, this is not ideal; a sudden burst of demand for supplementary power from the power grid or other sources is not easy to deal with. The same problem occurs when excess power is generated that must be curtailed or disposed of in some other manner. Instead, it is desirable to avoid such large drop-offs as seen in Fig. 5. Using a RHO horizon of $N = 1$ results in a SSE of roughly 210,000 MW-h^2. The following sections compare the capabilities of the SOFC/CAES system utilizing RHO to the original case without RHO as depicted in Fig. 5. For the sake of calculation times and comparison purposes, the same week of operation is simulated in each case study since it is a typical example of the diurnal power demand profile. Issues such as bulk energy storage for following seasonal trends in electricity demand is another important consideration, and is left to future work.

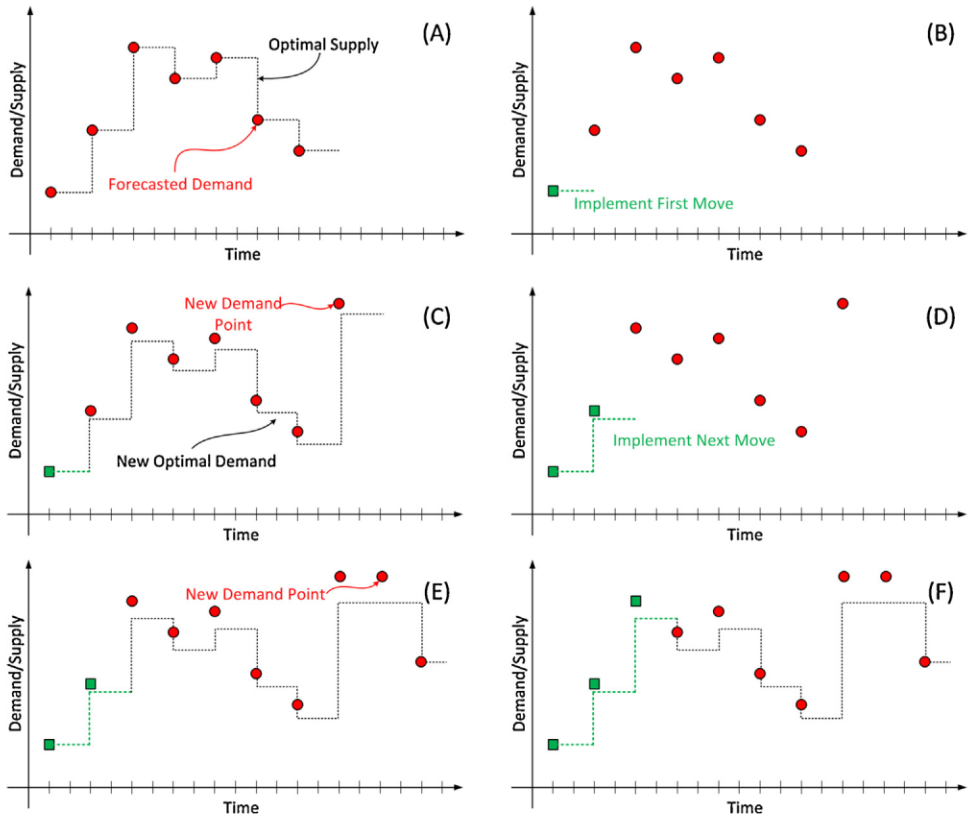

Fig. 4. Example RHO trajectories and implementation. (A), (C) and (E) show the RHO program's optimal trajectory based on available demand, and (B), (D) and (F) show the implementation of the first three control moves to the real plant.

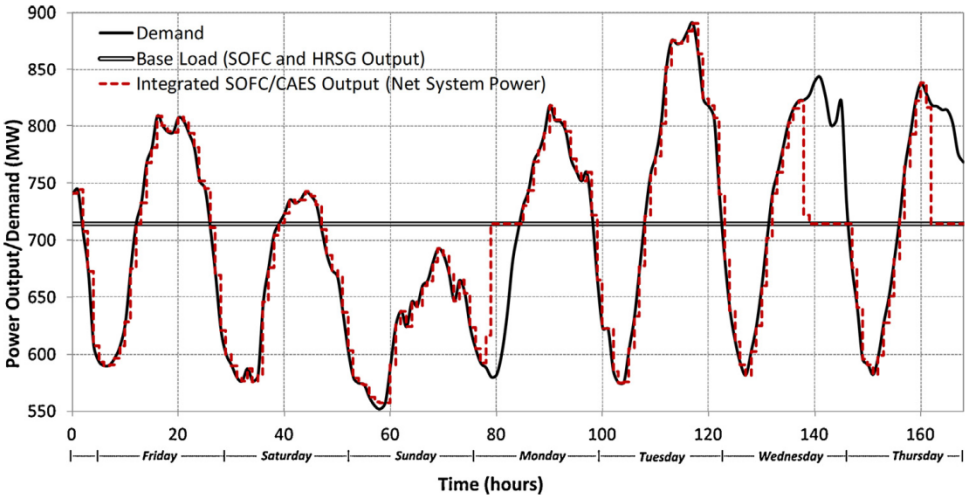

Fig. 5. Simulation results of the SOFC/CAES system for one selected week of operation using a RHO prediction horizon of $N = 1$ (June 17–23, 2011) – which essentially means that the RHO is disabled and the plant instead uses a policy of meeting the predicted demand for the next time step as closely as it possibly can. Times in which the output of the SOFC/CAES system matches the base load when demand is less than supply denote times when the cavern is full (at maximum allowable pressure). Times in which the SOFC/CAES system matches the base load when demand exceeds supply denote times when the storage cavern is empty (at minimum allowable pressure). Analogous to Nease and Adams (2013).

4.1. Base case performance

The base case considered for this investigation refers to having a 24 h prediction/optimization horizon ($N = 24$) with $\psi = 0$. Very accurate demand forecasts for at least 24 h ahead are available to the public from the IESO which are updated hourly, and as such a 24-h optimization horizon is realistic and achievable. However, to establish the base case scenario, instead of using the predictions of hour-by-hour demand 24 h ahead of each time point, the actual historical power demand is used. Thus, the base case is also the "best realistic case" scenario since it does not incorporate any demand uncertainty. Then, beginning in Section 4.2.2, inaccuracies in the demand predictions are considered by incorporating stochastic forecasting.

The critical constraint on the SOFC/CAES combined system's ability to meet demand is typically the storage capacity of the CAES cavern. The sensitivity of the CAES system's load following capabilities based on storage capacity was addressed in our prior work (Nease & Adams, 2013). An optimal storage size of 600,000 m^3 was chosen based on a marginal returns analysis, and is used consistently throughout the following analysis.

4.1.1. Week-long simulation results

The resulting supply and demand profiles for the same week of operation as reported in Fig. 5 is given in Fig. 7. Furthermore, the pressure profile for the same week (as was originally reported in Fig. 6) using the RHO scheme is given as Fig. 8. It is clear that the RHO scheme with a 24 h prediction horizon is able to avoid large gaps between supply and demand when compared to the previous results. During the time periods $60 \leq t \leq 80$, the RHO acknowledges that the cavern pressure will be at its upper bound, and therefore overproduces (and therefore diverts less cathode exhaust to the CAES storage space) by a small amount spread over multiple time steps. Similarly, the large peaks occurring toward the last three days of operation are accounted for by under-producing as necessary to avoid large drop-offs corresponding to the CAES cavern being at minimum pressure. There are even some points ($t \approx 135$ and $t \approx 150$) where the CAES is used to drop the output below the (already less than base-load) demand so additional stored air may be used to meet the peaks later. The SSE for this week of operation using RHO with $N = 24$ is 67,500 MW-h^2, which corresponds to a 68% reduction in SSE over the original method. The use of RHO therefore clearly improves the load-following

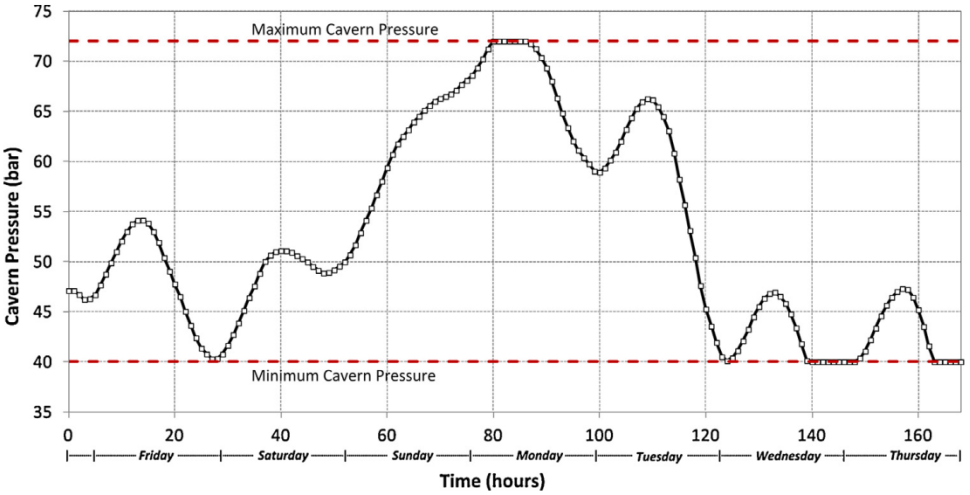

Fig. 6. Pressure profile for one week of simulated operation using a RHO horizon of $N = 1$ (June 17–23, 2011). Analogous to Nease and Adams (2013).

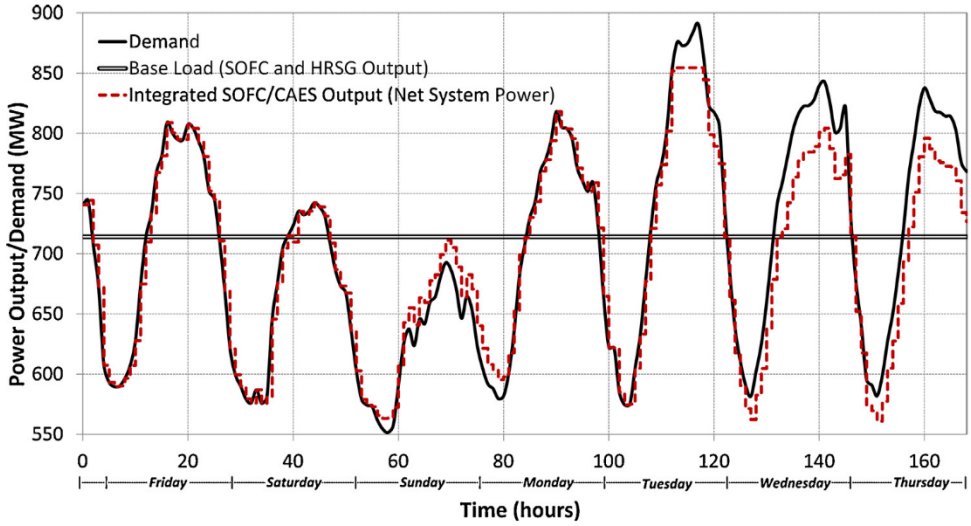

Fig. 7. Simulation results of the SOFC/CAES system for one selected week of operation (June 17–23, 2011) using a RHO prediction horizon of 24 h.

capabilities of the SOFC/CAES plant while at the same time reducing the gap between supply and demand, therefore improving operability by not requiring drastic supplements to the plant's power output.

4.2. Load-following case studies

For each of the case studies discussed below, the one-week simulation period was assumed to be representative of the overall performance capabilities of the RHO system. Full-year simulations were avoided due to extensive computation times without a corresponding gain of useful information for analysis purposes. This particular week used was selected because it includes periods of consistently low or consistently high demand, resulting in a scenario that, based on the size restrictions of the CAES cavern, precludes the ability of the SOFC/CAES system to achieve perfect load-following. This allows for the effects of the most important factors of load-following performance to be emphasized. Finally, each of the case studies uses a forecasting horizon of $N = 24$ h and a weighting factor of $\psi = 0$ to be compared to the base case.

4.2.1. Effect of demand forecast horizon

It is assumed in this scenario that future demand is known exactly up to 24 h ahead at every control move. The relaxation of this assumption is addressed in the stochastic demand considerations discussed in Sections 4.2.2 and 4.2.3.

As expected, increasing the optimization horizon by increasing the amount of future demand data known improves the ability of the RHO to reduce the SSE. When the demand forecast and optimization horizon is extended, more about the upcoming profile is known to the RHO scheme. Consequently, upcoming periods of excessively high or low demand are known earlier, which allows the RHO scheme to compensate for these highly divergent periods ahead of time. Fig. 9(A) shows the performance of the SOFC/CAES system using the base-case optimization horizon of $N = 24$, which has the largest N and hence the best load-following capabilities with an SSE of 67.5×10^3 MW-h^2. When a prediction horizon of $N = 12$ is used (Fig. 9(B)), higher peaks such as those at $t = 140$ and $t = 160$ are not as well followed due to the CAES not being used to store supplemental energy during the troughs associate with each peak as they are when $N = 24$ is used. This results in a higher overall SSE of 85.9×10^3 MW-h^2

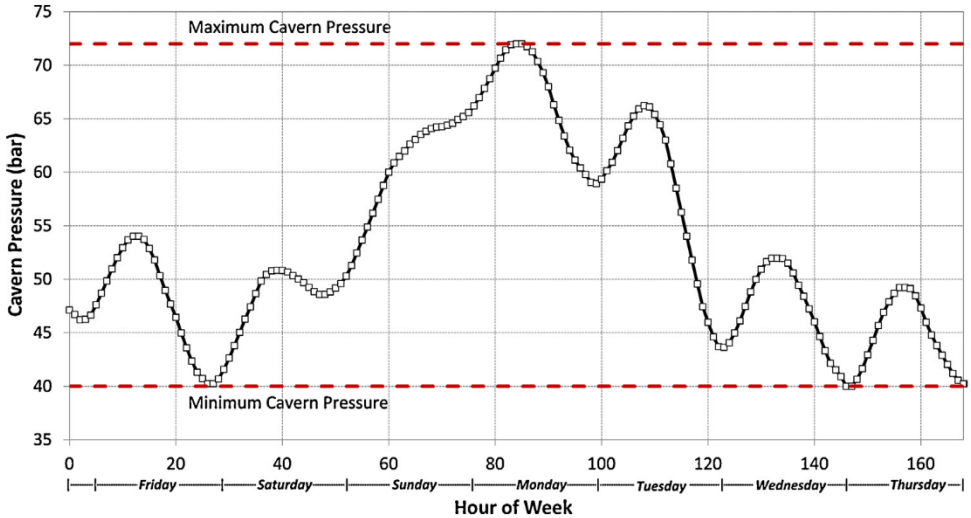

Fig. 8. Pressure profile of the SOFC/CAES system for one selected week of operation (June 17–23, 2011) using a RHO prediction horizon of 24 h.

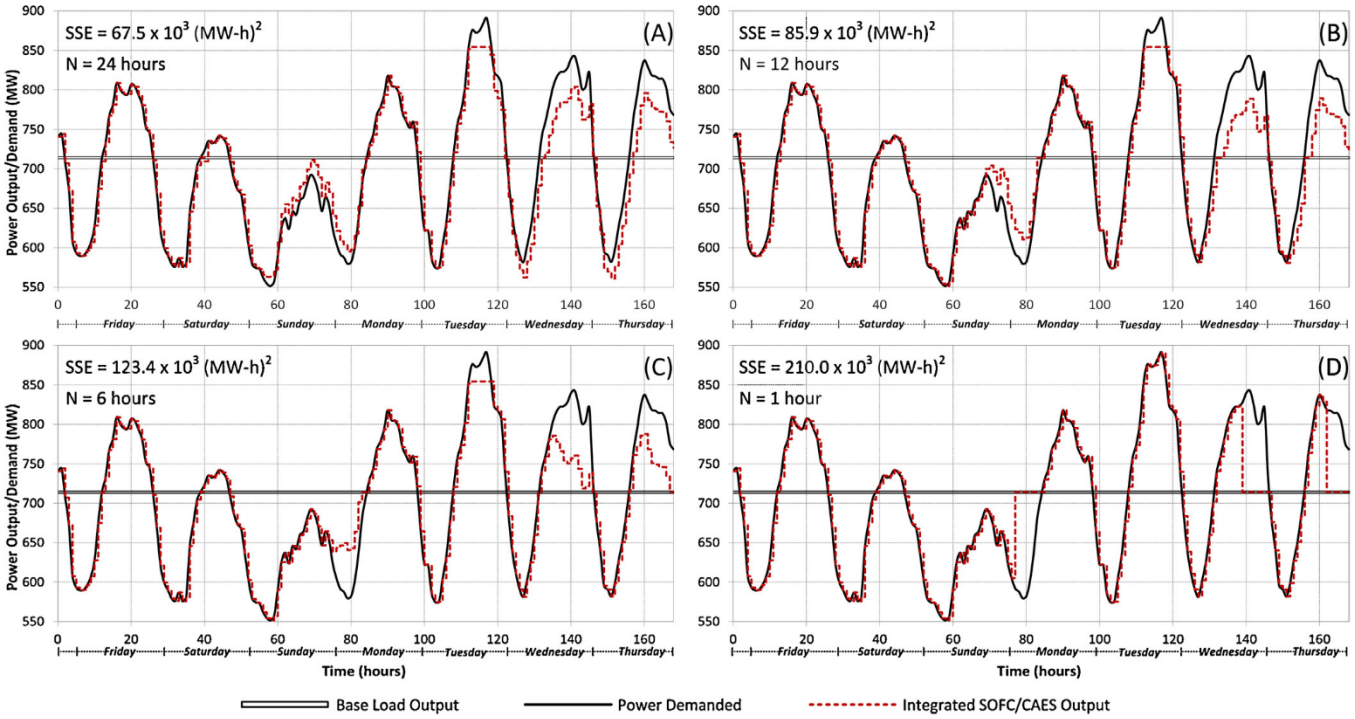

Fig. 9. Load-following results for the selected week of operation using different prediction horizons (N).

(a 27.3% increase from the base case). Using $N = 6$ (Fig. 9(C)) further accentuates this problem at those times, while also failing to compensate for the consistently low demand over the middle of the simulated week (Sunday). The overall SSE when a RHO horizon of $N = 6$ is used is 123.4×10^3 MW-h^2, nearly double (82.3%) of that of the base case. Fig. 9(D) is analogous to Fig. 7 where the prediction horizon of the RHO is $N = 1$ and exhibits the worst results.

As the RHO horizon increases, it can be seen in Fig. 10 that SSE improves with diminishing marginal returns. The best possible result of 42.9×10^3 MW-h^2 occurs when the entire week is known ahead of time, or $N = 168$. Although such a long optimization horizon is not realistically achievable, it serves to demonstrate the best possible improvement that RHO can make on the SOFC/CAES process. Furthermore, this shows that reducing the prediction horizon to a very reasonable 24 h does not decrease the RHO's performance by a large amount, indicating that using a realistic and achievable RHO scheme nearly maximizes the load-following capabilities of the SOFC/CAES plant.

4.2.2. Effect of demand forecast uncertainty

Although the improvement of the SOFC/CAES plant using RHO is significant, it is unreasonable to assume that the demand forecast for the entire prediction horizon is perfect. Instead, it is much more reasonable to assume that there is error associated with the forecasted demand over the optimization horizon. To this end, Gaussian noise was introduced to the RHO formulation to reflect this uncertainty. Gaussian noise was chosen based on the forecasting performance indicators reported by the IESO (IESO, 2012), where the greatest error for a 24-h ahead forecast for the year 2010 (the most recent performance data available) was ±18.2% of the forecasted demand for that time. The vast majority of forecasting errors were in the range of ±3%. Thus, we chose to generate white Gaussian noise with standard deviations in the range of 4–12% of the forecasted demand, resulting in a "worst-case" uncertainty analysis. Unfortunately, an archive of what the future predictions of demand were at each point in time was unavailable, and only the real demand data were available. The noise addition strategy used is shown graphically in Fig. 11. It was assumed that the

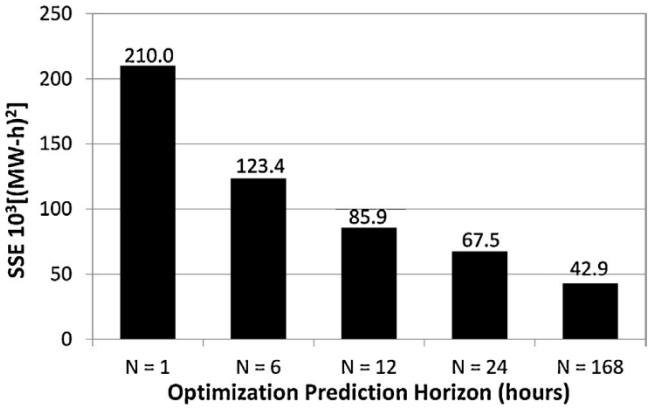

Fig. 10. Summary of load-following performance as measured by SSE for several tested prediction horizons (N).

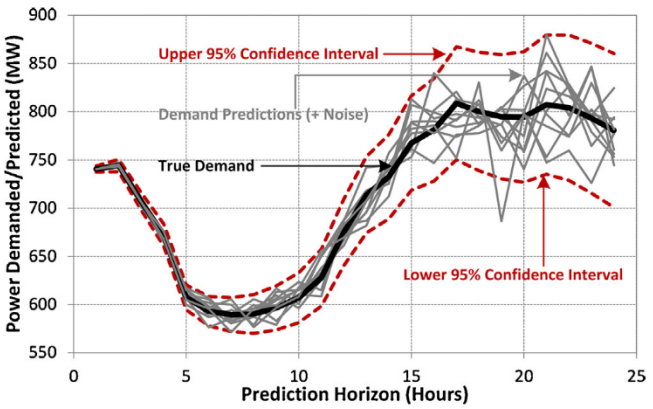

Fig. 11. Model of prediction error from the current simulation point i looking $t - 1$ time steps in the future as described in Eqs. (13) and (14).

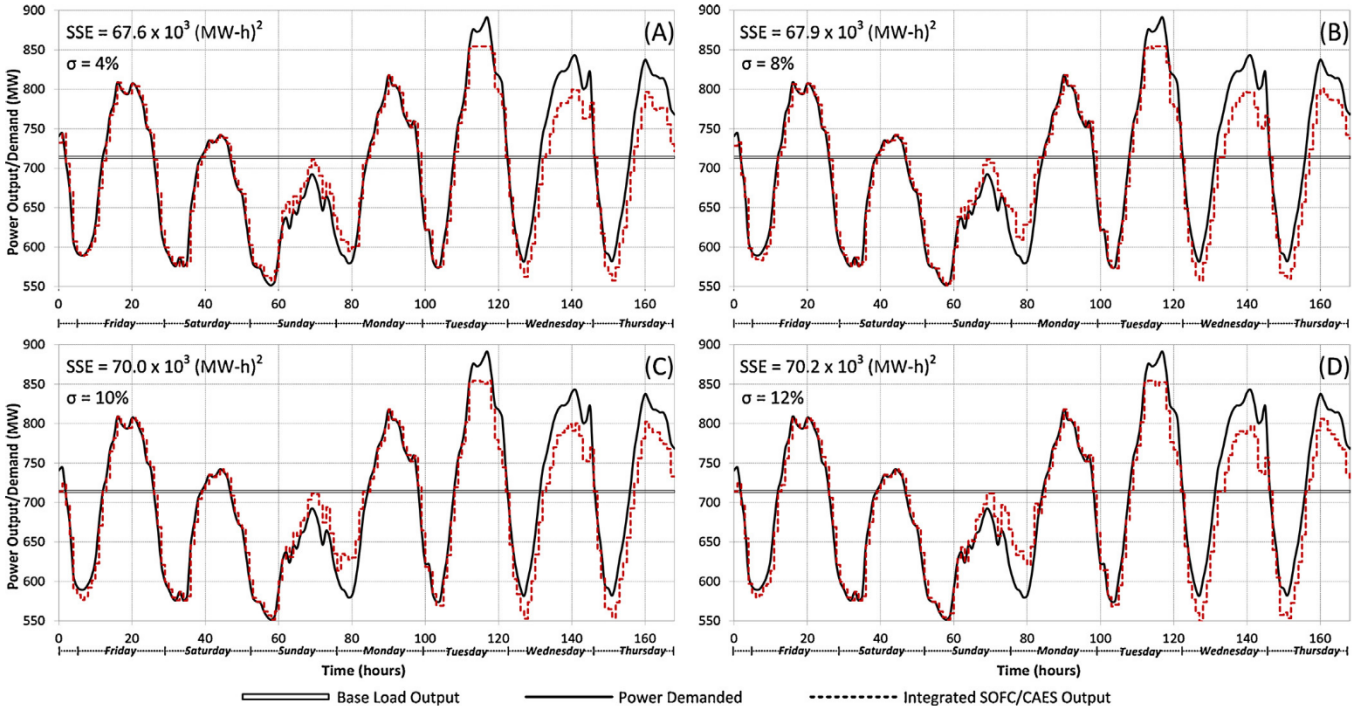

Fig. 12. Load-following results for the selected week of operation using different noise levels (σ, in % of demand) for the demand forecasts.

current demand is known exactly at each RHO control step, and that the size of the noise distribution increases linearly as the forecast extends away from the current point. Specifically, each demand forecast $D_{i,1} \ldots D_{i,N}$ is calculated as:

$$D_{i,t} = \mathcal{N}\{\bar{D}_{i+t-1}, \bar{D}_{i+t-1} w_t \sigma_D\} \quad [\forall t = (1 \ldots N)] \tag{14}$$

where $\bar{D}_i$ is the actual historical demand at timestep i, $D_{i,t}$ is (once again) the forecasted demand profile $t-1$ timesteps ahead of timestep i, σ_D is the standard deviation of the Gaussian noise of demand used to generate uncertainty and $\mathcal{N}\{\mu, \sigma\}$ is a randomly selected point based on a normal Gaussian distribution centered at the mean μ ($\bar{D}_i$ is the demand point on which the distribution is centered) and standard deviation σ. w_t is the linear weighting factor corresponding to the increasing uncertainty with forecasting horizon according to:

$$w_t = \frac{t-1}{N-1} \quad [\forall t = (1 \ldots N)] \tag{15}$$

which allows for the current demand to be known exactly, and the last point in the prediction horizon to be subjected to the highest potential noise. Note that a Monte Carlo simulation involving 20 individual simulations (each with different, randomly generated noise based on different results for $\mathcal{N}\{\mu, \sigma\}$) was performed in order to obtain an accurate average effect of the prediction noise.

Fig. 12 shows the resulting week demand/supply profiles under demand uncertainty using different standard deviations as high as $\sigma_D = 12\%$. It can be seen that increasing σ_D does not have a significant adverse effect on the RHO scheme's performance. Since the forecasted demand becomes increasingly accurate as it nears the current time interval, the RHO is only affected when it greatly over-compensates for a highly divergent prediction many hours in advance. Furthermore, it should be noted that in our analysis, the RHO forecast has no "memory", meaning that fresh noise is added to each forecasted point at each optimization interval. It is therefore possible that a severe over-prediction for the demand N time steps ahead will be followed by a severe under-prediction at the next optimization interval, when it is now $(N-1)$ time steps in the future. The pure randomness of the noisy forecasts have the chance of compensating for one another, therefore resulting in a relatively consistent set of RHO decisions. Fig. 13 shows that using values of σ_D as high as 8% do not have an adverse effect on the load-following capabilities of the SOFC/CAES plant as measured by the SSE (an increase in SSE of only 0.6%). Using very high values of σ_D does increase the SSE to as high as 70.2×10^3 MW-h^2, corresponding to a 4% increase over the base-case. However, even under these extremely uncertain demand forecasting conditions, the RHO is able to provide significant load-following performance improvements over our prior work (Nease & Adams, 2013).

4.2.3. Effect of consistent over- or under-prediction of demand

Although adding random noise introduces a more realistic and uncertain forecasting scenario, it is likely that entirely random changes in forecasted demand is unrealistic. Instead, it is more likely that certain forecast methods consistently under-predict or

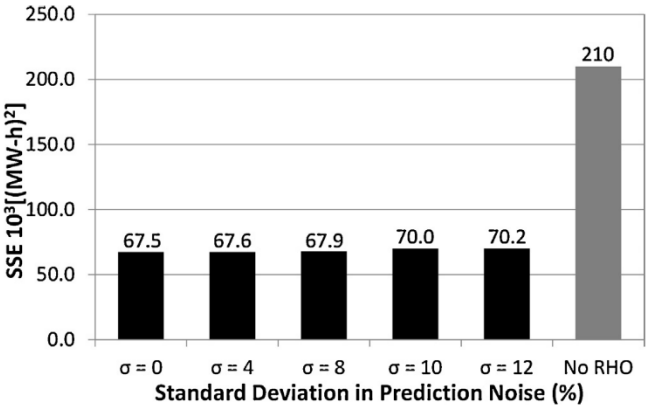

Fig. 13. Summary of load-following performance as measured by SSE for several tested standard deviations (in % of demand) of noise for prediction uncertainty (σ).

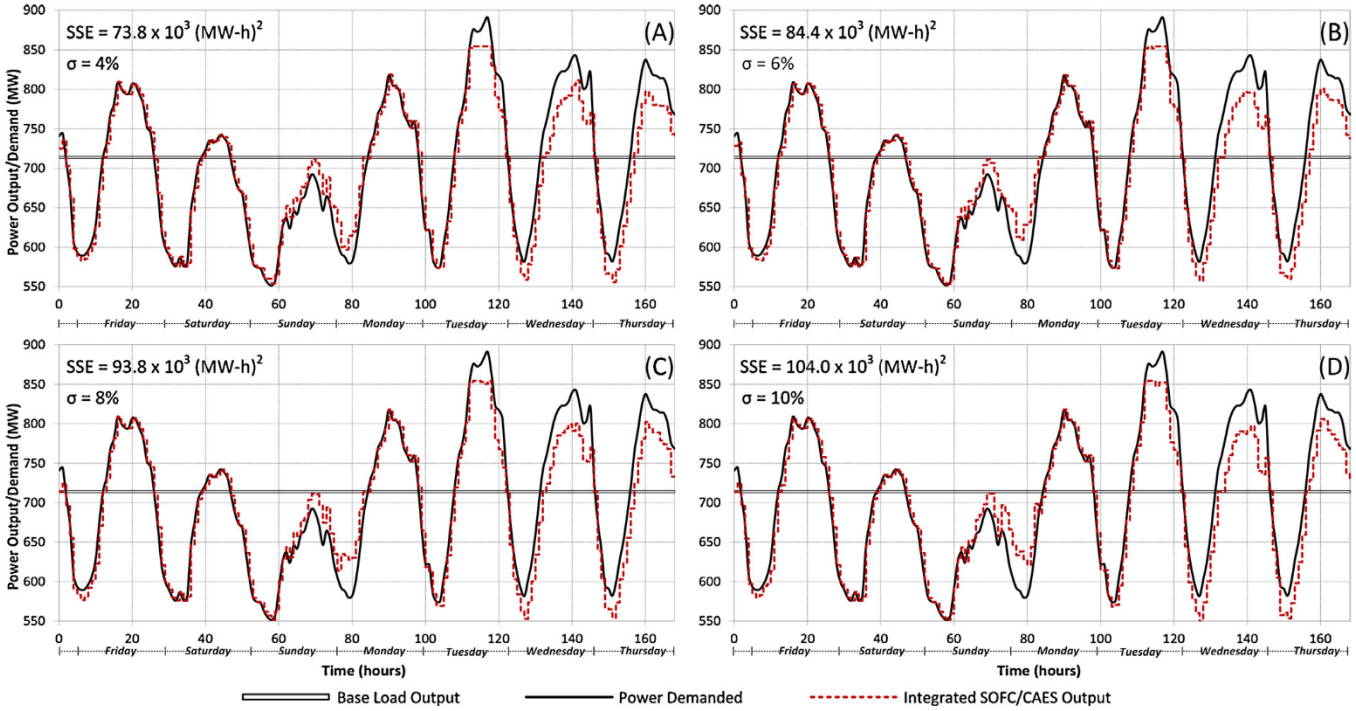

Fig. 14. Load-following results for the selected week of operation using various noise levels for the demand forecasts (σ, in % of demand) when demand is consistently over-predicted.

over-predict demand. From the perspective of the CAES system, more consistent under- or over-prediction of future demand can lead to a propagation of error due to the restrained space in the CAES storage cavern. To this end, the noise added to the demand forecast was altered to consistently over or under-predict demand while maintaining some level of randomness via the Gaussian noise. For this investigation, the demand adjustment for uncertainty described in Eq. (14) was altered as:

$$D_{i,t} = \bar{D}_{i+t-1} \pm |\mathcal{N}\{0, \bar{D}_{i+t-1} w_t \sigma_D\}|, \quad [\forall t = (1 \ldots N)] \tag{16}$$

Where $|\mathcal{N}\{0, \bar{D}_{i+t-1} w_t \sigma_D\}|$ represents the absolute deviation from the actual demand in the same fashion as Eq. (14), and is either added or subtracted from the true demand if consistent over- or under-predictions are desired, respectively.

Fig. 14 shows the resulting weekly supply/demand profiles when demand is consistently over-predicted for a range σ_D from 4% to 10% of demand. It can be seen that if demand is over-predicted, the RHO scheme is likely to over-produce during consistent periods of low demand, such as the period beginning at approximately $t \approx 60$. This is because the volume limitations of the CAES cavern are not expected to be as prevalent when this time period is at the high-noise end of the prediction horizon. As such, the net power output of the SOFC/CAES plant must be higher than ideal during those times. Furthermore, consistent over-prediction of demand also leads to falsely anticipated peaks during periods of high demand. For example, leading up to the peaks occurring at times $t \approx 140$ and $t \approx 160$, the net SOFC/CAES plant output goes lower than the actual demand as an anticipatory response to meeting high peaks later. As the standard deviation of prediction error increases, it can be seen that the gap between demand and supply during these charging periods expands. Not only does this increase the SSE, but it also increases the amount of power that must be supplied from an external source during those periods, which is wasteful. As expected, Fig. 15 shows the much more significant effect that uncertainty has on SSE when the prediction error is always in the same direction. With $\sigma = 4\%$, the SSE for the week-long simulation increases to 73.8×10^3 MW-h^2, corresponding to an increase of 9.3% over the base case and even higher than using purely random prediction noise with $\sigma_D = 12\%$. As the demand uncertainty increases to $\sigma_D = 12\%$, the SSE reaches 107.5×10^3 MW-h^2, and is 59.3% higher than the base case. The performance of the RHO is therefore clearly dependant on the quality of the forecasted demand, but even under unrealistically bad scenarios ($\sigma_D = 10\%$ is considered to be a worst possible prediction quality) the RHO scheme is able to improve performance over the case where RHO goes unused by roughly 50%.

Consistently under-predicting demand, as one might expect, exhibits inverted results from the over-prediction case. Fig. 16 shows that when demand is consistently anticipated to be lower than reality while below the base-load, the RHO over-produces in the time steps leading up to this phenomena to free up additional space that is expected to be needed in the CAES cavern. This is evident by examining the time step preceding $t \approx 60$ in Fig. 16, where there is clearly a demand/supply mismatch that

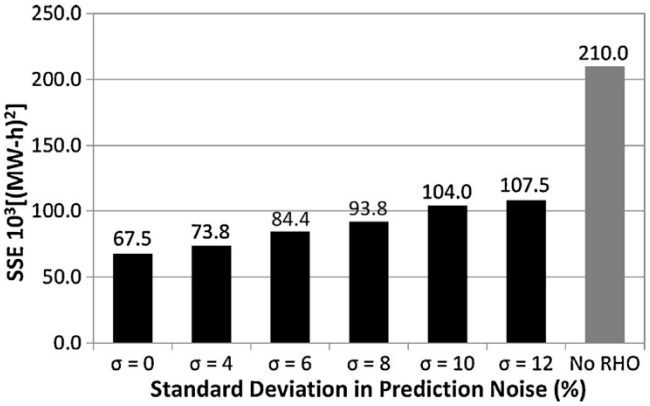

Fig. 15. Summary of load-following performance as measured by SSE for several tested standard deviations (in % of demand) of noise for over-prediction of demand (σ).

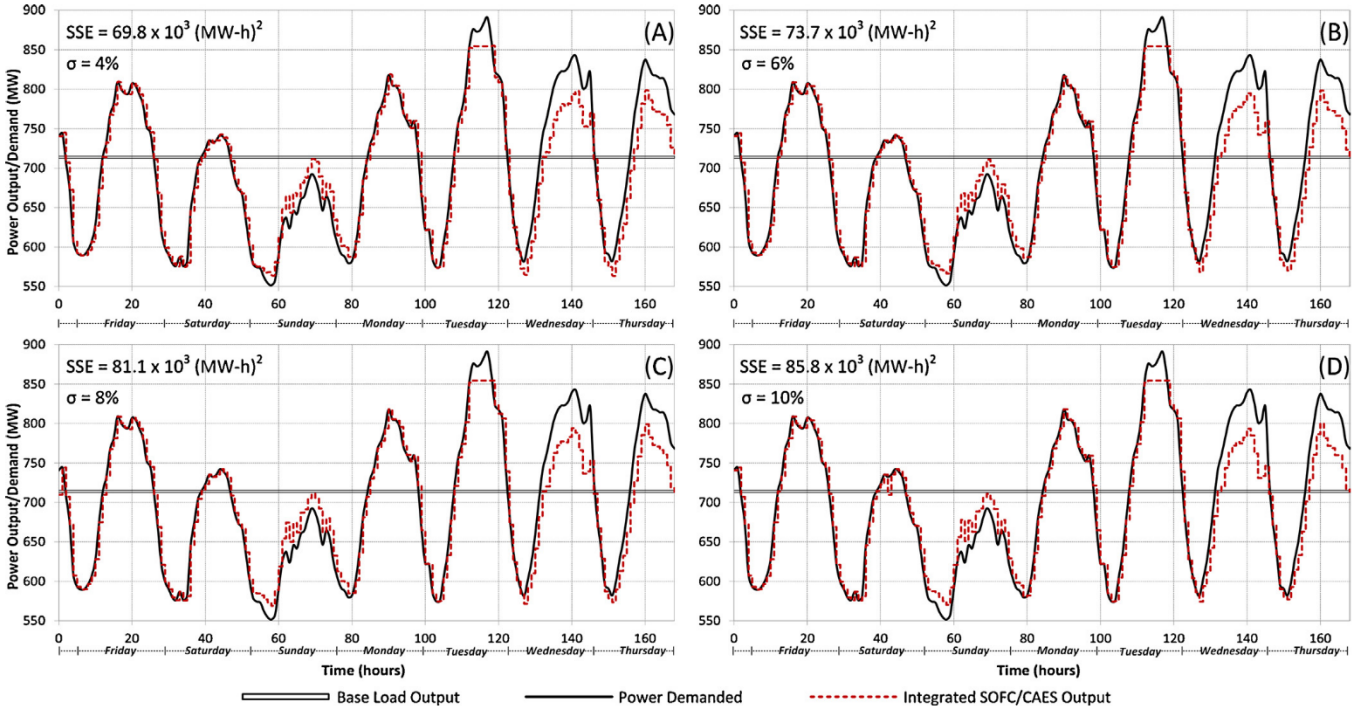

Fig. 16. Load-following results for the selected week of operation using various noise levels for the demand forecasts (σ, in % of demand) when demand is consistently under-predicted.

does not occur in the random or over-prediction cases exhibited in Figs. 12 and 14, respectively. Furthermore, under-prediction anticipates lower peaks than reality during periods of high demand. As such, the CAES storage cavern is charged less than the ideal amount during the times leading up to these peaks, resulting in a larger supply/demand gap during peak times. However, Fig. 17 shows that, for the same σ_D, under-prediction results in a lower SSE than when demand is always over-predicted. The worst-case SSE for the under-prediction case corresponding to $\sigma_D = 12\%$ is an SSE of 96.3×10^3 MW-h^2, which is still significantly lower than the results for the over-predicting case for the same conditions. This is likely due to the relative change in SSE associated with certain parts of the week-long demand profile; during the high peaks toward the end of the week, increasing the already high supply/demand gap by under-predicting demand does not have an adverse effect on SSE. However, the relative increase in the supply/demand gap at consistently low demand such as the area spanning $t \approx 60$ due to over-production has a significantly more pronounced effect on the increase of SSE. Regardless of the amount of uncertainty or how it is applied, it is clear from this analysis that the RHO scheme allows for significant load-following performance and operability improvements over the basic greedy algorithm used in our prior work (Nease & Adams, 2013).

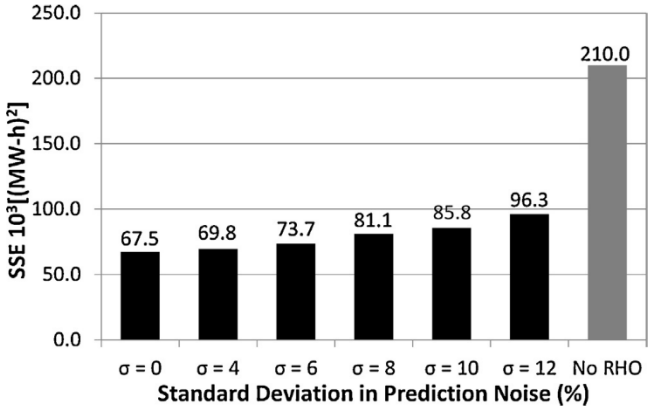

Fig. 17. Summary of load-following performance as measured by SSE for several tested standard deviations (in % of demand) of noise for under-prediction of demand (σ).

4.3. Economic case studies

4.3.1. Revenue maximization objective

The objective function given in Eq. (4) with the weighting factor $\psi \approx 60$ attempts to maximize revenue based on the spot price of electricity at each optimization interval, and each forecasted interval. Data for the hourly price of electricity for Ontario, Canada was obtained from the IESO for the operating year of 2011 (IESO, 2012). Note that the following assumptions were made for this analysis: (a) the SOFC/CAES plant is a price taker and therefore has no impact or control over the selling price of electricity, and (b) the hourly spot price of electricity is known with a very high degree of accuracy for the entire forecast/optimization period (which is maintained at 24 h for this analysis). Assumption (b) is very simplifying as the price of electricity is subject to multiple market factors and therefore is much more volatile when compared to the demand for electricity. As such, this analysis will serve as the absolute "best-case" scenario with regards to forecasting and RHO performance.

Fig. 18 shows the power demand/supply profile for the same week of data used for the load-following case studies. Several observations can be drawn from this graphic. First, it is clear that the revenue maximization RHO scheme does not attempt to follow demand in any way. An objective penalty through the variation of ψ is used to balance load following with revenue maximization in the proceeding section, but a purely revenue-maximization objective was used in this case to determine the maximum revenue

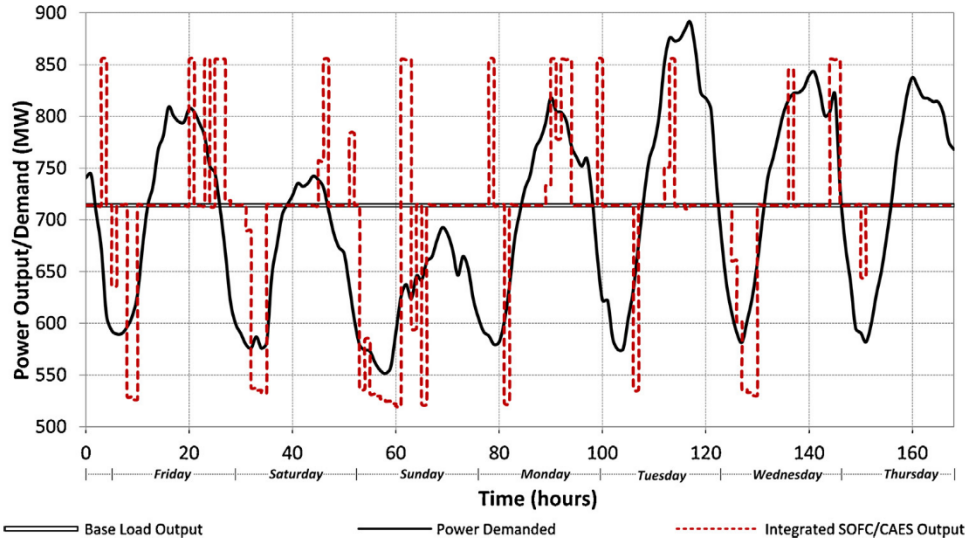

Fig. 18. Week long demand/supply price based optimization.

attainable by the plant over one week of operation. Consequently, this RHO method precludes the use of the SOFC/CAES system as a peaking plant, and would instead have to be used as a base-load supplement driven by purely financial motivations. Second, the SOFC/CAES plant usually charges or discharges at the maximum allowable air flow rate to or from the CAES cavern, hence minimizing or maximizing the net plant output, respectively. This is an expected result, since as much energy as possible should be stored during periods of sufficiently low electricity prices, and the power generation of the overall plant should be maximized during periods of high prices. One final observation that can be made is that the plant produces at base-load for a significant number of control periods. This can be explained by the inherent efficiency losses captured by the reduced models described in Eq. (8), whereby the use of the CAES compressors/turbines introduces net plant efficiency losses as high as two percentage points as described in our prior work (Nease & Adams, 2013). The price of electricity must therefore, over the prediction horizon of 24 h, vary by a relative amount that is higher than the portion of energy that would be lost to inefficiencies to make the use of the CAES system economically advantageous. Over this week-long period, the economic RHO is able to generate $3.97 million, which is a 3.9% increase over operating at the base-load alone ($3.82 million). However, the SSE reaches 1.30×10^6 MW-h^2, which makes it little better than the base-load plant (1.42×10^6 MW-h^2) with regards to load-following capabilities.

In order to compare the economic potential of using an economic objective function in the RHO scheme, it was used to

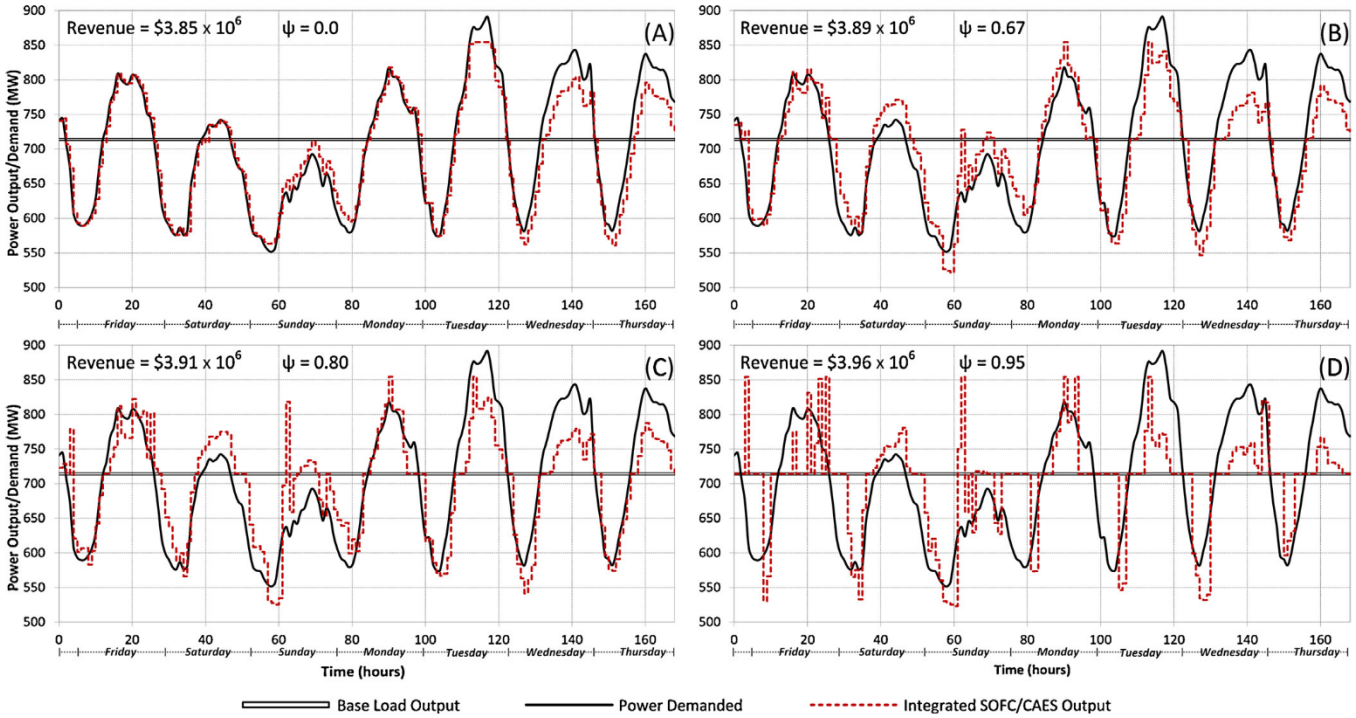

Fig. 19. Supply profiles and economic performances for the selected week of operation using different economic weighting values (ψ).

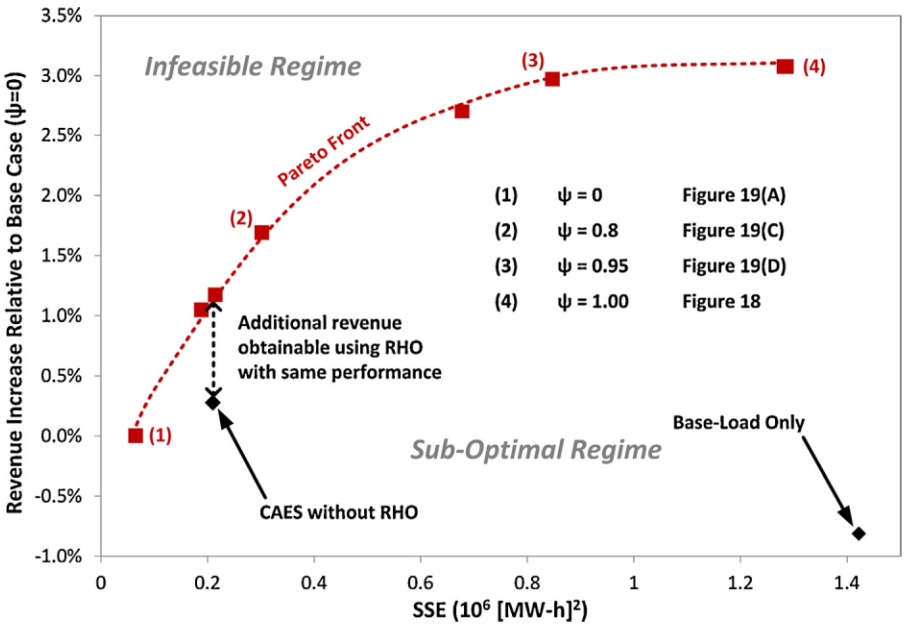

Fig. 20. Pareto plot showing the trade-offs between economic and load-following objective functions. The results for a base-load SOFC plant is outside of the view of this figure (SSE = 1.4 × 106 MW-h^2 and relative revenue = −0.8%).

simulate a typical year of operation so as to compare it to the SOFC/CAES plant described in our prior work from a cost standpoint. When a year of operation is considered, the results are similar to that of the week-long simulation. The revenue generated over one year of operation using the economic RHO is $196.9 million, which is a 4.65% increase over the original greedy-algorithm based SOFC/CAES plant that is able to generate $188.2 million and a 4.2% increase over the base-load plant which generates $188.6 million. Although the RHO scheme is able to generate additional revenue, it does so at the loss of load following capabilities; the revenue-maximizing RHO simulation has an annual SSE of 149.2×10^6 MW-h^2, which is roughly 8.4% higher than the original SOFC/CAES plant (137.7×10^6 MW-h^2).

4.3.2. Effect of economic weighting factor

Shown below in Fig. 19 are the supply/demand plots for the SOFC/CAES plant operating with an economic weight $0 \leq \psi < 1$, which results in a trade-off optimization that attempts to maximize revenue while also matching demand to a degree depending on the value of ψ. In Fig. 19(A), the $\psi = 0$ (load-following) case from Fig. 7 is shown again for easy comparison. As ψ increases across Figs. 19(B)–(D), the total revenue accrued by the plant increases. However, these increases in revenue are coupled with decreasing load-following performance. For example, Fig. 19(D) shows that when $\psi = 0.95$ the supply profile approaches the results of the purely economic-optimizing case in Fig. 18, albeit with marginally lower revenue generation.

The trade-off between the potential load-following and economic performance of the SOFC/CAES plant may be conveniently represented via the Pareto Plot shown in Fig. 20. The Pareto front represents the optimal trade-off between load-following and economic performance. It can be seen in Fig. 20 that the SOFC/CAES plant without RHO investigated in our prior work (Nease & Adams, 2013) falls within the sub-optimal regime away from the Pareto front, which further reinforces that the RHO scheme serves to improve the performance of the SOFC/CAES plant. The Pareto plot also exhibits that the improvement in revenue generation when targeting an economic objective (point (4) in Fig. 20) is only 3% greater than when economics are disregarded (point (1) in Fig. 20), but it comes with an over 20-fold increase in SSE. Another interesting comparison is that, compared to the CAES without RHO case, it is possible to generate an additional 1.1% ($42,000 weekly) in revenue using RHO while still achieving the same load-following performance result (Nease & Adams, 2013). Finally, note that the base-load only case without CAES or RHO is not shown in the diagram because it is too far from the Pareto front.

5. Conclusions and recommendations

In this study, the application of RHO to an integrated SOFC/CAES plant for load-following purposes was investigated. Reduced models of the SOFC/CAES plant developed in Aspen Plus v7.3 were implemented in GAMS in order to optimize the net power production of the combined system in order to minimize SSE over a sample week of operation. Real demand data available from the IESO was used to apply the integrated SOFC/CAES system with RHO to a realistic and applicable scenario. Several optimization forecasting horizons from one to 168 h were simulated in order to assess the impact of prediction horizon on load-following capabilities. Performance data from the IESO was also used to introduce realistic forecasting errors as Gaussian noise, the impacts of which were investigated using multiple Monte Carlo simulations for both realistic (±4% of demand) and exceedingly high (±12% of demand) noise severities. Lastly, an economic objective function was used to determine the impact of RHO in a revenue maximization scenario.

It was found that the addition of RHO with a prediction horizon of 24 h, when compared to the use of a CAES system not incorporating RHO, was able to reduce SSE by 68% to 67.5×10^3 MW-h^2 over the sample week simulated. Increasing the forecasting and optimization horizon was found to improve SSE with diminishing marginal returns beyond a horizon of 6 h. Adding random Gaussian noise to the RHO scheme to model error in the demand predictions had a marginal impact on SSE, increasing it by only 0.6% to 67.9×10^3 MW-h^2 when a conservatively high standard deviation of 8% of demand was used. Consistently over- or under-predicting demand was found to have a greater impact on the ability of the RHO to minimize SSE; using a standard deviation of 8% increased

SSE by 20% to 81.1×10^3 MW-h^2 when all forecasted demand was under-predicted, and by 39% to 93.8×10^3 MW-h^2 when all forecasted demand was over-predicted using a forecast horizon of 24 h. However, even under worst-case forecasting scenarios the use of RHO provides a more than 50% reduction in SSE when compared to the original SOFC/CAES system. Using an economic objective function was able to increase the gross revenue of the SOFC/CAES plant by as much as 4.7% ($8.7 million per year), and can be balanced with a load-following objective to optimize revenue based on a given performance threshold.

Overall, the SOFC/CAES process utilizing RHO shows great promise as a realistic day-to-day load following system capable of meeting peaking power demands with high accuracy and reliability. Since this is the first time RHO has been applied to a SOFC/CAES peaking plant to the best of our knowledge, our further work will investigate the use of more rigorous dynamic system models. Furthermore, dynamic control systems will be designed and implemented to demonstrate the feasibility of this process in a real-world and implementable scenario. One final area for expansion will involve the use of seasonal power storage opportunities (such as molten salts or electrolysis for hydrogen storage) in order to obtain both seasonal and daily load-following capabilities with zero emissions.

Acknowledgements

The authors would like to graciously acknowledge the Ontario Research Fund and Ontario Graduate Scholarship Program for their financial support of this project.

References

Achenbach E. Response of a solid oxide fuel cell to load change. Journal of Power Sources 1995;57:105–9.
Adams, T. A., II, Barton, P. I. (2009). *US Patent App. 12/434486*. Systems and methods for the separation of carbon dioxide from water.
Adams TA, Barton PI I. I. High-efficiency power production from coal with carbon capture. AIChE Journal 2010a;56:3120.
Adams TA, Barton P I. I. High-efficiency power production from natural gas with carbon capture. Journal of Power Sources 2010b;195:1971–83.
Adams TA II, Nease J, Tucker D, Barton P. Energy conversion with solid oxide fuel cell systems: A review of concepts and outlooks for the short- and long-term. I&EC Research 2013;52:3089–111.
Almutairi G, Kendall K, Bujalski W. Cycling durability studies of IP-SOFC. International Journal of Low-Carbon Technologies 2012;7:63–8.
Barelli L, Bidini G, Ottoviano A. Part load operation of SOFC/GT hybrid systems: Stationary analysis. Hydrogen Energy 2012;37:16140–50.
Becker WL, Braun RJ, Penev M, Melaina M. Design and technoeconomic performance analysis of a 1 MW solid oxide fuel cell polygeneration system for combined production of heat, hydrogen, and power. Journal of Power Sources 2012;200:34–44.
Campanari S. Carbon dioxide separation from high temperature fuel cell power plants. Journal of Power Sources 2002;112:273.
Cavallo A. Controllable and affordable utility-scale electricity from intermittent wind resources and compressed air energy storage (CAES). Energy 2007;32:120–7.
Chachuat B, Srinivasan B, Bonvin D. Adaptation strategies for real-time optimization. Computers & Chemical Engineering 2009;33(10):1557–67.
Copelin L. As Texas worries about power generation, is answer underground? Statesman; April 2013, Available online http://www.statesman.com/news/business/as-texas-worries-about-power-generation-is-answe-1/nRmpY/
De Souza G, Odloak D, Zanin AC. Real time optimization (RTO) with model predictive control (MPC). Computers & Chemical Engineering 2010;34(12):1999–2006.
Dressler-Rand. Dresser-Rand Awarded Compressed Air Energy Storage (CAES) Project [press release]; 2013, Available online: http://investor.dresser-rand.com/releasedetail.cfm?ReleaseID=774720
EG&G Technical Services. DOE/NETL fuel cell handbook. seventh ed.; November 2004.
Electric Power Research Institute. Wind Power Integration Technology Assessment and Case Studies. In: EPRI Report 1004806; 2004.
Fuel Cell Today. The fuel cell today industry review 2011. In: Corporate report; September 2011.
Fertig E, Apt J. Economics of compressed air energy storage to integrate wind power: A case study in ERCOT. Energy Policy 2009;39:2330–42.
Greenblatt JB, Succar S, Denkenberger DC, Williams RH, Socolow RH. Base load wind energy: Modeling the competition between gas turbines and compressed air energy storage for supplemental generation. Energy Policy 2007;35:1472–92.
Herzog HJ, Golomb D. Carbon capture and storage from fossil fuel use. In: Cleveland CJ, editor. Encyclopedia of energy. New York: Elsevier Science; 2004. p. 277–87.
Hoffeins H. Huntorf air storage gas turbine power plant. In: Energy supply. Brown Boveri Publication DGK 90 202 E; 1994, Available HTTP: http://www.eon.com/content/dam/eon-content-pool/eon/company-asset-finder/asset-profiles/shared-ekk/BBC_Huntorf_engl.pdf. Accessed 20.03.2013.
Hounslow DR, Grindley W, Louglin RM. The development of a combustion system for a 110 MW CAES plant. Journal of Engineering for Gas Turbines and Power 1988;120:875–83.
Independent Electricity System Operator. Ontario demand and market prices 2012, Available HTTP: http://www.ieso.ca/imoweb/siteShared/demand_price.asp?sid=ic. Accessed 19.03.2012.
Jin H, Larson ED, Celik FE. Performance and cost analysis of future, commercially mature gasification-based electric power generation from switchgrass. Biofuels, Bioproducts and Biorefining 2009;3:142.
Khajuria H, Pistikopoulos EN. Optimization and control of pressure swing adsorption processes under uncertainty. AIChE Journal 2012., http://dx.doi.org/10.1002/aic.13783.
Komatsu Y, Kimijima S, Szmyd JS. Performance analysis for the part-load operation of a solid oxide fuel cell-micro gas turbine hybrid system. Energy 2012;35:982–8.
Krulla K. Assesment of the distributed generation market potential for solid oxide fuel cells. In: SECA conference proceeding; 2013.
Kuramochi T, Turkenburg W, Faaij A. Competitiveness of CO_2 capture from an industrial solid oxide fuel cell combined heat and power system in the early stage of market introduction. Fuel 2011;90:958–73.
Liso V, Oleson A, Nielson M, Kaer S. Performance comparison between partial oxidation and methane steam reforming processes for solid oxide fuel cell (SOFC) micro combined heat and power (CHP) system. Energy 2011;35:4216–26.
Luyben WL. Compressor hueristics for conceptual process design. Industrial & Engineering Chemistry Research 2011;50(24):13984–9.
Mason J, Fthenakis V, Zweibel K, Hansen T, Nikolakakis T. Coupling pv and case power plants to transform intermittent pv electricity into a dispatchable electricity source. Progress in Photovoltaics Research and Application 2008;16(8):649–68.
Ming NQ. Coal based solid oxide fuel cell technology development. ECS Transactions 2007;7:45.
Mueller F, Tarroja B, Maclay J, Jabbari F, Brouwer J, Samuelson S. Design, simulation and control of a 100 MW-class solid oxide fuel cell gas turbine hybrid system. Journal of Fuel Cell Science and Technology 2010;7:031007-1–12.
Nagel FP, Schildhauer TJ, Biollaz SMA. Biomass integrated gasification fuel cell systems. Part 1: Definition of systems and technical analysis. International Journal of Hydrogen Energy 2009;34:6809.
Nease J, Adams TA II. Systems for peaking power with 100% CO_2 capture by integration of solid oxide fuel cells with compressed air energy storage. Journal of Power Sources 2013;228(15):281–93.
Nease J, Adams TA II. Coal-fuelled systems for peaking power with 100% CO_2 capture through integration of solid oxide fuel cells with compressed air energy storage. Journal of Power Sources 2014;251:92–107.
National Energy Board. Canada's energy future: Energy supply and demand projections to 2035 – electricity outlook highlights [online] 2012, Available HTTP: http://www.neb-one.gc.ca/clfnsi/rnrgynfmtn/nrgyrprt/nrgyftr/2011/fctsht1134lctrct-eng.html. Accessed June, 2012.
Ontario Ministry of Natural Resources. Underground storage – reservoirs [online] 2013, Available HTTP: http://www.mnr.gov.on.ca/en/Business/OGSR/2ColumnSubPage/STEL02_167108.html. Accessed 11.10.13; 2013.
Raju M, Khaitan SK. Modeling and simulation of compressed air storage in caverns: A case study of the Huntorf plant. Applied Energy 2012;89:474–81.
Rosenthal R. GAMS – a user's guide. Washington, DC, USA: GAMS Development Corporation; 2012.
Smith JM, Van Ness H, Abbot M. Introduction to chemical engineering thermodynamics. 7th edition New York, NY, United States: McGraw-Hill; 2005.
Stiller C, Thorund B, Bolland O. Safe dynamic operation of a simple SOFC/GT hybrid system. Journal of Engineering for Gas Turbines and Power 2006;128:551–9.
Succar S, Williams RH. Compressed air energy storage: Theory, resources and applications for wind power. Princeton Environmental Institute, Princeton University; 2008, Available HTTP: https://www.princeton.edu/pei/energy/publications/texts/SuccarWilliams_PEI_CAES_2008April8.pdf. Accessed 03.10.2013.
Trabold TA, Lylak JS, Walluk MR, Lin JF, Trojani DR. Measurement and analysis of carbon formation during diesel reforming for solid oxide fuel cells. International Journal of Hydrogen Energy 2012;37:5190.
US Energy Information Administration, AEO2012 Early Release Outlook, US DOE/EIA-0383ER (2012); January 2012.
US Energy Information Administration. U.S. underground natural gas storage by storage type [online] 2013, Available HTTP: http://www.eia.gov/dnav/ng/ng_stor_type_s1_m.htm. Accessed 11.10.13; 2013.
Vora SD. Fuel cells program overview. In: SECA conference proceeding; 2013.
Williams MC, Strakey JP, Surdoval WA. U.S. Department of Energy's solid oxide fuel cells: Technical advances. International Journal of Applied Ceramic Technology 2005;2:295.
Woods MC, Capicotto PJ, Haslbeck JL, Kuehn NJ, Matuszewski M, Pinkerton LL. Cost and Performance Baseline for Fossil Energy Plants. Volume 1: Bituminous Coal and Natural Gas to Electricity Final Report, DOE/NETL-2007/1281, Revision 1; August 2007.

Yang L, Weng Y. Performance study of a solid oxide fuel cell and gas turbine hybrid system designed for methane operating with non-designed fuels. Journal of Power Sources 2010;196:3824–35.

Young RE. Petroleum refining process control and real-time optimization. IEEE Control Systems 2006;26(6):73–83.

Zanin AC, Tvrska de Gouvea M, Odloak D. Industrial implementation of a real-time optimization strategy for maximizing production of LPG in a FCC unit. Computers & Chemical Engineering 2010;24:525–31.

Zhao C, Fu J, Xu Q. Real-time dynamic hoist scheduling for multistage material handling process under uncertainties. AICHE Journal 2013;59(2):465–82.

Chapter 7

Application of a Two-Level Rolling Horizon Optimization Scheme to a Solid Oxide Fuel Cell and Compressed Air Energy Storage Plant for the Optimal Supply of Zero-Emissions Peaking Power

The content of the following chapter has been **accepted** (with minor revisions) as the following peer-reviewed journal for publication consideration:

Nease J, Monteiro N, Adams TA II. Application of a two-level rolling horizon optimization scheme to a solid-oxide fuel cell and compressed air energy storage plant for the optimal supply of zero-emissions peaking power. *Computers & Chemical Engineering*. 2016 (Submitted).

Application of a Two-Level Rolling Horizon Optimization Scheme to a Solid-Oxide Fuel Cell and Compressed Air Energy Storage Plant for the Optimal Supply of Zero-Emissions Peaking Power

*Jake Nease [a], Nina Monteiro [b], Thomas A. Adams II [a]**

[a] Department of Chemical Engineering, McMaster University. 1280 Main Street West, Hamilton, Ontario, Canada

[b] Engenharia Química, Universidade Federal do Paraná. Avenida Coronel Francisco Heráclito dos Santos, Jardim das Américas, Curitiba, Brazil

* Corresponding author. 1280 Main Street West, Hamilton, Ontario, Canada, L8S 4L7. Tel.: +1 (905) 525-9140 x24782; E-mail address: tadams@mcmaster.ca

Abstract

We present a new two-level rolling horizon optimization framework applied to a zero-emissions coal-fueled solid-oxide fuel cell power plant with compressed air energy storage for peaking applications. Simulations are performed where the scaled hourly demand for the year 2014 from the Ontario, Canada market is met as closely as possible. It was found that the proposed two-level strategy, by slowly adjusting the SOFC stack power upstream of the storage section, can improve load-following performance by 86% compared to the single-level optimization method proposed previously. A performance analysis indicates that the proposed approach uses the available storage volume to almost its maximum potential, with little improvement possible without changing the system itself. Further improvement to load-following is possible by increasing storage volumes, but with diminishing returns. Using an economically-focused objective function can improve annual revenue generation by as much as 6.5%, but not without a significant drop-off in load-following performance.

7.1 Introduction

Due to pressure from governmental regulations, the constant knowledge of waning resources, and the rapidly improving technologies for generating reliable electricity from renewable resources, classic power plants utilizing fossil fuels such as coal and natural gas (NG) are being eschewed in favour of more environmentally friendly alternatives, particularly in North America. In fact, it is projected that by 2035 the United States and Canada will each generate approximately 10% [1] and 16% [2] of their power from non-hydroelectric renewable resources, respectively. However, a current prohibitive feature of renewable resources is that they are typically intermittent in nature (variable and unpredictable wind/cloud patterns, day/night cycles, *etc*.), which makes them unsuitable for use in a bulk supply scenario, which requires high reliability and consistency. Although it is possible to use large-scale intermittent energy storage techniques such as pumped hydro storage [3], compressed air energy storage (CAES) [4], molten salt loops [5], material phase changes [6] and others in order to levelized the power supply from intermittent renewables, the high variability of renewables coupled with the limited capacity of energy storage techniques

make for significantly difficult planning and operability concerns. These problems are further exacerbated by the low capacities of renewables and round-trip efficiency losses in potential energy storage systems, both of which must be improved before renewable energy sources will be capable of fully displacing fossil fuel-based power.

While the paradigm in energy sources for electricity generation moves to renewables, the use of fossil fuels still constitutes a major portion of the power generated worldwide. In fact, it is estimated that the United States will still supply approximately 34% of its electricity demand through the consumption of coal [1]. Furthermore, at its current usage rate it is estimated that North America possesses sufficient reserves for over 250 years of domestic coal consumption [7]. This large supply of coal, combined with the forecasted importance of it as a future resource, provides an opportunity and challenge to make the most efficient usage of this resource as possible.

Solid oxide fuel cells (SOFCs) can be used to generate reliable "peaking" electric power at the bulk scale with minimal environmental impact when appropriate carbon capture strategies are used [8]-[10]. To do this, SOFCs fueled by coal [11],[12] or natural gas (NG) [13] can be integrated with compressed air energy storage (CAES) in order to exploit some process synergies that enable the system to meet an ever-changing electricity demand through the day despite having no direct CO_2 emissions. The electric power can be generated at a competitive market price, even without government subsidies, once the SOFC technology reaches maturity. Furthermore, detailed life cycle analyses have shown that these proposed SOFC plants have significantly lower environmental impacts than other state of the art options such as the NG combined cycle (NGCC) [14] or supercritical pulverized coal (SCPC) [15] process.

In the SOFC/CAES system, the SOFCs produce power at a constant, steady rate, and the CAES system either stores or releases compressed air in different amounts that can change hourly or even more frequently. The goal is to adjust the amount stored or released throughout the day in order to change the total net electricity production needed to meet the demand. However, because the SOFC output is limited and the CAES storage capacity is finite, the power demand cannot always be met every hour of every day, week, and month. Therefore, an operating policy is required which must decide how well to match the production and demand at any given time. For example, the original proof-of-concept used a naïve (or "greedy") operating policy, which was to always store or release energy at any given moment such that power demand at that moment would be met exactly. Although this worked sometimes, it also led to significant "large misses" when the CAES storage volume reached minimum or maximum capacity, leading to all flexibility in the system being lost instantaneously [11]-[13]. The concept of real-time optimization [16]-[19] being used in chemical plants and even with small SOFC experimental setups [20] led to the eventual development of a rolling horizon optimization (RHO) technique that uses forecasts of future demand to optimally plan the next series of control moves based on the operating and storage constraints of the SOFC/CAES system [21]. With this approach, the system would predict a potential problem and then avoid it by scheduling a series of "small misses" over time in order to prevent a more serious large miss. Although this method improves the day-to-day performance and peak-following capability of the SOFC/CAES plant, it does not

solve the problem of seasonal changes in demand, such as a generally higher demand (up to 30% more) during the summer and winter months compared to autumn and spring.

Therefore, to better solve this problem, we present a new, expanded version of the RHO concept by formulating a two-stage RHO methodology that exploits the modular nature of the upstream SOFC stacks by turning some of them on or off safely, infrequently, and in incremental amounts. This leads to a modular step increase or decrease in the steady-state output of the plant, and thus the baseload can be optimally selected in order to track seasonal changes in demand as closely as possible. This allows for the CAES storage volume to be much more efficiently utilized, and significantly improves season-to-season and overall annual load-following performance. To demonstrate, this concept is applied to a SOFC/CAES plant with zero direct CO_2 emissions using gasified coal as a fuel source, showing for the first time that it is possible to use coal for clean, reliable and efficient electrical peaking power at the 100 megawatt scale over the entire year.

7.2 The Process and Simulation Models

7.2.1 SOFC/CAES Plant Layout

The integrated SOFC/CAES system used for this work is shown in Figure 5, which was studied in a prior work using the "greedy" operational strategy [11] but has not been examined using a RHO framework. This system is capable of providing reliable power with system-limited peaking capabilities and 100% capture of direct CO_2 emissions. The essential operating principle of this plant is as follows: The plant is designed for an annual average expected power demand subject to diurnal fluctuations. During periods of low demand, the CAES system consumes electricity provided by the base-load SOFC portion to charge the CAES storage of a completely independent (save for heat integration) CAES plant. The air source for the CAES, instead of atmospheric air, is the already-compressed cathode exhaust stream (mostly N_2) from the SOFC power island, resulting in significant savings and efficiency losses during the compression step. The consumption of power by the CAES compressors results in a net plant output lower than the base load output of the plant, and the diverted cathode exhaust into the CAES storage may be adaptively selected in order to result in a net plant output equal to (or very close to) the demand at any given time. When demand increases beyond the base load capacity, the CAES system is discharged, pre-heated by exchanging heat with the hot SOFC exhaust streams, and expanded to generate supplemental power in order to reach the required demand.

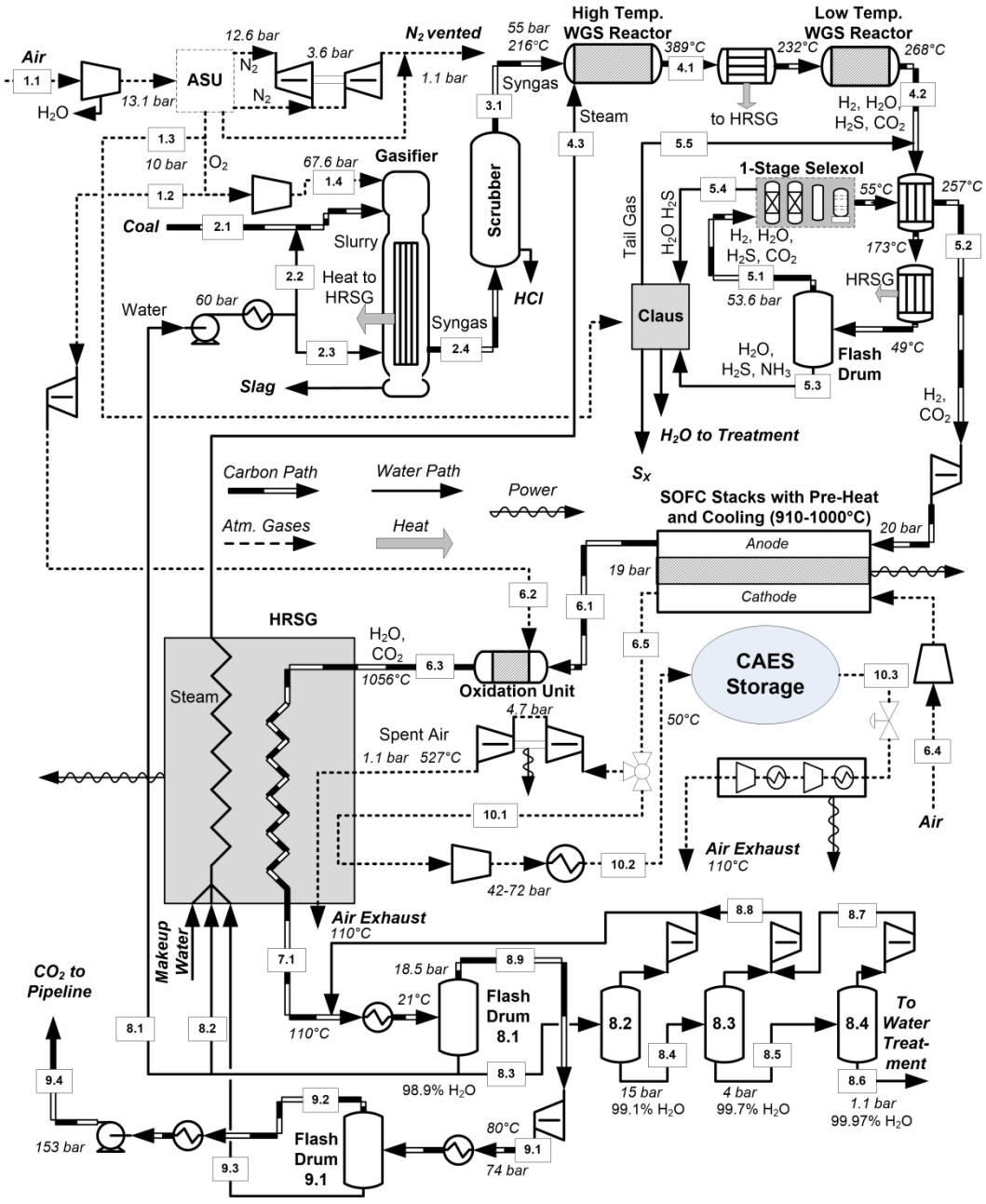

Figure 5: SOFC/CAES plant fueled by gasified coal that is simulated with the two stage RHO scheme presented in this work. Reproduced with permission from [11]

By synergistically using the excess heat available from the SOFC stacks (preventing the consumption of NG for pre-heating) and compressing the cathode exhaust instead of atmospheric air (reducing the overall compression ratio from 40-70 to approximately 4-7 depending on the operating pressure of the storage volume), SOFCs and CAES can be shown to complement each other nicely and result in peaking systems with higher efficiencies than any current alternative. For further details regarding the plant design and analyses,

the reader is encouraged to refer to the prior studies on the design of the system [11],[21]. Please note that although this design was chosen for the case study, many other design variations, including variations using other fuels such as natural gas, are also possible.

Once constructed, some operating parameters of the SOFC/CAES plant can be changed during operation. The two key operating parameters which are changed hourly during transient operation are (1) the percentage of the cathode exhaust sent to either CAES or the heat recovery and steam generation (HRSG) section, which is controlled by the three-way valve immediately downstream of stream 6.5, and (2) the amount of compressed air released from the CAES which is controlled by the valve immediately downstream of stream 10.3. The number of SOFC stacks in operation (or equivalently, the total power output of the SOFC stacks themselves) can also be changed as a third operating variable, although only once per week.

7.2.2 Rigorous SOFC/CAES Model in Aspen Plus

Since the rigorous SOFC/CAES system model used in this work was the same as in the prior work and is described in detail there, [11] only a brief summary is provided for brevity. Rigorous simulations of the SOFC portion of the proposed plant were performed using Aspen Plus v8.6 using the Peng Robinson equation of state (EOS) employing the Boston-Mathias modification, with a few exceptions (the Redlich-Kwong-Soave EOS and Electrolyte-NRTL packages were used for CO_2/H_2O streams below and near the critical point of CO_2, respectively). The coal feedstock to the gasification step is assumed to be Illinois #6 Bituminous, and thus has a higher heating value (HHV) of 27.267 MJ/kg [23] and contains 63.75% C, 4.5% H, 1.25% N, 0.29% Cl, 2.51% S, 11.12% H_2O and the remainder ash by weight [22]. The plant uses an optional water-gas shift (WGS) step upstream of the SOFC stacks to upgrade the H_2 content of the anode fuel stream, the trade-offs of which were addressed in the prior work. The SOFC plant is sized to produce a maximum output of approximately 820 MW, which was chosen to be consistent with our prior work and is also the size of a typical SCPC or other comparable coal-fueled base-load plant according to Woods et al. [24].

Although this is a much larger SOFC plant than any currently existing example, the US Department of Energy is anticipating that MW-scale SOFCs will exist by 2020 and should be commercially available by approximately 2030 [25],[26],[27]. In fact, Bloom Energy already has 210 kW modules available, further showing the advancement in technology is proceeding as anticipated [28]. Large-scale simulations of SOFC plants are also common in current literature [29]. It should be noted that the units in the SOFC plant are assumed to reach equilibrium, and thus the throughput of the plant may be reduced to as low as 600 MW in response to seasonal changes in base load due to the modular nature of the SOFCs. A detailed description of the SOFC plant was the topic of a prior paper and is thus not repeated here for the sake of brevity. For design decisions and stream conditions for the SOFC plant, the reader is referred to a prior work [22].

The CAES operating parameters were chosen based on the design recommendations by Luyben [30], and are comparable to the E.N. Kraftwerke plant as simulated by Raju and Khaitan [31]. Details regarding the operation and integration of the CAES system with the SOFC plant was the main topic of a prior work, and is thus not repeated here. The reader is referred to Table 1 in [11] for the assumptions related to the CAES system. The base case size of the underground CAES cavern is assumed to be 600,000 m^3, which was chosen based on a Pareto-optimal trade-off in the original investigation. However, with the proposed RHO framework allowing for better utilization of CAES storage volume, the size of the CAES cavern is varied in a sensitivity analysis (See section 7.4.2).

7.2.3 Reduced-Order SOFC/CAES Model

The Aspen Plus simulation takes approximately 5 minutes to converge, since the model itself requires several different iterative solves to converge tear streams, design specifications, and local optimization problems. This makes it unsuitable to use in a RHO framework because the RHO algorithm, which is described in Section 3, requires around 500 simulations for the algorithm to complete (or about 40 CPU-hours) *every timestep*, which in this work is once every hour of the year. So for the entire year of interest, this would require about 40 CPU-years to compute. Furthermore, the nature of the RHO algorithm is such that it cannot be easily parallelized, so using more CPUs in parallel does not solve this problem.

Therefore, a much faster reduced-order model representing the SOFC/CAES plant was identified from the rigorous Aspen Plus model. The reduced-order model was fit by running the Aspen Plus simulation at a variety of values for three key independent state variables. These are the pressure in the CAES cavern (P) at the beginning of the time step, a variable related to the amount of cathode exhaust diverted to the CAES storage volume (S), and the current baseload capacity of the steady-state plant (BL). Latin hypercube sampling was used for each independent variable. For each combination of variables, the net power output of the SOFC/CAES system $f(P,S,BL)$ was computed with the Aspen Plus model and recorded. This was performed twice, such that two models were identified, one for the charging mode and another for the discharging mode. A least-squares regression method was used to identify the coefficients of the model, which had the form:

$$f(P,S,BL) = \sum_{x=0}^{2}\sum_{y=0}^{2}\sum_{z=0}^{2} a_{xyz}\left(\frac{P}{\bar{P}}\right)^{x}\left(\frac{S}{\bar{S}}\right)^{y}\left(\frac{BL}{\overline{BL}}\right)^{z}. \quad (7.1)$$

Note that the indexed form of this model used in the optimization routine is discussed in section 7.3.1.1. In the model in Eq. (1), a_{xyz} is the model coefficient for the x^{th}, y^{th} and z^{th} powers of the normalized independent variables. The list of identified model parameters is shown in Table 1. The overbar denotes the value at which each of the variables were normalized to improve the scaling accuracy of the model. It is convenient to note the relationship between the variable used to describe the exhaust flow rate (S), the flow rate of the cathode exhaust (F), and BL is:

$$S = \begin{cases} 1 - \frac{F}{50.257BL - 3123.4} & [when\ charging\ CAES] \\ F & [when\ discharging\ CAES] \end{cases} \quad (7.2)$$

A plot showing the nonlinear fit of the model and sampled data points for a variety of baseloads (each represented by a different plane) are shown in Figure 6. It can be seen that the model fits the data very well without spurious curvature or significant biases, with an overall testing R^2 value of 0.989 and a root-mean squared error of estimation (RMSEE) of 2 MW (0.4%). A testing set was used to validate the model, which had a similar R^2, and the model was never used outside the range of variables of which it was identified. Higher order polynomial terms did not increase the R^2 significantly and had small coefficient values, and so only 2nd order terms were used in the final reduced model.

Table 1: Reduced-order model coefficients for revised RHO formulation

Coefficient	**Value** when $\boldsymbol{m = c}$ **(charging mode)**	Value when $\boldsymbol{m = d}$ **(discharge mode)**
$\mathbf{a_{000}}$	173.3	0.1
$\mathbf{a_{100}}$	-158.0	0
$\mathbf{a_{200}}$	24.6	0
$\mathbf{a_{010}}$	-55.8	25.5
$\mathbf{a_{020}}$	6.2	0
$\mathbf{a_{001}}$	369.4	696.8
$\mathbf{a_{002}}$	79.6	0
$\mathbf{a_{011}}$	94.5	0
$\mathbf{a_{101}}$	12.7	0
$\mathbf{a_{110}}$	70.7	0
$\mathbf{a_{111}}$	-25.4	0

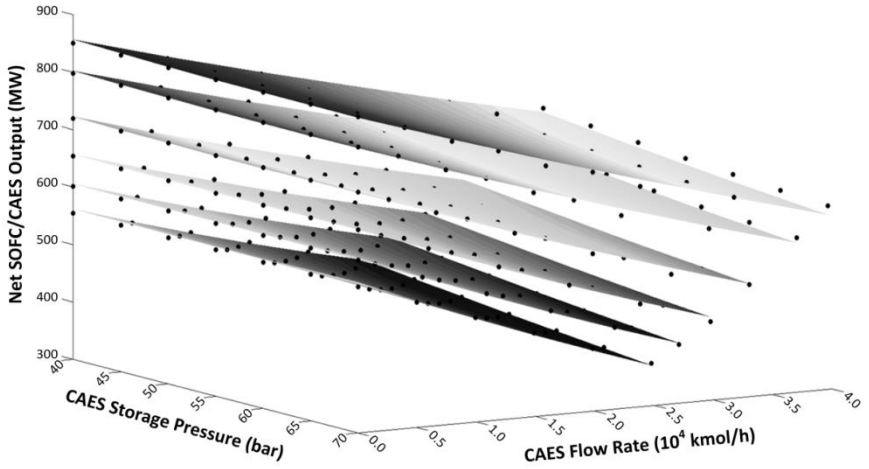

Figure 6: Predicted (planes) and simulated (dots) performance of the reduced-order SOFC/CAES model used in this work for six selected baseline capacities (BL).

7.3 Two-Stage Rolling Horizon Optimization Framework

The reduced-order model was implemented in GAMS [32]. The RHO algorithm was implemented in MATLAB, which communicated with GAMS to perform the optimization routine at each simulated time step. The RHO problem formulation for both stages and a discussion of what solvers were used in GAMS is presented in this section.

7.3.1 Problem Formulation

In the load-following optimization case, it is the objective of the RHO to determine the SOFC/CAES operating parameters over the control horizon that will either minimize the sum-of-squared errors (SSE), maximize the total revenue, or some weighted combination of both over the optimization's horizon ($\mathcal{R}$). The primary decision variables of interest determined by the RHO program are the flow rate to or from the CAES cavern (F) and what the baseload for the coming week should be (BL), which is then used to calculate the power output of the combined SOFC/CAES plant at each time step.

7.3.1.1 First Stage Objective Function Formulation

The problem formulation for this investigation is inspired by the formulation in our prior work [21] with some significant changes to the formulation and solution strategy for improved load-following and revenue generation performance. Overall, the RHO objective attempts to maximize a weighted objective function Φ that balances the total revenue generated by the SOFC/CAES plant ($\mathcal{R}$) and the load following performance of the plant as measured by the negative of the sum of squared error (SSE) between the plant output and demand as follows:

$$\max_{\delta_{i,t},\, F_{i,t}} \Phi_i = \{\psi \mathcal{R}_i - (1-\psi) SSE_i\}, \tag{7.3}$$

$$SSE_i = \sum_{t=1}^{N} \left(E_{i,t} - D_{i,t}\right)^2, \tag{7.4}$$

$$\mathcal{R}_i = \sum_{t=1}^{N} \left(E_{i,t}\omega_{i,t}\right), \tag{7.5}$$

where SSE_i is the sum of squared error difference at each simulation time step i between the power produced $E_{i,t}$ and forecasted demand $D_{i,t}$ (both in MW) at each control move t across the forecast time horizon N, $\omega_{i,t}$ is the forecasted market spot-price of electricity (POE) for each one-hour optimization interval over the optimization horizon (both forecasts are obtained from the IESO [33]), and $\psi \in [0,1]$ defines the emphasis on which of the two objectives should be met. Selecting $\psi = 1$ results in a pure revenue maximization problem while selecting $\psi = 0$ yields a load-following problem. $F_{i,t}$ is the flow rate to or from the CAES storage volume at each simulation time step, the direction of which is denoted by $\delta_{i,t}$, which is a binary variable that denotes whether the CAES storage is being charged ($\delta = 1$; the net plant output is reduced below the base-load) or discharged ($\delta = 0$; the net plant output is increased beyond the base-load). For the demonstrative purposes of this work, i ranges from 1 to 8760, for each of the 8760 hours in one simulated year of plant

operation. However, it is possible for this routine to be used indefinitely in real time, thereby not having a terminal value of ξ.

7.3.1.2 Process Model Equations

For the purposes of this investigation, the optimization or "control move" interval is one hour. $E_{i,1}$ is therefore the power actually produced at simulated timestep i, and $E_{i,t}$ is the power the optimizer plans on producing t–1 timesteps in the future for $t = (2 \dots N)$, which may or may not be implemented depending on future decisions since the entire forecasted output is recalculated at each update of i. The optimal production of the plant at the current simulation time i for the prediction horizon $t = 1 \dots N$ is calculated as:

$$E_{i,t} = \delta_{i,t} f_{c,i,t}\left(P_{i,t}, S_{i,t}, BL_i\right) + \left(1 - \delta_{i,t}\right) f_{d,i,t}\left(P_{i,t}, S_{i,t}, BL_i\right), \tag{7.6}$$

where BL_i is the baseload selected for the current simulation timestep i (the optimization sub-routine to select BL_i is discussed later), $E_{i,t}$ is the electrical output of the SOFC/CAES plant for RHO horizon $t = 1 \dots N$ at simulation time step i, $D_{i,t}$ is the demand for the RHO horizon $t = 1 \dots N$ at simulation time step i. The variables $S_{i,t}$ and $P_{i,t}$ are the variable related to the molar flow rate to/from the storage cavern (in kmol/hr) and the pressure (in bar) in the cavern at each time step, respectively, and $f_{m,i,t}$ are the indexed versions of the reduced-order models for the charging and discharging of the CAES cavern where $m \in \{c, d\}$, respectively and take the form:

$$f_{m,i,t}\left(P_{i,t}, S_{i,t}, BL_i\right) = \sum_{x=0}^{2} \sum_{y=0}^{2} \sum_{z=0}^{2} a_{xyz} \left(\frac{P_{i,t}}{\bar{P}}\right)^{x} \left(\frac{S_{i,t}}{\bar{S}}\right)^{y} \left(\frac{BL_i}{\overline{BL}}\right)^{z}, \tag{7.7}$$

$$S_{i,t} = \begin{cases} 1 - \frac{F_{i,t}}{50.257 BL_i - 3123.4} & when\ m = c \\ F_{i,t} & when\ m = d \end{cases}. \tag{7.8}$$

Note that the description of the coefficients is given in the previous section and the values of which are listed in Table 1. The mass balance constraint on the CAES cavern is described by:

$$\begin{aligned} n_{i,1} &= n_{i-1,1} + F_{i,1}\delta_{i,1}\Delta - F_{i,1}\left(1 - \delta_{i,1}\right)\Delta, \\ n_{i,t} &= n_{i,t-1} + F_{i,t}\delta_{i,t}\Delta - F_{i,t}\left(1 - \delta_{i,t}\right)\Delta, \qquad [\forall\ t = (2 \dots N)] \end{aligned} \tag{7.9}$$

where $n_{i,t}$ is the number of moles of cathode exhaust contained in the CAES storage volume at any given timestep i and Δ is the length of the simulation time step in which the output of the plant is held constant via a zero-order hold. Note again that $n_{i,1}$ is the actual molar holdup of the cavern as a result of executing the decision variables $F_{i,1}$ and $\delta_{i,1}$, and $n_{i,t}$ for $t = (2 \dots N)$ is the predicted molar holdup $N-1$ timesteps in the future based on the current optimization results, and may or may not change in the future. The pressure $P_{i,t}$ of the CAES storage volume is calculated using the SRK equation of state:

$$P_{i,t} = \frac{RT_{i,t}}{\mathcal{V}_{i,t} - b_{SRK}} - \frac{a_{SRK}}{T^{0.5}\mathcal{V}_{i.t}(V + b_{SRK})}, \qquad [\forall\, t = (1 \dots N)] \qquad (7.10)$$

where a_{SRK} and b_{SRK} are the SRK model coefficients for the cathode exhaust (assumed to be pure N_2) with values of $1.56 \times 10^{-5}\ \frac{m^6\ bar}{mol^2}$ and $2.67 \times 10^{-5}\ \frac{m^3}{mol}$, respectively [34]. The symbol R is the universal gas constant and T is the uniform temperature in the storage volume (assuming the contents of the volume itself are well-mixed). The molar volume of the CAES cavern contents at each control step is denoted by $\mathcal{V}_{i,t}$ and is determined as a function of the CAES storage volume V as:

$$\mathcal{V}_{i,t} n_{i,t} = V. \qquad [\forall\, t = (1 \dots N)] \qquad (7.11)$$

Note that the molar volume calculations given above in Eq. (7.11) combined with the material balances in Eq. (7.9) result in nonlinear relationships between the pressure in the CAES cavern and the flow rate to or from its control volume, which increases the complexity of the constraint in Eq. (7.10). Pressure is calculated at each time step to ensure that it never exceeds the operating limits of the CAES system, specifically:

$$P_{min} \leq P_{i,t} \leq P_{max}. \qquad [\forall\, t = (1 \dots N)] \qquad (7.12)$$

Finally, the flow rate into the CAES cavern is bounded by the cathode exhaust flow rate denoted by F_{max}:

$$0 \leq \delta_{i,t} F_{i,t} \leq F_{max}. \qquad [\forall\, t = (1 \dots N)] \qquad (7.13)$$

Inspection of the above equations shows that $E_{i,t}$ is a quadratic function in $P_{i,t}$, $BL_{i,t}$ and $S_{i,t}$. However, $P_{i,t}$ is itself a highly nonlinear function of $F_{i,t}$ and thus $S_{i,t}$ due to the SRK equations of state and material balances on the CAES storage volume. It can therefore be concluded that the objective function for this problem is highly nonlinear and includes the binary variable $\delta_{i,t}$ at each simulation timestep. The RHO problem at each simulation timestep i is thus a mixed-integer nonlinear program (MINLP), the size of which increases depending on the forecasting and optimization horizon N.

7.3.2 Second Stage: Baseload Selection

The baseload BL_i is adjusted every ξ time steps of the simulation (chosen to be one week, or 168 hours, due to the desired low-frequency of changing the SOFC output) by solving the second stage optimization problem of the form:

$$\min_{BL_i} \Gamma = \begin{Bmatrix} \min \\ \delta_{\iota,\tau} F_{\iota,\tau} \end{Bmatrix} \left[\sum_{\iota=i}^{i+\xi} \sum_{\tau=1}^{N=1} \left(E_{\iota,\tau} - D_{\iota,\tau} \right)^2 \right], \qquad (7.14)$$

$$BL_\iota = BL_i, \qquad [\forall\, \iota] \qquad (7.15)$$

$$(BL_i - BL_{i-1})^2 \leq (\Delta BL_{max})^2, \qquad (7.16)$$

where ΔBL_{max} is the maximum permitted change in the baseload (40 MW was used in this work) every ξ timesteps. It can immediately be seen that the objective function in Eq. (7.14) is the minimization of the original RHO objective function focused entirely on the minimization of SSE as described in equations (1) and (2). However, the RHO horizon for the subproblem is restricted to one future time step ($N = 1$), a technique known as the greedy algorithm. The optimization problem in Eq. (7.14) is subjected to the same operating constraints as the original RHO problem, but in this case BL_i is adjusted to find the baseload that minimizes the SSE of the greedy algorithm for the coming week. The outer optimization problem is thus restricted to a nonlinear program of one dimension that can be solved much more quickly than the full-sized inner optimization problem outlined in Eq. (7.3). The only additional constraint for Eq. (7.14) is the restriction that BL_i must not move more than ΔBL_{max} from the previous value (Eq. 7.16).

As a final note, it should be stated that the final result of the outer-layer optimization problem in Eq. (7.14) is rounded to the nearest MW step change to represent the modular nature of the SOFC stacks and thus the gross output of the SOFC/CAES plant. Rounding to the nearest 5 MW has been found to not change the nature of the solution to the outer-layer RHO problem, and thus is not added as a hard constraint to avoid having BL_i appear as an integer variable

7.3.3 Optimization Scheme and Method

7.3.3.1 Summary of Optimization Algorithm

The optimization scheme in this work follows closely to that of the prior investigation [21]. However, in this case there is an additional outer-layer optimization that occurs every ξ time steps. A summary of the algorithm is as follows:

1. Select desired values of the objective weighting factor ψ, the storage cavern volume V, and the RHO horizon N.

2. Initialize the problem with the demand predictions for next N timesteps (The actual historical hourly operation of 2014 is used for this study).

3. Provide the initial guesses for the SOFC/CAES plant output ($\dot{E}$), number of moles in the cavern ($\dot{n}$), model selection variable ($\dot{\delta}$) and operating pressure of the cavern ($\dot{P}$) to improve the likelihood of locating an optimal solution:

   If $i = 1$
   $\dot{E}_{1,1} \dots \dot{E}_{1,N} = D_1 \dots D_N$
   $\dot{n}_{1,1} \dots \dot{n}_{1,N} = n_0$
   $\dot{\delta}_{1,1} \dots \dot{\delta}_{1,N} = 1$
   $\dot{P}_{1,1} \dots \dot{P}_{1,N} = P_0$
   Else

$$\dot{E}_{i+1,1} \dots \dot{E}_{i+1,N-1} = E_{i,2} \dots E_{i,N} \qquad \dot{E}_{i+1,N} = D_{i+N}$$
$$\dot{n}_{i+1,1} \dots \dot{n}_{i+1,N-1} = n_{i,2} \dots n_{i,N} \qquad \dot{n}_{i+1,N} = n_{i,N}$$
$$\dot{\delta}_{i+1,1} \dots \dot{\delta}_{i+1,N-1} = \delta_{i,2} \dots \delta_{i,N} \qquad \dot{\delta}_{i+1,N} = \delta_{i,N}$$
$$\dot{P}_{i+1,1} \dots \dot{P}_{i+1,N-1} = P_{i,2} \dots P_{i,N} \qquad \dot{P}_{i+1,N} = P_{i,N}$$

4. Assign the appropriate baseload:

   If $i = 1$ **OR** $\xi \ (mod\ t) = 0$:
   Perform **second stage RHO** to select optimal baseload BL_i

   Else
   $BL_i = BL_{i-1}$

5. Pass in demand, the current baseload, and the operating conditions of the CAES system to the **first stage RHO** and obtain results.

6. Recover the actual values at simulation step i for plant output ($\bar{E}_i$), cavern pressure ($\bar{P}_i$) and number of moles ($\bar{n}_i$) as the first value of each described by the rolling horizon optimizer.

   $\bar{E}_i = E_{i,1}$
   $\bar{P}_i = P_{i,1}$
   $\bar{n}_i = n_{i,1}$

7. Update simulation time step and save results: $i = i + 1$. Check if $i > N_{max}$, which denotes the end of the simulation:

   If $i > N_{max}$
   End the algorithm.

   Else
   Return to step 3.

It is important to note that for research purposes, the demand for the entire year was "known" up front so that each iteration of the algorithm could take place immediately. However, in a real application, demand forecasts for the next N timesteps would be used instead, and one iteration would take place each hour over the course of the year. Also, in the case of the Ontario grid, the existing 24-hour demand forecast prediction models are very good with a low prediction error (typically less than 4%) [33]. Our prior work for the one-layer RHO [21] showed that the difference in performance between using predictions with up to 12% error versus perfectly accurate predictions was small due to the structure of the RHO framework. Therefore, only perfectly accurate predictions are used in this study to determine a "best case" scenario.

7.3.4 Solver Selection

Two commercial solvers were used in GAMS in a hierarchical structure for this work: ANTIGONE and BARON [32]. ANTIGONE is used as the primary solver in this case because it was found to solve each optimization step of the simulation faster than BARON when provided with a feasible initial guess (solution time for $N = 24$ is approximately 20 seconds with ANTIGONE). However, if a feasible initial guess was not provided by the algorithm presented in section 7.3.3.1 due to a switch in δ or an unexpectedly large change in demand or price, ANTIGONE sometimes failed to converge to a feasible solution. In these cases, it was found that BARON was able to solve the problem to a feasible optimum (solution time for $N = 24$ is approximately 10 minutes) in all cases. Consequently, a feasible optimum was found at each simulation time step, which was recorded in MATLAB. The total time for one simulation of 8760 time steps (one year of operation with hour-long control intervals) was approximately 5 CPU days per run, on average. Note that if BARON were used exclusively, approximately 61 CPU days would have been required.

7.4 Results and Discussion

The following sections describe the impacts that the proposed two-stage RHO scheme has on the load-following and revenue-maximization capabilities of the studied SOFC/CAES plant fueled by gasified coal. All simulation case studies use a forecasting and optimization horizon of $N = 24$ hours (one full day ahead) and $\xi = 168$ hours (one full week ahead).

7.4.1 Effect of Two-Stage RHO Scheme on Plant Performance

The importance of being able to change the baseload output of the integrated SOFC/CAES plant is demonstrated in Figure 7, which shows the average weekly demand for the province of Ontario, Canada for the operating year of 2014 scaled to an average of 720 MW. Since the CAES system storage capacity is on the order of 100s of MW-h, it would be impossible to exclusively use CAES to account for seasonal drifts in demand such as those shown in Figure 7 without an intractably large storage volume. Furthermore, the maximum range of the power change achievable by the CAES system is constrained by the cathode exhaust flow rate (when charging, or dipping below the current baseload) and excess heat available from the SOFC for pre-heating (for discharging, or rising above the current baseload). This range, for a 720 MW baseload plant, is approximately 200 MW if the baseload is never changed. However, it can be seen in Figure 7 that the difference between the minimum and maximum average weekly demand is nearly 235 MW, with the actual difference between the highest and lowest moments of the year being 527 MW. Thus, the use of weekly optimal baseload changes allows for more efficient use of the CAES storage volume and operating constraints.

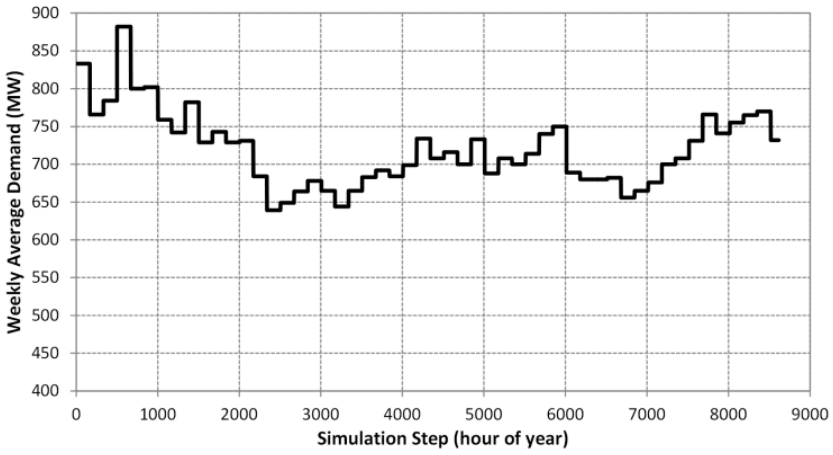

Figure 7: Weekly average demand for the simulated market over one year of operation

7.4.1.1 Load Following Performance

Shown in Figure 8 is the simulation results for one consistently high week of demand near the beginning of the year. Figure 8 (B) shows the performance of the SOFC/CAES system with the default selected initial value for BL of 720 MW (recall that this is the average demand over the entire simulated year) while Figure 8(A) shows the performance of the same system with an optimally selected BL of 830 MW (note that all subsequent changes to BL after this initial selection are subjected to the constraint of Eq. 15). It can readily be seen that the load-following capabilities of the integrated SOFC/CAES system are far greater when the baseload is chosen optimally, with over a 99% improvement in the load-following metric as measured by SSE. It is still clear in Figure 8(B) that the first-stage RHO scheme is attempting to use the forecasted demand to reduce large misses, but due to the low baseload output of the plant, the CAES storage volume cannot be utilized effectively. This result is demonstrated in Figure 9(B), which shows the operating pressure of the CAES storage volume for the same week of operation. It is clear that the entire energy storage capacity of the CAES system is underutilized, primarily due to demand being consistently higher than the base load can even achieve (and thus no excess energy is available for storage). Compare this result to Figure 9(A), which shows that the entire storage capacity of the CAES storage volume is utilized (both the maximum and minimum operating pressures are reached). Furthermore, it can be seen that the operating limits are touched upon but are not active for significant periods of time. This is due to the combined optimal selection of the baseload output of the plant via the second layer of the RHO scheme and the optimal hourly output as chosen by the first layer.

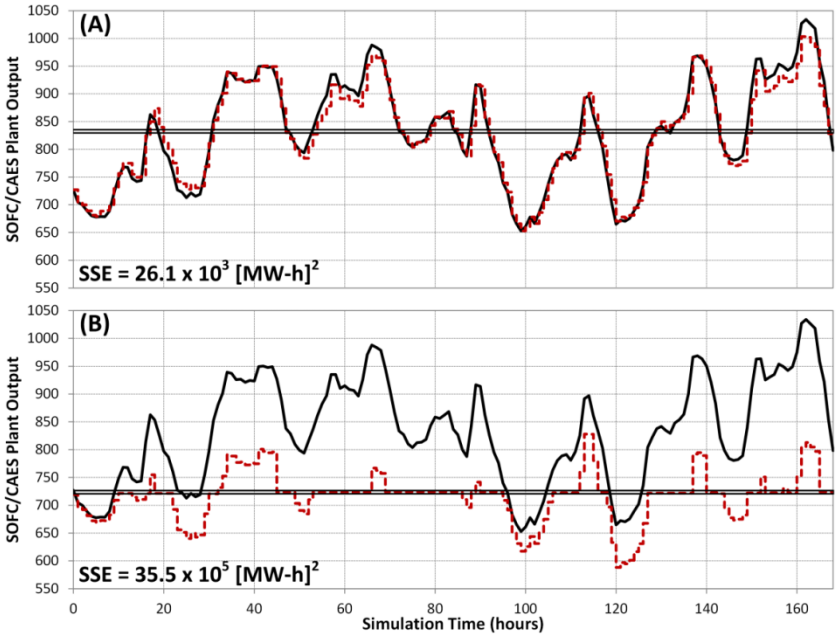

Figure 8: SOFC/CAES plant simulation results (red dashed line) and market demand (black line) for a high-demand week of operation near the beginning of the year. (A): with optimal base load selection using both layers of the RHO scheme. (B): With default base load selection using only the first layer of the RHO scheme

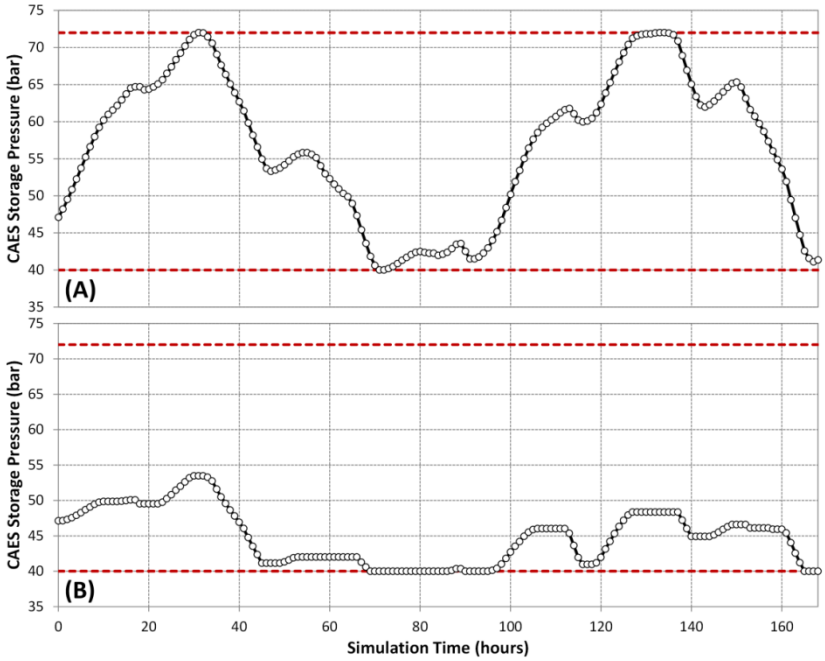

Figure 9: CAES storage volume pressure profiles for the high-demand simulated week of operation. (A): with optimal base load selection using both layers of the RHO scheme. (B): With default base load selection using only the first layer of the RHO scheme

Shown in Figure 10 is another case week that demonstrates the improvements brought about by the augmentation of the RHO scheme presented in this work, but for a week of consistently low-demand. In Figure 10(A), it is clear that the optimally selected baseload of 645 MW allows for more efficient use of the CAES storage, resulting in a load-following improvement of approximately 95% as measured by SSE for this week. It is clear in Figure 10(B) that the one-layer RHO scheme is optimizing the hourly output of the plant based on the constraints imposed by the CAES storage volume limits (and thus avoiding big misses by having a more consistent demand/supply mismatch), but in general the ability to provide the precise demanded power is nearly impossible. This is emphasized in Figure 11, which shows the pressure profiles for the CAES storage volume with (Figure 11[A]) and without (Figure 11[B]) the second layer of the RHO scheme choosing the optimal baseload for the week ahead. However, Figure 11(B) is in contrast to Figure 9(B) since in this case the CAES storage volume is always operating at or near its maximum limit due to the non-optimized baseload plant being too large and thus wasting power (and the resources used to make it). Compare this with Figure 11(A), which clearly shows that the entire operating range of the CAES storage is used, leading to a more efficient utilization of the available storage. In addition, it is also clear that simply oversizing the baseload and leaving it at that same level all year round as a strategy for ensuring that high-demand weeks are met is grossly inefficient and was the original motivation for the design of the integrated SOFC/CAES plant [11]. Note that the difference in initial pressures for each panel in Figure 11 are due to different operation decisions made prior to the highlighted week of operation.

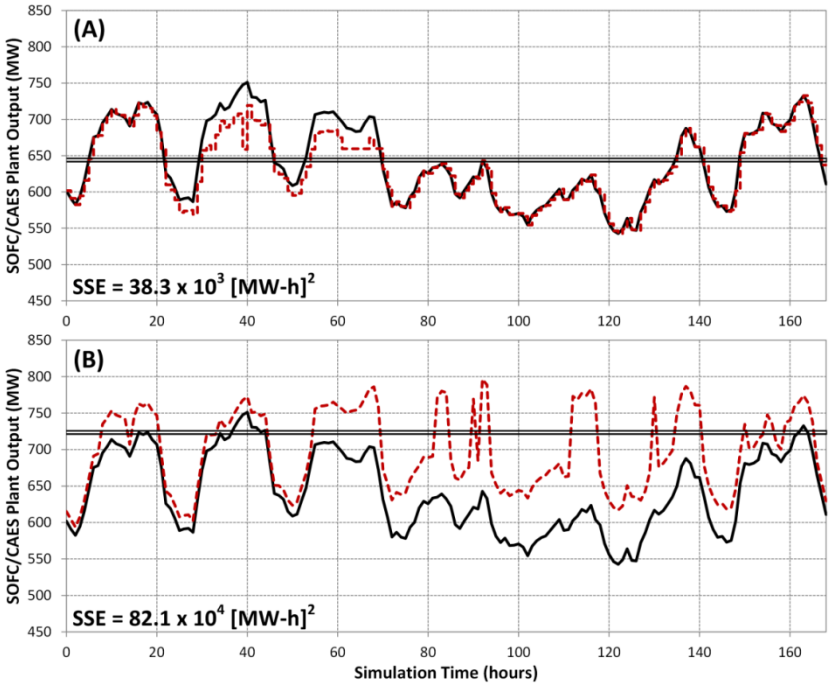

Figure 10: SOFC/CAES plant simulation results (red dashed line) and market demand (black line) for a low-demand week of operation near the beginning of the year. (A): with optimal base load selection using both layers of the RHO scheme. (B): With default base load selection using only the first layer of the RHO scheme

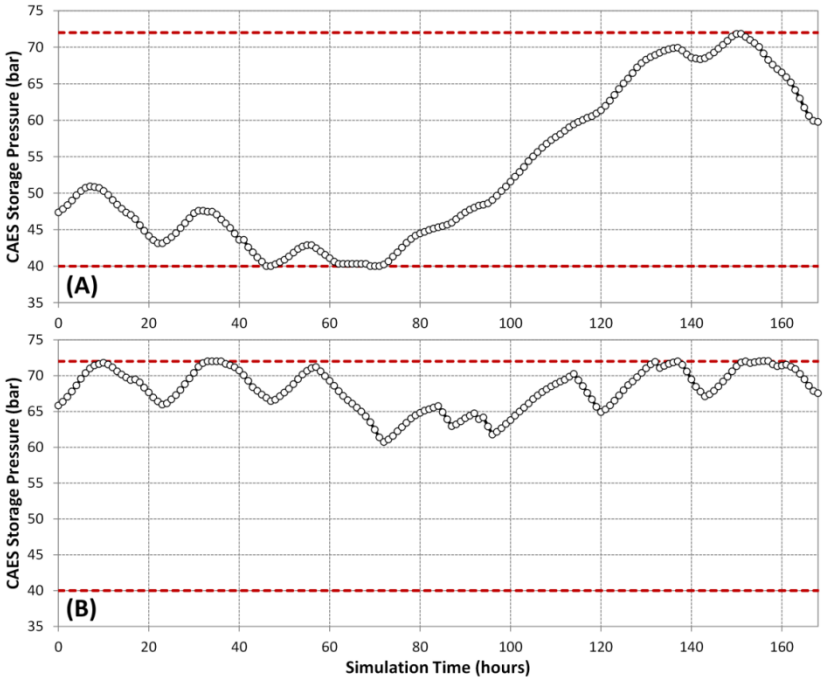

Figure 11: CAES storage volume pressure profiles for a low-demand simulated week of operation. (A): with optimal base load selection using both layers of the RHO scheme. (B): With default base load selection using only the first layer of the RHO scheme

In the previous work, the one-layer RHO scheme provided a significant load-following improvement for certain weeks of operation, but only those consistently at or near the default baseload output of 720 MW. The adaptive selection of the baseload output of the plant offered by the new second layer of the proposed RHO method allows for effective utilization of the CAES storage volume during any week of the year. This is further reinforced by the fact that the second layer takes the available CAES storage into account when selecting the baseload for the coming week. The importance of selecting the baseload each week is exemplified in Figure 12, in which it can be seen that the baseload is adjusted nearly every week to adapt to seasonal drifts in demand.

With regards to the annual load-following performance of the integrated plant, a figure is not shown since the high number of data points would make the plot virtually illegible. Rather, the SSE values for a one-year simulation are provided in Table 2. It is clear that, over an entire year of operation (8760 first-layer optimizations with $N = 24$ and 52 second-layer optimizations with $\xi = 168$) the proposed two-level RHO scheme can meet demand with a total SSE of 4.15×10^6 (MW-h)^2. This may be compared to the use of the single layer RHO developed in the prior work for the same year of demand using a fixed baseload of 720 MW, which is an order of magnitude higher at 30.3×10^6 (MW-h)^2. Furthermore, employing the greedy algorithm (hourly decisions with no forecasted optimization, equivalent to the one-layer scheme with $N = 1$) with a fixed baseload for this year of demand results in an SSE of 42.7×10^6 (MW-h)^2. The proposed two-level RHO method designed to exploit the modular nature of the SOFC stacks can thus improve the load-following performance of an integrated SOFC/CAES peaking plant by over 90% when compared to

using no optimization at all, and 86% when compared to optimizing the hourly operation of the CAES system exclusively. Although it is not possible to achieve perfect load-following from a stand-alone SOFC/CAES plant due to the operating limits and constraints of the CAES system, more efficient utilization of the CAES storage volume by appropriately optimizing the weekly baseload is possible; it is therefore likely that increasing the CAES storage volume beyond the base-case 600,000 m^3 will result in even better load-following, but with diminishing returns. The effect of CAES storage on annual load-following capabilities is discussed later in section 7.4.2.

Another metric in Table 2 that shows the improvements brought on by the two-level RHO is the number of times the CAES storage pressure is near its upper or lower bound. Over the year, the two-level RHO scheme results in the CAES storage pressure dipping below 41 bar (that is, the CAES storage is near or at the minimum allowable pressure) 423 times (4.8% of the total time steps). Of those 423 occurrences, the CAES pressure was stuck at the lower bound for more than one time step in a row at only 83 of them (0.9% of all time steps). Compare this to the one-layer RHO scheme for the same simulation, in which the CAES storage pressure was at or near its minimum constraint 990 times (11.3%). Of those 990 instances, 384 of them (4.4%) occurred consecutively. This indicates that nearly 4.5% of all demand instances, even with the one-layer RHO active, resulted in consecutive time steps in which the CAES system went unused due to capacity constraints. By reducing this occurrence to less than 1% of all time steps simulated, it is clear that the two-level RHO is much more effective at utilizing the limited CAES storage volume when demand is consistently lower than the average value of 720 MW. A similar result occurs with regards to the CAES storage volume operating at or near its maximum allowable pressure. Throughout the year, the two-level RHO results in the CAES storage pressure rising above 71 bar (within 1 bar of maximum) 288 times (3.3% of the year), whereas the one-layer RHO allows this to happen 622 times (7.1% of the year). Of the 288 instances where the two-level RHO results in operation near the maximum pressure constraint, only 38 of them (0.4%) result in consecutive time steps at maximum pressure, compared to 96 (1.1%) for the one-layer RHO.

Moreover, the two-level RHO results in the maximum and minimum pressures of the CAES storage volume being reached during the *same week* on 21 occasions versus only 5 for the one-layer RHO, indicating that the baseload is being selected so as to optimally utilize the available CAES storage. These pressure constraint results further reinforce that the two-level RHO makes much better use of the limited CAES storage capacity, which allows for much better load-following on an annual basis.

Note finally that in order for the two-level RHO scheme to be effective, a larger baseload amount of SOFC stacks would have to be purchased than the averaged-out 720 MW. The total size of the baseload SOFC power island would therefore have to be its maximum output of 830 MW, which is approximately 15% higher than the size of the plant used in the one-layer RHO. Although a full economic impact analysis is outside of the scope of this work, the increase in capital investment comes with two inherent benefits that should be considered: (1) because more of the demand is met, more power can be sold, and (2) the fuel consumption of the plant, which is the largest contributor to operating cost, is actually

lower for the 830MW plant using the two-level RHO than the one-layer RHO case by a small margin (0.7%) while meeting higher peaks than possible for the one-layer method.

Table 2: Load following metrics comparing this work to the methods used in prior studies

	Greedy Policy (no RHO)	One-Level RHO	Two-level RHO (This Work)
SSE (10^6 [MW-h]^2) *Lower is better*	42.7	30.3	4.15
Time steps within 1 bar of pressure bound *Lower is better*	4715	1612	711
Consecutive time steps at upper or lower bound *Lower is better*	3781	480	121
Weeks in which maximum and minimum pressure are both visited *Higher is better*	2	5	21

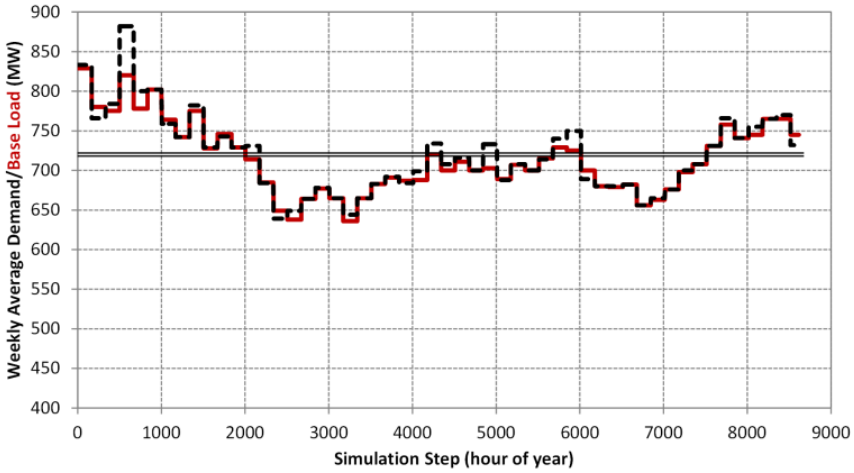

Figure 12: Weekly average demand (black line) for the simulated market over one year of operation alongside the optimally selected weekly baseload (red line) via the second stage of the proposed RHO method. The double-line is the constant average 720 MW chosen by the one-level RHO

7.4.1.2 Economic Performance

Shown in Table 3 are the resulting revenues generated by the SOFC/CAES plant over the simulated year of operation based on the actual market spot-price of electricity over that span. For each result, the same values of $N = 24$ and $\xi = 168$ are used as in the load-following scenario, but in this case the economic parameter ψ is varied from 0 (a purely load-following objective) to 1.0 (a purely economically driven objective that foregoes matching supply and demand in an attempt to maximize revenue) for the first layer of the RHO scheme. Note that price forecasting models are generally much less reliable than demand forecasting models, and thus the use of the proposed RHO scheme is likely better suited for a load-following scenario as concluded in the prior work. Also note that the use of a revenue maximization objective in the first stage of the proposed two-level RHO scheme results in an attempt to maximize revenue while still following the seasonal trends

of demand. The reason for this is simply because it is unrealistic to expect to be able to sell the maximum possible capacity of the SOFC/CAES plant to the market for the entire year, which would be the exclusive optimization decision since there is no negative cost associated with overproduction included in the given problem formulation. Consequently, the second stage of the simulation selects a baseload most appropriately suited to the coming week of demand in the same fashion as the load following objective, but the first level of the RHO is free to produce whatever results in the highest revenue generation possible. In reality, there are a multitude of potential objective function reformulations that may consider operating cost, annualized capital costs, or any combination of these that also consider operating constraints (such as minimum production constraints or constraints on maximum allowable misses). The following case study results are meant to show that the proposed two-level RHO is adaptable and may readily be implemented with an economic objective of the user's choosing.

Results for this case study show that it is possible to use the two-level RHO to increase annual revenue by as much as $14.1 million (6.3%) over the load-following scenario by using the CAES storage to exploit future jumps or drops in the spot price of electricity. This is unsurprising, since the currently existing CAES plants use this concept as their primary motivation to employ CAES technology, as mentioned earlier. However, this increase in revenue does not come without a trade-off, as the load-following portion of the objective function is eschewed entirely, leading to a very sporadic supply profile such as that shown in Figure 13. Based on the results in Figure 13, any scenario requiring distributed power generation or other cases in which high reliability and availability is needed would not be an appropriate opportunity to use the revenue maximization method. The application of the economic objective function is rather to utilize the available CAES storage for a given week of operation based on a previously selected baseload.

Given the continuous nature of the economic weight ψ, it is possible to achieve a hybridized objective function that balances revenue generation and delivering reliable power. A discussion revolving around this concept and the trade-offs associated with it are provided in section 7.4.3.

Table 3: SSE results comparing this work to the methods used in prior studies

Economic Parameter ψ	Revenue Generated (10^6 $)	Revenue Relative to Base Case
0.00	**224.6**	**100.0%**
0.50	**229.2**	**102.0%**
0.75	**233.8**	**104.1%**
0.90	**238.4**	**105.6%**
0.95	**238.6**	**106.2%**
1.00	**238.7**	**106.3%**

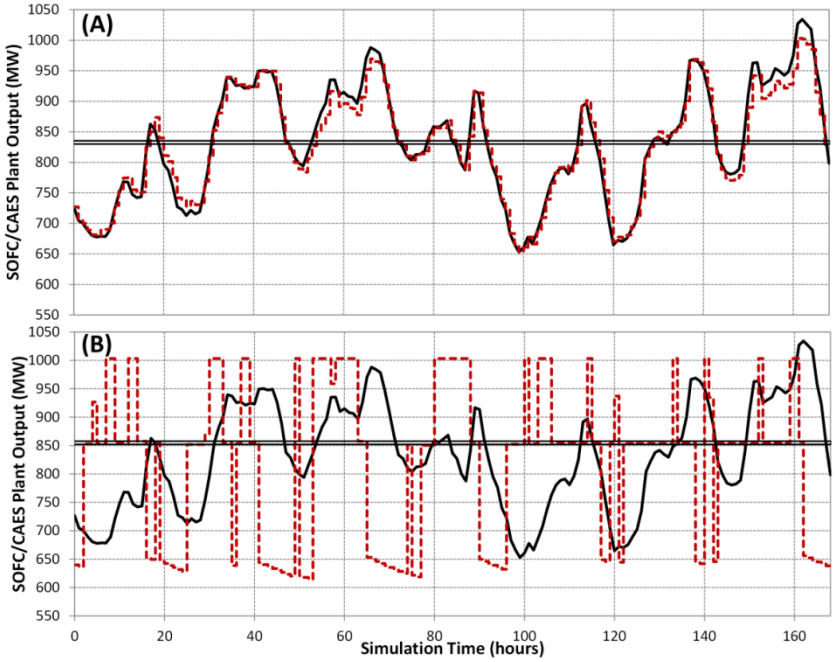

Figure 13: SOFC/CAES plant simulation results (red dashed line) and market demand (black line) for the consistently high week of operation near the beginning of the year using the proposed two-level RHO. (A): with the economic weighting parameter $\psi = 0$. (B): with the economic weighting parameter $\psi = 1$

7.4.2 Effect of Storage Volume on Plant Performance

In the original work defining the conceptual plant design of an integrated SOFC/CAES system for peaking power, it was postulated that increasing the CAES volume would improve the load-following capabilities of the integrated plant [13]. Although a sensitivity analysis in that work showed that such improvements are possible, they were not without significant added cost and exhibited a significant case of diminishing marginal return for increasing the size of the CAES storage volume. This result was primarily due to the CAES system only capable of storing intermediate amounts of energy (hundreds of MW-h), but the seasonal drifts in demand required massive amounts of energy storage (nearly millions of MW-h) that were not possible with CAES unless an excessively large volume was available. Moreover, as previously mentioned, the maximum amplitude of the CAES system is not sufficient to handle the maximum and minimum swing in demand observed by a typical market.

However, the adaptive baseload selection routine introduced in this work allows for a much more efficient utilization of the CAES volume throughout seasonal drifts in demand. As a result, a sensitivity analysis was performed to assess what improvements to load following would be possible with modest increases in the base case CAES volume size. The results showing the annual SSE for the integrated SOFC/CAES plant using the proposed

two-level RHO with $N = 24$, $\xi = 168$ and $\psi = 0$ versus the available CAES storage volume (with all other operational constraints the same) are shown in Figure 14. As expected, Figure 14 shows diminishing marginal returns as a function of CAES storage volume size. However, doubling the CAES cavern to (a very reasonable) 1.2×10^6 m^3 results in a 53% reduction in SSE (from 4.15×10^6 to 1.95×10^6 [MW-h]^2) over a year of operation. Furthermore, doubling the storage size results in its operating pressure being within 1 bar of the maximum or minimum constrained range for only 339 time steps (or 3.9% of the year). This is nearly a 20% reduction compared to the base case cavern size. Along with this reduction in operation near the constraints, the number of instances where the CAES pressure constraint is nearly active for consecutive time steps is only 45 times in this scenario, further reinforcing that the larger CAES volume is being efficiently used by the RHO scheme to improve the load-following capabilities of the plant. Any cavern size beyond 1.2×10^6 m^3 offers only a small improvement to the plant's load following capabilities with a significant increase in cost and further restriction on available locations.

One further interesting observation that can be made from Figure 14 is that the integrated SOFC/CAES plant will be unable to provide perfect load following even with an infinitely large storage volume. This is since the maximum amplitude of weekly demand variation is too high for the CAES capacity to compensate for without the external use of atmospheric air (for charging) or the combustion of NG for pre-heating (for discharging). However, as a stand-alone plant meant to supply a demand profile with a moderate amplitude, it is conceivable that a SOFC/CAES system would be able to supply efficient power with nearly 100% reliability.

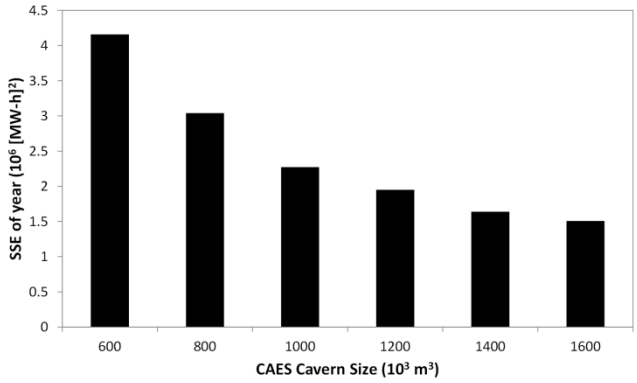

Figure 14: SSE using the base case parameters for the two-level RHO scheme for various CAES storage volume sizes

7.4.3 Pareto Trade-off Analysis Between Revenue and Load-Following Objectives

A trade-off plot between the potential load-following and economic performance of the SOFC/CAES system using the proposed two-level RHO method for various values of ψ is shown in Figure 15. Note that the base case CAES storage volume of 600,000 m^3 was used to generate this plot. It can immediately be seen that greedy algorithm (used in the original work demonstrating the applicability of an SOFC/CAES plant for load following) falls well

below the Pareto frontier denoting the optimal achievable combinations of revenue generation and load following. In fact, using the proposed two layer RHO method offers both an increase in revenue (1.5%) and a reduction in SSE simultaneously. Alternatively, it is possible to choose ψ to be a value between 0.75 and 0.90 in order to obtain approximately an increase in revenue of 6.5% ($14.6 million) relative to the base case study in this work with the same load-following performance. Any points beyond the Pareto front in Figure 15 is an infeasible operating condition based on the constraints of the CAES system when integrated with the SOFC power island. However, increases in storage volume size, external air and heat sources, and lower demand profile amplitudes can push the frontier further upwards and to the left.

It is also interesting to note that a base-load only SOFC plant sized to the average demand for the year (720 MW) has an excessively high SSE and is thus not included on the Pareto front axes, clearly making it a sub optimal method of operation. Furthermore, such a plant would have to be sized to always meet the highest possible demand, which would be very wasteful from a resource consumption perspective.

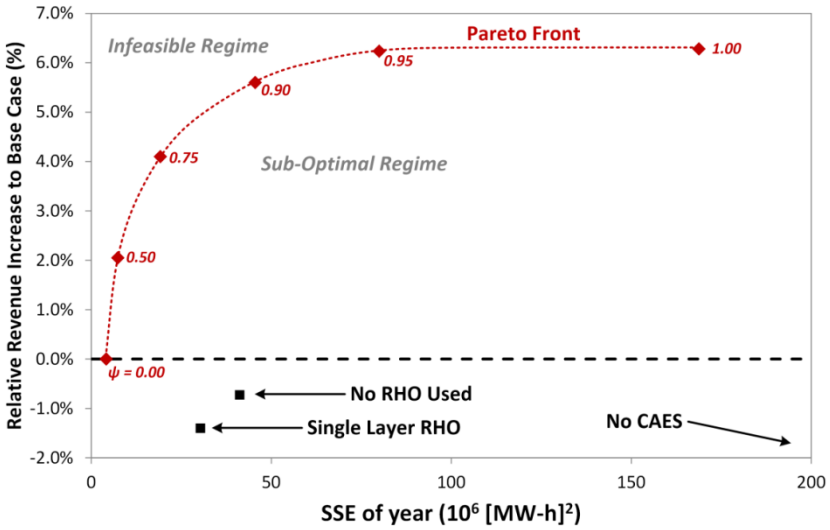

Figure 15: Pareto frontier showing the trade-off between revenue generation and load-following capabilities of the SOFC/CAES plant for various values of ψ

7.5 Conclusions and Recommendations

This study focused on the development of a two-stage RHO method that takes advantage of the hourly variability of CAES and the modular nature of SOFCs to provide reliable peaking power from an integrated SOFC/CAES plant with no CO_2 emissions. The first layer of the proposed RHO method used forecasted hourly demand to optimally operate the CAES portion of the integrated plant over the optimization time horizon (24 time steps were used in this case). The second layer of the RHO framework made adjustments to the SOFC baseload power island in order to adapt to seasonal drifts in demand throughout the year, a significant shortcoming of the single layer RHO previously proposed. The method was applied to a simulated SOFC/CAES plant fueled by coal designed in Aspen

Plus v8.6. Simulations for one year of scaled demand data from the Province of Ontario, Canada were performed using a reduced-order model in MATLAB with all optimization calculations performed in GAMS using ANTIGONE and BARON. All simulation and control intervals were chosen to be one hour in order to use the demand data available. Since the impact of demand forecasting uncertainty was addressed in a prior work for individual weeks, this work focused on the performance of the plant when its baseload is selected optimally at the beginning of each week of operation.

It was found that the proposed two-layer RHO method improved the load following performance of the SOFC/CAES plant by over 86% (from 30.3×10^6 to 4.15×10^6 [MW-h]^2) as measured by the SSE between demand and the power supplied by the plant for the 2014 year of operation. This is also a 90% improvement over the load-following capability of the integrated plant operating on an hour-by-hour basis (the so-called Greedy algorithm). It is worth noting that this improvement in demand/supply matching comes with no alterations to the plant design at all, but rather a more optimal utilization of the CAES peaking capabilities for hourly variations and the SOFC modularity to handle seasonal drifts in demand. Furthermore, it is possible to increase the revenue of the same plant by over $14 million (6.5%) per year if load following is not required via the tuning of the first-level objective function toward an economic focus. However, it should be noted that the proposed plant would require a larger SOFC power island (and hence capital investment), so a full techno economic trade-off analysis of the increased revenue should be the subject of a future work. A sensitivity analysis on the effect of CAES storage volume showed marked improvements in load following performance when more CAES storage is available, yielding a 53% improvement over the base case down to 1.95×10^6 (MW-h)^2. However, it was concluded that it would not be possible to completely eliminate supply/demand mismatches even with an infinitely large storage volume without significantly over-designing the power generation equipment.

Future work on this topic should include the investigation of uncertainty on the performance of the two stage RHO framework. Although prior studies found that demand forecast uncertainty did not significantly affect the hourly performance of the SOFC/CAES plant, it is possible that longer forecasts (and thus a greater degree of prediction error) could bias the second layer of the proposed technique and thus affect the baseload selection. Although it is not anticipated that this will significantly affect the results, it is something that should be addressed to test the robustness of this strategy to real-world noise and other sources of error.

Overall, the method showcased in this work has shown that, with the proper use of optimization strategies and by exploiting the advantages of the technologies therein, SOFC/CAES plants can be used to generate clean, reliable and efficient peaking power by using coal, which is a resource typically associated with the negative stigmas in all of these categories. The proposed RHO method overcomes the main weakness of the SOFC/CAES plant for peaking power by allowing it to slowly and safely adjust to seasonal changes in demand in an optimal manner, thereby more efficiently using the CAES system to save resources, money, and unnecessary wear on equipment. With these results, it is now apparent that technologies such as SOFCs and CAES are emerging as exciting opportunities that

will permit the use of North America's abundant natural resources in a sustainable future for electricity production.

7.6 Acknowledgements

The authors would like to graciously acknowledge the Ontario Research Fund, the NSERC Vanier Canada Graduate Scholarship Program, and the Canada-Brazil Science Without Borders program for their financial support of this project.

7.7 Nomenclature

7.7.1 Abbreviations

CAES	Compressed Air Energy Storage
CCS	Carbon Capture and Sequestration
EOS	Equation of State
GT	Gas Turbine
HHV	Higher-Heating Value
HRSG	Heat Recovery and Steam Generation
IESO	Independent Electricity Systems Operator
RHO	Rolling Horizon Optimization
SOFC	Solid Oxide Fuel Cell
SSE	Sum of Squared Error

7.7.2 Mathematical Symbols

E	Power produced by SOFC/CAES plant (via optimization)
$\bar{E}$	Actual power produced at each time step
$\dot{E}$	initial guess for E for proceeding simulation step
P	Pressure in CAES storage (via optimization)
$\bar{P}$	Actual pressure recorded in CAES storage at each time step
$\dot{P}$	Initial guess for P for proceeding simulation step
n	Number of moles in CAES storage (via optimization)

$\bar{n}$	Actual number of moles in cavern at each time step
$\dot{n}$	Initial guess for n for proceeding simulation step
$\mathcal{R}$	Total revenue
D	Demand
F	Molar flow rate of cathode exhaust
N	RHO forecasting horizon
R	Universal gas constant
V	Volume
a	Model coefficient
$f(\cdots)$	SOFC/CAES reduced model
δ	Binary charge/discharge decision variable
$\dot{\delta}$	Initial guess for δ for proceeding simulation step
ω	Price of electricity
ψ	User-defined economic/load-following weight factor
Φ	Economic/load-following objective function
BL	Base load
S	Cathode exhaust diversion parameter
$\mathcal{V}$	Molar volume
Δ	Time step length
a_{SRK}, b_{SRK}	SRK model coefficients

7.7.3 Subscripts

i	First-stage simulation/control time step
ι	Second-stage simulation/control time step
t	First-stage RHO calculation time horizon step
τ	Second-stage RHO calculation time horizon step
m	Reduced model identifier
k	Reduced model variable identifier
a, b, c	Reduced model order/coefficient identifiers
max	Maximum allowable value
min	Minimum allowable value

7.8 References

[1] US Energy Information Administration, Annual Energy Outlook 2014, US DOE/EIA-0383(2014). April 2014.

[2] National Energy Board. Canada's Energy Future: Energy Supply and Demand Projections to 2035 - Electricity Outlook Highlights. [online] Accessed June, 2012. [online]. Available HTTP: http://www.neb-one.gc.ca/clfnsi/rnrgynfmtn/nrgyrprt/nrgyftr/2011/fctsht1134lctrct-eng.html.

[3] D. Beevers, L. Branchini, V. Orlandini, A. De Pascale, H. Perez-Blanco. Pumped hydro storage plants with improved operational flexibility using constant speed Francis runners. *Applied Energy*. **2015**, *137*, 629-637.

[4] H. Sun, X. Luo, J. Wang. Feasibility study of a hybrid wind turbine system – Integration with compressed air energy storage. *Applied Energy*. **2015**, *137*, 617-628.

[5] A.k. Srivastava, J.Y. Kudariyawar, A. Borgohain, S.S. Jana, N.K. Maheshwari, P.K. Vijayan. Experimental and theoretical studies on the natural circulation behaviour of molten salt loop. *Applied Thermal Engineering*. **2016**, *98*, 513-521.

[6] G. Zanganeh, M. Commenford, A. Haselbacher, A. Pedretti, A. Steinfeld. Stabilization of the outflow temperature of a packed-bed thermal energy storage by combining rocks with phase change materials. *Applied Thermal Engineering*. **2014**, *70*, 316-320.

[7] BP Energy. BP Statistical Review of World Energy June 2014 (2014). Available HTTP: http://www.bp.com/content/dam/bp/pdf/Energy-economics/statistical-review-2014/BP-statistical-review-of-world-energy-2014-full report.pdf.

[8] T.A. Adams II, P.I. Barton. Systems and methods for the separation of carbon dioxide from water. US Patent App. 12/434486 (2009).

[9] EG&G Technical Services, DOE/NETL Fuel Cell Handbook, seventh ed., November 2004.

[10] M.C. Williams, J.P. Strakey, W.A. Surdoval. U.S. Department of Energy's solid oxide fuel cells: Technical advances. *International Journal of Applied Ceramic Technology.* **2005**, *2*, 295.

[11] J. Nease, T.A. Adams II. Coal-Fuelled Systems for Peaking Power with 100% CO_2 Capture Through Integration of Solid Oxide Fuel Cells with Compressed Air Energy Storage. *J. Power Sources*. **2014**, *251*, 92.

[12] N.Q. Ming. Coal based solid oxide fuel cell technology development. *ECS Transactions.* **2007**, *7*, 45.

[13] J. Nease, T.A. Adams II. Systems for peaking power with 100% CO_2 capture by integration of solid oxide fuel cells with compressed air energy storage. *J. Power Sources*. **2013**, *228*, 281.

[14] J. Nease, T.A. Adams II. Life Cycle Analyses of Bulk-Scale Solid Oxide Fuel Cell Power Plants and Comparisons to the Natural Gas Combined Cycle. *The Canadian Journal of Chemical Engineering*. **2015**, *93*, 1349-1363.

[15] J. Nease, T.A. Adams II. Comparative life cycle analyses of bulk-scale coal-fueled solid oxide fuel cell power plants. *Applied Energy*. **2015**, *150*, 161-175.

[16] B. Chachuat, B. Srinivasan, D. Bonvin. Adaptation strategies for real-time optimization. *Computers & Chemical Engineering*. **2009**, *33(10)*, 1557–1567.

[17] G. De Souza, D. Odloak, A.C. Zanin. Real time optimization (RTO) with model predictive control (MPC). *Computers & Chemical Engineering*. **2010**, *34(12)*, 1999–2006.

[18] A.C. Zanin, M. Tvrska de Gouvea, D. Odloak. Industrial implementation of a real-time optimization strategy for maximizing production of LPG in a FCC unit. *Computers & Chemical Engineering* **2010**, *24*m 525–531.

[19] C. Zhao, J. Fu, Q. Xu. Real-Time Dynamic Hoist Scheduling for Multistage Material Handling Process Under Uncertainties. *AICHE Journal*. **2013**, *59(2)*, 465–482.

[20] G.A. Bunin, Z. Wuillemin, G. Francois, A. Nakajo, L. Tsikonis, D. Bonvin. Experimental real-time optimization of a solid oxide fuel cell stack via constraint adaptation. *Energy.* **2012**, *39,* 54-62.

[21] J. Nease, T.A. Adams II. Application of rolling horizon optimization to an integrated solid oxide fuel cell and compressed air energy storage plant for zero-emissions peaking power under uncertainty. *Computers & Chemical Engineering*. **2014**, *68*, 203-219.

[22] T.A. Adams II, P.I. Barton. High-efficiency power production from coal with carbon capture. *AIChE Journal*. **2010**, *56*, 3120.

[23] GREET, The Greenhouse Gases, Regulated Emissions, and Energy Use In Transportation Model, GREET 1.8d.1, developed by Argonne National Laboratory, Argonne, IL, released August 26, 2010. Available HTTP: http://greet.es.anl.gov/.

[24] M.C. Woods, P.J. Capicotto, J.L. Haslbeck, N.J. Kuehn, M. Matuszewski, L.L. Pinkerton, M.D. Rutkowski, R.L. Schoff, V. Vaysman. Cost and Performance Baseline for Fossil Energy Plants. Volume 1: Bituminous Coal and Natural Gas to Electricity Final Report, DOE/NETL-2007/1281, Revision 1, August 2007.

[25] K. Krulla. Assesment of the Distributed Generation Market Potential for Solid Oxide Fuel Cells. United States Department of Energy – National Energy Technology Laboratory. SECA Conference proceeding. Pittsburgh, PA. July 23-24, 2013.

[26] S. D. Vora, Fuel Cells Program Overview. United States Department of Energy – National Energy Technology Laboratory. SECA Conference proceeding. Pittsburgh, PA. July 23-24, 2013.

[27] Fuel Cell Today, *The Fuel Cell Today Industry Review 2011*. September 14, 2011. Corporate report.

[28] T.A. Adams II, J. Nease, D. Tucker, P. Barton. Energy Conversion with Solid Oxide Fuel Cell Systems: A Review of Concepts and Outlooks for the Short- and Long-Term. *I&EC Research*. **2013**, *52(9)*, 3089-3111.

[29] F. Mueller, B. Tarroja, J. Maclay, F. Jabbari, J. Brouwer , S. Samuelson. Design, Simulation and Control of a 100 MW-Class Solid Oxide Fuel Cell Gas Turbine Hybrid System. *Journal of Fuel Cell Science and Technology*. **2010**, *7*, 031007-1-12.

[30] W.L. Luyben. Compressor heuristics for conceptual process design. *Industrial and Engineering Chemistry Research.* **2011**, *50*, 13984-13989.

[31] Raju M, Khaitan SK. Modeling and simulation of compressed air storage in caverns: A case study of the Huntorf plant. *Applied Energy.* 2012; 89:474-481.

[32] Rosenthal R. GAMS – A User's Guide. *GAMS Development Corporation.* Washington, DC, USA. 2012.

[33] Independent Electricity System Operator. *Ontario Demand and Market Prices*. Accessed March 19, 2012. Available HTTP: http://www.ieso.ca/imoweb/siteShared/ demand_price. asp?sid =ic.

[34] Smith JM, Van Ness H, Abbot M. *Introduction to Chemical Engineering Thermodynamics – 7th Edition*. McGraw-Hill. New York, NY, United States. 2005.

Chapter 8

Conclusions and Recommendations

8.1 Conclusions

Throughout this thesis project, meaningful steps have been taken toward the industrialization of SOFC power plants with integrated CAES for the production of clean, renewable peaking power from fossil fuels. With this objective in mind, this thesis objectively compares and contrasts SOFC power plants to the current SOTA from the perspective of the triple-bottom-line of sustainability, which focuses on the economic, environmental and political feasibility of each plant.

8.1.1 Economic Feasibility

Unique bulk-scale SOFC/CAES plants were designed for natural gas (chapter 2) and gasified coal (chapter 3) as fuel sources in order to demonstrate the flexibility and economic competitiveness of plants featuring the use of SOFCs. Full techno-economic analyses of each configuration were performed and compared to the current SOTA (NGCC, SCPC, and IGCC plants) in cases with and without carbon capture, and for a variety of carbon tax scenarios. Rigorous simulation models were used to determine the performance of each plant configuration with respect to peaking capabilities and overall system efficiency with the objective of saving as much fuel as possible. Results show that an SOFC plant fueled by natural gas is economically competitive with NGCC plants when only a modest CO_2 tax of approximately $15-20/tonne is introduced and the price of natural gas is moderately high ($8/GJ). With regards to coal, a CO_2 tax of approximately $22/tonne makes the SOFC process with CCS more economically attractive than any SOTA alternative. In both cases, the addition of CAES to the SOFC plant provides a substantial improvement to load-following capabilities with a modest 0.3 ¢/kW-h increase in the levelized cost of electricity generation. Moreover, at high fuel and CO_2 prices it was even found that SOFC/CAES systems with planned partial plant shutdowns, due to their ability to better utilize fuel by exploiting the CAES peaking functionality, are the least expensive options of all plants considered. Sensitivity analyses on the SOFC plants found that the economics of such systems is strongly dependant on the price of the SOFC stacks themselves, which were already assumed to be very high since the technology is in its early commercial stages.

8.1.2 Environmental Performance

In order to make a meaningful claim that the environmental impact of SOFC plants with CCS are less harmful to the environment (as opposed to a gate-to-gate emissions study), it was imperative that the entire life cycle impact of the SOFC plants and the competing SOTA options was performed. As such, the boundary regions, life cycle impacts and complete long-term impact analyses for the natural gas-fueled (chapter 4) and coal-fueled (chapter 5) SOFC plants and their competitors were compared using the *ReCiPe 2008* method. It was found that, unsurprisingly, the addition of CCS to *any* plant fails to reduce its global warming potential by 100% regardless of the efficiency of the CCS system. This is due to the significant contributions of up- and down-stream uncontrolled substances and fugitive emissions. However, the SOFC plant with CCS fueled by natural gas was found to have a 50% lower life cycle impact when compared to the NGCC plant, and a 30% lower life cycle impact compared to an NGCC plant using CCS, while also (according to chapter 2) having

a lower cost of electricity. However, perhaps the most significant discovery in chapter 4 is that, when all facets of life cycle impacts are considered (resource depletion, ecosystem destruction, and human health), there is no significant difference between the life cycle impacts of the NGCC plant with CCS and the SOFC plant *without* CCS; both plants have a total life cycle impact of 37 ecoPoints /MW-h (note that 1,000 points is defined to be the total impact of one human over one year). This is a very important result to argue in favour of the industrialization of SOFC plants fueled by natural gas. This way, SOFC plants may be constructed now without CCS, which may then be added in the future to even further improve their environmental impact. In chapter 5, it was found that adding CCS to a coal-fueled SOFC plant reduced its end-point impact by more than 55% to 27 points/MW-h, which is significantly lower than any alternative SOTA plant by a significant margin. Not only does this mean that coal can be used in a more sustainable manner going forward, but coal power plants using SOFCs have even lower life cycle impacts than SOTA plants using natural gas as a fuel source. This is a very strong argument for the development of SOFCs for bulk power generation since it would unlock the otherwise unfavourable use of coal.

It should be noted that the LCA results presented in this thesis feature the SOFC plants mentioned above without the inclusion of CAES. However, the impacts of CAES on the LCA results can be estimated to be inversely proportional to the decrease in system efficiency observed while using CAES (less than one percentage point in most cases). Furthermore, the very small contributions of the commissioning and decommissioning of the CAES system would have only a marginal impact on the results, and would change no conclusions about the system versus the current SOTA. To repeat these results would be unnecessary, and thus the analysis for the baseload SOFC plants only was considered.

8.1.3 Reliability and Load Following Capabilities (Political Performance)

The final component of this thesis was to test the reliability of the proposed SOFC/CAES with regards to its ability to provide on-demand peaking power. In the original process designs presented in chapters 2 and 3, a so-called “greedy” algorithm was used to demonstrate that the CAES system is able to, generally speaking, provide rudimentary peaking capabilities to an otherwise base-load only plant setup. In chapters 6 and 7, the forecasts of coming hourly and seasonal demand profiles was exploited in an RHO scheme aimed at matching the supply of the SOFC/CAES plant to demand as often as possible, and distributing problematic sudden “large misses” as a series of “small misses” in order to improve the load-following capabilities of the SOFC/CAES plant. Chapter 6 detailed the primary formulation of the RHO method, including all operating and capacity constraints of the CAES portion of the integrated plant. It was found that significant improvements to load-following on a day-to-day basis was possible with the use of RHO, even in the presence of significant demand uncertainty. It was also found that altering the objective function to consider the market spot-price of electricity made it possible to improve revenues and thus the profitability of the proposed plant. However, one significant operational issue still remained: the demand profile used in simulations (which was a scaled sample of the real demand pattern from the Ontario market for 2013 and 2014) contained much larger, slower seasonal drifts that were unable to be handled by the CAES system. Consequently, certain

months of the year still showed very poor load-following performance. This led to the development of the two-stage RHO proposed in chapter 7, which uses the modularity of the SOFC stacks in the first optimization level to make small, deliberate changes in the base-load output of the SOFC plant at weekly intervals by optimizing the forecasted load-following performance of the plant at the beginning of each week. The resulting formulation was found to vastly improve the load-following performance of the SOFC/CAES plant to nearly perfect levels (an 86% improvement compared to the single-layer RHO method and a 96% improvement to the naïve greedy algorithm), any improvements on which would only be made possible by the use of another long-term energy storage method and a larger plant.

8.1.4 Concluding Thoughts and Outlooks

This thesis has taken significant strides toward the industrialization of SOFC power plants on a number of levels. However, a more far-reaching conclusion may be drawn from the results of this work. In an era of dwindling natural resources deemed to be non-renewable coinciding with a time in which their use has never been higher, more effective and efficient use of these resources is imperative as a transition is made to a landscape in which renewable energy sources are able to more significantly contribute to global power generation. A critical observation from the life cycle analyses performed in chapters 4 and 5 are that carbon capture and sequestration, although important, do not provide a single answer to the issue of global warming. Moreover, carbon capture, particularly for combustion-based systems, does nothing but exacerbate the issue of fossil fuel consumption by significantly decreasing overall plant efficiency. The SOFC plants, on the other hand, not only do not suffer from this parasitic energy loss, but also start with a higher overall system efficiency in all cases, making them superior to any state-of-the-art plant by a significant margin. The key takeaway here is that the SOFC plants, in all cases, are more efficient, meaning they not only consume less fuel, but also have a smaller upstream life cycle impact due to lower fuel consumption.

These results show that improved system efficiency is not only a way to reduce fuel consumption, but also a method for reducing environmental impact as well. Moreover, improved system efficiency, as was shown in chapters 2 and 3, is a method to reduce operating costs, leading to improved economic performance as well. SOFC plants, with their high system efficiency, therefore represent a forward-looking method to deliver on all three facets of the triple-bottom-line of sustainability via their higher efficiencies versus any currently used power plant design consuming fossil fuels.

8.2 Recommendations for Further Work

The following section describes some possible projects that would further this research, or works-in-progress that were incomplete at the time of publication.

8.2.1 System Dynamics and Control Studies

It is acknowledged that the dynamics studied in this work, particularly those of the CAES charging and discharging system, were simplified in order to prove the conceptual

applicability of an SOFC/CAES plant for load-following scenarios. However, it would be more suitable for detailed dynamic models, either from first principles or based on empirical data, to be used to design control systems capable of effectively adjusting the many interconnected parts of the proposed plant. Such models could be used for the design of a variety of control structures including but not limited to classical controllers (proportional-integral), model predictive controllers, or even advanced stability-oriented methods such as Lyapunov-based model predictive control. Explicitly accounting for modeling uncertainties and disturbances would also clarify the true controllability of a dynamic SOFC/CAES process. Furthermore, the impact of input constraints in any MPC control implementation or in a more rigorous RHO study would be important to improve the validity of the RHO and control study results.

8.2.2 Pilot Plant Design, Construction and Operation

At this point, the next step for this SOFC/CAES concept would be to build and test a small scale experimental setup. Detailed drawings of a potential are included as Appendix A. In the future, it would be considered the final step of this research project, and the last key demonstration of the potential of the use of SOFC/CAES plants for peaking power, to have an operating system available for demonstration at McMaster. It would then be possible to analyze the true efficiency and performance of the system for a variety of fuel compositions to obtain experimental validation of the process design conclusions in chapters 2 and 3. Analysis of outlet streams could validate the life cycle impact conclusions in chapters 4 and 5. Finally, the combination of the proposed RHO framework with a control system designed as mentioned above would demonstrate the true physical peaking capabilities of the integrated SOFC/CAES plant. Should the pilot plant successfully confirm the results of this thesis, it would make a very strong case for the industrial adaptation of SOFC power plants.

Appendix A: Pilot Plant Piping and Instrumentation Diagrams and Floorplans

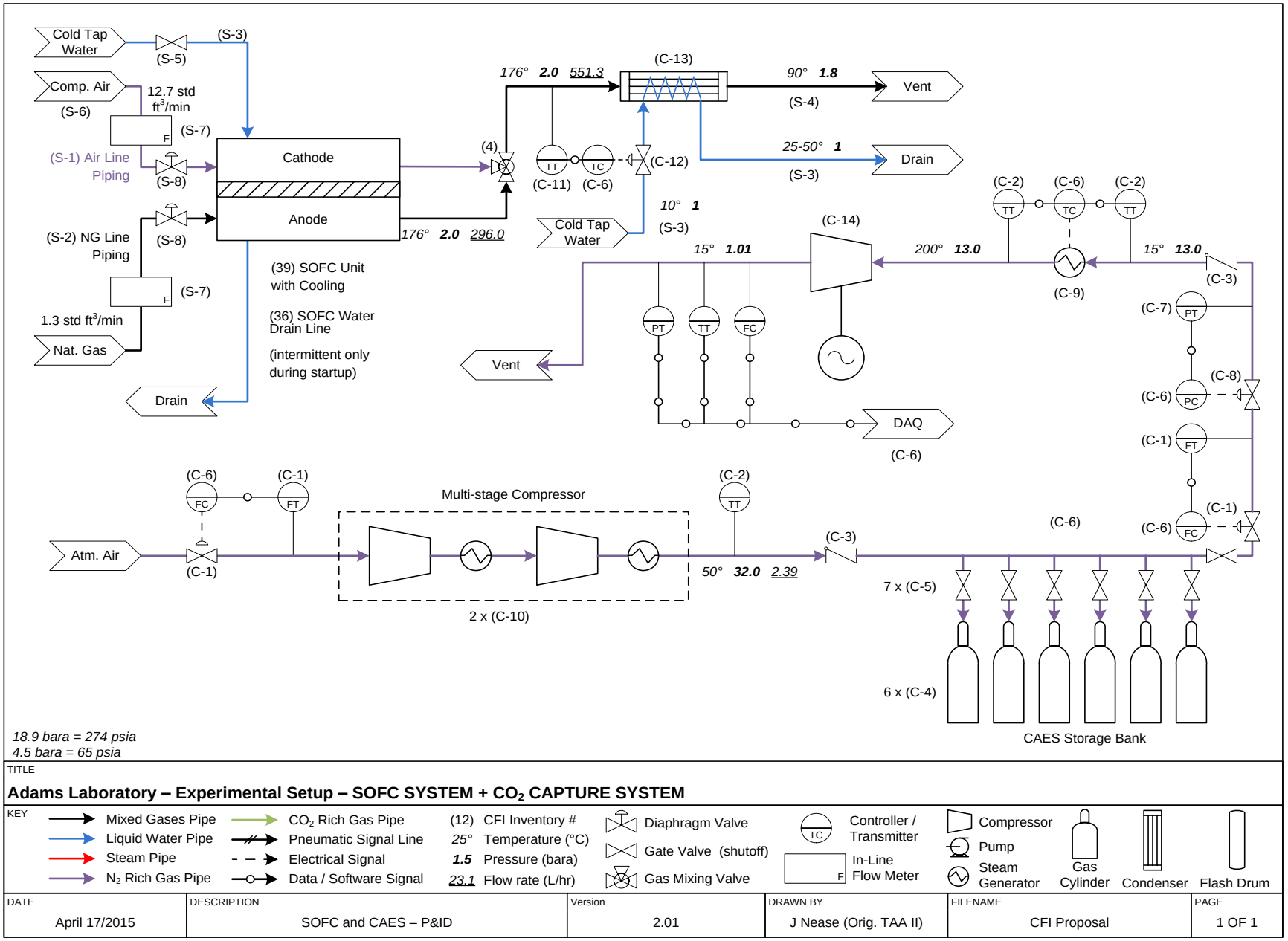

Figure 16: SOFC/CAES pilot plant P&ID

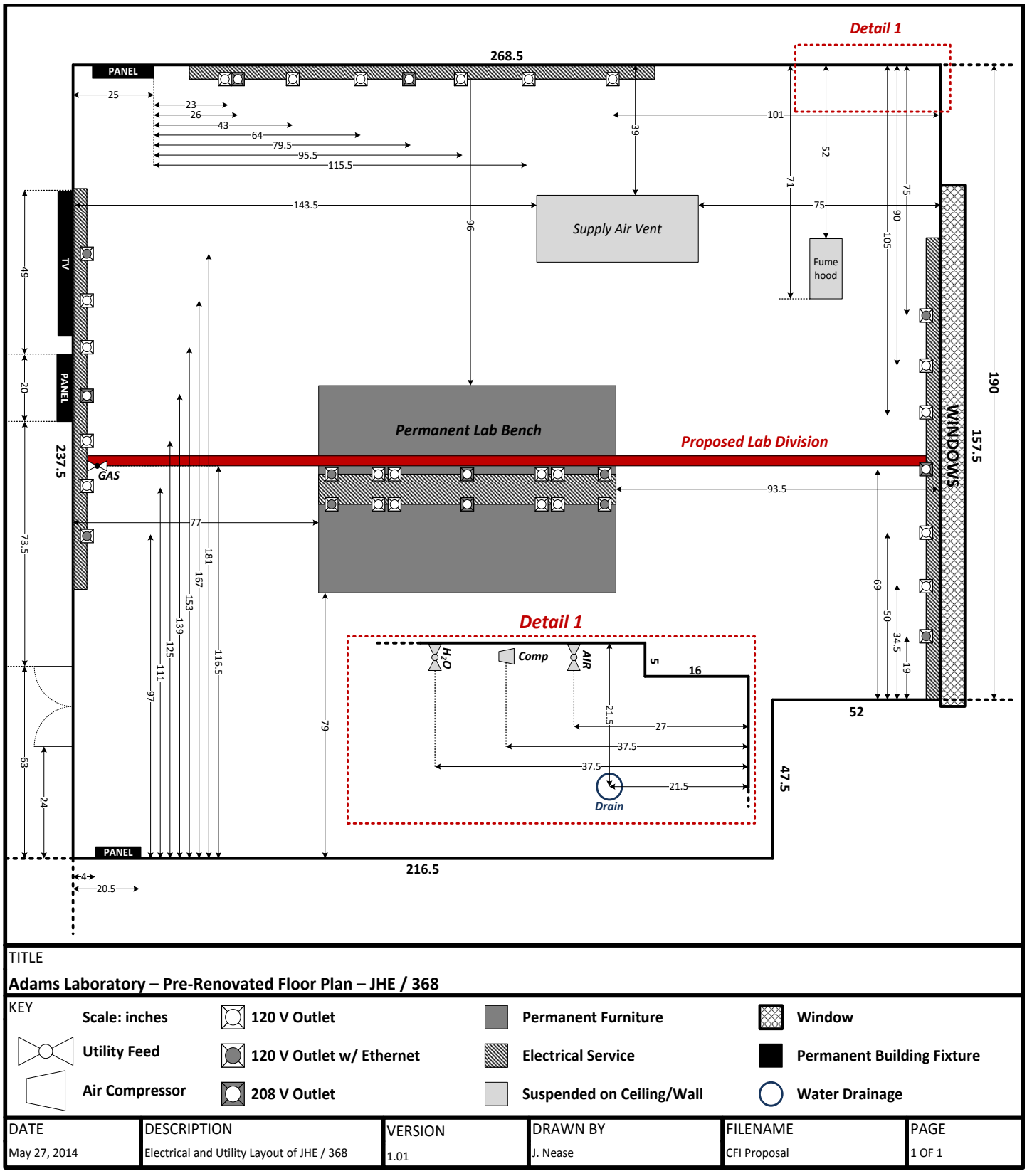

TITLE

Adams Laboratory – Pre-Renovated Floor Plan – JHE / 368

KEY			
Scale: inches	120 V Outlet	Permanent Furniture	Window
Utility Feed	120 V Outlet w/ Ethernet	Electrical Service	Permanent Building Fixture
Air Compressor	208 V Outlet	Suspended on Ceiling/Wall	Water Drainage

DATE	DESCRIPTION	VERSION	DRAWN BY	FILENAME	PAGE
May 27, 2014	Electrical and Utility Layout of JHE / 368	1.01	J. Nease	CFI Proposal	1 OF 1

Figure 17: SOFC/CAES lab layout prior to pilot plant renovations

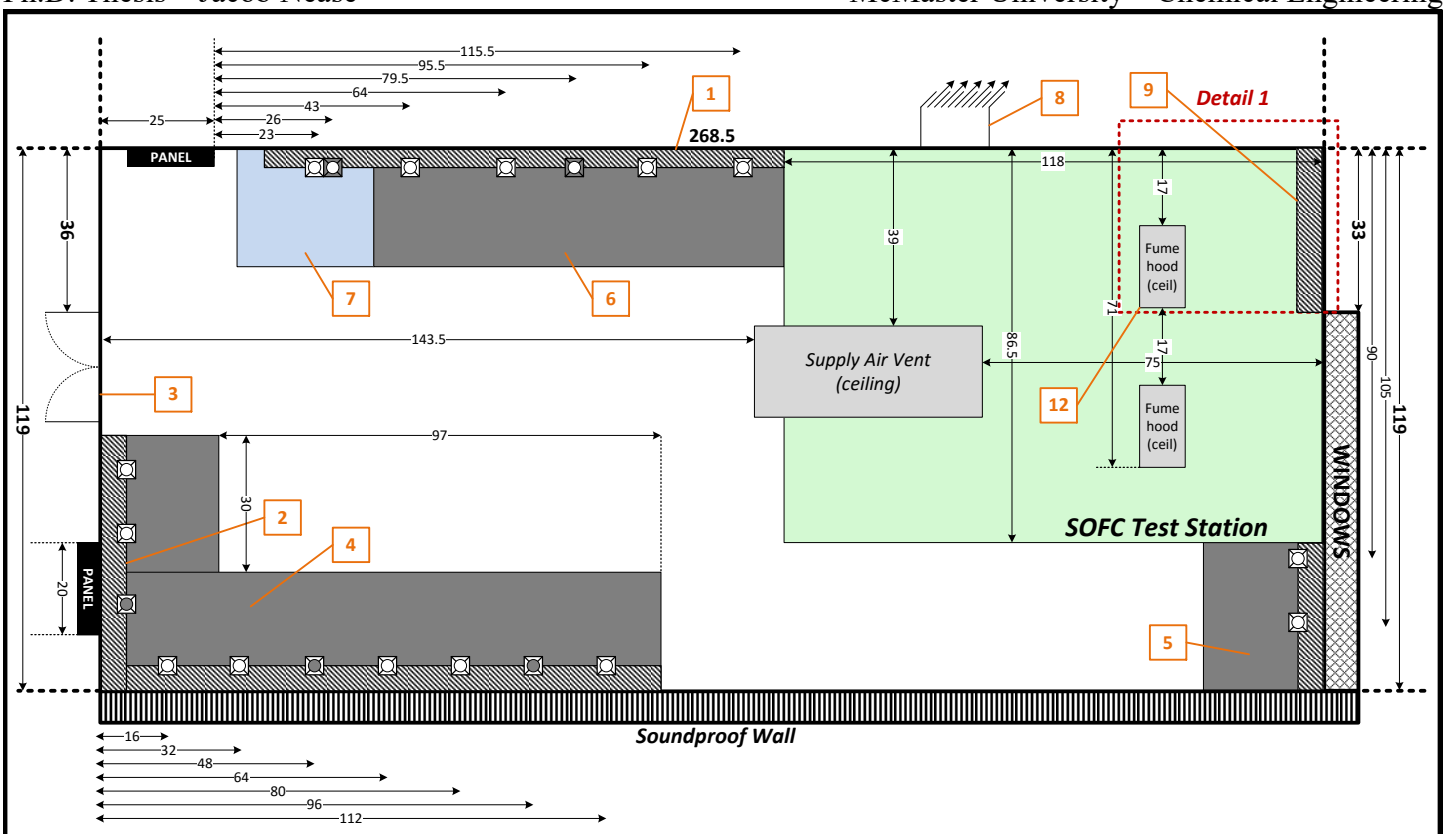

CALLOUT DEFINITIONS

(1) Slight alteration required for East wall electrical service (shortened from south end to fit SOFC station)
(2) North wall electrical service must be bisected and shortened from East side for door placement
(3) New door location (requires departmental TV to be moved)
(4) Additional Lab bench for data and analysis equipment
(5) South wall electrical service must be bisected, shortened from East side to add SOFC test station and workspace must be added
(6) Additional lab bench area for CAES and CCS equipment
(7) Open space available for CAES storage and compressed gas cylinders (N_2, H_2, O_2, CO, CO_2)
(8) Dedicated SOFC exhaust vents (to outside)
(9) New 230 V power sources required (see Detail 1)
(10) 230 V power source to run SOFC equipment (as per manufacture recommendations) **NB** – 208 V may be used with decreased performance
(11) Gas feeds from compressed cylinders in blue section (piping required on wall)
(12) Additional fume hood for safety

DETAIL 1

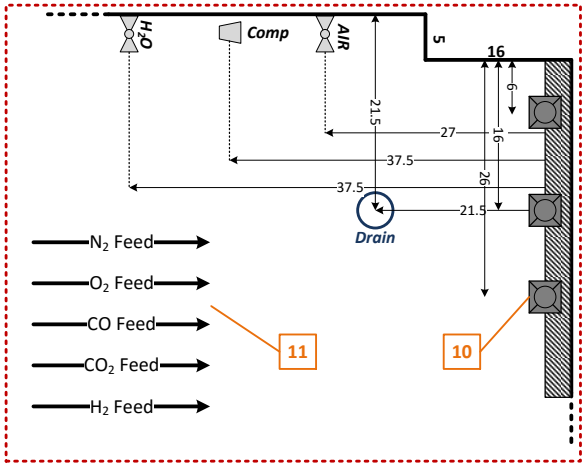

TITLE

Adams Laboratory – Post-Renovated Floor Plan – JHE / 368A (Working Name, East Side)

KEY

Scale: inches
Utility Feed
Air Compressor
120 V Outlet
120 V Outlet w/ Ethernet
208 V Outlet
230 V Outlet
Lab Bench
Electrical Service
Suspended on Ceiling/Wall
SOFC Test Station
Window
Permanent Building Fixture
Compressed Gas Storage
Water Drainage

DATE	DESCRIPTION	VERSION	DRAWN BY	FILENAME	PAGE
May 27, 2014	Proposed Layout of JHE / 368A (Adams Half)	1.01	J. Nease	CFI Proposal	1 OF 1

Figure 18: SOFC/CAES lab layout after pilot plant renovations